

GIS/RS-based Integrated Eco-hydrologic Modeling in the East River Basin, South China

WANG, Kai

A Thesis Submitted in Partial Fulfillment
of the Requirements for the Degree of
Doctor of Philosophy
in
Geography and Resource Management

The Chinese University of Hong Kong
December 2010

UMI Number: 3491982

All rights reserved

INFORMATION TO ALL USERS

The quality of this reproduction is dependent on the quality of the copy submitted.

In the unlikely event that the author did not send a complete manuscript and there are missing pages, these will be noted. Also, if material had to be removed, a note will indicate the deletion.



UMI 3491982

Copyright 2011 by ProQuest LLC.

All rights reserved. This edition of the work is protected against unauthorized copying under Title 17, United States Code.



ProQuest LLC.
789 East Eisenhower Parkway
P.O. Box 1346
Ann Arbor, MI 48106 - 1346

Thesis/Assessment Committee

Professor LEUNG Yec (Chair)
Professor CHEN Yongqin (Thesis Supervisor)
Professor FUNG Tung (Committee)

ABSTRACT

Land use/cover change (LUCC) has significantly altered the hydrologic system in the East River (Dongjiang) Basin. Quantitative modeling of hydrologic impacts of LUCC is of great importance for water supply, drought monitoring and integrated water resources management. An integrated eco-hydrologic modeling system of Distributed Monthly Water Balance Model (DMWBM), Surface Energy Balance System (SEBS) was developed with aid of GIS/RS to quantify LUCC, to conduct physically-based ET (evapotranspiration) mapping and to predict hydrologic impacts of LUCC.

To begin with, in order to evaluate LUCC, understand implications of LUCC and provide boundary condition for the integrated eco-hydrologic modeling, firstly the long-term vegetation dynamics was investigated based on Normalized Difference Vegetation Index (NDVI) data, and then LUCC was analyzed with post-classification methods and finally LUCC prediction was conducted based on Markov chain model. The results demonstrate that the vegetation activities decreased significantly in summer over the years. Moreover, there were significant changes in land use/cover over the past two decades. Particularly there was a sharp increase of urban and built-up area and a significant decrease of grassland and cropland. All these indicate that human activities are intensive in the East River Basin and provide valuable information for constructing scenarios for studying hydrologic impacts of LUCC.

The physically-remote-sensing-based Surface Energy Balance System (SEBS) was employed to estimate areal actual ET for a large area rather than traditional point measurements. The SEBS was enhanced for application in complex vegetated area. Then the inter-comparison with complimentary ET model and distributed monthly water balance model was made to validate the enhanced SEBS (ESEBS). The application and test of ESEBS show that it has a good accuracy both monthly and annually and can be effectively applied in the East River Basin. The results of ET mapping based on ESEBS demonstrate that actual ET in the East River Basin decreases significantly in the last two decades, which is probably caused by decrease of sunshine duration.

In order to effectively simulate hydrologic impact of LUCC, an integrated model of ESEBS and distributed monthly water balance model has been developed in this study.

The model is capable of considering basin terrain and the spatial distribution of precipitation and soil moisture. Particularly, the model is unique in accounting for spatial and temporal variations of vegetation cover and ET, which provides a powerful tool for studying the hydrologic impacts of LUCC. The model was applied to simulate the monthly runoff for the period of 1980-1994 for model calibration and for the period of 1995-2000 for validation. The calibration and validation results show that the newly integrated model is suitable for simulating monthly runoff and studying hydrologic impacts of LUCC in the East River Basin.

Finally, the newly integrated model was firstly applied to analyze the relationship of land use and hydrologic regimes based on the land use maps in 1980 and 2000. Then the newly integrated model was applied to simulate the potential impacts of land use change on hydrologic regimes in the East River Basin under a series of hypothetical scenarios. The results show that ET has a positive relationship with Leaf Area Index (LAI) while runoff has a negative relationship with LAI in the same climatic zone, which can be elaborated by surface energy balance and water balance equation. Specifically, on an annual basis, ET of forest scenarios is larger than that of grassland or cropland scenarios. On the contrary, runoff of forest scenarios is less than that of grassland or cropland scenarios. On a monthly basis, for most of the scenarios, particularly the grassland and cropland scenarios, the most significant changes occurred in the rainy season. The results indicate that deforestation would cause increase of runoff and decrease of ET on an annual basis in the East River Basin. On a monthly basis, deforestation would cause significant decrease of ET and increase of runoff in the rainy season in the East River Basin.

These results are not definitive statements as to what will happen to runoff, ET and soil moisture regimes in the East River Basin, but rather offer an insight into the plausible changes in basin hydrology due to land use change. The integrated model developed in this study and these results have significant implications for integrated water resources management and sustainable development in the East River Basin.

土地利用變化嚴重改變了東江流域的水文系統，因此定量模擬土地利用變化對水文系統的影響對區域供水，乾旱監測及流域水資源綜合管理具有重要意義。為此，本研究建立了一套集分布式月水文模型，能量平衡系統，遙感和地理信息系統為一體的綜合模擬系統，分析了東江流域土地利用變化，並用基於遙感具有物理基礎的能量平衡系統模擬區域實際蒸散發，最後定量評價了由人類活動引起的土地利用變化對東江水資源量及其時空變化的影響。

為分析土地利用變化及為後文的生態水文模擬提供邊界條件，論文首先利用 NDVI 數據分析了東江流域植被動態長期變化情況。其次，論文利用分類後比較方法分析了東江流域的土地利用/覆蓋變化情況并用马尔科夫链模型對未來土地利用/覆蓋進行了初步預測。結果表明，在此 20 年間，此區域植被活動在夏季有減弱趨勢。土地利用變化較為嚴重，尤其以城市化和草場耕地退化最為嚴重。該結果亦揭示人類活動在此區域尤為頻繁。以上分析為後文的水文響應研究的邊界條件設定提供了重要信息。

其次，傳統蒸散發估算都首先通過點的估算進而通過空間插值來推及到面，其精度和物理基礎值得商榷。為了更合理的估算區域實際蒸散發，論文採用基於遙感的具有明確物理基礎的能量平衡系統。由於該系統比較適合低矮均勻植被區域，因此，為使其適應南方複雜下墊面和植被覆蓋情況，本研究對其進行了改進，並用水文模型和互補蒸發模型對其結果進行了驗證。模擬和驗證結果表明，改進後該模型精度較高，實用性強。實際蒸散發的模擬結果表明，此 20 年間，實際蒸發明顯的減少趨勢。通過分析對比相關氣象因素如溫度，相對濕度，日照時間，風速的變化趨勢，實際蒸散發的減少很可能是由太陽輻射減少所引起。

再次，為了能夠更好模擬土地利用變化的水文響應，本研究開發了集改進的蒸散發模型 ESEBS、基於 LAI 的截留子模型以及分布式月平衡模型為一體的綜合模擬模型。該耦合模型可以考慮降雨，地形及土壤水的空間變化，特別是能夠考慮植被和蒸散發的空間變化。該特性使模型建立了水文過程與植被的直接聯繫，為研究土地利用變化引起的水文響應提供了有力的工具。該綜合模型以 1980 至 1994 年為率定期，以 1995 至 2000 年驗證期，對東江流域的生態水文過程進

行了模擬。率定和驗證結果表明該模型具有較高精度很適合東江流域的降雨徑流模擬及生態水文效應研究。

最後，應用此綜合模型，結和情景分析方法，對土地利用變化對區域可利用水資源的可能影響作出了定量分析。結果表明，對於同一氣候區，實際蒸散發和葉面指數具有正相關關係而徑流與葉面指數具有負相關關係。該結論可以很好的用能量平衡和水量平衡理論來解釋。具體結果如下：就年尺度而言，林地情景的蒸發量比草地和耕地的都高，但林地情景的徑流量比草地和耕地的都低。就月過程而言，也有與年相似的結論。并且，跟現狀相比，各情景的月最大變化量都集中在雨季。因此，可以得出以下結論：就年總量而言，森林退化將會引起蒸散發的顯著減少以及徑流的顯著增加。就月過程而言，森林退化將會引起雨季蒸散發的顯著減少以及徑流的顯著增加。

由於現有科技水準和觀察資料的限制，要準確模擬土地利用變化對區域水文水資源的影響非常困難。本文探索性地建立了結合水量平衡，能量平衡和遙感地理信息系統的綜合模擬方法，探討了土地利用變化對東江流域水文水資源的影響，對區域的水資源綜合管理和社會可持續發展具有重要的科學意義和實用價值。

Acknowledgement

Many people have provided me with support, encouragement, and assistance during my Ph.D. study period at The Chinese University of Hong Kong. First and foremost, I would like to express my deep and sincere gratitude to my supervisor, Prof. Chen Yongqin, for his guidance, support and encouragement. His academic advice and professional mentorship have helped me establish a solid foundation for my career development. He provided me with patient supervision, important advice and many helpful suggestions during my PhD study. His friendly smile and constant encouragement exceptionally helped me to recover my self-confidence when I encountered difficulties and enable me to complete this work.

I would also like to thank other members of my Advisory Committee: Prof. Leung Yee and Prof. Fung Tung for their advice and helpful suggestions throughout my doctoral study. I have been fortunate to have Prof. TUNG Yeou-Koung as the External Examiner in my thesis committee. He has extensive knowledge and experience in hydrologic science and gave me many valuable suggestions. I should pay my special appreciation to him.

I am deeply grateful to Prof. Chen Xi at Hohai University, who has given me many advices and suggestions on my research and offered me much help in my Ph.D. study. All of his efforts have not only broadened my research scope but also benefited me a great deal. Therefore, I must say a hearty thank-you to Prof. Chen Xi for everything he has done to me that no words could explain.

I also want to express my sincere thanks to my friends and colleagues at CUHK during the past years of my Ph.D. study. I have been accompanied and supported by them who made this long journey easier.

Last but not the least, I wish to extend my deepest gratitude to my parents, sister for their love and support throughout my education and academic career. Their love and support accompany me throughout my life and this thesis is simply impossible without them and I thank them all from the bottom of my heart.

Table of content

CHAPTER 1 INTRODUCTION	1
1.1 Background	1
1.2 Research objectives.....	10
1.3 Research significance.....	10
1.4 Organization of the dissertation	12
1.5 Research framework	12
1.6 Study Area.....	15
CHAPTER 2 REVIEW	17
2.1 Eco-hydrology: definition and recent development.....	17
2.2 Effects of land use/cover change on watershed hydrology	18
2.3 Modeling hydrologic impacts of land use change	26
2.4 Remote sensing in eco-hydrologic modeling.....	33
CHAPTER 3 LAND USE/COVER CHANGE ANALYSIS WITH THE AID OF GIS/RS	52
3.1 Introduction.....	52
3.2 Spatial-temporal analysis of vegetation dynamics based on NDVI.....	53
3.3 Land use/cover change detection based on post-classification comparison	63
3.4 Land use/cover change prediction.....	71
3.5 Summary and conclusion	78
CHAPTER 4 EVAPOTRANSPIRATION (ET) MAPPING WITH AID OF GIS/RS	80
4.1 Introduction	80
4.2 Data	84
4.3 Surface energy balance system (SEBS).....	91
4.4 Enhancement of SEBS for application in complex vegetated area.....	105
4.5 Validation of ESEBS	114
4.6 Results and discussion	122
4.7 Summary and conclusion	130

CHAPTER 5 INTEGRATED DISTRIBUTED MONTHLY WATER BALANCE MODEL (IDMWBM)	131
5.1 Introduction	131
5.2 Conceptual framework of Monthly Water Balance Model.....	133
5.3 Distributed Monthly Water Balance Model.....	137
5.4 Integration of ESEBS and LAI-based interception model into DMWBM	143
5.5 Application of the integrated DMWBM in the East River Basin	148
5.6 Summary and conclusion	166
CHAPTER 6 ASSESSMENT OF HYDROLOGIC IMPACTS OF LAND USE/COVER CHANGE	168
6.1 Introduction	168
6.2 Effects of land use/cover on hydrologic regimes.....	169
6.3 Hydrologic response to land use/cover change.....	177
6.4 Summary and conclusion.....	189
CHAPTER 7 SUMMARY AND CONCLUSIONS	191
7.1 Summary of the study	191
7.2 Major findings and conclusions	192
7.3 Recommendation for future study.....	200
REFERENCES	203

List of Figures

Figure 1.1 The integration of hydrology and ecology.....	2
Figure 1.2 The delicate balance between water for livelihood and water as a resource ...	2
Figure 1.3 Research gaps of hydrologic impacts of LUCC and ET as a link to bridge the gaps	6
Figure 1.4 Illustration of ET as a link for water and energy balance system.....	9
Figure 1.5 Research framework	14
Figure 1.6 Geography and major tributaries of the East River Basin	16
Figure 2.1 Empirical model.....	27
Figure 3.1 Summary of land use/cover change detection and quantification	53
Figure 3.2 Long-term variation of monthly NDVI from 1982 to 2003	58
Figure 3.3 Long-term variation of seasonal NDVI (Spring and Summer)	59
Figure 3.4 Long-term variation of seasonal NDVI (Autumn and Winter)	60
Figure 3.5 Long-term variation of annual NDVI from 1982 to 2003	60
Figure 3.6 Spatial distribution of annual mean NDVI	61
Figure 3.7 Monthly mean NDVI of the upper-part, middle-part and lower-part.....	62
Figure 3.8 Land use map in 1980.....	64
Figure 3.9 Land use map in 2000.....	64
Figure 3.10 Illustration of land use centroid movement model	66
Figure 3.11 Centroids movement of different land use types from 1980 to 2000.....	70
Figure 3.12 Land cover maps in 2002 and 2008 (MODIS 500 m * 500 m).....	72
Figure 3.13 Ratios of different land cover in different years	73
Figure 3.14 Projected Land use land cover for 2010 (unit: km ²).....	78
Figure 4.1 Summary of ET as a core in the studies of hydrologic impacts of LUCC	82
Figure 4.2 Location of rainfall, hydrologic and weather stations	85
Figure 4.3 Areal mean monthly pan evaporation, rainfall, runoff and temperature of the East River Basin from 1980 to 2000.....	85
Figure 4.4 Spatial distribution of annual mean temperature.....	87
Figure 4.5 Spatial distribution of annual mean wind speed.....	87
Figure 4.6 Field work for Ground-truthing and LAI measurement conducted from December 2008 to December 2009.....	88
Figure 4.7 Measured LAI by field work from December, 2008 to December, 2009.....	89
Figure 4.8 Selected photos for land use/cover in the East River Basin	90

Figure 4.9 Typical structure of the atmospheric boundary layer	92
Figure 4.10 Surface Energy Balance for ET	93
Figure 4.11 Surface radiation balance.....	94
Figure 4.12 Map of solar zenith.....	94
Figure 4.13 Scheme representation of SEBS	103
Figure 4.14 The procedures for enhancing SEBS for application in complex vegetated area.....	107
Figure 4.15 Relationship of LAI~NDVI.....	109
Figure 4.16 Curve fitting results for identification of LAI-NDVI relationship.....	112
Figure 4.17 Comparison of LAI estimated by different methods	113
Figure 4.18 Illustration of complimentary relationship ET model	116
Figure 4.19 ESEBS output on 02/02/1992.....	123
Figure 4.20 Annual variation of annual mean ET from 1982 to 2000.....	124
Figure 4.21 Spatial distribution of annual mean ET from 1982 to 2000	124
Figure 4.22 Inter-comparison of ET estimated by different models.....	125
Figure 4.23 Monthly mean ET process of different models	126
Figure 4.24 Variation of annual mean ET and T from 1982 to 2000.....	127
Figure 4.25 Variation of annual mean relative humidity from 1982 to 2000	127
Figure 4.26 Variation of annual mean sunshine duration from 1982 to 2000	127
Figure 4.27 Variation of annual mean wind speed from 1982 to 2000.....	128
Figure 4.28 Comparison of monthly ET, NDVI and LAI from 1982 to 2000.....	128
Figure 4.29 Monthly process of ET estimated by ESEBS	129
Figure 5.1 Integration of ESEBS and LAI-based interception sub-model into monthly water balance model for assessing hydrologic impact of LUCC.....	132
Figure 5.2 Regional terrestrial hydrological processes in warm and humid area	136
Figure 5.3 Field capacity curve of soil moisture and rainfall-runoff relationship	140
Figure 5.4 Flowchart for integration of ESEBS and LAI-based interception model into DMWBM with aid of GIS/RS	145
Figure 5.5 Flow chart for the delineation of subbasin from a DEM	149
Figure 5.6 DEM for the East River Basin.....	150
Figure 5.7 Depressionless DEM for the East River Basin.....	150
Figure 5.8 Flow directions for the East River Basin.....	151
Figure 5.9 Flow accumulation for the East River Basin.....	151
Figure 5.10 Division of the East River Basin into 17 sub-basins	152

Figure 5.11 Cumulative frequency distributions of IRDRG for 17 sub-basins in the East River Basin.....	154
Figure 5.12 Model calibration interface.....	158
Figure 5.13 Spatial distribution of the runoff regulation coefficient α	161
Figure 5.14 Spatial distribution of the pan coefficient η	161
Figure 5.15 Comparison of monthly observed and simulated runoff for the calibration period at the Boluo station	164
Figure 5.16 Comparison of monthly observed and simulated runoff for the validation period at the Boluo station	164
Figure 5.17 Comparison of monthly observed and simulated runoff for the validation period at the Heyuan station.....	164
Figure 5.18 Comparison of monthly observed and simulated runoff for the validation period at the Longchuan station.....	165
Figure 5.19 Sensitivity of parameters to runoff in the East River Basin	166
Figure 6.1 Spatial distribution of annual mean ET in 1980 and 2000	171
Figure 6.2 Spatial distribution of annual mean runoff from 1980 to 2000	172
Figure 6.3 Spatial distribution of annual runoff in 1980.....	173
Figure 6.4 Spatial distribution of annual runoff in 2000.....	173
Figure 6.5 Spatial distribution of monthly soil moisture in January of 1980	175
Figure 6.6 Spatial distribution of monthly soil moisture in February of 1980	175
Figure 6.7 Spatial distribution of monthly soil moisture in January of 2000	176
Figure 6.8 Spatial distribution of monthly soil moisture in February of 2000	176
Figure 6.9 Illustration of scenario setting	179
Figure 6.10 Comparison of ET processes for different scenarios.....	184
Figure 6.11 Monthly mean ET for different scenarios.....	185
Figure 6.12 Change of ET compared with current situation for different scenarios.....	185
Figure 6.13 Comparison of runoff processes for different scenarios.....	187
Figure 6.14 Monthly runoff depth for different land cover	188
Figure 6.15 Change of monthly runoff depth compared with current situation for different scenarios	188

List of Tables

Table 2.1 Summary of the advantages and disadvantages of the different approaches used to estimate ET from remote sensing data.....	50
Table 3.1 Statistic values for inter-annual variation of monthly mean NDVI.....	56
Table 3.2 Land use in 1980 for different regions of the East River Basin (unit: km ²)...	66
Table 3.3 Land use in 2000 for different regions of the East River Basin (unit: km ²)...	67
Table 3.4 Change range of land use for different regions (unit: km ²).....	67
Table 3.5 Change dynamic degree of land use for different regions (unit: %).....	68
Table 3.6 Land use transition matrix for 1980 and 2000 (unit: km ²).....	68
Table 3.7 Centroid movement of different land use types (unit: km).....	69
Table 3.8 Transitional Probability table derived from the land use/cover maps of 2002 and 2008.....	77
Table 4.1 Summary of measured LAI for different land cover.....	88
Table 4.2 Vegetation height for different land cover (LDAS, 2010).....	107
Table 5.1 Watershed Characteristics.....	154
Table 5.2 Distributed parameters at sub-basin scale.....	159
Table 5.3 Calibration and validation results for the integrated model.....	161
Table 5.4 Comparison of mean monthly observed and simulated runoff (mm).....	162
Table 6.1 Summary of mean ET for different land use.....	170
Table 6.2 Summary of annual mean runoff depth for different land use.....	171
Table 6.3 Summary of monthly soil moisture for different land use.....	173
Table 6.4 Summary of six hypothetical scenarios.....	178
Table 6.5 Summary of estimated ET for different scenarios (unit: mm).....	182
Table 6.6 Summary of runoff depth for different scenarios (unit: mm).....	185

ABBREVIATIONS

AA	Advection-aridity
AVHRR	Advanced Very High Resolution Radiometer
BAHC	Biospheric Aspects of the Hydrological Cycle
CARE	Complementary relationship areal evapotranspiration
CAS	Chinese Academy of Science
DEM	Digital Elevation Model
DMWBM	Distributed Monthly Water Balance Model
ENVI	The Environment for Visualizing Images
ESEBS	Enhanced Surface Energy Balance System
ESRI	Environmental Systems Research Institute
ET	Evapotranspiration
FAO	Food and Agriculture Organization
GCM	General Circulation Model
GG	Granger and Gray
GIS	Geographic Information System
GLC	Global Land Cover 2000 Project
GWP	Global Water Partnership
IDL	Interactive Data Language
IDMWB	Integrated Distributed Monthly Water Balance Model
IGBP	International Geosphere-Biosphere Programme
IPCC	Intergovernmental Panel on Climate Change
LAI	Leaf Area Index
LDAS	Land Data Assimilation System
LUCC	Land Use/Cover Change
M-K	Mann-Kendall
MSS	Multispectral Scanner
MODIS	Moderate Resolution Imaging Spectroradiometer
NDVI	Normalized Difference Vegetation Index
NOAA	National Oceanic and Atmospheric Administration
PBL	Planetary Boundary Layer
RS	Remote Sensing
SEBAL	The Surface Energy Balance Algorithm for Land
SEBS	Surface Energy Balance System
SCS	Soil Conservation Service
SLURP	Semi-distributed Land Use-based Runoff Processes
SPOT	Systeme Probatoire d'Observation de la Terre
TM	Thematic Mapper
UNESCO	United Nations Educational, Scientific and Cultural Organization
USDA	United States Department of Agriculture
WCRP	World Climate Research Programme

CHAPTER 1

INTRODUCTION

1.1 Background

Water, as the liquid of life, is the most essential component for the life of all beings. Hardly any economic activity can be sustained without water (Munther, 2001). Water is always on the move in the hydrological cycle. It is the very foundation for all biological life on Earth, and the basic link between the biosphere and the anthroposphere.

Knowledge of the general laws governing the distribution and movement of water – the hydrologic cycle - is of practical importance for the rational use and protection of water resources. The hydrologic cycle describes the continuous movement of water on, above and below the surface of the Earth. It is a complex phenomenon involving the interaction of biological and atmospheric processes and over many scales.

The water cycle links human society with ecosystems (Figure1.1). There is a delicate balance between water system and ecosystem (Figure1.2). In the last several decades, with the progress of civilization, human activities gradually intrude on the natural water environment and ecosystem by altering the dynamic equilibrium of the water cycle and initiating new processes and events, consequently, freshwater ecosystems have experienced reductions in biodiversity at least as great as the most impacted terrestrial ecosystems (Paul et al., 2008). In recent years, environmental protection, sustainable development and climate change are becoming issues of major concern to nations all around the world.

In view of the problems mentioned above, the traditional hydrology can not satisfy the needs for integrated water resources management and sustainable development, therefore, a better idea is now needed of the roles and functions of water in the integrated social-ecologic system, which has created a background for integration of ecology and hydrology and resulted in the evolution of a field of study called ecohydrology. UNESCO, under the International Hydrological Programme IHP-V, has initiated and provided a framework for such an interdisciplinary effort. In the programme, the conceptual background and principles of the surficial processes of ecohydrology were defined: first, by integration and quantification of biological and

hydrological processes at the basin scale; second, by the enhancement of basin ecosystem absorbing capacity against human impact; and third, by using ecosystem properties as a management tool. Those principles are targeted, not only to eliminate threats, but also to amplify the opportunities for sustainable development as far as the control and regulation of nutrients and water cycling at the basin scale become possible.

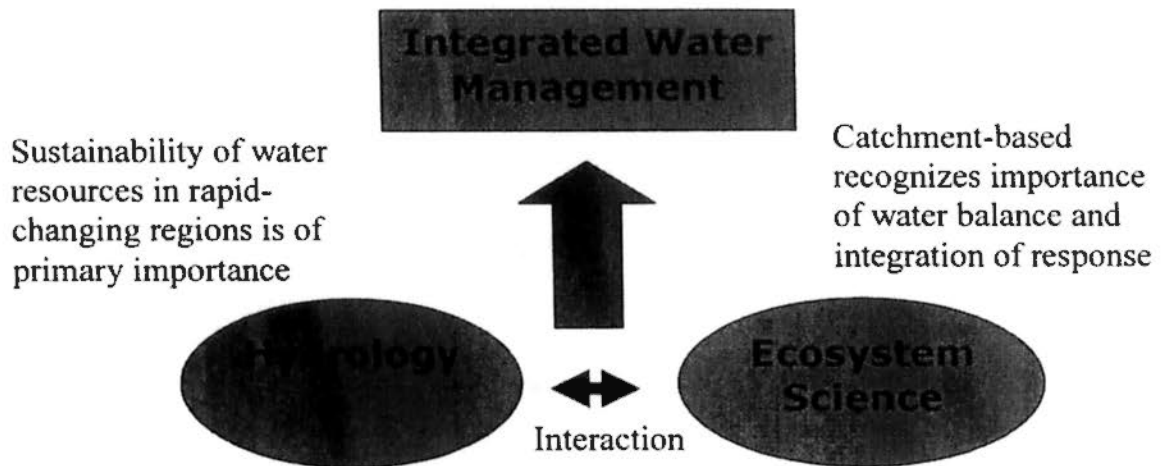


Figure 1.1 The integration of hydrology and ecology (Modified from Nuttle, 2002)

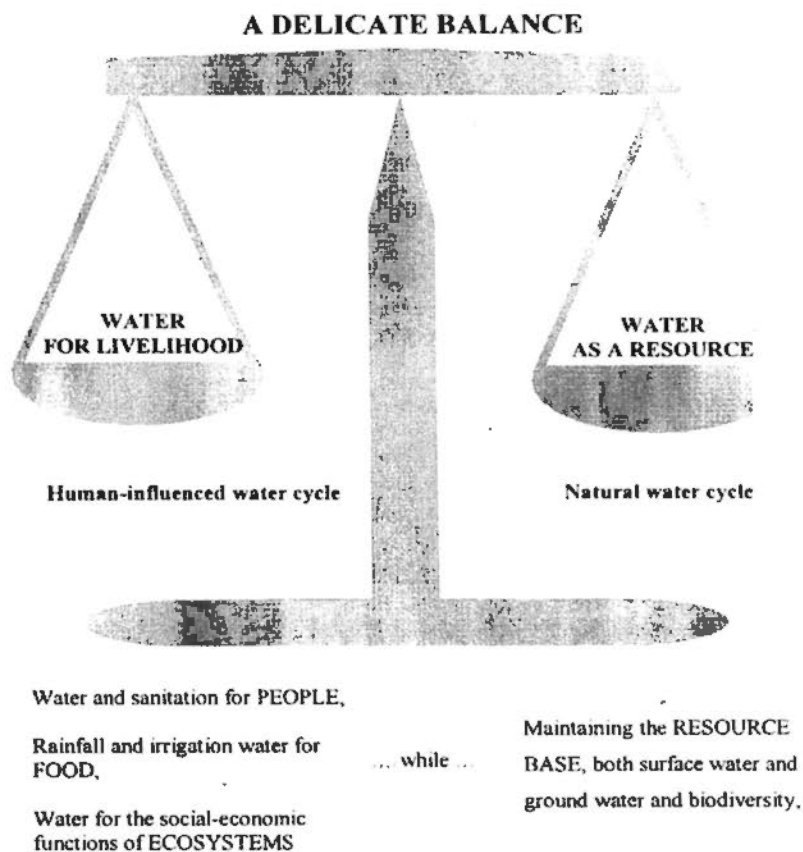


Figure 1.2 The delicate balance between water for livelihood and water as a resource (Modified from GWP/WATAC, 2000)

To date, there has been no ubiquitously and unanimously accepted definition of the term eco-hydrology. Although it might not appear from the definitional struggle, eco-hydrology started with the notion that vegetation plays an important role in the hydrological cycle. There is a consensus that vegetation and land use significantly affect watershed hydrology.

On one hand, vegetation is one of the essential components that significantly influences water and energy balances, establishing bi-directional links with the climate (Jonathan et al., 2000). The effect of vegetation on the water recycling of a land ecological system is considerably significant. Understanding the relationship between vegetation and runoff changes will benefit regional eco-environmental and water resources management (Gao et al., 2009). Moreover, the role of vegetation in the dynamics of soil moisture, runoff, and ET has been acknowledged to be very important (e.g. Fernández-Illescas, 2004; Neave, 2002; Newman et al., 1998; Wilcox et al., 2003), and understanding the influence of vegetation on hydrological changes is part of the foundational basis of eco-hydrology (e.g. Newman et al., 2006; Azzali, 2000; Bradford et al., 2003; Li et al., 2006). Therefore, studies on quantifying the relationship between the vegetation and water resources represent a critical step in developing advanced eco-hydrological approaches, supporting resource management and environmental change.

On the other hand, the study on hydrologic response to land use/cover changes is an important theme in eco-hydrology (BAHC, 1993; IGBP, 1994; Wang, 2007). As mentioned previously, human activities influence hydrologic processes and cycles to varying extents on different spatial and temporal scales. On local, regional and global scales, the most significant human impacts on the hydrologic system are caused by land-use change. Conversion of land to agriculture, mining, industrial, or residential uses significantly alters the hydrologic characteristics of the land surface and modifies pathways and rates of water flow. If this type of major shift in the hydrologic balance occurs over large or critical areas of a watershed or region, it can have significant short- and long-term impacts. The importance of investigating LUCC and its impacts as a baseline requirement for land use planning and sustainable management of natural resources has been highlighted by many researchers (Petit et al., 2001; Read et al., 2002). Some suggest that the consequences may outweigh those from climate change (Sala et al., 2000; Vorosmarty et al., 2000).

Identifying and quantifying the hydrological consequences of land-use change are not trivial exercises, and are complicated by: (1) the relatively short lengths of hydrological records; (2) the relatively high natural variability of most hydrological systems; (3) the difficulties in 'controlling' land-use changes in real catchments within which changes are occurring; (4) the relatively small number of controlled small-scale experimental studies that have been performed; and (5) the challenges involved in extrapolating or generalizing results from such studies to other systems (Defries & Eshleman, 2004). Given the diversity and complexity of land-use changes that are taking place about the globe, powerful techniques for analyzing the hydrological consequences of land use must be considered to be in an early stage of development.

Investigating the hydrologic impacts of land use/cover change involves two issues: land use/cover changes and the responses of hydrologic systems. Both of them are complicated problems involving interactions and feedbacks between atmospheric, hydrologic and biologic system. In order to better understand this problem, it has been customary to use hydrologic models, which are mathematical descriptions of the large-scale physical processes governing the integrated systems that all the terms of the water balance can be estimated, including actual ET, over an unlimited time frame. Several types of hydrologic models have been developed for simulating the large-scale physical processes governing the integrated systems. However, they are still limited in practice. On one hand, conceptual lumped models do not consider the spatial variability and have no direct links with vegetation. On the other hand, physically distributed models have limited applicability because of data availability and model complexity. Therefore, there is no universally accepted hydrologic model for hydrologic impacts of LUCC studies (Figure 1.3). The development of hydrologic models for reliably predicting the hydrological effects of future land-use changes is literally in its infancy (Beven, 2000).

Figure 1.3 illustrates research gaps of hydrologic impacts of LUCC using hydrologic model and ET as a link to bridge the gaps. First, a large amount of hydrologic model for assessment of the hydrologic impacts of land-use change is typically performed on an event-specific basis. However, it is important to estimate the long-term impacts of land-use change on water quantity that are dominantly controlled by the cumulative effects of smaller storm events rather than by rare high magnitude storm events (McClintock et al., 1995). Second, although some of the existing distributed hydrologic models are capable

of assessing long-term impacts, they are not often suitable for preliminary assessment because of their complexity and a lack of extensive input data. Initial assessment of hydrologic impacts of land-use change requires a simple model that can be run with readily available input data to provide preliminary estimates of the absolute and relative impacts of watershed development and to identify the need for more advanced modeling in some cases or areas (Bhaduri et al., 2008). Lastly, there are numerous conceptual lumped-parameter hydrologic models widely used in China (Zhao, 1984; Chen et al., 2006). Such models may produce reasonable results but they can not be expected to accurately represent the watershed conditions because of the distributed nature of hydrologic properties like soil type, slope and land-use, therefore, they are limited in assessing the effect of land use and other changes in basin hydrology.

One of the most promising hydrological modeling techniques for assessing regional effects of land use change is water balance modeling on a monthly basis. Since the objective of land use change impact studies is to project the average hydrological behavior of a watershed under different land use change scenarios, the use of monthly water balance models for studying the hydrological impact of potential land use change has several merits (Figure 1.3). First, hydrological modeling on a large spatial scale which is not data intensive and requires only averages of watershed characteristics as model input can be performed. Second, the structure of monthly water balance models is not so complicated and the physical basis is clear that make them applicable. Third, monthly water balance models are suitable for assessing hydrologic impacts of LUCC because land use changes are often studied on monthly basis. Fourth, water resources management and planning for a large basin or region is generally on monthly or longer time scales. However, most of water balance models applied in China, for example, the distributed monthly water balance model (DMWBM) developed by Chen et al. (2006) for the East River Basin, have no direct links with vegetation and have only one set of parameters for the whole basin (Chen et al., 2006; Wang, 2007), which makes them not capable of predicting hydrologic impacts of LUCC.

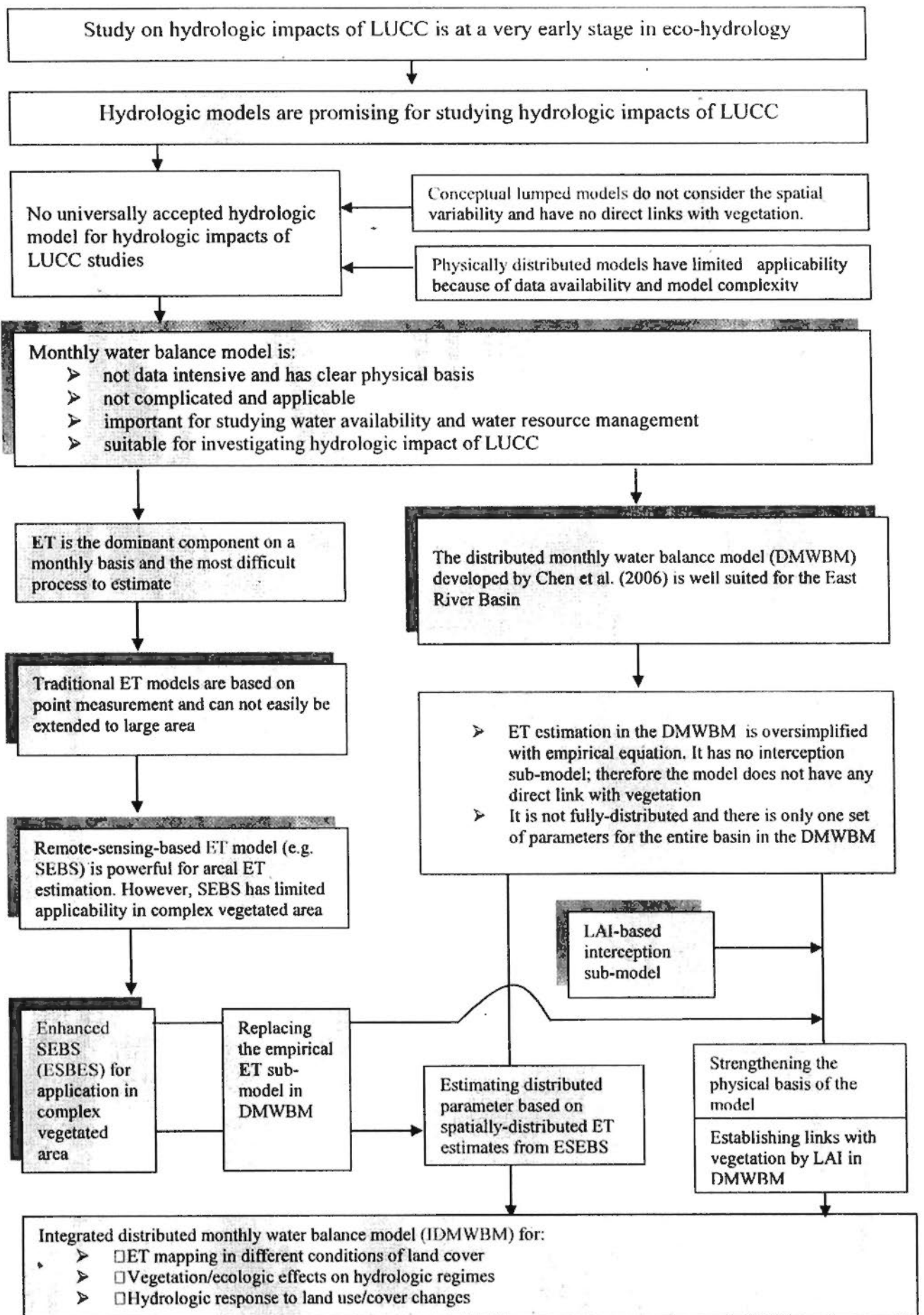


Figure 1.3 Research gaps of hydrologic impacts of LUCC and ET as a link to bridge the gaps

ET (evapotranspiration) is a major hydrologic component as well as an important ecological element (plant physiological processes) that can establish direct links between hydrologic processes and vegetation dynamics in monthly water balance models. On one hand, land use change has a direct effect on hydrology through its link with the ET regime (Dunn & Mackay, 1995). The dominant process for driving the water yield in response to land use/cover change is ET (Turner, 1991; Zhang et al., 2001). On the other hand, ET is one of the most important processes occurring at the land-surface and affecting the atmosphere and hence, climate. It plays the dual roles of providing water vapor to the atmosphere as well as absorbing incident radiation in the processes. ET has long been recognized as playing an essential role in determining exchanges of energy and mass between the hydrosphere, atmosphere, and biosphere (e.g. Bowen, 1926; Jia et al., 2003; Monteith, 1965; Penman, 1948; Priestley et al., 1972; Su, 2002). These roles make it a key process in the water budget and the energy budget as well as providing a strong link between them (Figure 1.4). Moreover, in distributed hydrological modeling accurate estimates of evapotranspiration are indispensable both for water balance studies and for assessment of hydrological impact of man-made changes such as land use changes. Therefore, mapping ET becomes a very important step in establishing links with vegetation in integrated eco-hydrologic modeling.

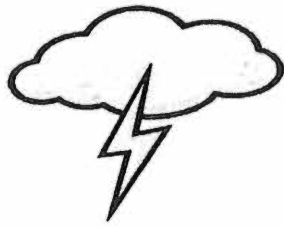
Conventional ET estimation techniques that employ point measurements to estimate the components of energy balance are only representative at local scales and can not be extended to large areas. Remote sensing is probably the only technique which can provide reliable measurements of several relevant physical parameters at scales from a point to the macro scale. One of the most famous ET models, the remote-sensing-based surface energy balance system (SEBS) developed by Su (2002) has been widely applied in estimating area ET in Northern China and Europe (Zhan, 2005; Lin, 2005; Su, 2002). However, it is only suited for homogeneous low-vegetation region and has some limitations in complex vegetated area (Zhan, 2005; Lin, 2004). Therefore, enhancement of SEBS should be made for application in complex vegetated area in south China.

Rainfall interception is also an important hydrological component that has a close link with vegetation. The amount of water intercepted by the canopy and the net precipitation reaching the ground surface depend on the type and density of vegetation (Getu, 1998; Yi, et al., 1996). Some experiments indicate that the percentage of rainfall intercepted by forest canopies to total annual rainfall varies from 11.4 to 34.3% (Wang & Xue, 1997). However, it has received little attention in most traditional monthly water

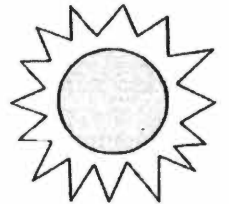
balance models (Yuan, 2006). Therefore, simulation of interception in monthly water balance model can strengthen the physical basis of model and establish a direct link between hydrologic processes and vegetation, which is important for studying hydrologic impact of LUCC.

In view of the problems and research gaps mentioned above, there is an urgent need for a suitable model that can be capable of accounting for spatial variations of vegetation and ET to predict hydrologic impacts of LUCC for a large scale on a monthly basis. An integrated eco-hydrologic modeling system of the enhanced SEBS and the distributed water balance model with aid of GIS/RS is a promising way to assess hydrologic impacts of land use change on a monthly scale.

Water and Energy Balance System



Precipitation



Shortwave Radiation

Transpiration

Reflected long wave radiation

Water Balance:
 $ET = P - R - \Delta S$
 P: Net precipitation
 R: Runoff
 ΔS : Storage

Energy Balance:
 $ET = R_n - H - G$
 R_n : Net radiation
 H: Sensible heat flux
 G: Soil heat flux

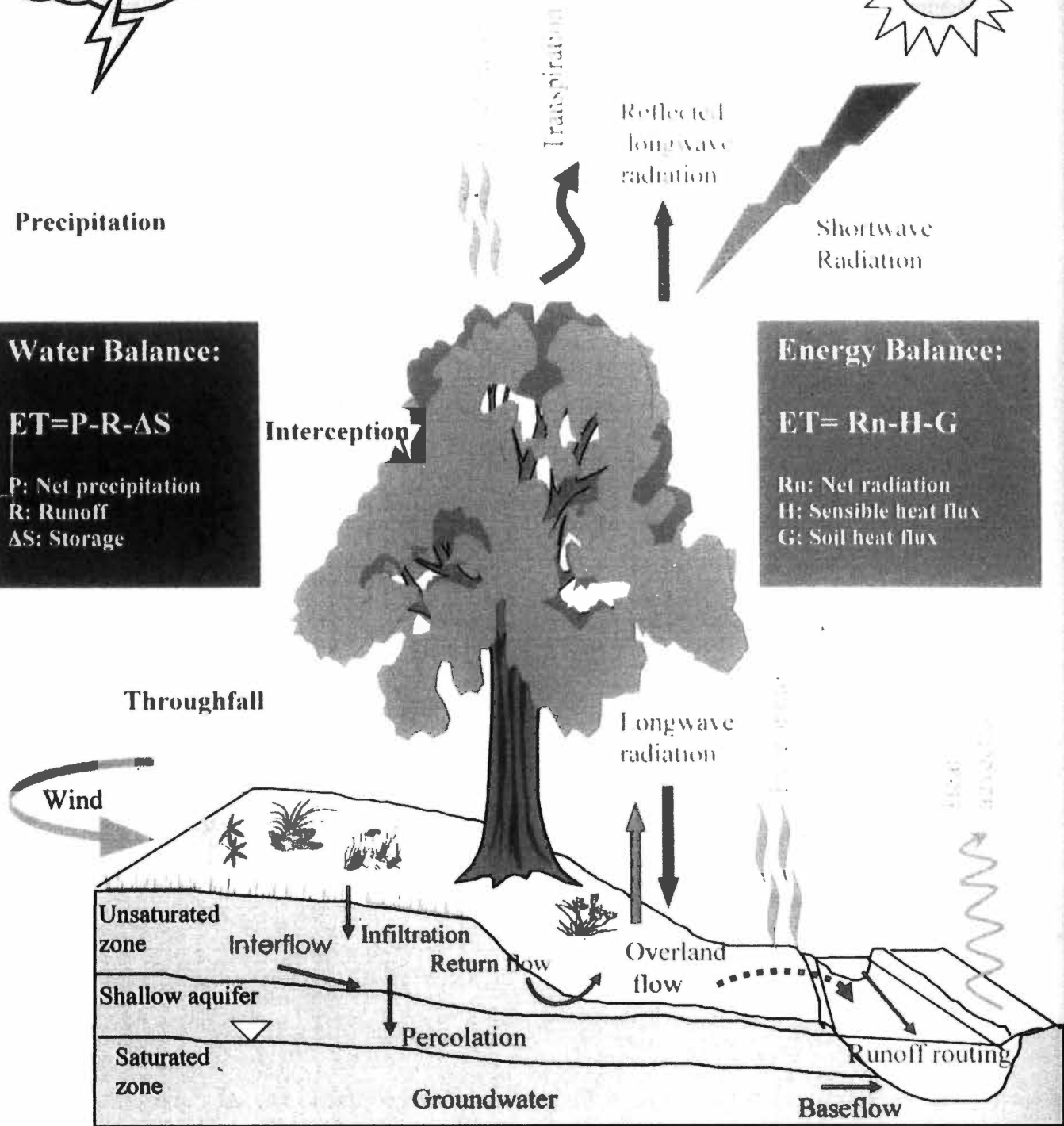


Figure 1.4 Illustration of ET as a link for water and energy balance system

1.2 Research objectives

Overall, this study aims to develop an integrated modeling system of enhanced surface energy balance system, LAI-based interception model and distributed monthly water balance model to conduct eco-hydrologic simulation for predicting hydrologic impacts of LUCC in the East River Basin with aid of GIS/RS. Specifically, this research aims:

- (1) To analyze and detect spatial-temporal changes of land use/cover with aid of GIS /RS;
- (2) To estimate areal ET for a large area using the physically-remote-sensing-based SEBS and enhance the SEBS for application in southern China under complicated vegetation conditions, validate the results of ESEBS by distributed monthly water balance model and complementary relationship ET models;
- (3) To integrate the ESEBS and LAI-based interception models into the distributed monthly water balance model with aid of GIS/RS, for strengthening the physical basis of the model, establishing direct links between hydrologic process and vegetation, estimating distributed parameters at sub-basin scale and modeling hydrologic impacts of LUCC;
- (4) To study vegetation effects on hydrologic regimes and investigate hydrologic responses to land use/cover changes by using the integrated model with the aid of GIS.

1.3 Research significance

Eco-hydrology, as a new discipline, seeks to deal with the delicate balance between water system and ecosystem, which plays a crucial role in satisfying the needs for integrated water resources management and sustainable development. The study on hydrologic impacts of land use/cover changes is an important theme in eco-hydrologic modeling. Furthermore, the importance of investigating LUCC and their impacts as a baseline requirement for land use planning and sustainable management of water resources has been highlighted by many researchers (Verburg et al., 1999; Petit et al., 2001; Read et al., 2002). Therefore, understanding hydrologic impacts of LUCC is of great importance for integrated water resources management, eco-environment protection and sustainable development of society.

The East River (Dongjiang) is located in Guangdong and Jiangxi provinces in South China. Since Hong Kong has very limited water resources by itself, inter-basin water

transfer from the East River Basin to Hong Kong has been a vital factor in the great economic success and prosperity of the territory in the past three decades. The proportion of the East River water in Hong Kong's annual water supply has steadily increased from only 8.3% in 1960 to about 70% or even slightly over 80% in recent years. However, the water resources of the East River Basin are already heavily committed, rapid economic development and population growth in the region have caused serious concerns over the adequacy of the quantity and quality of water withdrawn from the East River in the future.

Moreover, as a major growth engine of Guangdong economy, the East River Basin has experienced fast and continuous economic growth over the past three decades and intensive human activities such as land use/cover changes and urbanization have caused enormous influences on the environment which has been changing rapidly. The hydrologic changes in response to land use/cover changes may have increased the risk and vulnerability of natural and environmental hazards such as floods, landslide and degradation of ecosystems. Any significant change in the magnitude or timing of runoff, ET or soil moisture in the East River Basin induced by changes in ecologic variables (e.g. land use/cover) would thus have important implications for the great economic success and prosperity of the East River Basin and Hong Kong. Failure in accounting for these hydrologic impacts in water resources planning and management may lead to great economic losses and environmental damages.

Accordingly, a modeling study is practically needed on the potential impacts of future land use change on water availability in this basin. However, there is no universally accepted hydrologic model for hydrologic impacts of LUCC studies. Therefore, the contribution of this research is that it presents an integrated eco-hydrologic modeling system to quantify LUCC and their impacts on hydrological regimes. This can be achieved through a combined use of Distributed Monthly Water Balance Model, Surface Energy Balance System and GIS/RS to quantify LUCC, conduct physically-remote-sensing based ET mapping and simulate the hydrologic impacts of LUCC. Using the integrated model to simulate the hydrologic response to land use/cover changes and find out the possible driving forces carries not only important scientific merit, but also valuable practical significance for integrated water resources

management, eco-environment protection and sustainable development of the East River Basin.

1.4 Organization of the dissertation

The thesis is organized in seven chapters. Chapter 1 is an introduction chapter where the background, problem statement, objectives and significant of the study are discussed. Chapter 2 presents an extensive review of the literature on hydrological impact studies of LUCC, the use of hydrological modeling LUCC studies, land use/cover mapping and change detection with aid of remote sensing and ET estimation with the aid of remote sensing and GIS. Concepts of LUCC, methods, data acquisition, detection and quantification of LUCC and analysis made at watershed and sub-watershed levels are elaborated in Chapter 3.

Chapter 4 presents ET mapping with the aid of GIS/RS. In this chapter, first and foremost, the surface energy balance system (SEBS) is described. Moreover, the SEBS was enhanced for application in area with complicated vegetation conditions. Furthermore, in order to validate the simulation results, inter-comparison is made with complimentary ET model and distributed water balance model. Last but not least, the spatial-temporal analysis of ET is made. Chapter 5 focuses on the development and test of the newly integrated distributed monthly watershed model for predicting the hydrologic impacts of LUCC with the aid of GIS/RS. Simulations of hydrological responses to LUCC are elaborated in Chapter 6. In this chapter firstly impact of LUCC on the hydrological regimes in past and present are analyzed and then future land use scenarios are developed and examined. Summary and conclusions are presented in Chapter 7.

1.5 Research framework

The research framework is presented in Figure 1.5. Firstly a large number of data, e.g. meteorological data, vegetation data, soil data, DEM data, remote sensing data and field measurement data are collected and manipulated, which can lay a solid foundation for studying hydrologic impacts of LUCC. Secondly, LUCC analysis based on long-term trend analysis of vegetation dynamics and post-classification comparison is conducted

with the aid of GIS/RS, which provide valuable information for understanding LUCC and constructing scenarios for studying hydrologic impacts of LUCC.

The physically-remote-sensing-based SEBS is employed to estimate areal ET for a large area rather than traditional point measurement on a local scale. As the SEBS has limited applicability in complex vegetated area, an enhancement is made to improve SEBS for application in complex vegetated area by estimating LAI, aerodynamic roughness height and displacement height for different land cover in the East River Basin. The results of ESEBS are validated by inter-comparison with distributed monthly water balance model (DMWBM) and complimentary ET models.

The enhanced SEBS (ESEBS) is integrated into the distributed monthly water balance model (DMWBM) by replacing the empirical ET sub-model in the original DMWBM with aid of GIS/RS. In addition, a LAI-interception model (Yi et al., 1996) as new component is integrated into the DMWBM. Through the integration, the physical basis of DMWBM can be strengthened, a direct link between vegetation and hydrologic processes can be established in DMWBM and distributed parameters can be estimated at sub-basin scale. Consequently, the newly integrated distributed model can not only account for spatial variations in basin terrain, rainfall, soil moisture but also consider spatial and temporal variation of vegetation and ET in particular, which provides a powerful tool for modeling effects of land use changes on hydrologic regimes. Finally, based on the integrated modeling system of ESEBS, LAI-based interception model and DMWBM and scenario analysis, vegetation effects on hydrologic regimes and hydrologic responses to land use/cover changes are investigated.

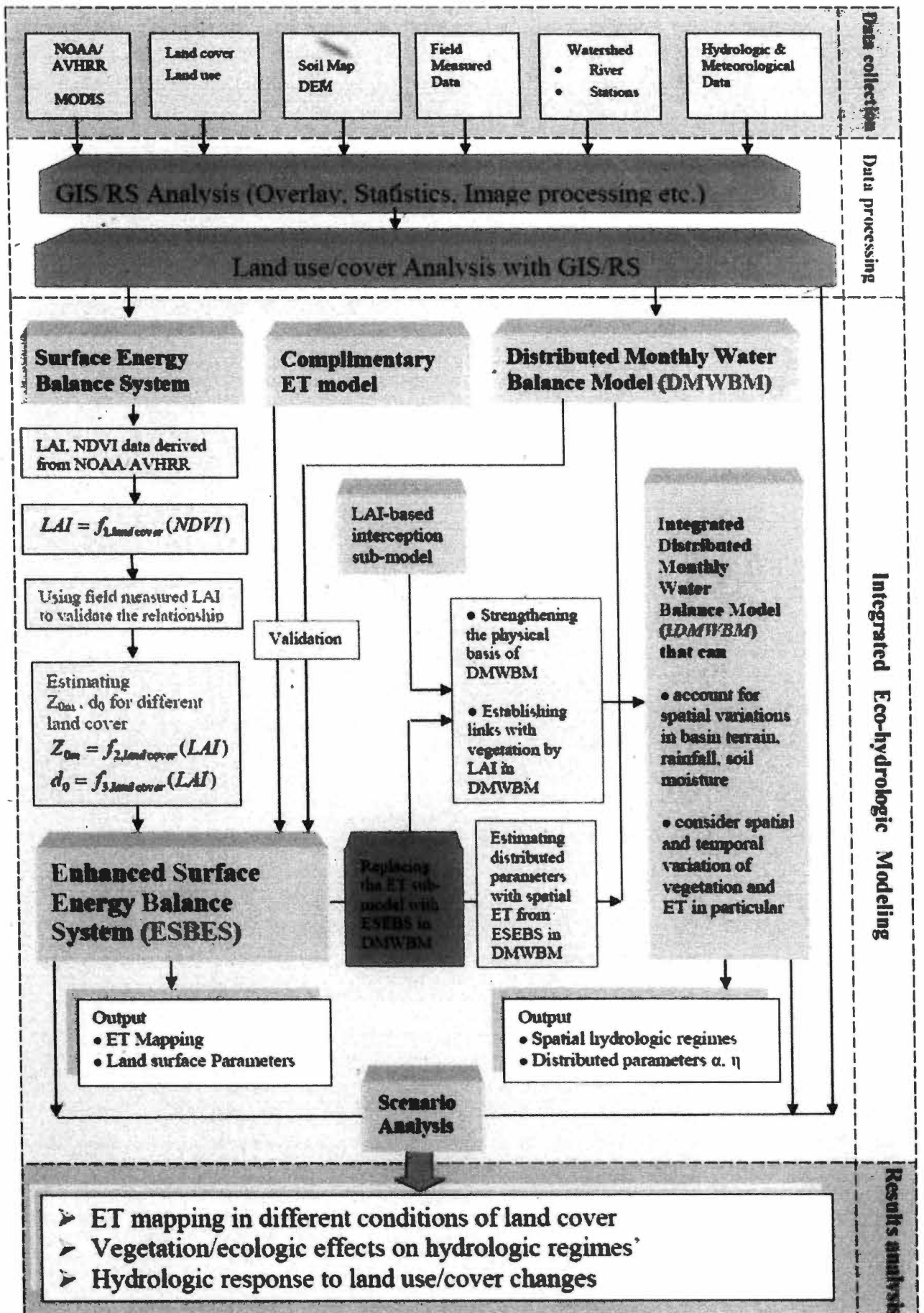


Figure 1.5 Research framework

1.6 Study Area

The East River Basin is located in Guangdong and Jiangxi provinces in the southern China. Originating in Xunwu county of Jiangxi province, the river flows from north-east to south-west and discharges into the Zhujiang estuary with an average gradient of 0.39 ‰. Three major metropolises, Guangzhou, Hong Kong and Shenzhen, are situated just outside of the lower part of the basin (Figure 1.4). Its mainstream length is 562 km, of which 435 km is in Guangdong province. The river drains an area of 35,340 km², about 90% of which is in Guangdong province. The geology of the catchment is complex. Precambrian, Silurian, and Quaternary geological formations are encountered at the surface with granites, sandstone, shale, limestone, and alluvium. The landscape is characterized by hills and plains, comprising 78.1% and 14.4% of the basin area, respectively. Forest covers the upper elevations and intensive cultivation dominates the hills and plains.

The East River Basin has a sub-tropical climate with a mean annual temperature of about 21°C and only occasional incidents of winter daily air temperature dropping below 0°C in the mountainous areas of the upper basin. The average annual rainfall for the period of 1980 ~ 2000 is 1,747 mm, and the average annual runoff is 935 mm, or roughly 54% of the annual rainfall. Precipitation is generated mainly in two forms: front-type and typhoon-type rainfalls. There are large seasonal changes in rainfall and runoff in the catchment: about 80% of annual rainfall and runoff occur in the wet season from April to September, and about 20% occurs during the dry period of October to March. Elevation in the catchment ranges from a few meters below the mean sea level at the basin outlet to the highest point at 1336 m. The basin topography is controlled by five parallel ridges extending from north-east to south-west. Because of the mountainous terrain and the large differences in elevation, the precipitation in the basin is spatially distributed. Generally more precipitation falls in the south-west part than in the north-east part and more in mountainous areas than in lower elevations.

CHAPTER 2

LITERATURE REVIEW

2.1 Eco-hydrology: definition and recent development

Eco-hydrology has sprung up since 1990s, the 20th Century. In the face of water resources declining on a global scale, the international scientific community has emphasized the need for new solutions. According to the World Science Report (UNESCO, 1998), the safeguarding of the sustainability of water resources in the face of increasing deterioration of the global environment has been defined implicitly as one of the priority goals for science. The gravity of the problem was already appreciated and so it was the urgent need for new solutions that was emphasized at the International Conferences on Water and the Environment held in Dublin (1992) and Paris (1998). Eco-hydrology, as an independent discipline, was put forward in this context. Eco-hydrology is in close tie with various programmes such as the World Climate Research Programme (WCRP), the Intergovernmental Panel on Climate Change (IPCC), the Global Environmental Monitoring System (GEMS), particularly with the implementation of Biospheric Aspects of the Hydrological Cycle (BAHC) and the International Geosphere-Biosphere Programme (IGBP), eco-hydrology has received a great deal of attention and become a hot topic.

Although eco-hydrology has been called “the next big thing in hydrology” recently (Nuttle, 2002), there has been no ubiquitously and unanimously accepted definition of the term Eco-hydrology (hydro-ecology). Baird & Wilby (1999) thought that eco-hydrology is the study of plant-water interactions and the hydrological processes related to plant growth. Rodriguez-Iturbe et al. (2001) defined eco-hydrology as a discipline seeks to describe the hydrological mechanisms that underlie ecological pattern and processes. Nettle (2002) considered eco-hydrology as the sub-discipline shared by ecological and hydrological sciences that is concerned with the effects of hydrological processes on the distribution, structure and function of ecosystems, and on the effect of biological processes on the elements of the water cycle. This combines Rodriguez-Iturbe’s (2000) definition with his subsequent observation that “the connection between the role of plants in the water balance” is central to ecohydrology (Rodriguez-Iturbe et al., 2001). Dolman et al. (2003) had an idea that eco-hydrology seeks to understand the interaction between the hydrological cycle and terrestrial ecosystems. Xia et al. (2003)

and Huang et al. (2003) presented that definition and study scope of eco-hydrology depends on scale. For small scale, it focuses on soil moisture dynamic and the mechanism of vegetation impacts through plant water stress; for meso-scale or large scale, the core of eco-hydrology is to study the vegetation effects on hydrologic processes, in other words, the hydrologic impacts of land use/cover changes (Wang, 2007).

In short, eco-hydrology is remarkably poorly defined and has different definitions and focuses at different scales (Xia et al., 2003). Eco-hydrology as new discipline is still very much at an early stage. The area of interest of eco-hydrology is so vast and manifold, which is beyond the scope of this dissertation. This research focuses on one of the most important theme in eco-hydrology-the hydrologic response to land use/cover change.

2.2 Effects of land use/cover change on watershed hydrology

As mentioned previously, the study on hydrologic response to land use/cover changes is an important topic in eco-hydrology. The importance of investigating LUCC and their impacts on hydrologic cycle has been highlighted by many researchers (Petit et al., 2001; Read et al., 2002). Land use/cover change has a direct effect on hydrologic processes through its link with the evapotranspiration regime on one hand and on the other hand the degree and type of ground cover has an enormous impact on the initiation of surface runoff (Fohrer, 2001). Specifically, the natural circulation of water in the soil-vegetation-atmosphere continuum is an important process and it is central to the energy, carbon, and solute balances of the system. There are many pathways that water may take in its continuous cycle of falling as rainfall and returning to the atmosphere as evapotranspiration. It may be intercepted by vegetation and evaporated directly to the atmosphere. It may infiltrate into the soil to be evaporated from the soil surface or be transpired by vegetation. It may become surface runoff and it may percolate through the soil to groundwater as recharge. Vegetation plays an important role in the hydrological cycle through the exchange of energy, water, carbon, and other substances (Zhang et al., 2001). The key hydrological processes and the impact of vegetation on hydrologic cycle will be reviewed in what follows.

2.2.1 The vegetation effects on canopy interception

Interception, or canopy interception, refers to precipitation that does not reach the soil, but is instead intercepted by the leaves and branches of plants. It occurs in the canopy, and in the forest ground litter. Because of evaporation, interception of liquid water leads to loss of that precipitation for the drainage basin. Their needles give them more surface area for droplets to adhere to, and they have foliage in spring and fall, therefore interception also depends on the type of vegetation in a wooded area.

Rainfall interception by vegetation is an important hydrological process, especially in forested catchments. The intercepted water may be retained on leaves, flow down the plant stems to become streamflow, or drop off the leaves to become part of the throughfall, or be evaporated from wet canopy surface during the period of storm (Zhang et al., 1999). Some experiments indicate that the percentage of rainfall intercepted by forest canopies to total annual rainfall varies from 11.4 to 34.3% (Wang & Xue, 1997), and the kinetic energy of raindrops will decrease significantly after passing through the forest canopy. Dickinson (1984) found that canopy interception is appropriately 0.2 times of leaf area index, therefore the change from sparse-canopy vegetation to densely-canopy vegetation might cause a decrease in canopy interception. In addition, forest litter also has a great influence on overland runoff. By absorbing rainfall, forest litter can decrease overland runoff and increase soil water storage. The amount of water absorbed by forest litter may reach 40%–260% of the weight of forest litter itself. Both litter and favorable forest structure may improve water infiltration and storage, which reduce overland runoff volume and lag the runoff peak. Soil water infiltration rate in forests was two to three times more than that in grassland. Meanwhile soil water-holding capacity in forest land was higher than that in shrub land, grassland and bare land. When moss-fire forest was converted to shrub forest, soil water-holding capacity at 0–80 and 0–20 cm in depth decreased by 42.13 and 66.1%, respectively (Zhou et al., 2001).

For annual flow afforestation for example can cause an increased interception during the wet periods of the year and increased transpiration during dry periods through augmented water availability to deep root systems of trees. For the seasonal flow this can lead to a rise of soil moisture deficits and a reduction of dry season flow. The higher interception of forest reduces floods by removing a proportion of the storm rainfall and

by allowing a build-up of soil moisture storage (Fohrer, 2001). This effect is in general small but greatest for small storm events. High infiltration rates under forest and an effective soil cover reduce surface runoff and erosion (Garbrecht & Martz, 1998).

Interception processes affect redistribution of rainfall in the system and there is large variation in interception loss among different vegetation types. It is evident that the proportion of rainfall intercepted by vegetation varies considerably between species. According to Zhang et al. (2001), on average, pine forests intercept 28 % of rainfall compared to 14 % for eucalyptus forests. Short grass and crops intercept 20 to 48 % of rainfall during the growing season. However, on an annual basis the percentage is much smaller compared to forests. The absolute interception values may not be accurate and may vary from year to year depending on the nature of rainfall. However, these values are useful for catchment scale water balance modeling.

In conclusion, rainfall interception is affected by a number of factors such as canopy characteristics and rainfall regime. Detailed studies of interception processes require accurate and frequent measurements. In practice, such data are not always available. However, for most catchments water balance modeling the interception process can be approximated using a simple equation related to LAI (Getu, 1998; Yi, et al., 1996).

2.2.2 Vegetation effect on ET

The total evaporation from a given land use is influenced by aerodynamic resistance to transportation of vapor between the evaporating surface and the atmosphere. The balance between the atmospheric and radiation demand leads to the occurrence of water at the evaporating surface (Chen & Hu, 2004; Sullivan et al., 2004). Concretely, depending on the rate of abstraction the extent of the free water surface in the lake and the swamps will be reduced. Also altered will be the availability of soil water to the plants in the case of the deep rooted oil plants that will replace short rooted grass and decreases in the availability of water during the dry season (Mo et al., 2004; Nachabe et al., 2005; Suleiman & Ritchie, 2003).

Total leaf area per unit ground area known as the leaf index will be increased when the proposed crops replace the grassland. There will be increased availability of evaporating water through transpiration (James et al., 2003; Li & Wang, 2003). These changes in the

availability of water at the evaporating surface will cause changes in the evaporation rate leading to a change in the near surface atmospheric conditions, and considering the extent of the land use, this will lead to a basin scale climatic change (Schneide et al., 2004; Tomo'omi et al., 2005). At the same time, replacing the grasses with the taller vegetation will increase the aerodynamic roughness and lower aerodynamic transport resistance. The overall effect of altering the surface fluxes of heat and water vapor is an increase in the total evaporation thus altering the mass balance of lake and swamp water shade (Shao, 2005).

Therefore, ET, as the second or third largest term in the water balance equation and it is closely linked with vegetation characteristics. Dunn & Mackay (1995) conducted some experiments in Tyne small basin and found that the same land use change may have a significant effect on the hydrology of the lowland sub-catchment, but an insignificant effect on the hydrology of the upland sub-catchment. Zhang & Dawes (1999) pointed out that catchment evapotranspiration is a complex process and it is affected by rainfall interception, net radiation, advection, turbulent transport, canopy resistance, leaf area, and plant available water capacity. Under dry conditions, the principal controls on evapotranspiration are plant available water capacity and canopy resistance, and actual evapotranspiration is only a small fraction of the potential evapotranspiration. Under wet conditions, the dominant controls are advection, net radiation, leaf area, and turbulent transport. Under intermediate conditions, the relative importance of these factors is likely to vary depending on climate, soil, and vegetation. The challenge in modeling catchment scale evapotranspiration is to be able to represent these processes and factors in a simple fashion allowing practical prediction of the effect of vegetation changes on evapotranspiration.

In conclusion, regional evapotranspiration is a complex process and it is affected by rainfall interception, net radiation, advection, turbulent transport, canopy resistance, leaf area, and plant available water capacity. There is no universe consensus on the relationship between ET and land cover/use. More efforts have to be made to quantify the relationship.

2.2.3 Effects of land use/cover change on runoff

How much water percolates or forms surface runoff depends on the soil type and the land cover type. Soil type in a watershed can be considered as a constant since soil can change only in a geological perspective of time, which is far beyond the study period presented here. However, land cover can change very quickly, from year to year, even from day to day. Thus, the only process that can affect percolation rates in the study period is the land cover change. Land cover, especially forests, is one of the most influencing factors in the runoff behavior (Axayacatl, 2007).

2.2.3.1 Effects of forest change on runoff

Many researchers focused on the relationship between forest changes and runoff (Lørup et al., 1998; Zhao et al., 2001). It is generally accepted that forests can retard overland runoff, reduce and delay flood peaks effectively, and play a major role in many components of the water cycle. Meantime, there were many debates on the effects of forest changes on annual runoff, which may originate from the spatial and temporal differences of the study area in question. To date, there is no consensus that whether forest can increase or decrease annual runoff.

Some authors believed that forestation could reduce runoff and deforestation could increase runoff. The impact of forest cover on stream flow has been studied in sub-Mediterranean mountain watersheds by a modeling approach and the results suggested that with respect to the unexploited site, felling in a forest site subject to gradual clearance induced a significant increase in high flow rate and may increase runoff by 10% (Cognard-Plancq et al., 2001).

Hibbert (1967) reviewed results from 39 such experiments. Bosch & Hewlett (1982) updated Hibbert's review to include an additional 55 catchments. Results from these experiments show a large variation in catchment responses to changes in vegetation cover. However, a clear conclusion was that reduction of forest cover increases water yield.

Stadimir et al. (1998) conducted a fifteen-year study and compare runoff in three small forested watersheds in Serbia, found that forest cover has a considerable effect on the runoff regime of the watersheds. Forest cover is 70% in the most forested watershed,

while it is 49% and 40% in the other two watersheds. With all other conditions such as rainfall, topography, and soil type being equal or similar, the most forested watershed has a balanced runoff regime or a constant runoff through the year. However, the other two watersheds have large intervals of drought and the runoff was mainly in form of flood waves. Thus, forest cover increases percolation of water into the soil, which minimizes surface runoff and transforms potential surface runoff into groundwater preventing floods. This underground water travels slowly to springs and major streams which prevents the streams from being dry during the dry season of the year.

Nevertheless, some authors assert that forest coverage would cause an increase in runoff. For example, Lørup et al. (1998) identified and assessed long-term impacts of land use change on catchment runoff in semi-arid Zimbabwe, based on analyses of long hydrological time series (25–50 years) from six medium-sized (200–1000 km²) non-experimental rural catchments and the results indicated a decrease in the annual runoff for most of the six catchments. Zhao et al. (2001) summarized runoff and sediment yield and hydrological effect in forest watersheds and pointed out that increase of forest could cause increase in runoff.

In addition, some authors point out that forest vegetation basically has little impact on runoff. For example, Cosandey et al. (2005) chose three valleys, Draix, Loze`re and Collobrier, located in southern France, as study areas and analyzed the effects of forest felling and fire disturbance on hydrology. The results demonstrate that disturbance of forests did not necessarily imply an increase in runoff and the differences between bare soil and vegetation-covered soil could better explain the hydrological behavior.

2.2.3.2 Effects of land use structure on runoff

The structure of land use is being altered significantly by intensive human activities with the social-economic development and industrialization. The proportion change of different land use types may have a great effect on annual runoff.

Williamson et al. (1987) conducted a study comparing five small watersheds in southwest Australia. Paired watershed approach, i.e., comparing watershed with similar rainfall conditions, is used for this research. Three watersheds were converted from forest to agriculture. Complete clearing was applied to two watersheds and partial

clearing was applied to another one. The rest of the watersheds in the study, two, remain unaltered. Streamflow increased four times and surface runoff increased four times to 16% of the annual streamflow in the transformed watersheds immediately after clearing for agriculture.

Li et al. (2007) conducted numerical simulation of idealized deforestation and overgrazing for Niger and Lake Chad in West Africa. This study shows that tropical forests have a disproportionately large impact on the water balance in the watershed since they are highly localized in regions with the highest rainfall. Total deforestation increases the runoff ratio from 0.15 to 0.44 and the annual stream flow by 35% although forests only cover 5% of the watershed. Complete removal of grassland and savanna, which occupy much greater areas of the watershed, results in an increase of simulated annual streamflow of 33%.

Owe (1985) conducted a 51-year study in Chester Creek Basin in southeastern Pennsylvania. Relationships between streamflow and historical trends of five land cover types including forest, urban, residential, cultivated crop land, and open grass were analyzed. During the study period urban and residential areas increased, while crop lands decreased. Forest areas increased and open grass areas decreased. The final effect of these processes on the watershed is an increase in surface runoff. Annual streamflow increased 51 %, which is the direct result of changes in the land cover type in the basin.

Andrea adapted three models (ProLand model, ELLA model and SWAT model) to examine the effects of land use change on eco-hydrological effects in the Aar watershed in central Germany. The result indicates that the percentage of forested areas declined significantly, the area of grassland increased from 20 to 41%, and stream flow and surface runoff increased due to these changes in land use (Andrea et al., 2001).

Urbanization could increase, to some extent, the areas of impermeable underlying surface, which may diminish concentration time of runoff and induce an increase in overland runoff coefficients. Campana & Tucci (2001) applied a hydrological model IPHIV together with GIS to predict the hydrological graph corresponding to alternative urbanization scenarios in Diluvio Creek, located in Porto Alegre, Brazil. The simulation results suggests that when 50% of the free space is turned into an impermeable

underlying surface in the city, urbanization increases the peak flow by 20–50% compared with the urban conditions of the Diluvio basin in 1979. In Taihu Basin, China, cultivated land decreased by 3,385 km² and construction area increased by 2,460 km² during 1986–1996, and runoff in 1996 was increased by 10.18×10⁸ m³ compared with in 1986 under the same rainfall conditions (Gao & Wen, 2002).

Research that relates changes in land cover with changes in mean annual river discharge for small watersheds (< 1 km²) are very common, but assessment on effects of changes in large river basins (> 100 km²) usually have not found similar relationships. Costa et al. (2003) conduct an analysis to find any relationship between the land cover of Tocantins River watershed and the water flow in the river. Researchers use a 50-year, from year 1949 to 1998, riverflow dataset to conduct the analysis. Tocantins River is located within a 175,360 km² watershed in Brazil. At the beginning of the study period, 30% of the watershed was used for agriculture; and at the end of the study period, 49 % percent of the watershed was used for agriculture. While precipitation was not statistically different during the study period, annual mean river flow was 24 % greater and the rain season river flow was 28% greater at the end of study period compared to the data collected at the beginning of the study period. Changes in vegetation cover in this watershed altered its hydrological response (Axayacatl, 2007).

From the review above, it can be concluded that there is no universe consensus on effects of land use/cover change on runoff, particularly annual runoff. Moreover, much of our present understanding of land-use effects on hydrology is derived from controlled, experimental manipulations of the land surface, coupled with pre- and post-manipulation observations of hydrological processes, commonly precipitation inputs and stream discharge outputs. Most notable are studies of the effects of forest management practices (including cutting, removal activities, and re-growth of forest vegetation) on annual and seasonal water yields, evapotranspirative losses, interception rates, and flood peaks that have been conducted in forests throughout the world,

A major limitation of such paired watershed studies is the obvious lack of experimental replication across a full range of natural conditions. Therefore, what expect is that experimental approaches combining hydrometric measurements from paired watersheds with process modeling will serve to unravel rapidly the response to land-use change of

watersheds of varying size, topography, and spatial configuration and contribute to a progressive 'whitening' of the watershed 'black box'. What follows will review hydrologic modeling approach for studying hydrologic impacts of LUCC.

2.3 Modeling hydrologic impacts of land use change

The methods for assessing hydrologic impacts of LUCC can be generally be grouped into 3 categories: the first involves the "paired catchment experimental techniques". This method is based on two similar catchments which are studied for a calibration period; then one catchment is subject to a change (i.e. clearing), and the other remains unchanged (i.e the 'control'). Paired catchment studies try to minimize differences between control catchments and treated catchments in terms of rainfall, soil, topography, and other factors that may influence catchment water balance. A major limitation of paired watershed studies is the obvious lack of experimental replication across a full range of natural conditions (Defries & Eshleman, 2004).

The second level is statistic method. Double mass curves and flow duration curve are two of the most frequently used methods for assessing land use impacts on hydrology by analyzing runoff in a statistical way. The major disadvantage of statistics methods is that they don't have a strong physical basis. Furthermore, these models need a long series of observation data (more than 50 years). Moreover; statistic method can not distinguish the effects from land use and climate change. Last but not least, it can not be used to know more details at a sub-basin scale in a distributed way.

The third level comes from hydrologic modeling. These studies are not specifically designed to examine the effects of vegetation on water yield, but the fact that they represent catchments with diverse climate, vegetation, and soil can provide useful information about the role of vegetation in catchment water balance. Therefore, it has become the most widely used method for hydrologic impacts of assessing land use change in modern hydrology.

Hydrologic modeling approaches are various and hydrologists over the years have developed a plethora of surface hydrology models, spanning a wide range of complexity, which are able to reproduce observations well. Hydrological models are developed for different reasons and therefore have different forms. The different forms reflect a wide range of modeling purposes, spatial and temporal scales that influence the

conceptualization and parameterization of hydrological processes. Beven (2001) mentioned his attempt to draw an exhaustive list of rainfall runoff models nearly 25 years ago and his abandoning of the task when he reached 100 models. Given the broad range of hydrological models thus far developed, there are many ways of classifying hydrological models using different criteria (Dooge, 1992; Singh, 1995). Therefore, a clear classification system is very difficult if not impossible, but the most commonly used system classifies the models as metric, conceptual and physically-based. In the following section, the modeling approaches, hydrological process and application studies of these models has been briefly reviewed.

2.3.1 Empirical Models

According to Wheater et al. (1993) 'The essential characteristic of empirical models is that they are based primarily on observations and seek to characterize system response from those data.'

As the definition suggests, empirical models treat the catchment as a single unit and relate its output (the flow $Q(t)$) to its input (the rainfall $P(t)$) where t is the time, through an operator Φ (Figure 2.1). Φ is called a transfer function.

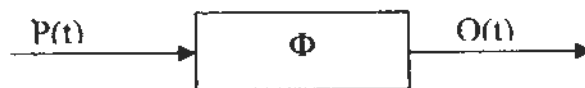


Figure 2.1 Empirical model

This approach was developed primarily in the early days of hydrological modeling and can be traced to the development of unit hydrograph theory for catchment scale storm flow simulation (Sherman, 1932). The unit hydrograph concept considers only event response. The unit hydrograph $h(t)$ is the stormflow response at time t to a unit input of effective rainfall $u(t)$. Effective rainfall is that part of the rainfall that eventually becomes stormflow, which is rainfall minus losses (evapotranspirative and aquifer). Stormflow is modeled explicitly as a linear, time invariant function of effective rainfall, i.e. its convolution with the unit hydrograph.

$$x^{(q)} = \int_0^t h(t-s)u(s)ds \quad (2-1)$$

The unit hydrograph concept has been extended to include modeling of baseflow and hence allow simulation between events when stormflow has waned. One such model is the CLS model of Natale & Todini (1977).

In empirical models, one considers the fact that a great amount of information is held in measured data that the model can extract to conduct predictions. It is therefore a mainly empirical approach and is also called the black box approach. Because it is based on data, the techniques employed do not all originate from the hydrological sciences but also from other domains of science. Metric models usually treat the catchment as a single element, therefore they are lumped.

Empirical models can be very successful at mimicking the observations, but they do not necessarily have a physical basis (e.g. neural networks). This characteristic of metric models can be a major limitation for their application in assessing hydrologic impacts of land use/cover changes. Therefore, they are not well suited for eco-hydrologic modeling.

2.3.2 Conceptual hydrologic models

Conceptual hydrologic models can be described as all the other models that can not be classified as metric or physically-based. They represent the important processes in a simplified conceptualization – often by the means of reservoirs or buckets. They are formulated by a number of conceptual elements, each of which is a simplified representation of one process element of the system being modeled.

Conceptual hydrologic models were introduced in hydrology to improve the black box, system theoretical approach which depends mainly on some general, yet flexible relationships between input and output data without much physics within the system. Conceptual models are generally designed to account for the soil moisture phase of the hydrologic cycle at basin scale. The primary approach is to transform rainfall to stream flow through a number of interconnected mathematical functions, each representing a certain component of the hydrologic cycle (Crawford & Linsley, 1966). Examples of conceptual models include the following: STANFORD IV (Crawford & Linsley, 1966), TANK (Sugawara et al., 1983), SFB (Boughton, 1984), HBV (Bergstrom, 1995).

There are also few applications of conceptual hydrologic model for modeling relationship of hydrologic regimes. Zhang et al. (2001) find that a close relation between long-term evapotranspiration and precipitation for a given forest acreage existed. He proposes a simple two-parameter model (Rational Function Approach) to estimate actual annual evapotranspiration by precipitation, potential evapotranspiration and the water capacity coefficient of plant-available w , where different vegetation types have different w values. However, this application is limited before of ignoring spatial heterogeneity and empirical parameters.

In summary, conceptual hydrologic models have generally been a very useful and successful approach in simulating runoff from catchments in different parts of the world for the last three decades (WMO, 1975, 1992). However, conceptual models ignore the spatial variability of hydrological and meteorological variables, so conceptual models are suitable for the prediction of spatially averaged catchment response but limited in assessing the effect of land use and other changes in basin hydrology (e.g. Gan & Biftu, 1996). Their applicability is limited to areas where runoff has been measured for some years and to places where no significant changes in catchment conditions have occurred over the period of simulation since model parameters that are calibrated, not measured, are assumed to remain constant (Getu, 1998).

2.3.3 Physically-based models

According to Wheater et al. (1993), physically-based models represent the component hydrological processes 'in a more classical mathematical-physics form, based on continuum mechanics, through numerical solution of the relevant equations of motion using a finite difference or finite element spatial discretization. Beven (2001) argued that it is not currently possible to build this true representation and that empiricism has to be introduced. He mentioned these models as almost deductive.

They are developed following the bottom-up approach (Sivapalan, 2003) and are based on a priori perception of the importance of the various physical processes and how they interact. Also, they are spatially distributed since the equations from which they formed generally involve one or more space coordinates.

Physically based distributed model can in principle be applied to almost any kind of hydrological problem. Obviously, there are many problems for which the necessary

solutions can be obtained using cheaper and less sophisticated empirical, lumped conceptual or statistical models. However, for the more complicated problems there may be little alternative, but to use a physically-based distributed model.

The parameters of a physically-based, distributed model have a direct physical interpretation, which means that they can be evaluated for the new state of the catchment before the change actually occurs. This enables the effects of changes to be examined in advance of such changes. In addition, the characteristically localized nature of catchment changes can easily be accounted for within the spatially distributed model structure.

Examples of physically-based models include the Institute of Hydrology Distributed Model (IHDM) (Beven et al., 1987), the Système Hydrologique Européen (SHE) (Abbott et al., 1986a, b), WSHS (Al-Soufi, 1987) and TOPOG (Dawes & Short, 1994). Typically, these models use the Richards equation for subsurface flows and a kinematic wave equation for surface flow. In theory, the parameters of these models have explicit physical meanings and can be measured a priori (Evans, 2000). In practice, however, one problem with physically-based distributed models was that the detailed information required as input was rarely available making calibration difficult. Therefore, they tend to function as lumped conceptual models due to lack of data and limitations in computer processing time. While the latter problem will decrease in the future no clear solution on the data problem seems evident. Although the present study on use of remotely sensed data is a step in this direction there are still many processes, e.g. in the unsaturated and saturated zone, that can not be parameterized in a physically-based way by the presently or near-future available data sources.

There are a plethora of successful application examples of using physically distributed hydrologic model for assessing hydrologic impacts on LUCC all around the world. The Soil Conservation Service (SCS) curve number method, developed by the Soil Conservation Service of United States Department of Agriculture (USDA), has been widely used for runoff simulations. The popularity of the method is due to its simplicity, not its accuracy (Thompson, 1999). One of the key issues of the SCS curve is to determine the appropriate CN (Curve Number), which is a function of soil type, land use and cover type, cultivation practice and antecedent soil moisture.

Other examples include the MIKE SHE Model (Andersen, 2002), which establishes the relationship between losses(interception, evapotranspiration)and features such as leaf area index (LAI), vegetation root system and soil moisture content can describe the effects of LUCC on the hydrologic process. In a case study on the Qinhuai River Basin, Wang & Lu (2003) divided land use into four types: surface water body, paddy field, dry land and impervious surface. They then established corresponding runoff generation patterns separately for the four land-use types and analyzed the influence of LUCC on the water resource system, especially water balance and flood controls. In addition, in the Bagrov formula (Terpstra & Mazijk, 2001), the actual evapotranspiration was also calculated from the most important influence parameters of precipitation and potential evapotranspiration with a parameter N called the efficiency parameter, reflecting the storage properties of the evaporative zone and being related to land use and soil type.

There have been many related studies, which heavily relied on remote sensing information (Wu et al., 2004; Zhao et al., 2004). Most of the studies were conducted in regard to evapotranspiration. However, the SCS method calculated runoff directly while considering evapotranspiration indirectly. Meanwhile, to describe the characteristics of land use and cover using a parameter set, two kinds of methods can be adopted: one is with dispersed functions, i.e. one-to-one correspondence, such as the CN values in the SCS Model and the efficiency parameter N in the Bagrov formula; the other is through continuous functions, like LAI in the MIKE SHE Model. The literature reveals conflicting impacts of LUCC on runoff. For example, in some studies, deforestation produced more stream flow and higher flow peaks, while in others the opposite occurred (Beven, 2001). This means uncertainties exist in predicting hydrologic responses with LUCC. In fact, many simulations have been conducted only paying close attention to changes in vegetation or land surface and neglecting any accompanying changes (Chen et al., 2004). Some examples include forest land being converted to meadow that could change the soil structure, and construction of water conservation projects that could not only change the state of land use but also reallocate water resources in time and space, thus altering the natural process of water cycle.

Techniques for the analysis of effects due to land use and cover change on modeled hydrologic responses are still very much at an early stage. The prediction of effects

from future changes (and validation of these predictions) has hardly even started (Beven, 2001).

Although physically-based hydrologic model struggle with data availability and model complexity, they still can provide valuable understanding of the physical processes at the scale where the required input can be adequately defined. Moreover, all these practical applications have proven that physically distributed hydrologic model are well suited for evaluating the effects of land-use change within a watershed.

2.3.4 Lumped vs Distributed

On the basis of the spatial representation, the hydrological models can be classified into three main categories: lumped models, semi-distributed models, distributed models. Lumped generally refers to a model which deals with the catchment in its entirety, while distributed refers to a model which subdivides the catchment into smaller spatial units often using a grid system. Whole catchment models are referred to as lumped since they take all the sub-catchment variability and 'lump' that into a set of effective parameters for the entire catchment. Distributed models on the other hand, have a set of effective parameters for each cell or spatial unit (Evans, 2000).

This distinction is somewhat artificial when you consider that within each cell of a distributed model the parameters are effectively lumped parameters for that cell. Also a lumped model may be applied to several neighboring catchments or sub-catchments and hence give a distribution of parameter values for the basin.

According to Singh (1995), distributed models take explicit account of spatial variability of process, input boundary conditions, and/or system (catchment) characteristics. However, in practice, a lack of data prevents such a general formulation of distributed models. He further noted that in a majority of cases, the catchment characteristics are lumped, many of the processes are lumped, the input is lumped, and even some of the boundary conditions are lumped, but some of the processes that are directly linked to the output are fully distributed; rather they are quasi-distributed/semi-distributed at best. Semi-distributed models recognize that in a catchment area can have similar hydrological behavior and react in the same way. The aim is thus to define these areas and to group them together to simplify the computation.

Therefore, a semi-distributed hydrologic model can account for spatial variation and avoid the problems of data availability and model complexity (overparameterization and uncertainty), which seems to be well suited for investigating hydrologic impacts of LUCC at a basin scale.

In summary, over the last several decades, hydrological model has evolved from 'black box' models, through conceptual models, to physically-based models, and have been applied at different spatial scales from a few square kilometers to ten of thousands of square kilometers, for research purposes and operational purposes. Under most circumstances there are several alternative hydrologic models that can be used. However, there have yet been no objective criteria for making the best choice between alternative models. The selection of a model depends to a larger extent on the objective of the modeling and the availability of the necessary model input data. Generally, empirical models are applied to large-scale basin and regional analyses at time scales of months to seasons to years, while conceptual lumped are needed for detailed estimation of runoff in small basins at daily or shorter time scales and physically distributed hydrologic models are used for simulation of spatial patterns of hydrologic response within a watershed (Jiang, 2005).

2.4 Remote sensing in eco-hydrologic modeling

Hydrology is a science built on observation and measurement. Looking at the historical development of hydrologic modeling one comes easily to the conclusion that all hydrologic models are data limited. Models are generally not built the way which would be scientifically most sound, but rather according to data availability (Schultz, 2000).

Remote sensing (RS) has held a great deal of promise for hydrology, mainly because of the potential to observe areas and entire river basins rather than merely points. In addition, as the remote sensing science has developed we have learned of the potential to make entirely new measurements of hydrologic variables not generally possible with traditional techniques.

In spite of this promise, applied or engineering hydrology has been slow to embrace remote sensing as a useful source of data, presumably because existing techniques and data have been satisfactory for limited applications. Most of the advances in using remote sensing for hydrology have come from new areas of hydrologic analysis; areas where existing methods were unsatisfactory or limiting and areas where sufficient data were sparse or nonexistent. These areas include General Circulation Model (GCM) land parameterizations, advances in snow hydrology and the measurement of soil moisture. Moreover, the prediction in ungauged basin (PUB) and the research on hydrologic changes has resulted in the development of more complex, physically realistic, distributed hydrological models, which has dramatically increased the demand for spatial data. At the same time, the data collection agencies are under pressure to reduce the sizes of their conventional ground-based data networks. Therefore, using remote sensing methods to understand eco-environmental changes in eco-hydrologic studies has emerged to be a current research topic of wide interest.

It should be kept in mind, that RS data are not only used for monitoring of hydrologic state variables, but also as the basis for parameter estimation of hydrologic models. Remote sensing, particularly from various satellites in various spectral bands, can provide information on catchment characteristics (e.g. land cover, land use, slope, and vegetation), from which the parameters of hydrological models can be gathered. Particularly in combination with other spatial information, such as digital elevation models, digital terrain models, digital soil maps. RS will allow the spatial estimation of hydrologic model parameters, e.g. the maximum soil water storage capacity in a river basin.

Salomonson (1983) argued that the use of remote sensing in hydrological models can be divided into three broad categories or levels of use. The simplest of these is the use of remote sensing imagery to identify items of interest such as flood areas. The second level is to obtain data such as land cover, geological features, or other hydrological parameters through interpretation and classification of remotely sensed data. This interpolation of satellite data is often used in conjunction with existing hydrological models such as the SCS watershed runoff model. The third level involves the use of digital data to estimate hydrological parameters directly. This is normally achieved through correlation of known hydrometric data with remotely sensed data. Estimates of

soil moisture and precipitation have been obtained in this fashion. All three categories have been used successfully in hydrological applications with the second category being particularly well suited to hydrological models.

Although the usefulness of remote sensing data is widely recognized, there remain few cases where remote sensing data have been actually used in hydrological simulations. Difficulties still exist in choosing the most suitable spectral data for studying hydrological processes as well as in interpreting such data to extract useful information (Abbott & Refsgaard, 1996; Engman, 1996; Kite & Pietroniro, 1996).

A review on the second and the third level will be provided as follows, with special regard to application of remote sensing in detecting and monitoring land use cover change and ET estimation with aid of remote sensing.

2.4.1 Land use/cover mapping and change detection with aid of remote sensing

The International Geosphere-Biosphere Program, The International Human Dimension Program and the Land Use and Land Cover Change project have referred to land use and land cover change as follows (IGBP-IIIDP, 1999). Land cover refers to the physical and biophysical characteristics or state of Earth's surface and immediate, captured in the distribution of vegetation, water, desert, ice and other physical features of the land, including those created solely by human activities e.g., settlements. Land use refers to the intended use or management of the land cover type by human beings. Thus, land use involves both the manner in which the biophysical attributes of land are manipulated and intent underlining that manipulation (the purpose for which the land is used e.g., agriculture, grazing), which are more subtle changes that affect the character of the land cover without changing its overall classification. Definition of land use in this way establishes a direct link between land cover and the actions of people in their environment (FAO, 1998).

Conventional ground methods of land use mapping are labor intensive, time consuming and are done relatively infrequently. These maps soon become outdated with the passage of time, particularly in a rapid changing environment. In fact according to Olorunfemi (1983), monitoring changes and time series analysis is quite difficult with traditional method of surveying. In recent years, satellite remote sensing techniques

have been developed, which have proved to be of immense value for preparing accurate land use land cover maps and monitoring changes at regular intervals of time. In case of inaccessible region, this technique is perhaps the only method of obtaining the required data on a cost and time – effective basis.

2.4.1.1 Land use/cover mapping with remote sensing

The most established application of remote sensing to eco-hydrologic modeling is mapping patterns of the Earth's surface. Vegetation mapping allows quantification of actual vegetation on the ground. This provides eco-hydrologic studies with realistic information instead of potential natural vegetation maps based on observed vegetation relationships to climatic factors. This type of analysis is fundamental to the study of land cover and land use, and much land-use/land-cover research still focuses on this type of work. First, it provides the current spatial distribution of land cover and land use for any given area that has been imaged by a sensor. Much of the global land-use classification is done with 1-kilometer (km) and 8-km AVHRR data. Other sensors, especially Landsat TM and SPOT, are used for finer-scale classifications. Second, repeat coverage allows temporal studies of change. Three decades of satellite imagery allow decadal studies of land-cover change. These archives of satellite imagery also serve as a baseline for future monitoring and change assessments. Change detection is accomplished by creating algorithms to quantify the magnitude and direction of change. Overall the assessments of land-use/land-cover change can be quantitative and comprehensive. This type of spatial analysis can also help to target study areas.

As land cover classification was one of the earliest products of satellite data it has often been used to provide data for conventional hydrological techniques. For example, Rango et al. (1983) describe the use of land cover from Landsat MSS data as input to flood frequency models for urban planning. The cost of obtaining the land cover information from Landsat was estimated at about one third that of conventional techniques for basins exceeding 25 km².

Land cover may also be used as a classifier for parameters of a hydrological model (Kite, 1989). For example, each type of land cover will have a distinct roughness coefficient and a distinct infiltration rate. This parameterization is included implicitly in the early Soil Conservation Service (SCS) hydrological model (USDA, 1972) in which

runoff curve numbers (RCN) based on land type and soil group are used to parameterize interception, depression storage and infiltration and then to derive runoff volumes. The land types were conventionally derived from observation or aerial photography.

Blanchard (1973) and Ragan & Jackson (1980) have all used remotely sensed land cover data to estimate runoff curve numbers for further input into the SCS model. In those two studies Landsat data were used for the estimation of the land cover and subsequently, the runoff curve numbers, time to peak and peak flow; the third study used GOES data and restricted the classification to three land types. This use was extended by Duchon et al. (1992) using Landsat MSS data to divide a watershed into land cover types before applying the USDA SWRRB model (a variation on the SCS RCN concept) to each land cover separately. In all cases the results obtained from the remote sensing land covers were acceptable. Tao & Kouwen (1989) also showed that using remotely sensed data for land cover meant that information was no longer lumped, thus allowing modellers to estimate rainfall excess and runoff separately for each land cover class (Kite & Pietroniro, 1996).

2.4.1.2 Monitoring land cover change with Vegetation Indices

Beyond spatial description of change, scientists are interested in the amount of change. Vegetation indices offer quantitative information about vegetation productivity based on spectral information found in satellite imagery.

There are various spectral vegetation indices in use, which have been reviewed by Bastiaanssen (1998). The most widely used vegetation index, the Normalized Difference Vegetation Index (NDVI), relates near infra-red to visible red reflectance $(NIR-VIS)/(NIR+VIS)$ in order to take advantage of the differential reflectance characteristics of vegetation in these two spectra. This index, like most vegetation indices, relates a measure of "greenness", which is empirically related to vegetation structure and function, through variables such as LAI, vegetation cover, above-ground biomass, photosynthetic efficiency, FAPAR, and stomata conductance. Moreover, as being representative of vegetation growth and vigor at the land surface, it is also an indicator of photosynthetic activity of plants and has been widely used for assessing vegetation phenology and estimating landscape patterns of primary productivity (Tucker & Sellers, 1986). The NDVI was designed to quantitatively evaluate vegetation growth:

higher NDVI values imply more vegetation coverage, lower NDVI values imply less or non-vegetated coverage, and zero NDVI indicates rock or bare land (Jin, 2009).

There are numerous studies on application of remote sensing in large-scale global assessments of vegetation distribution and land cover with the Normalized Difference Vegetation Index (NDVI) data from Advanced Very High Resolution Radiometer (AVHRR) and the Moderate Resolution Imaging Spectroradiometer (MODIS) (Defries & Townshend, 1994). Kite (1995) used monthly NDVI values for the Upper Columbia Basin from two sources. NDVI directly from NOAA-AVHRR 1.1 km data were compared to the 10-minute (about 20 km) Global Ecosystem Database (NOAA-EPA, 1992) in the SLURP hydrological model (Kite, 1995). Wang et al. (2006) employed NDVI as an important vegetation indicator to analyze the spatial-temporal variation in the Pearl River Delta and found that the plant activity decreased in the area. Fang et al. (2003) pointed out that the vegetation activity in China increased during the last 20 years.

Another important vegetation index is Leaf Area Index (LAI), the area of leaf above a given area of ground, has been identified by Running et al. (1986) as the single most important variable for quantifying energy and mass exchange by plant canopies over landscapes. Gholz et al. (1976) showed that knowledge of leaf area index and its spatial distribution is essential for estimating photosynthesis, transpiration, respiration, interception and energy transmission to the ground. Denisenko & Lozinskaya (1994), in computing evaporation and transpiration for the KUREX88 field experiment in Russia, computed actual transpiration, E_a , as a function of maximum possible (potential) evaporation under a closed canopy by introducing LAI.

The importance of these results for hydrological modeling is that LAI is land cover specific and fits well with models which use land cover information as the basis for parameter definition (Kite & Kouwen, 1992). If a relationship can be defined relating LAI to actual ET, a much more dispersed representation of E_a can be used in the hydrological model. In the Semi-distributed Land Use-based Runoff Processes (SLURP) model (Kite, 1995) daily values of LAI are used in transpiration algorithms for each land cover type.

Leaf area index has traditionally been calculated using species-specific allometric equations relating stem diameter and foliage biomass. This is very laborious and imprecise (Gower & Norman, 1991) and so Running et al. (1986) suggested the use of satellite data to estimate LAI. The visible and infrared bands of the AVHRR sensor can be used to derive indices of stomatal activity. The Normalized Difference Vegetation Index (NDVI) is the most commonly used. However, AVHRR channels 1 and 2 are subject to differential atmospheric scattering and absorption and so other, less susceptible, indices have also been proposed (Pinty & Verstraete, 1992).

All of these vegetation indices are correlated with vegetation cover, although to varying degrees in different environments. New techniques for extracting ecological variables from satellite imagery include combining NDVI with texture analysis to constrain LAI better and performing multiple regression analyses directly on spectral bands instead of using vegetation indices. Most likely, these empirical methods will never be exact, so quantitative methods also have been explored.

In a word, Vegetation Indices, particularly NDVI and LAI, has been widely applied in land use change detection and ecohydrologic modeling with aid of remote sensing. With the development of remote sensing and hydrologic modeling, vegetation index is one of the most promising ways to conduct eco-hydrologic modeling.

2.4.1.3 Land use & cover change detection

An increasingly common application of remotely sensed data is for change detection. Change detection is the process of identifying differences in the state of an object or phenomenon by observing it at different times (Singh, 1989). Change detection is an important process in monitoring and managing natural resources and urban development because it provides quantitative analysis of the spatial distribution of the population of interest. Change detection is useful in such diverse applications as land use change analysis, monitoring shifting cultivation, assessment of deforestation, study of changes in vegetation phenology, seasonal changes in pasture production, damage assessment, crop stress detection, disaster monitoring, day/night analysis of thermal characteristics as well as other environmental changes (Singh, 1989).

Macleod & Congalton (1998) listed four aspects of change detection which are important when monitoring natural resources: (1) Detecting the changes have occurred;

(2) Identifying the nature of the change; (3) Measuring the aerial extent of the change and (4) Assessing the spatial pattern of the change. Efficiency of the techniques depends on several factors such as classification schemes, spatial and spectral resolution of remote sensing data, ground reference data and also an effective implementation of the result.

The basic premise in using remote sensing data for change detection is that changes in land cover result in changes in radiance values which can be remotely sensed. Techniques to perform change detection with satellite imagery have become numerous as a result of increasing versatility in manipulating digital data and increasing computing power.

A wide variety of digital change detection techniques have been developed over the last two decades. Singh (1989) and Coppin & Bauer (1996) both provide excellent and comprehensive summaries of methods and techniques of digital change detection. Coppin & Bauer (1996) summarize eleven different change detection algorithms that were found to be documented in the literature by 1995. These include:

1. Mono-temporal change delineation;
2. Post classification comparisons;
3. Multidimensional temporal feature space analysis;
4. Composite analysis;
5. Image differencing;
6. Multitemporal linear data transformation;
7. Change vector analysis;
8. Image regression;
9. Multitemporal biomass index;
10. Background subtraction;
11. Image rationing.

The scientific literature reveals that digital change detection is a difficult task to perform accurately and unfortunately, many of the studies concerned with comparative evaluation of these applications have not supported their conclusions by quantitative analysis (Singh, 1989). All digital change detection is affected by spatial, spectral, temporal, and thematic constraints. The type of method implemented can profoundly affect the qualitative and quantitative estimates of the change. Even in the same

environment, different approaches may yield different change maps. The selection of the appropriate method therefore takes on considerable significance. Not all detectable changes, however, are equally important to the resource manager. On the other hand, it is also probable that some changes of interest will not be captured very well or at all by any given system.

An image differencing technique is powerful in change detection study. According to recent research by Coppin & Bauer (1996), image differencing appears to perform generally better than other methods of change detection; and such monitoring techniques based on multispectral satellite data have demonstrated potential as a means to detect, identify, and map changes in forest cover. Image differencing is probably the most widely applied change detection algorithm for a variety of geographical environments (Singh, 1989). It involves subtracting one date of imagery from a second date that has been precisely registered to the first.

Post-classification comparison is the commonly reported technique for classification based change detection (Weismiller & Momin, 1977; Wickware & Howarth, 1981; Singh, 1989). This method was found to be the most suitable for detecting LUCC (Larsson, 2002; Liu & Zhou, 2004). In this technique, two types of images from different dates are independently classified. The use of independently produced classifications has the advantage of compensating for varied atmospheric and phonological conditions between dates, or even the use of different sensors between dates, because each classification is independently produced and mapped. This approach is very powerful when land use maps are available. Particularly, it is also very useful for interdisciplinary studies, i.e., the studies of LUCC on hydrologic cycles from hydrologic perspectives.

To date, there are numerous researches on land use change detection using post-classification comparison with aid of remote sensing. For example, Dimiyati (1995) made an analysis of land use and land cover changes using the combination of MSS Landsat and land use map of Indonesia, the results reveal that land use land cover change were evaluated by using remote sensing to calculate the index of changes which was done by the superimposition of land use land cover images of 1972, 1984 and land use maps of 1990. This was done to analyze the pattern of change in the area, which

was rather difficult with the traditional method of surveying as noted by Olorunfemi (1983) in 1983 when he was using aerial photographic approach to monitor urban land use in developing countries with Ilorin in Nigeria as the case study.

Daniel et al. (2002) in their comparison of land use land cover change detection methods, made use of 5 methods viz, traditional post – classification cross tabulation, cross correlation analysis, neural networks, knowledge – based expert systems, and image segmentation and object – oriented classification. A combination of direct T1 and T2 change detection as well as post classification analysis was employed. Nine land use land cover classes were selected for analysis. They observed that there are merits to each of the five methods examined, and that, at the point of their research, no single approach can solve the land use change detection problem.

Arvind et al. (2006) carried out a post-classification comparison study on land use land cover mapping of Panchkula, Ambala and Yamunanger districts, Haryana State in India. They observed that the heterogeneous climate and physiographic conditions in these districts has resulted in the development of different land use land cover in these districts, an evaluation by digital analysis of satellite data indicates that majority of areas in these districts are used for agricultural purpose. The hilly regions exhibit fair development of reserved forests. It is inferred that land use land cover pattern in the area are generally controlled by agro – climatic conditions, ground water potential and a host of other factors.

It can be concluded that over time through series of studies that satellite image is adequate for general extensive synoptic coverage of large areas. As a result, this reduces the need for expensive and time consuming ground surveys conducted for validation of data. Generally, satellite imagery is able to provide more frequent data collection on a regular basis unlike aerial photographs which although may provide more geometrically accurate maps, is limited in respect to its extent of coverage and expensive; which means, it is not often used. Moreover, due to the complexity of land use change detection, there is no universally accepted approach can solve the land use change detection problem. However, post-classification comparison seems be one of the most popular approach for change detection, particularly on condition that land use classification maps are available. This approach is very powerful when land use maps

are available. Particularly, it is also very useful for interdisciplinary studies, i.e., the studies of LUCC on hydrologic cycles from hydrologic perspectives.

2.4.2 ET Estimation with the aid of remote sensing and GIS

Evaporation is one of the important phases of the hydrological cycle. Evapotranspiration from land surfaces, together with precipitation, governs the amount of run-off from a river basin. Evapotranspiration from vegetated surfaces also plays a major role in the global water cycle, in the natural and essential processes of plants, and in modifying weather and climate (Shuttleworth, 1991). Therefore, it is essential to estimate ET accurately for hydrologic modeling, water resources estimation, and drought monitoring. However, evaporation has traditionally been one of the most difficult hydrological processes to estimate since direct measurements present many problems. The methods for estimating ET can generally be grouped into 4 categories i.e. the hydrological methods (water balance), direct measurement (lysimeters), micrometeorological (energy balance) and empirical or combination methods (Thornthwaite) based on energy balance or climatic factors (Thornthwaite & Mather, 1955). Most of these methods can only provide point estimates of ET which are not sufficient for system-level water management. Theoretically, distributed physically-based hydrological models can compute ET patterns; however, in practice it is often not applicable due to model complexity and data availability.

During the last two to three decades, significant progress has been made to estimate actual evapotranspiration (ET_a) using satellite remote sensing (Engman & Gurney, 1992; Kustas & Norman, 1996; Bastiaanssen et al., 1998, 2002). Techniques are now becoming available to use satellite data to provide areal estimates of skin temperature, cloud cover/sunshine duration and surface albedo and to compute evapotranspiration from different land covers. These methods provide a powerful means to compute actual ET (ET_a) from the scale of an individual pixel right up to an entire raster image.

Furthermore, there are numerous remote sensing based ET estimation models; therefore, it is always difficult to classify these methods, because there are often intermediate approaches which combine physical and empirical relationships. Nevertheless, according to Courault (2005), four model categories which are based on:

(1) Empirical direct methods where remote sensing data are introduced directly in semi-empirical models to estimate ET (for example, the simplified relationship using Thermal Infra Red (TIR) remote sensing and meteorological data). All these methods are based on semi-empirical relationships between net radiation R_n and cumulative temperature difference ($T_s - T_a$), where the surface temperature T_s is obtained by satellite images, while the air temperature T_a is given by ground based observations.

(2) Residual methods of the energy budget combining some empirical relationships and physical modules. Most current operational models (such as SEBAL, S-SEBI, SEBS described further) use remote sensing directly to estimate input parameters and ET.

(3) Deterministic methods generally are based on more complex models such as Soil-Vegetation-Atmosphere Transfer models (SVAT), directly computing all the different components of energy budget. Remote sensing data are used at different modeling levels, either as the input parameters to characterize the different surfaces, or in assimilation procedures which aim at retrieving adequate parameters for the ET computation. Some examples of this approach will be shown in the third section.

(4) The last category is that of vegetation index methods or inference methods based on the use of remote sensing to compute a reduction factor (such as K_c or Priestley Taylor- α parameters) for the estimation of the actual evapotranspiration. These approaches consider a potential or reference ET obtained from ground measurements. Different papers deal with these approaches in this special issue (Allen et al., 2005; Neale et al., 2005; Garatuza & Watt, 2005).

Below the four model categories will be reviewed, with special regard to the Residual methods. Before presenting these different approaches, a brief review about energy budget is required for a better understanding of the relationships between ET and the driving variables such as surface temperature (T_s). Then many models using remote sensing to estimate ET will be discussed.

2.4.2.1 Evapotranspiration estimates and surface energy balance budget

The surface energy balance is commonly written as

$$R_n = G + H + \lambda E \quad (2-1)$$

Where R_n is the net radiation, G the soil heat flux, H the sensible heat flux and λE is the latent heat flux, which can be expressed as height of water, i.e. evapotranspiration.

The equation to calculate the net radiation is given by

$$R_n = (1 - \alpha) \cdot R_{swd} + \varepsilon \cdot R_{lwd} - \varepsilon \cdot \sigma \cdot T_0^4 \quad (2-2)$$

where, R_{swd} , R_{lwd} is incoming shortwave and outgoing longwave radiation respectively, α is the surface albedo, ε the emissivity of the surface, σ the Stefan-Boltzmann constant, equals to 5.67×10^{-8} and T_0 the surface radiative temperature.

The available net radiant energy R_n is shared between the soil heat flux G and the atmospheric convective fluxes (sensible heat flux H and latent energy exchanges λE). Soil heat is normally considered a fixed fraction of the net radiation (Norman & Kustas, 1995), and since previous studies have shown that net-radiation can be accurately determined from RS data (e.g. Boegh et al., 1999), the main task becomes the determination of sensible heat flux from remote sensing data (Overgaard et al., 2006).

Given the aerodynamical resistance r_a between the surface and the reference height z_a in the lower atmosphere (generally 2m) above the surface, H is expressed as:

$$H = \rho c_p (T_s - T_a) / r_a \quad (2-3)$$

where r_a is a function of wind speed u_a , atmospheric stability and roughness (z_0 , z_{01}), depending on vegetation height and geometry).

This means that LE is linearly related to the surface air temperature difference at the time of T_s measurement, if the second order dependence of r_a on this gradient is ignored.

$$LE = R_n - G - \rho c_p (T_s - T_a) / r_a \quad (2-4)$$

This equation is widely used for the estimation of instantaneous LE (residual method). At midday it is a good indicator of plant water status for irrigation scheduling. For estimation of LE over longer periods (seasonal, monthly, daily estimations), the use of ground-based ET from weather data is necessary to make temporal interpolation.

2.4.2.2 Empirical Direct Methods

These methods are essentially simplified relationships based on the theoretical assumption that ratio H/R_n is constant during the day and that the daily value of G is null. The relationships, proposed by various authors (e.g. Jackson et al., 1977; Lagouarde, 1991; Courault et al., 2005), have the following typical formulation:

$$ET_{24} = R_{n24} + A \cdot B(T_s - T_a) \quad (2-5)$$

where ET_{24} and R_{n24} are the daily values of evapotranspiration and net radiation, $(T_s - T_a)$ is the instantaneous difference in temperature measured around midday, and A and B are parameters to be calibrated. The accuracy of the method can reach 10 - 15% at local scale (Calcagno et al., 2007), but apart from the problems due to calibration, issues linked to the spatial interpolation of the quantities have to be considered. In fact, also assuming that solar radiation can be spatially estimated through remote sensing techniques, geostatistical models used to interpolate T_a reduce the accuracy around 20 to 30%.

Since vegetation indices and surface temperature are related (higher ET values are usually associated with lower surface temperatures), Carlson et al. (1995) and Moran et al. (1994) explored the relationship between the cumulated temperature difference $(T_s - T_a)$, also known as stress degree day (SDD), and the NDVI, drawing up a trapezoidal scheme by which a classification of the different soil moisture conditions can be obtained.

2.4.2.3 Residual methods

SEBI, SEBS, and S-SEBI

Surface Energy Balance Index (SEBI), proposed by Menenti and Choudhury (1993), is based on the Crop Water Stress Index (CWSI) (Jackson et al., 1981) concept in which the surface meteorological scaling of CWSI is replaced with planetary boundary layer (PBL) scaling. It uses the contrast between wet and dry areas appearing within a remotely sensed scene to derive ET from the relative evaporative fraction (Λ_r). The Λ_r is calculated by relating surface temperature observations to theoretical upper and lower bounds on the difference between T_s and T_a (Gowda et al., 2007). Evaporative fraction (Λ), as utilized by Bastiaanssen et al. (1998), is defined as the ratio of latent heat flux to the available energy ($AE = R_n - G$) and is assumed to remain nearly constant during the day.

Surface Energy Balance System (SEBS) was developed by Su (2002) using the SEBI concept. It uses a dynamic model for aerodynamic roughness length for heat (Su et al., 2001), bulk atmospheric similarity (BAS) (Brutsaert, 1975) and Monin - Obukhov similarity (MOS) theories for PBL to estimate regional ET, and atmospheric surface layer scaling for estimating ET at local scale. SEBS requires theoretically defined wet and dry boundary conditions to estimate H. Under dry conditions, the calculation of H_{dry} is set to the AE as evaporation becomes zero due to the limitation of water availability and H_{wet} is calculated using Penman - Monteith parameterization (Monteith, 1965). The main limitation with SEBS is that it requires aerodynamic roughness height. A potential weakness in the SEBS approach is the neglect of heat flux absorption along the temperature profile when extrapolating to and from the blending layer. The absorption, over a dry condition, can be large, and it disrupts the assumption of a smooth T gradient that conveys the H flux estimate all the way to the blending height. This results in an overstatement of the surface temperature for the dry condition and must be accounted for somehow empirically.

A great number of studies on SEBS's application in a semi-arid inland basin in Northwestern China (e.g. Li, 2001; Su et al., 2003), and drought disaster monitoring (Su et al., 2003), which have proved that it has clear physical meaning and reasonable accuracy. It is feasible and applicable for lowland-shrub region with relatively heterogeneous underlying surface. However, since NDVI saturates at higher LAI values, it is not suitable for complex vegetated area, particularly for areas with tall trees (Zhan, 2005).

Simplified SEBI (S - SEBI) (Roerink et al., 2000) is a simplified method derived from SEBS to estimate surface fluxes from remote sensing data. Consequently, this model is based on Λ and the contrast between the areas with extreme wet and dry temperature. The disadvantage of this method may be that it requires extreme T_s values, which cannot always be found on every image. However, the major advantages are that it is a simpler method that does not need additional meteorological data, and it does not require roughness length as in the case of SEBS.

SEBAL

The Surface Energy Balance Algorithm for Land (SEBAL) is a model with an intermediate approach using both empirical relationships and physical parameterizations (Bastiaanssen et al., 1998 a,b and Jacob et al., 2002). This model has been designed to calculate the energy partitioning at the regional scale with minimum ground data. Atmospheric variables (air temperature and wind speed) are estimated from remote sensing data by considering the spatial variability induced by hydrological and energetic contrasts. The determination of wet and dry surfaces on the studied area is necessary to extract threshold values. The model requires incoming radiation, T_s , $NDVI$ and albedo maps. Semi-empirical relationships are used to estimate emissivity, roughness length and G from $NDVI$. The sensible heat flux is computed from flux inversion at dry non evaporating land units and at wet surfaces types. Latent heat flux is computed as the residual of energy balance.

This model has been used for different applications to estimate monthly and seasonal ET by linearly interpolations the ET values for periods in between two adjacent images (Bastiaanssen, 2000) and applied under several irrigation conditions in different countries (Droogers & Bastiaanssen, 2002).

METRICTM

A full description of METRICTM can be found in Allen et al. (2007). The main difference between SEBAL and METRICTM is that the latter does not assume $H = 0$ or $LE = R_n - G$ at the wet pixel. Instead, it calculates the ET of the hot pixel by performing a soil water budget, using meteorological data from a nearby weather station, to verify that ET is indeed zero for that pixel. For the wet pixel, LE is set equal to $1.05 ET_r \lambda_v$, where ET_r is the hourly (or shorter time interval) tall crop reference (like alfalfa) ET calculated using the standardized ASCE Penman-Monteith equation applied to local meteorological observations. The second difference is that METRICTM selects extreme pixels purely in an agricultural setting, where particularly the cold pixel needs to have biophysical characteristics (hc , LAI) similar to the reference crop (alfalfa). The third difference is that METRIC uses the alfalfa reference evapotranspiration fraction (ET_rF) mechanism to extrapolate instantaneous LE flux to daily ET rates instead of using the Λ . The ET_rF is the ratio of ET_i (remotely sensed instantaneous ET) to the reference ET_r that is computed from weather station data at overpass time. The benefits of using ET_r

are the calibration around biases in R_n and G estimates at both ends of the temperature range (i.e., at the cold and hot pixels) as well as calibration around biases in T_s . An additional benefit of using ET_r and $ET_{r,F}$ is the ability to account for general advection impacts on ET . Disadvantages are the requirement for relatively high - quality weather data on an hourly or shorter time step and reliance on the accuracy of the ET_r estimate (Gowda et al., 2007).

2.4.2.4 Deterministic methods

Residual methods are able to supply ET estimates only if remote sensing images for the analyzed area are available. For the days without images (e.g. cloudy days) temporal interpolations are needed, that can be obtained locally from ground-based measurements. According to Courault (2005), there are two types of models in this category: remote sensing forced models, assimilation of numeric models. Generally these models (SVAT models) describe the exchanges between soil plant and atmosphere according to the physical processes occurring in each compartment with generally a fine time step (second, hour).

Deterministic models (SVAT models) can operate without having remote sensing data, because they use these data just as auxiliary input parameters or in data assimilation procedures. Therefore SVAT models are suitable for the estimate of energetic exchanges during the periods without remote sensing images. Furthermore, through SVAT models it is possible to obtain, together with the components of the energy balance, the estimates of many intermediate variables (e.g. LAI, soil moisture) strictly correlated to physiological and hydrological processes (Calcagno et al., 2007).

2.4.2.5 Inference Methods/ vegetation index methods

Vegetation indices are strictly correlated to parameters as fraction of vegetation cover or Leaf Area Index (LAI), that also affect the behavior of the crop coefficient K_c . Starting from these considerations, Heilman et al. (1982) investigated the relationships between percent cover and reflectance-based Perpendicular Vegetation Index (PVI) for alfalfa. Afterwards numerous studies have been conducted especially considering the NDVI (Neale et al., 1989; Choudhury et al., 1994; Allen et al., 2005) or similar indices as the Weighted Difference Vegetation Index (Consoli et al., 2006), retrieving various empirical equations to link these indices to the crop coefficient. However, especially

because of irrigation effects on soil moisture and water stress conditions, it has been verified that relationship between K_c and vegetation indices is not univocal (Allen et al., 2005).

Equations linking K_c to vegetation indices could be very useful for irrigation planning, particularly for K_c estimate in relatively dry soils, but results till now obtained are empirical, and it is necessary to work hard in order to develop more general relationships (Calcagno et al., 2007).

The advantages and disadvantages of the different approaches used to estimate ET from remote sensing data are summarized in Table 2.1. From the discussion above, one can easily come to the conclusion that evapotranspiration may be estimated from remote sensing data with different approaches: direct methods using TIR data, indirect estimates using assimilation procedures combining different wavelengths to get various input parameters (in particular related to vegetation water status). Some methods are based on the spatial variability present in remote sensed images (like the SEBAL or S-SEBI models), and try to use no additional meteorological data to estimate ET for routine application. The interest of using SVAT models is not only because they generally describe with more accuracy the crop functions, but also because they allow access to intermediate variables like soil moisture or LAI, which are related to physiologic and hydrologic processes that can be linked to other meteorological or hydrological models.

Although the remote sensing based ET models have been shown to have the potential to accurately estimate regional ET, however, the use of remote sensing for operational applications presents still several problems. However, research opportunities still exist to improve the spatial and temporal resolution of ET by developing data fusion/subpixel extraction algorithms to improve spatial resolution of surface temperature data derived from Landsat/ASTER/MODIS thermal images using same/other - sensor high resolution visible, NIR, and SWIR images. Moreover, the accumulation of very high quality experimental data and development of suitable distributed hydrologic has the potential to improve the accuracy of ET in terms of validation, which makes the future of accurate remote-sensing-based ET estimation promising.

Table 2.1 Summary of the advantages and disadvantages of the different approaches used to estimate ET from remote sensing data

Methods-models	Advantage	Disadvantage
Simplified models (Simplified Relationship)	Operational from local to regional scale	Spatial variations of coefficients
Inference models (K _c , f(NDVI))	Operational if combined with ground measurements or models estimating accurate ETR	<ul style="list-style-type: none"> • Requires calibration for each crop type • K_c varies according to water stress • Empirical no general relationship
Residual methods (SEBS, SEBAL, S-SEBI...)	<ul style="list-style-type: none"> • Operational, low cost, need no additional climatic data; • SEBAL: no atmospheric corrections for T_s; • SEBS: has clear physical basis, is not data intensive and particularly applicable for China) 	<ul style="list-style-type: none"> • Requires presence of wet and dry pixels • Some empirical relationships • Z_{0m} and T_{air} are sensitive to roughness length
Determinist (SVAT)	<ul style="list-style-type: none"> • Estimation of intermediate variables (LAI), possible links with climate, hydrological models, assimilation to find some parameters. • Allow continuous ET monitoring • Do not need thermal infrared remote sensing data. 	<ul style="list-style-type: none"> • Requires more parameters not easy to estimate • Requires accurate remote sensing data and continuous meteorological data

CHAPTER 3

LAND USE/COVER CHANGE ANALYSIS WITH THE AID OF GIS/RS

3.1 Introduction

As a major growth engine of Guangdong economy, the East River Basin, particularly the cities in the lower part (Shenzhen, Dongguan and Huizhou), has experienced fast and continuous economic growth over the past three decades and human activities have caused enormous influences on the environment which has been changing rapidly. Intensive human activities such as land use/cover changes and urbanization have significantly altered the hydrologic system in the East River Basin (Wang et al., 2006; Wei, 2010). The hydrologic changes in response to land use/cover changes may have increased the risk and vulnerability of natural and environmental hazards such as floods, landslide, and degradation of ecosystems. Therefore, analyzing land use/cover changes and finding out the spatio-temporal variation carry not only important scientific merit, but also valuable practical significance.

Land use/cover analysis is of primary importance in ecohydrologic modeling. On one hand, land use/cover analysis provides critical inputs for modeling water and energy balance in terrestrial ecosystems and is a basis for physically remote-sensing-based ET mapping. On the other hand, LUCC is linked to hydrologic cycle and human activities in complex ways, which is of utmost importance for understanding hydrologic impact of human activities. Moreover, LUCC studies can provide critical boundary condition for assessment of hydrologic response to LUCC. Therefore, understanding LUCC is an important step in integrated eco-hydrologic modeling.

The flowchart in Figure 3.1 shows the procedures for the LUCC detection and quantification in this chapter. As shown in the flowchart, this chapter firstly analyzes spatio-temporal variation of land use/cover using monthly NDVI with the aid of remote sensing and GIS, which can provide an insight into the long-term trend of vegetation growth and plant activities and the implications of NDVI variations in the East River Basin. Moreover, based on land use maps in 1980 and 2000, post-classification comparison methods, such as dynamic degree index model, land use transition model,

land use centroid movement model, are used to detect the land use changes and analyze the implications of the changes. Furthermore, Markov chain method is employed to predict the land use in 2010, which can be used as a boundary condition for future research on hydrologic impacts of LUCC. All of these provide a basis for understanding the LUCC and its implications at basin scale, which can also lay a solid foundation for providing input and constructing related scenarios for future research on hydrologic impacts of LUCC.

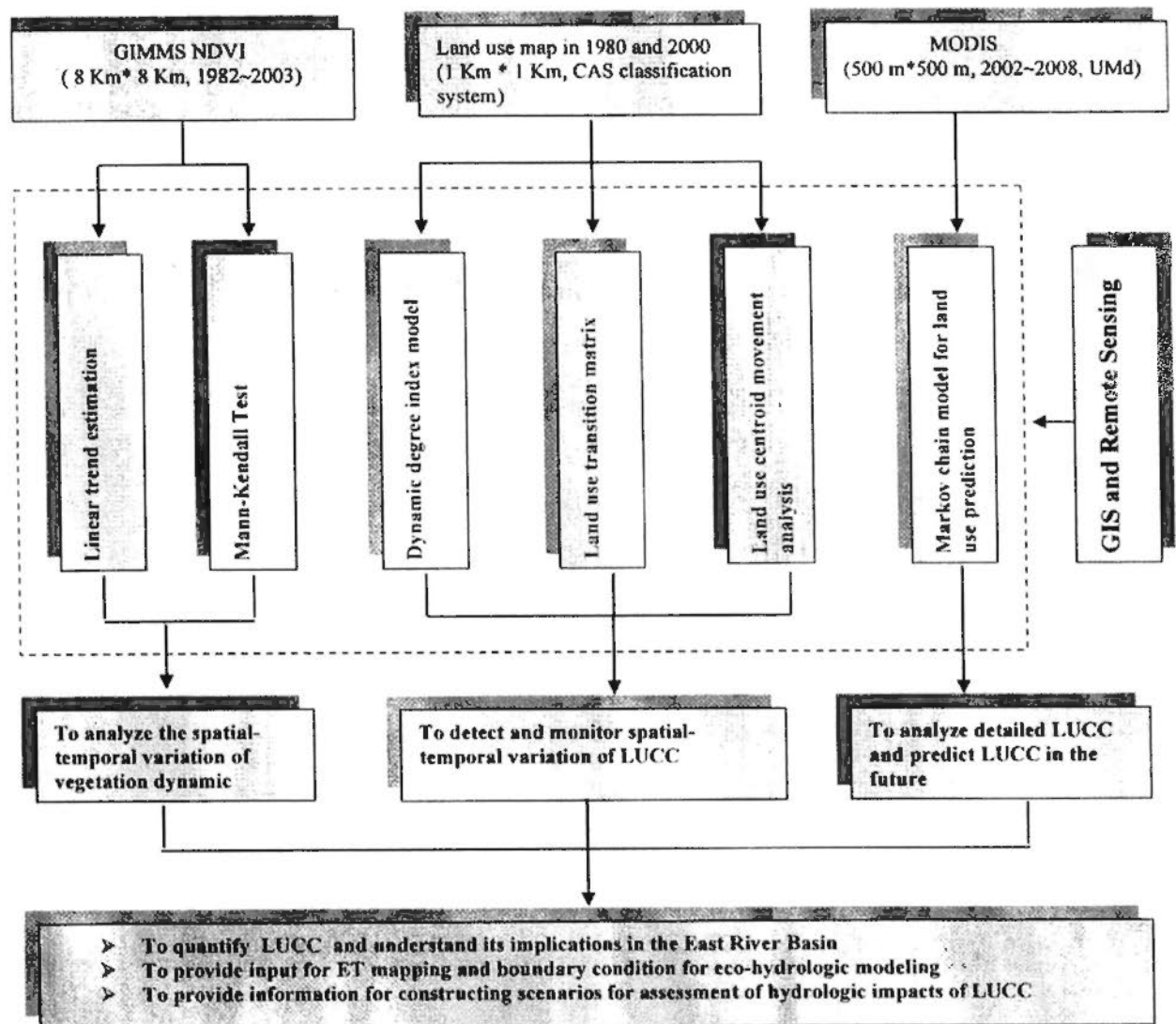


Figure 3.1 Summary of land use/cover change detection and quantification

3.2 Spatial-temporal analysis of vegetation dynamics based on NDVI

3.1.1 Review on NDVI for monitoring land use / cover changes

NDVI, calculated as the ratio of near infrared to red spectral response is well established in the literature (Justice et al., 1985; Reed et al., 1994) as being representative of vegetation growth and vigor at the land surface. NDVI is calculated from reflected solar

radiation in the near-infrared (NIR) and visible (VIS) wavelengths, using the following algorithm:

$$\text{NDVI} = (\text{NIR} - \text{VIS}) / (\text{NIR} + \text{VIS}) \quad (3-1)$$

NDVI is a nonlinear function that varies between -1 and 1 (undefined when NIR and VIS are zero). Values of NDVI for vegetated land generally range from about 0.1 to 0.7, with values greater than 0.5 indicating dense vegetation.

Currently, with the development of science and technology, remote sensing has become one of the powerful tools to study the spatial distribution of vegetation. Remote sensing has traditionally been used in large-scale global assessments of vegetation distribution and land cover with the NDVI data from Advanced Very High Resolution Radiometer (AVHRR) and the Moderate Resolution Imaging Spectroradiometer (MODIS) (e.g. Chen & Brutsaert, 1997; Defries & Townshend, 1994; Defries et al., 1995; Friedl et al., 2002; Loveland et al., 1999, 2000). As mentioned above, the NDVI is an index derived from reflectance measurements in the red and infrared portions of the electromagnetic spectrum to describe the relative amount of green biomass from one area to the next (Deering, 1978). This index is an indicator of photosynthetic activity of plants and has been widely used for assessing vegetation phenology and estimating landscape patterns of primary productivity (Sellers, 1985; Tucker & Sellers, 1986). Moreover, NDVI can also be designed to quantitatively evaluate vegetation growth: higher NDVI values imply more vegetation coverage, lower NDVI values imply less or non-vegetated coverage, and zero NDVI indicates rock or bare land (Jin, 2009).

There are numerous studies on analyzing vegetation dynamics based on NDVI. Globally, the vegetation activity is increased significantly in the recent 20 years. In China, the NDVI value in most parts of the country increased to different degrees. Several researches for some typical regions in China reveal that the vegetation activity increased in the Yangtze River Basin and the Yellow River Basin. However, in the arid or semi-arid areas in northwest part of China, the vegetation condition has become worse and, especially, the vegetation degradation is serious in Heihe River Basin (Wang et al., 2006; Jin, 2005).

In the last three decades, the East River Basin has experienced fast and continuous economic growth and human activities have caused enormous influences on the

environment which has been changing rapidly. In the upstream area, afforestation, irrigation and agricultural cultivation may have caused increase of vegetation activities (plant growth). The downstream area (Shenzhen, Dongguan and Huizhou), has experienced fast and continuous economic growth and intensive human activities like urbanization have significantly altered the hydrologic system. However, most studies on this topic are mainly focused on qualitative analysis (Wang et al., 2006). Therefore, it is important to quantify long-term LUCC at basin scale. In the following section a linear trend estimation model and Mann-Kendall test are employed to investigate long-term large-scale analysis of vegetation dynamics in the study area.

3.1.2 Data and Methodology

3.1.2.1 Data acquisition and pre-processing

In this study, the NDVI of the East River Basin was extracted from GIMMS (Global Inventory Modeling and Mapping Studies) dataset. The GIMMS data set is a NDVI product available for a 22-year period spanning from 1982 to 2003. The data set is derived from imagery obtained from the Advanced Very High Resolution Radiometer (AVHRR) instrument onboard the NOAA satellite series 7, 9, 11, 14, 16 and 17. This is a NDVI dataset that has been corrected for calibration, view geometry, volcanic aerosols, and other effects not related to vegetation change.

First and foremost, the NDVI from the dataset was extracted by the boundary of the East River Basin with the aid of GIS software (ARCGIS 9.2), remote sensing software (ENVI 4.0) and interface description language (IDL 6). Furthermore, because there are 792 satellite images, it is labor-intensive and time-consuming to do it one by one. Therefore, a program was developed to conduct the batch-processing of extraction works and output the results to Excel automatically in the IDL and ENVI environment.

3.1.2.2 Methodology

In order to detect vegetation dynamics in the East River Basin, linear trend model is firstly employed to analyze long-term trend of NDVI series from 1982 to 2003. A parametric test, T-test is employed to test whether the linear trend is statistically significant. Secondly, since we do not know whether the NDVI is normally distributed, a non-parametric test, Mann-Kendall test is employed to further assess significance of the trend.

Linear trend model

The simplest model of the time trend is the linear trend model:

$$T_t = \beta_0 + \beta_1 t, t = 1, 2, 3 \dots n \quad (3-2)$$

where T_t is the dependent variable, t is the independent variable, β_1 is the slope of the regression line, β_0 is the intercept of the regression line and n is the sample number.

The trend component is a straight line with intercept β_0 and slope β_1 . Note that $\beta_1 = dT_t/dt$. Therefore, $\beta_1 > 0$ if T_t has a positive trend and $\beta_1 < 0$ if T_t has a negative trend. The intercept, as is often the case in hydro-meteorological models, does not have a meaningful interpretation and its sign can be positive or negative, regardless of the trend's sign. A parametric test, T-test (Haan, 1977) is employed to test whether the linear trend is statistically significant.

Mann-Kendall test

There are many statistical techniques available to detect trends within the time series such as moving average, linear regression, Mann-Kendall (M-K) trend test. Each method has its own advantage and disadvantage in trend detection. However, non-parametric trend detection methods are less sensitive to outliers than parametric statistics such as Pearson's correlation coefficient. Moreover, the rank-based nonparametric Mann-Kendall test (Kendall, 1975; Mann, 1945) can test trends in a time series without requiring the assumption of normality or linearity. It is therefore highly recommended for general use by the World Meteorological Organization (Mitchell et al., 1966). The procedure of M-K trend test adopted in this study is as follows:

First the MK test statistic is calculated as

$$S = \sum_{i=1}^{n-1} \sum_{j=i+1}^n \text{sgn}(x_j - x_i) \quad (3-3)$$

$$\text{where } \text{sgn}(x_j - x_i) = \begin{cases} +1, & x_j > x_i \\ 0, & x_j = x_i \\ -1, & x_j < x_i \end{cases}$$

and n is the sample size. The statistics S is used to assess the monotonic trend. A positive S indicates an upward trend while a negative S indicates a downward trend.

The statistics S is approximately normally distributed when $n \geq 8$, with the mean and the variance as follows:

$$E(S) = 0 \quad (3-4)$$

$$V(S) = \frac{n(n-1)(2n+5) - \sum_{i=1}^m t_i(i-1)(2i+5)}{18} \quad (3-5)$$

where t_i is the number of ties of extent i and m is the number of ties of extent.

The standardized statistic (Z) for one-tailed test is formulated as:

$$Z = \begin{cases} \frac{S-1}{\sqrt{Var(S)}} & S > 0 \\ 0 & S = 0 \\ \frac{S+1}{\sqrt{Var(S)}} & S < 0 \end{cases} \quad (3-6)$$

Suppose that one wants to test the null hypothesis of no trend in the data against the alternative hypothesis of an upward linear trend at the significance level α . We reject the null hypothesis if $Z_i \geq Z_{\alpha}$, where the critical value Z_{α} can be found in the reference (Kendall, 1975; Mann, 1945). In this study, according to related studies in the Yellow River Basin and Pearl River Delta (Wang et al., 2006; Liu et al., 2006), one-sided M-K test is employed to detect the trend, say, at the significance level of 10%, the null hypothesis of no trend is rejected if $|Z| > 1.28$.

3.1.3 Spatial-temporal analysis of vegetation dynamics based on NDVI

3.1.3.1 Trend analysis of monthly NDVI

Linear trend model, T-test and M-K test were employed to analyze the long-term trend of monthly NDVI. The results are presented in Table 3.1 and Figure 3.2. As shown in Table 3.1 and Figure 3.2, it is observed that there are decreasing trends for most of the months, except for January, March, April, May and November. In terms of T-test, most of the P values are greater than 0.1 except September, which indicates that the linear trends are not significant. In terms of M-K test, June, July, August and September decreased significantly. However, the increasing trends for January, March, April, May and November are insignificant. In summary, there are significant decreasing trends of monthly NDVI in June, July, August and September over the years.

Table 3.1 Statistic values for inter-annual variation of monthly mean NDVI

Month	1	2	3	4	5	6	7	8	9	10	11	12
Regression coefficient	0.0004	-0.0003	0.0015	0.0012	0.0028	-0.0024	-0.0016	-0.0021	-0.0014	-0.0010	0.0001	-0.0004
Z value of M-K test	0.596	0.169	0.790	0.846	1.184	-1.635	-1.241	-1.805	-1.805	-0.677	-0.254	-0.056

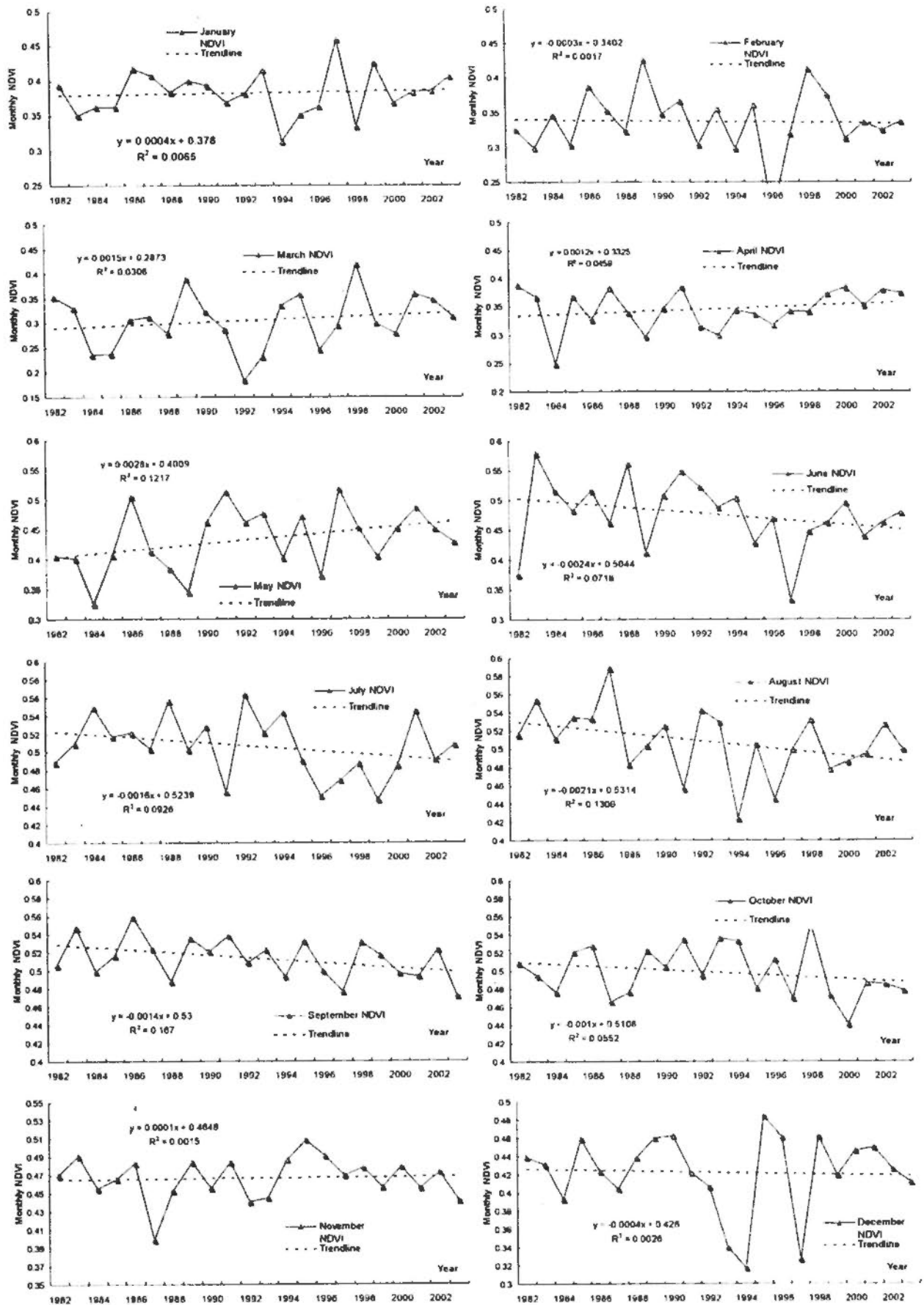


Figure 3.2 Long-term variation of monthly NDVI from 1982 to 2003

3.1.3.2 Trend analysis of seasonal NDVI

The results of long-term trend of seasonal NDVI are shown in Figure 3.3 and 3.4. For spring, the trend line is increasing, the regression coefficient is positive, the P value of T-test is 0.097 and the Z value of M-K test is 1.523 (>1.28). Therefore, it can be concluded that the NDVI of spring increased significantly during the past 22 years. For summer, the trend line is decreasing, the regression coefficient is negative, the P value of T-test is 0.042 (<0.05) and the Z value of M-K test is 1.607 (>1.28). Therefore, it can be concluded that the NDVI of summer decreased significantly during the past 20 years. For autumn and winter, both of the trend lines are decreasing and the regression coefficients are negative. Moreover, both of the P values of T-test are greater than 0.1 and both the Z values of M-K test are less than 1.28. Hence, it can be concluded that the NDVI of autumn and winter decreased insignificantly during the past 22 years.

In summary, the NDVI value of spring increased significantly at the rate of 0.0018 per year. However, the NDVI decreased in the other seasons. Specifically, for summer, the NDVI decreased significantly at a rate of -0.002. For winter and autumn, the NDVI decreased insignificantly. This conclusion agrees well with related studies in China (Zhou, 2005; Los, 2004).

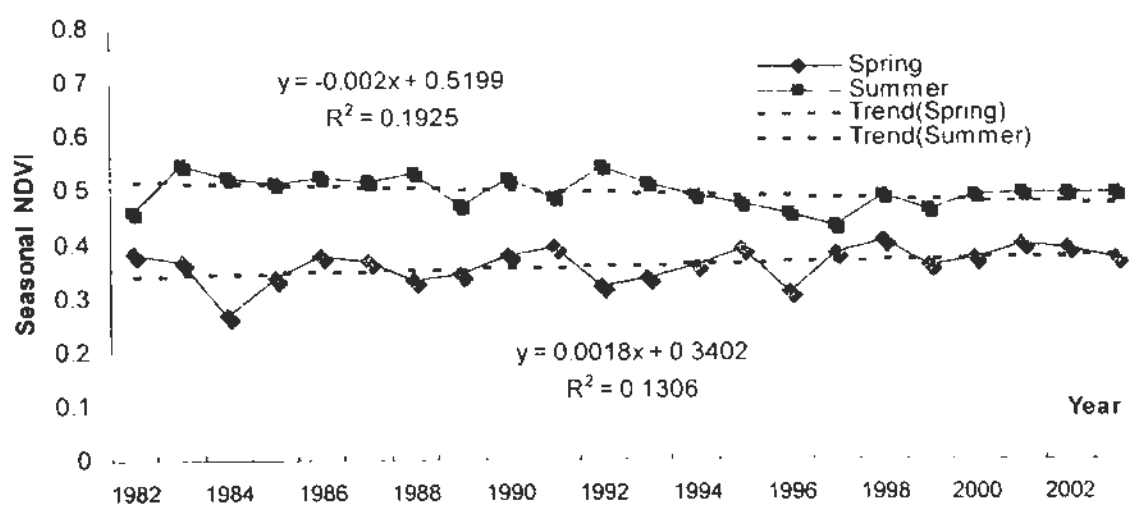


Figure 3.3 Long-term variation of seasonal NDVI (Spring and Summer)
($|Z_{spring}| = 1.523 > 1.28$; $|Z_{summer}| = 1.607 > 1.28$)

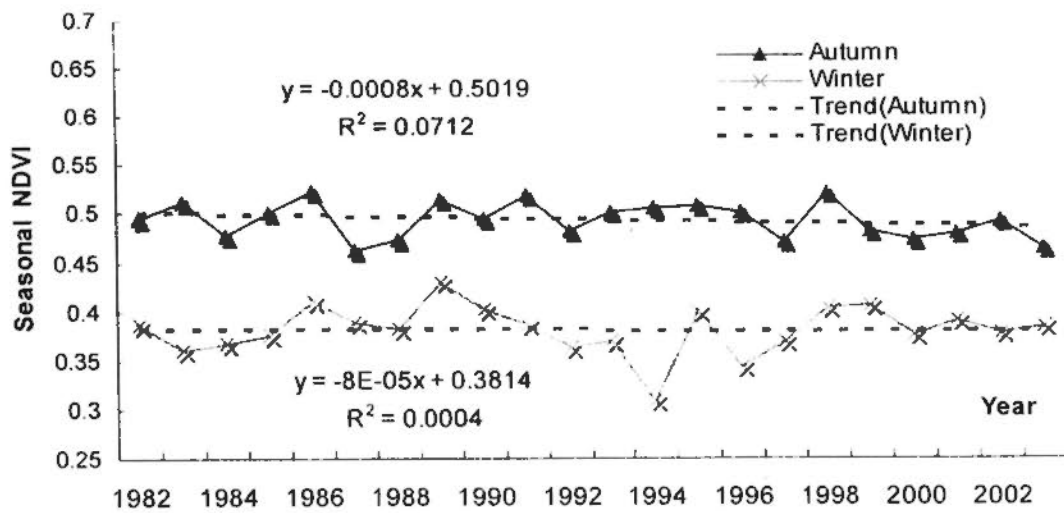


Figure 3.4 Long-term variation of seasonal NDVI (Autumn and Winter) ($|Z_{\text{autumn}}| = 1.128 < 1.28$; $|Z_{\text{winter}}| = 0.282 < 1.28$)

3.1.3.3 Trend analysis of annual NDVI

Long-term trend of annual mean NDVI was analyzed in the East River Basin by using linear trend model, T-test and M-K test. The results are presented in Figure 3.5. As shown in Figure 3.5, it can be found that the annual mean NDVI varied over the range of 0.402 and 0.459. The figures reached a peak at 0.459 in 1986 and bottomed out at 0.402 in 1996, which indicates vegetation cover was the best in 1986 but the worst in 1996. Generally speaking, there is a decreasing trend for annual mean NDVI with a rate of -0.0003. However, the P value of T-test is greater than 0.1 and Z value of M-K test is -0.733, which indicates that the decreasing trend is not insignificant.

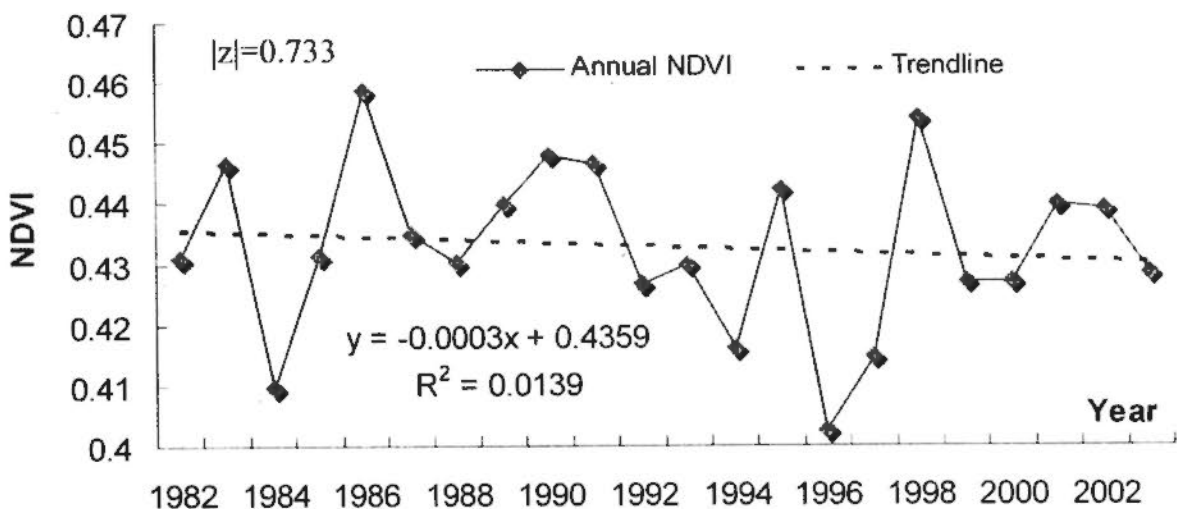


Figure 3.5 Long-term variation of annual NDVI from 1982 to 2003

3.1.3.4 Spatial variation of annual mean NDVI

The spatial distribution of annual mean NDVI is presented in Figure 3.6, and the monthly mean NDVI of the upper-part, middle-part and lower-part of the East River Basin are shown in Figure 3.7.

As shown in Figure 3. 6 and Figure 3.7, it can be observed that the NDVI decreased from the upper-middle-part to the lower-part. The average NDVI of the upper-part, middle-part and lower-part is 0.56, 0.53 and 0.41 respectively, with a decreasing trend towards the lower-part. The reasons are probably as follows. In the upper-middle-part, afforestation, irrigation and agricultural cultivation are frequent, which may have caused the increase of vegetation activities. However, in the lower-part, three big cities, Shenzhen, Dongguang, and Huizhou, have experienced fast and continuous economic growth and there are intensive human activities and fast city growth during the two decades, which can cause significant reduction in vegetation cover.

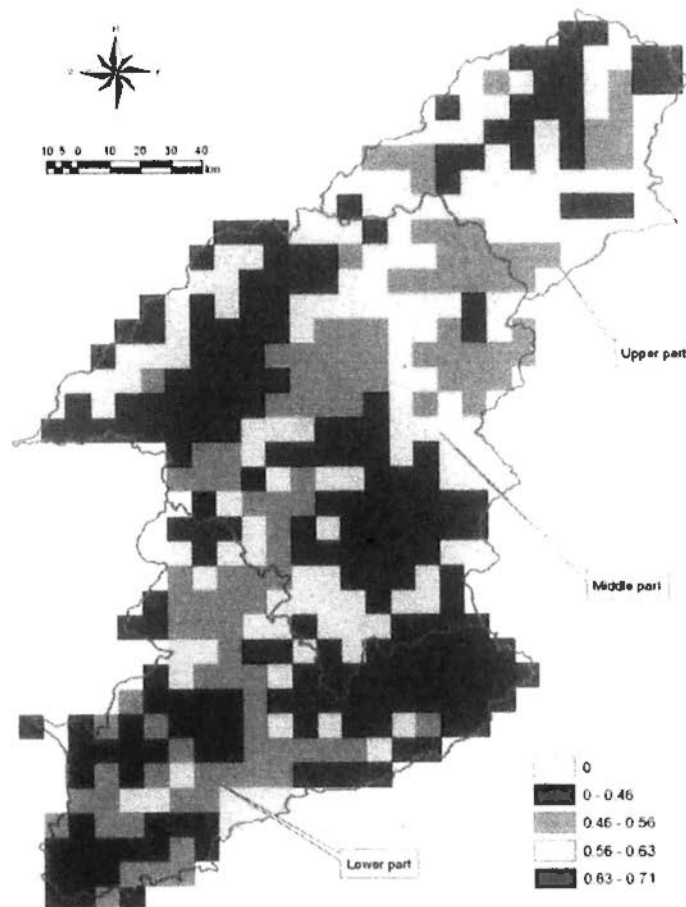


Figure 3.6 Spatial distribution of annual mean NDVI

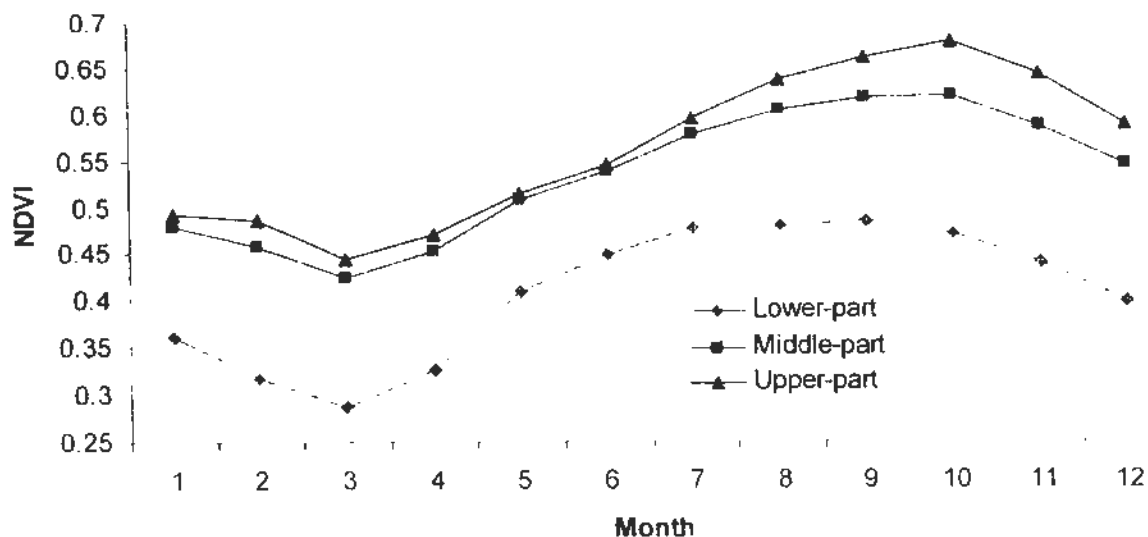


Figure 3.7 Monthly mean NDVI of the upper-part, middle-part and lower-part

3.1.3 Conclusions and discussions

In summary, from the discussion above, conclusions can be made as follows. (1) On a monthly basis, the NDVI values of June, July, August and September decreased significantly in the East River Basin from 1982 to 2003, which indicates that vegetation activities decreased in June, July, August and September over the years. (2) On a seasonal basis, NDVI value increased significantly at a rate of 0.0018 in spring and decreased significantly in summer over the years. Moreover, NDVI value decreased insignificantly in autumn and winter over the years. (3) On an annual basis, the annual mean NDVI value decreased insignificantly. (4) Spatially speaking, the NDVI value decreased from the upper-middle-part to the lower-part in the study area.

In conclusion, on one hand, spatially speaking, the NDVI value decreased from the upper-middle-part (agricultural region) to the lower-part (urban area) in the study area, which demonstrates that human activities can cause decrease of vegetation activities. On the other hand, temporally speaking, NDVI decreased significantly in summer (June to September) over the years. According to related studies conducted in this area (e.g. Wei, 2010; Hu, 2008; Wang et al., 2006), there is little influence of climate change on vegetation in southern China due to plentiful rainfall and suitable temperature, particularly in summer. Therefore, it can be concluded that the major driving force for the decrease of vegetation activities is probably human activity.

3.3 Land use/cover change detection based on post-classification comparison

LUCC in a watershed can be observed from processed aerial photographs and satellite images. Since remotely sensed data from the earth orbit can be obtained repeatedly over the same area, they have been very useful in monitoring and analyzing LUCC in various regions of the earth. A step-by-step evaluation of the images allows one to better understand the cause and effect relationship regarding the LUCC over time. Empirical evidence of LUCC delivered by repeated aerial photography and/or satellite images can greatly contribute to planning and management of available resources, especially in the developing countries where other kinds of background data are often lacking (Tekle & Redlund, 2000). In this section, combined use of remote sensing, GIS and post-comparison methods were employed to detect LUCC.

3.2.1 Data and methodology

Two land use maps of 1980 and 2000, respectively, which were obtained from Chinese Academy of Science (CAS, 2004), are used for LUCC analysis. The two land use maps are shown in Figure 3.8 and Figure 3.9, respectively.

Post-classification comparison is a commonly used technique for classification-based change detection (e.g. Weismiller & Momin, 1977; Rubec & Thie, 1978; Wickware & Howarth, 1981; Burns & Joyce, 1982; Estes et al., 1982; Likens & Maw, 1982; Singh, 1989). This method is found to be the most suitable for detecting LUCC (Larsson, 2002; Liu & Zhou, 2004). In this technique, two types of images from different dates are independently classified. The use of independently produced classifications has the advantage of compensating for varied atmospheric and phenological conditions between dates, or even the use of different sensors between dates, because each classification is independently produced and mapped. Thus, this study is based on post-classification comparison of independently developed and classified land cover maps of 1980 and 2000 from CAS.

Dynamic degree index model, land use transition matrix and land use centroid change model are three simple but powerful methods in post-classification comparison for studies of LUCC (Liu et al., 2006; Wang et al., 2005), which are employed in this study for change detection.

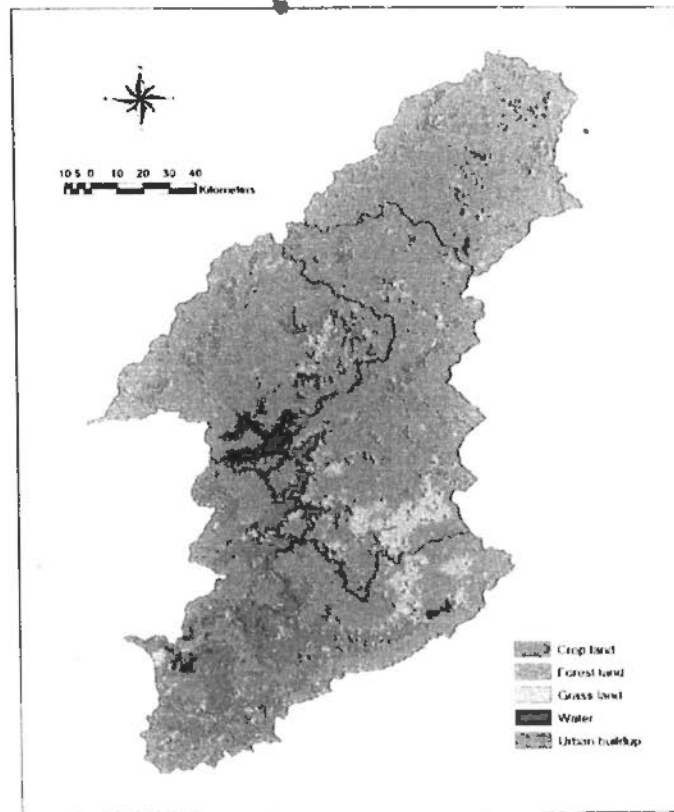


Figure 3.8 Land use map in 1980

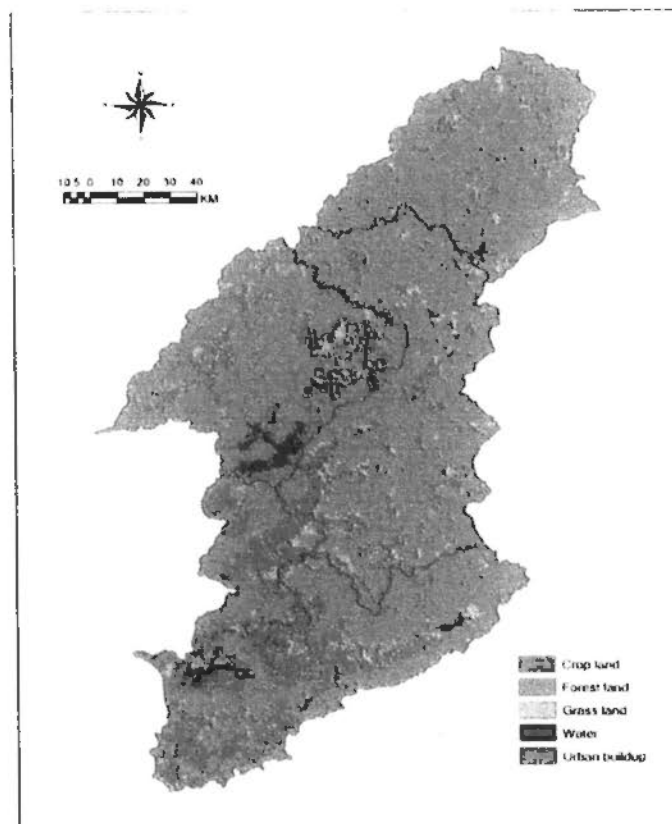


Figure 3.9 Land use map in 2000

3.2.1.1 Dynamic degree index model of land use change

The graphic information characteristics of land use change in difference regions can be expressed by the land use dynamic degree index, the equation form of land use dynamic degree index is:

$$K = \frac{Ua - Ub}{Ua} \times \frac{1}{T} \times 100\% \quad (3-7)$$

In the expression, K is a certain land use type dynamic degree in the period T ; Ua and Ub are total area of a certain land use type at the beginning and end of study period; T is the number of time periods between the beginning and the end (Dan, 2009).

3.2.1.2 The land use transition matrix

The land use transition matrix can be obtained through spatial overlay of the initial and final land use maps with the aid of ARCGIS 9.2. All the technical details of this method can be found in the manual of ARCGIS 9.2 (ESRI, 2007).

3.2.1.3 The centroid change model of land use

The land use centroid change model is illustrated as Figure 3.10. P_1, P_2, \dots, P_n represent different patches of one land use type and the corresponding areas are S_1, S_2, \dots, S_n respectively. The centroid for each patch is expressed as $G_1(x_1, y_1), G_2(x_2, y_2), \dots, G_n(x_n, y_n)$. The centroid for this type of land use can be expressed as follows:

$$X = \frac{\sum_{i=1}^n S_i x_i}{\sum_{i=1}^n S_i} \quad (3-8)$$

$$Y = \frac{\sum_{i=1}^n S_i y_i}{\sum_{i=1}^n S_i} \quad (3-9)$$

Using the centroid change model, the gravity center of land use in both 1980 and 2000 has been calculated in the East River Basin.

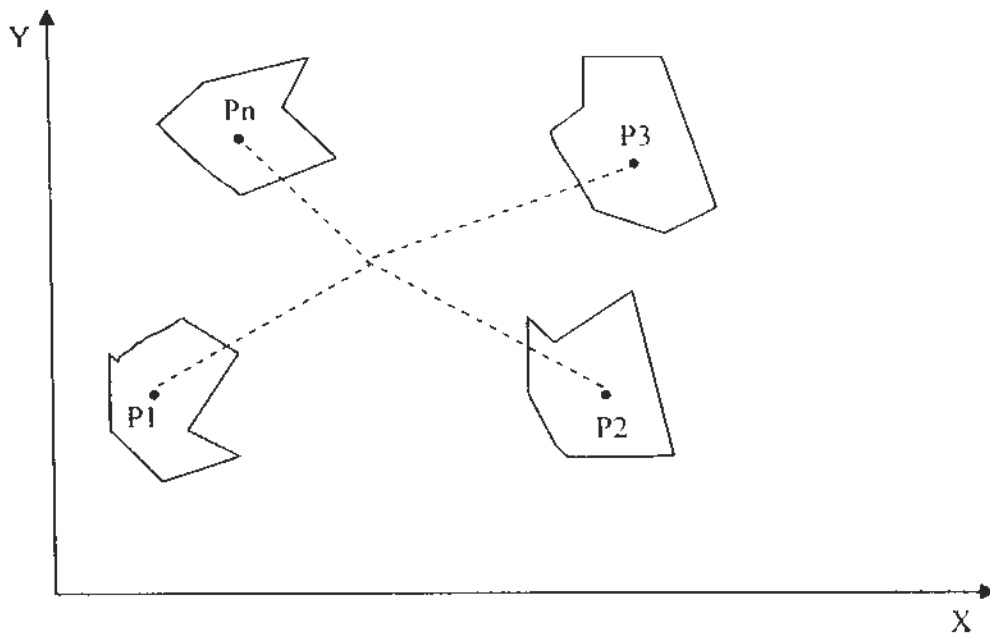


Figure 3.10 Illustration of land use centroid movement model

3.2.1.4 Results and discussion

The statistical summary of land use for different regions in different years is presented in Tables 3.2 ~ 3.5. From the tables, it is clear that there was a sharp increase in the area of urban and built-up from 323 to 841 km² and a slight rise in the area of forest from 20781 to 21814 km². However, the area of grassland decreased from 1581 to 721 km² and the area of cropland decreased from 4000 to 3299 km². The area of water remained constant between 526 and 530. From a single land use's perspective, the change ratio of Urban and built-up area was 7.63%/year, which is the maximum; the change ratio of cropland also reached to 2.6% per year. There was little variation in the change ratio of water area and forest area. From sub-area perspective, the change ratios for Dongguan, Huizhou urban and Baoan, Longgang were greater than others. It is in good agreement with the urban growth and economic development.

Land use transition matrix was employed to further understand land use transition procedure. The results are shown in Table 3.6. In the table, the rows represent the 1980 land use categories and the column represents the 2000 categories. The changed area accounted for 11.4% of the total watershed area, which indicates a high change degree. The increase of Urban and built-up area was mainly transferred from cropland (287 km²), forest (217 km²) and grass land (46 km²). Moreover, the decrease of grassland mainly transferred to forest land (984 km²). There were 284 km² of forest land

transferred to cropland. The decrease of cropland was mainly caused by a transfer of 675 km² cropland to forest land.

The results of land use centroid movement are shown in Table 3.7 and Figure 3.11. The results reveal that there were significant changes in land use centroids from 1980 to 2000. The centroid of grassland moved from east to west with a displacement of 10 km and from south to north with a displacement of 20 km, which is the greatest displacement compared with other land use types. The second largest centroid displacement is from urban and built-up, which moved from east to west with a displacement of 8.9 km and from north to south with a displacement of 18 km. In combination with the previous results, it is concluded that there were significant land use changes in the East River Basin during the two decades, particularly urbanization and grassland degradation were the most significant.

Table 3.2 Land use in 1980 for different regions of the East River Basin (unit: km²)

Region	Cropland	Forestland	Grassland	Urban and built-up	Water
Xunwu	265	1787	88	9	1
Anyuan	73	476	27	5	0
Dingnan	115	823	43	8	2
Xingning	26	247	12	1	1
Longchuan	276	1852	142	21	33
Heping	307	1884	125	13	7
Lianping	185	1761	139	15	3
Dongyuan	473	3219	163	2	214
Heyuan urban	86	194	18	27	10
Zijing	291	2415	144	21	14
Xinfeng	52	1128	213	4	2
Longmen	42	123	11	3	1
Boluo	335	1042	151	33	36
Huizhou Urban	373	661	56	62	93
Huiyang	262	531	45	18	22
Huidong	405	2127	135	44	53
Dongguan	202	284	25	18	17
Baoan	99	78	34	9	3
Longgang	134	148	9	12	13
Dongjiang	4000	20781	1581	323	526

Table 3.3 Land use in 2000 for different regions of the East River Basin (unit: km²)

Region	Cropland	Forestland	Grassland	Urban and built-up	Water
Xunwu	223	1976	21	2	2
Anyuan	62	529	5	1	0
Dingnan	84	950	11	4	3
Xingning	25	265	2	0	1
Longchuan	284	1923	30	14	36
Heping	288	2013	30	8	4
Lianping	176	1870	68	2	2
Dongyuan	435	3386	78	13	219
Heyuan urban	59	204	9	45	9
Zijing	269	2502	79	50	7
Xinfeng	46	1214	135	1	1
Longmen	36	130	8	0	1
Boluo	311	934	70	121	38
Huizhou Urban	273	636	34	166	98
Huiyang	223	449	39	78	23
Huidong	323	2345	58	37	56
Dongguan	98	287	18	98	16
Baoan	39	85	22	46	2
Longgang	45	114	10	156	14
Dongjiang	3299	21814	727	841	530

Table 3.4 Change range of land use for different regions (unit: km²)

Region	Cropland	Forestland	Grassland	Urban built-up	Water
Xunwu	-41	189	-67	-7	0
Anyuan	-11	52	-22	-4	0
Dingnan	-32	127	-32	-4	0
Xingning	-1	18	-10	-1	0
Longchuan	7	71	-112	-8	3
Heping	-19	130	-95	-5	-3
Lianping	-8	109	-71	-12	-2
Dongyuan	-38	167	-85	12	4
Heyuan urban	-27	10	-9	18	-1
Zijing	-22	87	-65	29	-6
Xinfeng	-6	87	-78	-4	0
Longmen	-7	7	-3	-3	0
Boluo	-25	-108	-81	87	2
Huizhou Urban	-99	-24	-22	104	5
Huiyang	-39	-82	-6	60	1
Huidong	-81	218	-78	-6	3
Dongguan	-103	3	-7	80	-2
Baoan	-60	7	-12	37	0
Longgang	-89	-34	1	144	1
Dongjiang	-700	1034	-855	518	3

Table 3.5 Change dynamic degree of land use for different regions (unit: %)

Region	Cropland	Forestland	Grassland	Urban and built-up	Water
Xunwu	-0.74	0.50	-3.61	-3.73	0.26
Anyuan	-0.69	0.52	-3.89	-3.95	0.26
Dingnan	-1.30	0.74	-3.60	-2.53	0.44
Xingning	-0.13	0.35	-4.07	-2.94	0.26
Longchuan	0.13	0.18	-3.77	-1.74	0.36
Heping	-0.29	0.33	-3.61	-1.88	-2.31
Lianping	-0.21	0.30	-2.44	-3.97	-2.57
Dongyuan	-0.39	0.25	-2.47	32.07	0.09
Heyuan urban	-1.50	0.25	-2.39	3.13	-0.55
Zijing	-0.36	0.17	-2.14	6.75	-2.22
Xinfeng	-0.55	0.37	-1.74	-4.15	-0.74
Longmen	-0.74	0.26	-1.49	-4.15	0.26
Boluo	-0.35	-0.49	-2.56	12.47	0.22
Huizhou Urban	-1.27	-0.18	-1.87	8.06	0.26
Huiyang	-0.72	-0.74	-0.60	15.85	0.26
Huidong	-0.96	0.49	-2.73	-0.70	0.26
Dongguan	-2.44	0.05	-1.37	21.30	-0.43
Baoan	-2.88	0.44	-1.67	18.59	-0.84
Longgang	-3.16	-1.09	0.41	57.33	0.26
Dongjiang	-0.83	0.24	-2.57	7.63	0.03

Table 3.6 Land use transition matrix for 1980 and 2000 (unit: km²)

Land use type	Cropland	Forestland	Grassland	Water	Urban and built-up	Total (1980)
Cropland	2907	675	90	40	287	4000
Forestland	284	20082	155	43	217	20781
Grassland	73	984	477	1	46	1581
Water	19	58	2	444	3	526
Urban and built-up	16	14	2	2	288	323
Total (2000)	3299	21814	727	530	841	27211
Changing area	700	1034	-855	3	518	3110
Changing ratio	17.51	4.97	-21.37	0.66	160.33	11.43

Table 3.7 Centroid movement of different land use types (unit: km)

Land use type	1980		2000		Displacement	
	$x_1(^{\circ})$	$y_1(^{\circ})$	$x_2(^{\circ})$	$y_2(^{\circ})$	Δx (km)	Δy (km)
Cropland	114.58	23.43	114.63	23.54	3.1	12.0
Forestland	114.91	24.02	114.92	23.98	1.0	3.0
Grassland	114.90	23.61	114.82	23.80	10.0	20.0
Water	114.56	23.60	114.55	23.57	0.7	2.0
Urban and built-up	114.38	23.06	114.28	22.89	8.9	18.0

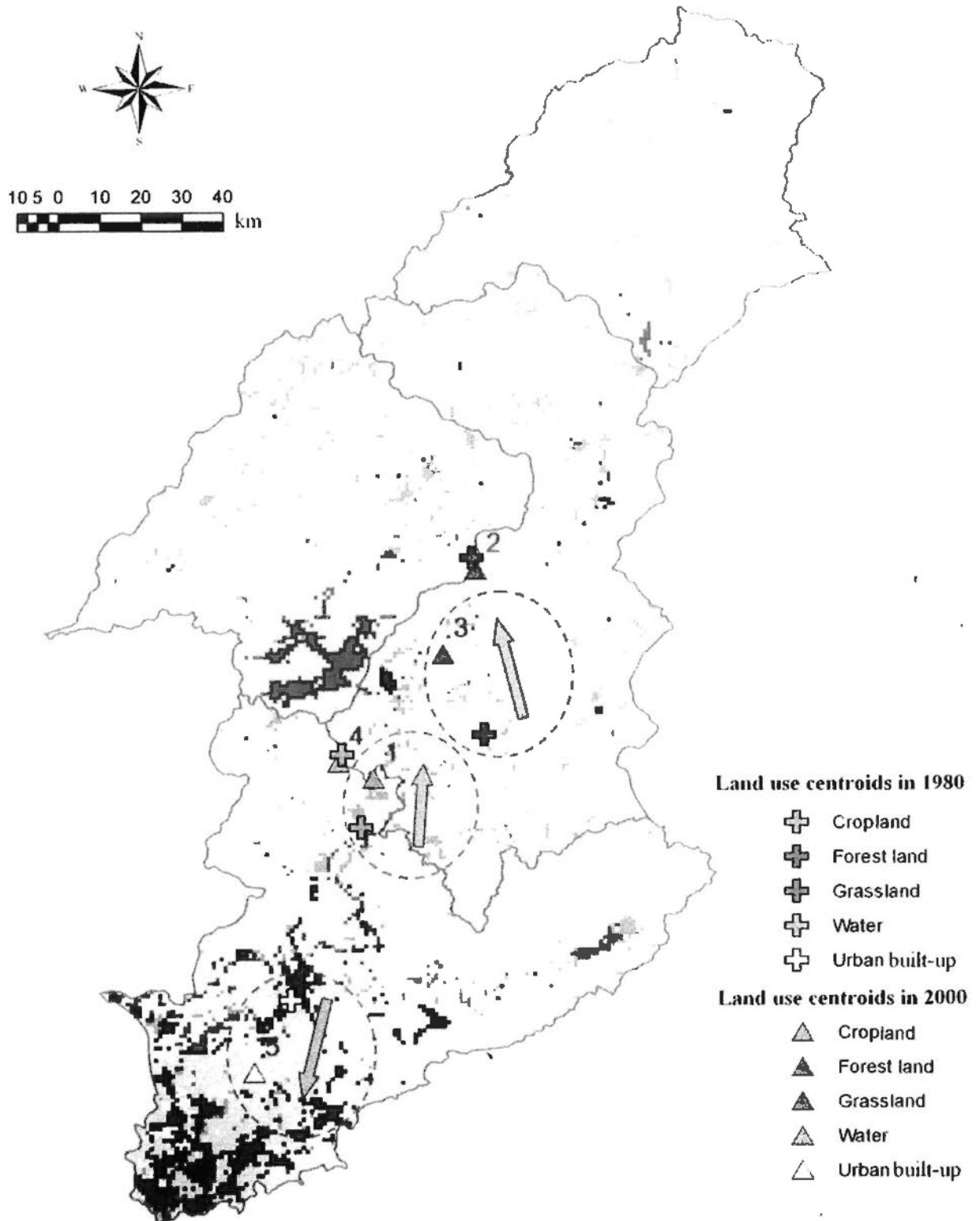


Figure 3.11 Centroids movement of different land use types from 1980 to 2000

3.4 Land use/cover change prediction

In order to offer an insight into the details of land use/cover change (e.g. broad-leaf forest, needle-leaf forest, mixed forest) and provide a boundary condition (Yuan, 2006) of projected LUCC for hydrologic impact studies, the land use maps from CAS are too coarse to satisfy the need. Therefore, detailed land use classification maps are needed to distinguish different tree species for a large area. However, land use classification for a large area is a hard nut to crack and needs intensive studies, which is not the focus of hydrology studies. The land use/cover products of MODIS can provide detailed land use classification and has a much higher accuracy (Ran, 2009) and high resolution in China comparing with other land use/cover products (e.g. IGBP, GLC 2000). Therefore there are amount of studies on LUCC in the East River Basin using MODIS DATA (e.g. Wang, 2006; Wei, 2010; Xie, 2009). Moreover, comparing with land use maps from CAS and groundtruthing of field works conducted in 2008, the land use/cover products of MODIS have good accuracy in the East River Basin. As a result, it can be adopted in this study.

On the other hand, LUCC is a very complicated process and is the result of complex interaction among climatic, socio-economic and biotic system. Therefore, accurate prediction of land use change calls for intensive studies due to so many driving forces, which is beyond the scope of this dissertation. Markov chain modeling is basically a simulation technique which has been widely applied to the analysis of land use change (e.g. Bell, 1974; Weng, 2002; Liu et al., 2005). Since LUCC is probably not a stationary process, the justification of Markov chain model for LUCC prediction should be made firstly. According to relevant LUCC studies in the East River Basin (e.g. Wei, 2010; Hu, 2009; Liu, 2005), the economic grows steadily and land management policy is strictly carried out in recent years in the East River Basin. Moreover, the projected year is 2010, which is a short-term prediction. Therefore, the short-term LUCC in the East River Basin can be considered as stationary Markov process.

In this section, in order to provide one scenario of projected LUCC for studying hydrologic response to changes of different vegetation types, land use change prediction is conducted using the MODIS DATA with a resolution of 500 m × 500 m with the aid of Markov chain method.

3.3.1 Data acquisition and pre-processing

Firstly the MODIS MCD12Q1 products of land use/cover data were downloaded from the website of the Land Processes Distributed Active Archive Center (LP DAAC, 2010), located at the U.S. Geological Survey (USGS) Earth Resources Observation and Science (EROS) Center (lpdaac.usgs.gov), and then extracted the data by boundary of the East River Basin with aid of ARCGIS 9.2. According to the manual of the products, the maps were recoded according to University of Maryland (UMd) Global Land Cover Classifications System (LPDAAC, 2010). Finally the accuracy of the data should be made by comparing with land use maps from CAS and ground truthing of field works conducted in 2008. The maps of 2002 and 2008 are presented in Figure 3.12.

The percentages of each land cover in different years are summarized in Figure 3.13. As shown in Figure 3.13, it is observed that the dominant land cover types are broadleaf forest and woodland, which occupy 69.63 % on average. There are significant changes in the 7 years, particularly the changing point occurs in 2005, broadleaf decreases to the lowest and woodland increases to the highest. However, cropland reaches to the lowest. The urban & built-up remains constant which indicates that urbanization reaches in a stationary state.

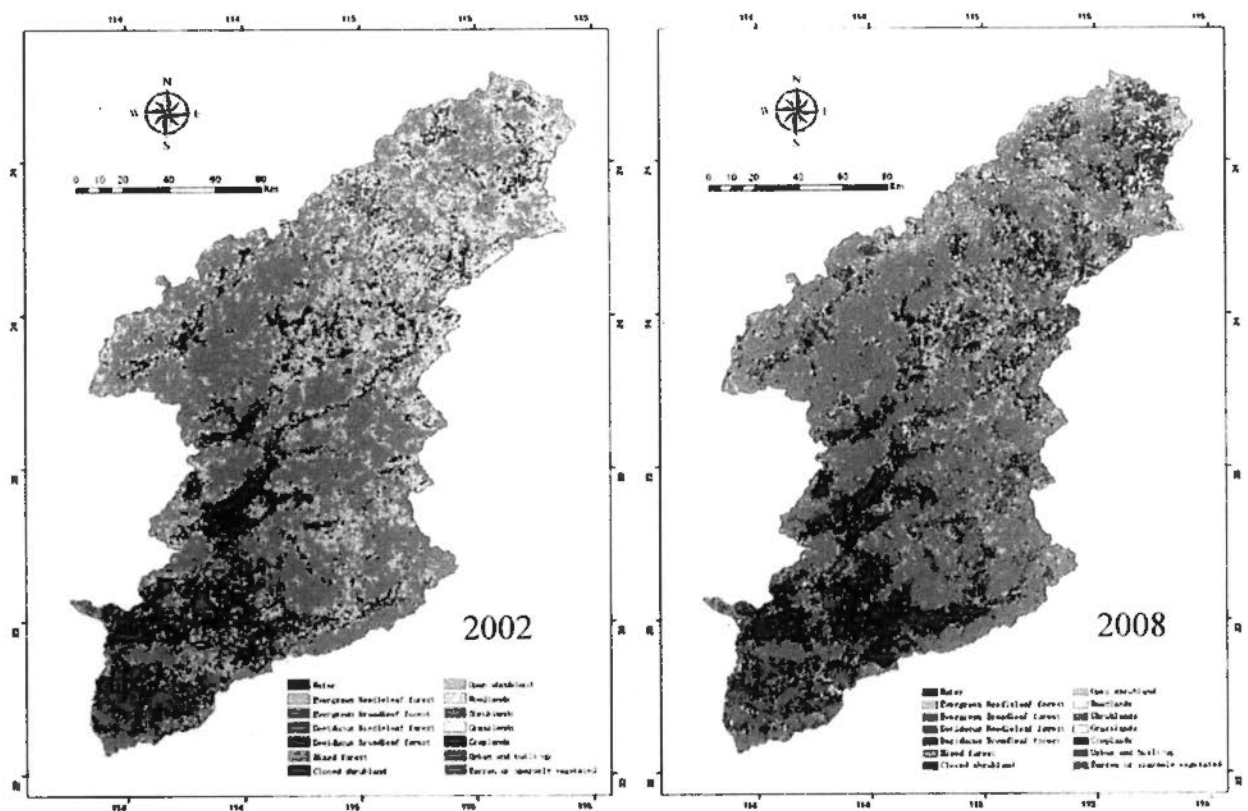


Figure 3.12 Land cover maps in 2002 and 2008 (MODIS 500 m * 500 m)

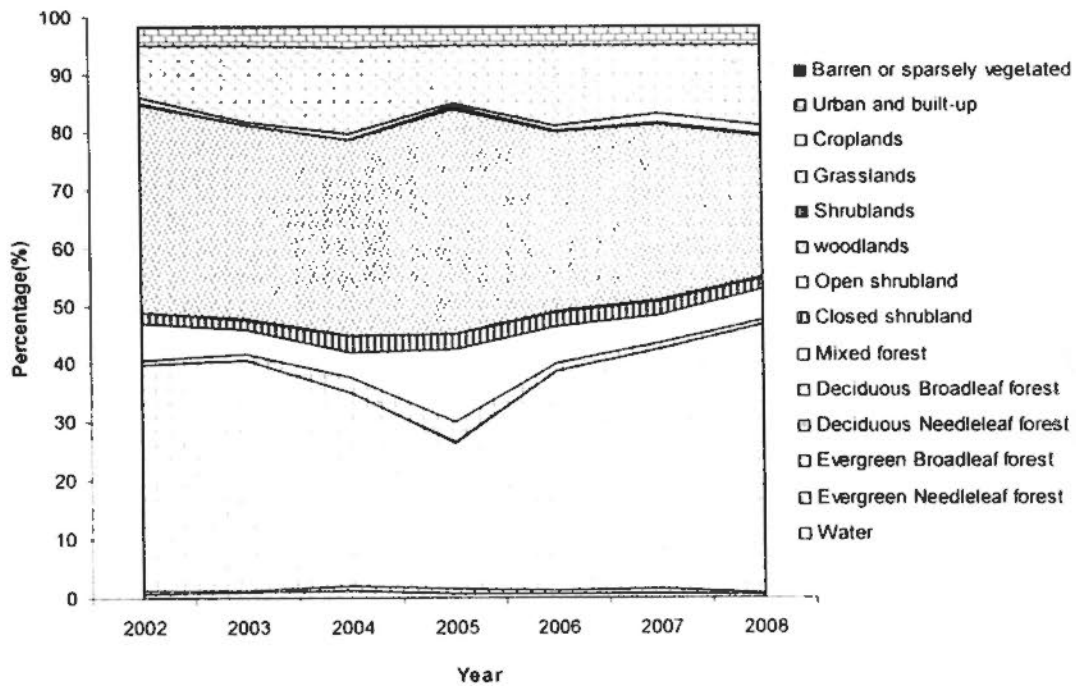


Figure 3.13 Ratios of different land cover in different years

3.3.2 Markov chain modeling of land use change

Markov chain modeling is basically a simulation technique which has been applied to the analysis of land use change. It is worth noting, however, that the application of Markov analysis for the prediction of long-term land use changes is included among the proposals of the LUCC Implementation Plan (LUCC, 1999). An earlier study is reported by Geoghegan et al. (1998).

A. Markov process is a stochastic process with particular characteristics which distinguish it from other stochastic processes. For a system of interest, i.e. a parcel of land, there is a set of discrete states (or classes) – S_1, S_2, \dots, S_n (i.e. different types of land use). The process can be in one and only one of these states at a given time. It moves successively from one state to the other with some probability which depends only on the current state and not on the previous states. This is a process without memory (Briassoulis, 2000).

Land use/cover change has several similar characteristics as Markov process (Wei, 2010): (1) For a specific area, there are mutual transformations among different land use types; (2) The mutual transformation processes are so complex that they contain a lot of processes that cannot be expressed in a physical/mathematical way. Therefore, Markov chain analysis provides a convenient tool for modeling land use change when changes

and processes in the landscape are difficult to describe. As mentioned previously, a Markov process is one in which the future state of a system can be modeled purely on the basis of the immediately preceding state. Markov chain analysis will describe land use change from one period to another and use this as the basis to project future changes. This is achieved by developing a transition probability matrix of land use change from time one to time two, which shows the nature of change while still serving as the basis for projecting to a later time period.

The probability of moving from one state i to another state j is called a transition probability, P_{ij} , and it is given for every ordered set of states. These probabilities can be represented in the form of a transition matrix, P , as shown below:

$$P = \begin{bmatrix} P_{11} & P_{12} & \dots & P_{1n} \\ P_{21} & P_{22} & \dots & P_{2n} \\ \dots & \dots & \dots & \dots \\ P_{n1} & P_{n2} & \dots & P_{nn} \end{bmatrix} \quad (3-14)$$

where P_{ij} is the transform probability of landscape types.

The transform probability P_{ij} can be calculated as shown in equation 3-15.

$$P_{ij} = CA_{ij} / CA_i \quad (3-15)$$

where CA_{ij} is the changing area from i type to j type and CA_i is total changing area of land use type i in the study period. The characters of P_{ij} are:

$$0 \leq P_{ij} \leq 1 \quad (3-16)$$

$$\sum_{i=1}^n P_{ij} = 1 \quad (3-17)$$

Given the matrix P of transition probabilities, its use to project future changes in land use is as follows. A vector, L_0 , depicting the distribution of land uses among the different types at the beginning of the period is required. The vector, L_t , showing the distribution of land use types at the end of the projection period is found by the following formula:

$$L_t = L_0 P \quad (3-18)$$

The distribution of land use types after k time periods (of a given length) is found by powering matrix P :

$$L_t^k = L_0 P^k \quad (3-19)$$

According to Briassoulis (2000), Markov chain analysis is a rather involved statistical method of analysis and its use requires thorough understanding of the mathematics and statistics involved as well as rigorous tests of the basic assumptions made; namely, that the observed processes are Markov processes and, in particular, stationary Markov processes. Moreover, Markov analysis of land use change is an aggregate, macroscopic modeling approach as it does not account for any of the drivers of land use change. Instead, it assumes that all forces that worked to produce the observed patterns and governed their transition probabilities will continue to do so into the future. However, it still can provide some information for constructing future scenarios for studying hydrologic impacts of LUCC.

In this section, according to related studies in the East River Basin (Wei, 2010; Hu, 2009; Liu, 2005), the economic grows steadily and land management policy is strictly carried out in recent years in the East River Basin. Moreover, the projected year is 2010, which is a short-term prediction. Therefore land use prediction based on Markov chain model can be made under the assumption that the future development is following the current socio-economic conditions, i.e. it does not consider any drivers of land use change, to project the land use in 2010 with Markov chain characteristics, which will be further used as one set of scenario for future research on hydrologic response to LUCC.

3.3.2 Results and discussion

The transition probability matrix records the probability that each land cover category will change to the other category, which is presented in Table 3.8. The rows represent the 2002 land cover categories and the column represents the 2008 categories.

As shown in the table, water area has a 0.7344 probability of remaining water area and a 0.0448 of changing to evergreen needle-leaf forest in 2010, which may not however be a true projection of this class except there is an occurrence of drought in the region. Deciduous broadleaf forest during this period will likely maintain its position as the highest class with a 0.5038 probability of remaining deciduous broadleaf forest in 2010. Built-up land also has a probability as high as 1.0 to remain as built-up land in 2010 which signifies the stability. On the other hand, the 0.4050 probability of change from mixed forest to deciduous broadleaf forest shows that there might likely to be a high

level of instability in forest land during this period. This would happen because eucalyptus is widely planted in the East River Basin.

Figure 3.14 shows the statistics of land use land cover projection for 2010. Comparing the percentage representations of Figure 3.13 and Figure 3.14, there are similarities in the observed distribution particularly in 2008. It is easy to come to the following conclusion: under the assumption that the future development is following the current social-economic conditions without any other driving forces, the dominated land cover in the study area in 2010 remain evergreen broadleaf forest, woodland and grassland. Woodland, which occupied 24.6% of the total in 2008, has a decrease of 9.84% in 2010; evergreen broadleaf forest, which accounted for 46.6% of the total in 2008, has an increase of 3.48% compared with 2008. The cropland and grassland increased by 7.76 and 7.23, respectively. However, there was a decrease in mixed forest with 5.88%.

Table 3.8 Transitional Probability table derived from the land use/cover maps of 2002 and 2008

2008 \ 2002	Water	Evergreen needleleaf forest	Evergreen broadleaf forest	Deciduous needleleaf forest	Deciduous broadleaf forest	Mixed forest	Closed shrublands	Open shrublands	Woodland	Shrubland	Grasslands	Croplands	Urban and built-up	Barren or sparsely vegetated
Water	0.7344	0.0448	0.0486	0.0008	0.0052	0	0	0.0017	0.0916	0	0	0	0	0.0728
Evergreen needleleaf forest	0.0274	0.1073	0.1517	0.0102	0.0359	0.0889	0.0187	0	0.5472	0	0	0	0	0.0128
Evergreen broadleaf forest	0	0.0017	0.8723	0.0002	0.0049	0.0518	0.0006	0	0.0684	0	0	0	0	0.0001
Deciduous needleleaf forest	0	0.226	0.4043	0	0.162	0	0	0	0.1911	0	0	0.0165	0	0
Deciduous broadleaf forest	0.0045	0	0.5038	0.0017	0.0539	0.0881	0.0016	0.0007	0.3329	0	0	0.0128	0	0
Mixed forest	0.0004	0.0008	0.5453	0	0.0057	0.226	0	0.0002	0.2167	0.0006	0	0	0	0.0001
Closed shrublands	0	0.0008	0	0.0019	0.0022	0.0061	0.3143	0.0579	0.2222	0.0056	0.1543	0.2332	0	0.0015
Open shrublands	0.009	0.0742	0	0	0.0096	0	0.2694	0.2059	0.134	0.0377	0.2421	0	0	0.0181
Woodland	0	0.0006	0.1631	0	0.0176	0.0384	0.022	0.0002	0.5359	0.0107	0.019	0.1924	0	0.0001
Shrubland	0.0076	0.0037	0.23	0	0.0182	0.043	0.0476	0	0.4139	0.0243	0.0111	0.2006	0	0
Grasslands	0.0109	0.0347	0.0094	0.0022	0.0163	0.0293	0.0709	0.0218	0.299	0	0.1667	0.3368	0	0.002
Croplands	0.0003	0	0	0	0.0096	0.0157	0.0403	0.0025	0.2152	0.0121	0.0375	0.6666	0	0.0001
Urban and built-up	0	0	0	0	0	0	0	0	0	0	0	0	1	0
Barren or sparsely vegetated	0.1244	0.1623	0	0	0.0063	0	0.0578	0.0135	0.1995	0	0	0.2965	0	0.1397

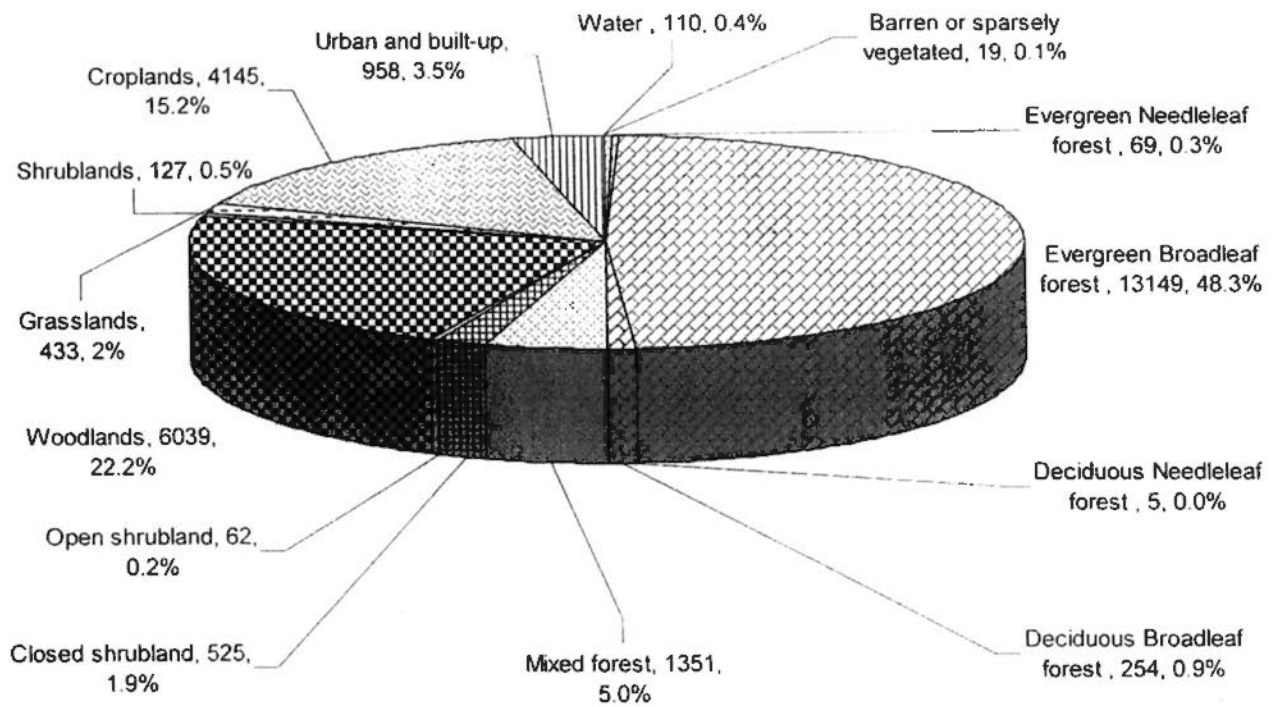


Figure 3.14 Projected Land use land cover for 2010 (unit: km²)

3.5 Summary and conclusion

The aims of this chapter are to evaluate LUCC, understand implications of LUCC and provide boundary condition for the integrated eco-hydrologic modeling in the future. From this study, it can be concluded that the East River Basin had experienced significant changes in land use and land cover over the past two decades.

From the spatio-temporal analysis of vegetation dynamics based on NDVI, it can be concluded as follows. On one hand, spatially speaking, the NDVI value decreased from the upper-middle-part (agricultural region) to the lower-part (urban area) in the study area, which demonstrates that human activities can influence vegetation activities (plant growth). On the other hand, temporally speaking, NDVI decreased significantly in summer (June to September) over the years. According to related studies conducted in this area (e.g. Wei, 2010; Hu, 2008; Wang et al., 2006), there is little influence of climate change on vegetation in southern China due to plentiful rainfall and suitable temperature, particularly in summer. Therefore, it can be concluded that the major driving force for the decrease of vegetation activities is probably human activity.

From post-classification comparison of LUCC, it is concluded that the East River Basin had experienced a significant change in land use and land cover over the past two decades. Particularly there was a sharp increase of Urban and built-up area and a significant decrease of grassland and cropland. It is identified that the increase of Urban and built-up area was mainly transferred from cropland (287 km²), forest (217 km²) and grassland (46 km²); moreover, the decrease of grassland mainly transferred to forest (984 km²). There were 284 km² of forest land transferred to cropland. The decrease of cropland was mainly caused by a transfer of 675 km² cropland to forestland. The analysis is very useful in understanding the mutual transition among different land use types, which can provide information for constructing scenarios for studying hydrologic impact of LUCC in the future.

From the results of land use change prediction based on MODIS MCD12Q1 data with aid of Markov chain model, it can be concluded that the dominant land cover in the study area in 2010 remain evergreen broadleaf forest, woodland and grassland. Woodland, which occupied 24.6% of the total in 2008, has a decrease of 9.84% in 2010; evergreen broadleaf forest, which accounted for 46.6% of the total in 2008, has an increase of 3.48% compared with 2008. The cropland and grassland increased by 7.76 and 7.23, respectively. However, there was a decrease in mixed forest with 5.88%. The predicted scenario can be used as one set of scenario for studying hydrologic impact of LUCC in the future.

In summary, the LUCC analysis in this chapter provides a basis for understanding the LUCC and its implications at basin scale, which can also lay a solid foundation for providing input and constructing related scenarios for future research on hydrologic impacts of LUCC.

CHAPTER 4

EVAPOTRANSPIRATION (ET) MAPPING WITH AID OF GIS/RS

4.1 Introduction

Evapotranspiration (ET) refers to the rate of the conversion of liquid water to water vapor from water, soil surfaces, and through vegetation at the land surface, which has long been recognized as the most important process in the determination of the exchanges of energy and mass among hydrosphere, atmosphere and biosphere (e.g. Bowen, 1926; Penman, 1948; Monteith, 1965; Priestley and Taylor, 1972; Brutsaert, 1982; Morton, 1983; Menenti, 1984; Famiglietti and Wood, 1994; Sellers et al., 1996; Su and Menenti, 1999). It is the result of complex interaction between water and energy fluxes subjected to changing atmosphere, soil and vegetation conditions. The complex variations in climate, terrain features, and vegetative covers complicate our attempt to quantify the ET at a regional scale adequately. Furthermore, ET estimation is further complicated by evaporative fluxes varying diurnally and seasonally (Getu, 1998). As a result, ET as a major hydrologic component has traditionally been one of the most difficult hydrological processes to determine.

On the other hand, ET is also an important ecological element (plant physiological processes) that can establish links between monthly water balance and vegetation dynamics. Firstly, land use change has a direct effect on hydrology through its link with the ET regime (Dunn & Mackay, 1995). The dominant process for driving the water yield in response to land use/cover change is ET (Turner, 1991; Zhang et al., 2001). Secondly, ET is one of the most important processes occurring at the land-surface and affecting the atmosphere and hence, climate. It plays the dual roles of providing water vapor to the atmosphere as well as absorbing incident radiation in the processes. ET has long been recognized as playing an essential role in determining exchanges of energy and mass between the hydrosphere, atmosphere, and biosphere (e.g. Bowen, 1926; Jia et al., 2003; Monteith, 1965; Penman, 1948; Priestley et al., 1972; Su, 2002). These roles make it a key process in the water budget and the energy budget as well as providing a strong link between them (Figure 1.3). Moreover, in modern eco-hydrological modeling accurate estimates of evapotranspiration are indispensable both for water and energy balance studies and for assessment of hydrological impact of man-made changes such as

land use changes. Therefore, ET has undoubtedly been one of the most difficult eco-hydrological processes to quantify. Mapping ET becomes a very important step in integrated eco-hydrologic modeling for assessment of hydrologic impact of LUCC.

Figure 4.1 summarizes the research gaps in ET studies and illustrates ET as a core in studying hydrologic impact of LUCC. As shown in the figure, conventional techniques that employ point measurements to estimate ET and the components of energy balance are only representative of local scales and cannot be extended to large areas because of the heterogeneity of the land surface and the dynamic nature of heat transfer processes. Remote sensing is probably the only technique which can provide representative measurements of several relevant physical parameters at scales from a point to the macro scale. Techniques using remote sensing information to estimate atmospheric turbulent fluxes and evapotranspiration are therefore essential when dealing with processes that can not be represented only by point measurements.

The remote-sensing-based areal ET estimation model, Surface Energy Balance System (SEBS) was developed by Su (2002) to estimate land surface fluxes using remotely sensed data and available meteorological observations. It has the most important advantage of including a physical model for the estimation of the roughness height for heat transfer which is the most critical parameter in the parameterization of the heat fluxes of land surface. SEBS has a very strong physical basis, which does not require too many parameters or other intensive meteorological data; therefore, it has been widely applied in Spain (van der Kwast et al., 2009) and Dutch (e.g., Weligepolage, 2005; Hailegiorgis, 2006) in Europe and northwestern China (Li, 2001; Su et al., 2003). The practical application has proved that it has a clear physical meaning and good accuracy for lowland-shrub region with relatively heterogeneous underlying surface (e.g., Su, 2002; Su et al., 2003; Zhan, 2005; Lin et al., 2008). However, there are few studies on its application in southern China. Moreover, the applicability in the area with heterogeneous underlying surface and complex vegetation conditions has been challenged by many scholars (e.g., Zhan, 2005; He et al., 2006; Lin et al., 2008). In the original SEBS, for LAI, the formula is strictly only good for low vegetation since NDVI saturates at higher LAI values; for aerodynamic roughness height (Z_{0m}) and displacement height (d_0), there is only one empirical equation for all types of land cover

can not represent the complex vegetation conditions. Therefore, an enhancement has to be made for SEBS's application in complex vegetated area.

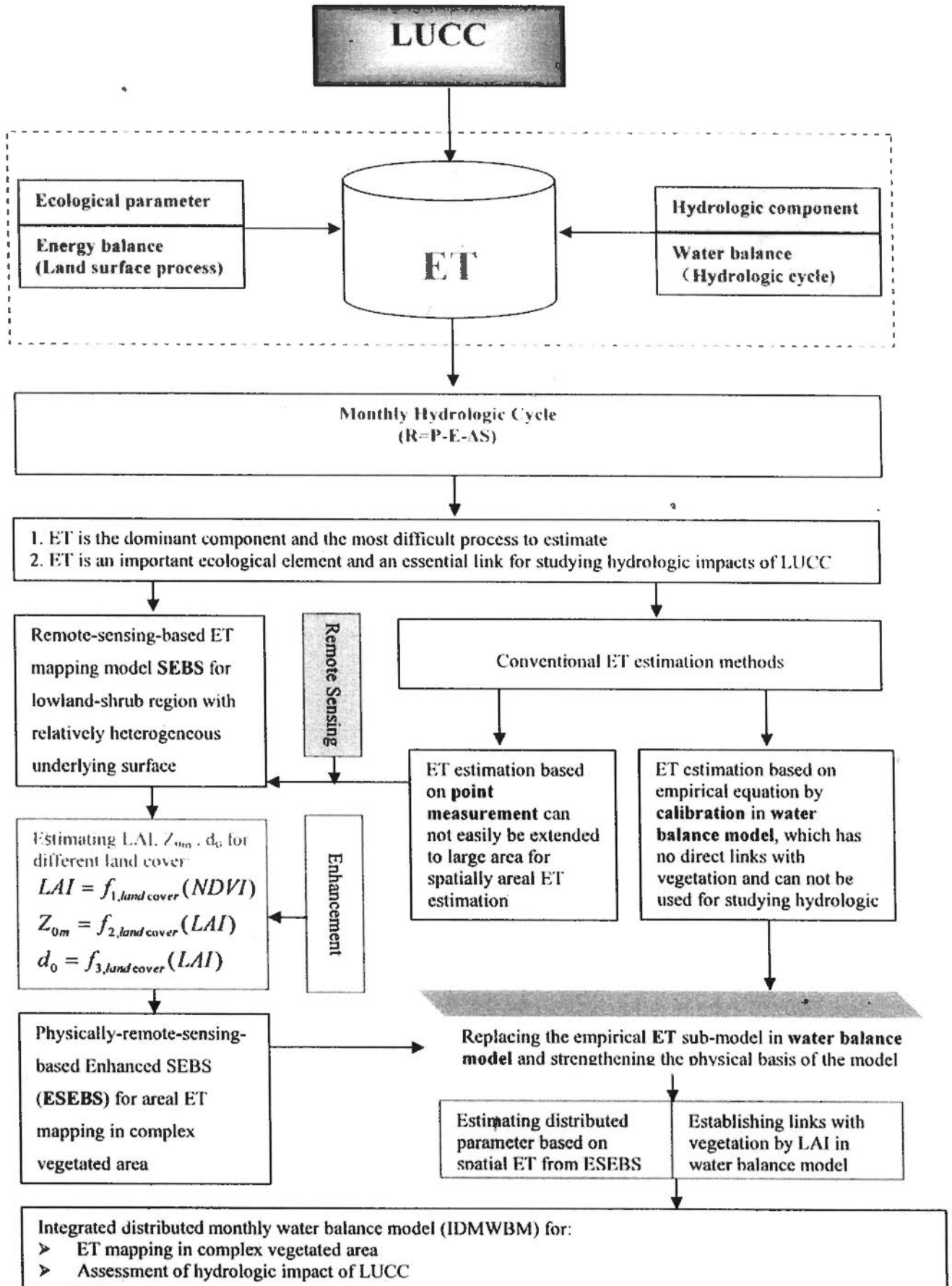


Figure 4.1 Summary of ET as a core in the studies of hydrologic impacts of LUCC

As shown in Figure 4.1, in order to enhance the SEBS for application in complex vegetated area, firstly relationship of LAI and NDVI are identified based on remote sensing data and field measured data using regression model. Secondly, based on the identified LAI-NDVI relationship mentioned above, in combination with the experiments in China as reported in Zhang (1996), estimation of aerodynamic roughness height z_{om} and the displacement height d_0 can be improved for application in complex vegetated area, which will be discussed in detail in the following section. Through model enhancement, the SEBS has a much stronger physical basis and a wider applicability, particularly for the complex vegetated area in southern China.

Furthermore, as most monthly water balance model oversimplify ET component with empirical equation and has no direct links with vegetation. The enhance SEBS has a clear physical basis and generates spatially-distributed ET, which can be further integrated into monthly water balance model for strengthening the physical basis and establishing links between hydrologic processes and vegetation.

This chapter firstly describes the data used in the ET mapping study. Secondly, in order to have a better understanding of remote-sensing-based ET model, the SEBS is described in details. Moreover, the SEBS is enhanced for application in complex vegetated area by estimating LAI, aerodynamic roughness height z_{om} and displacement height d_0 for different land cover. Furthermore, the enhanced SEBS (ESEBS) is employed to estimate the surface fluxes and estimate areal ET spatially over the East River Basin based on NOAA/AVHRR images. In addition, the results of SEBS are validated with complimentary relationship ET models (AA/GG/CARE) and Distributed Monthly Water Balance Model. Lastly, spatio-temporal variation of ET in the East River Basin is analyzed.

4.2 Data

4.2.1 Hydrologic data

The data for model calibration and validation include monthly potential evaporation data, monthly rainfall data, and monthly streamflow data. All the data are obtained from the published Yearly Hydrological Reports of China for the period from 1980 to 2000. Occasional missing data are estimated from the data of adjacent stations using the method of linear regression. A network of over 170 rainfall stations in the basin is operated by the hydrological institution of Guangdong at present, but about 90 stations of which were established between the end of 1960s and the beginning of 1970s. In this study, 46 major stations of relatively even distribution over the whole basin and 21-year continuous records (1980-2000), are selected for model calibration and validation (see Figure 4.2).

The model input of areal rainfall is calculated using the records of the 46 stations and the Thiessen polygon method. Pan evaporation ($\Phi 80$ cm) data of 3 weather stations are averaged to estimate areal potential evaporation. The three climate stations are located in Longchuan, Heyuan, and Boluo, respectively. The monthly streamflow data are from the Boluo stream gauging station, above which the drainage area is 25,325 km². River discharge at Boluo station is affected by three large reservoirs upstream (Fengshuba, Xinfengjiang, and Baipan Zhu). Streamflow records do not represent the flow regimes under natural conditions. Therefore, the streamflow data must be adjusted to the natural streamflow for calibrating and validating the monthly water balance models. Figure 4.3 presents the areal mean monthly values over the 21-year record (1980~2000) for observed pan evaporation, rainfall, runoff, and air temperature for the East River Basin.

4.2.2 Meteorologic Data

Long-series meteorological data from three meteorological stations (Heyuan, Lianping, Huiyang), which are derived from national meteorological database of China, State Meteorological Administration, is employed in this study, which includes:

- (1) Daily wind speed: 1980~2000
- (2) Daily air temperature: 1980~2000
- (3) Daily sunshine hours: 1980~2000
- (4) Daily relative humidity 1980~2000

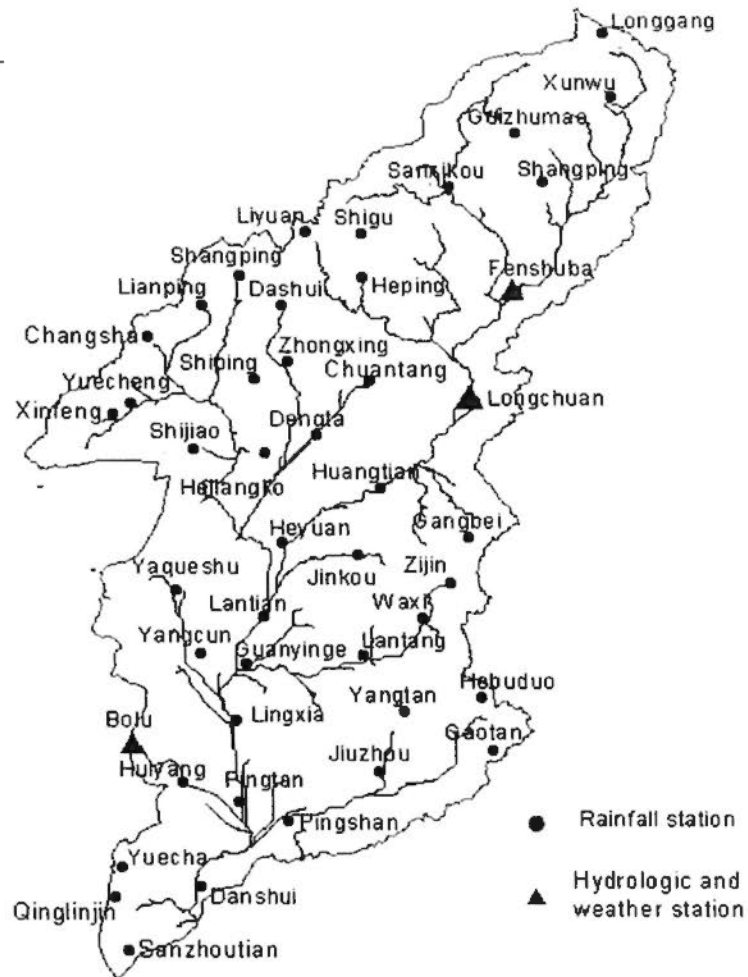


Figure 4.2 Location of rainfall, hydrologic and weather stations

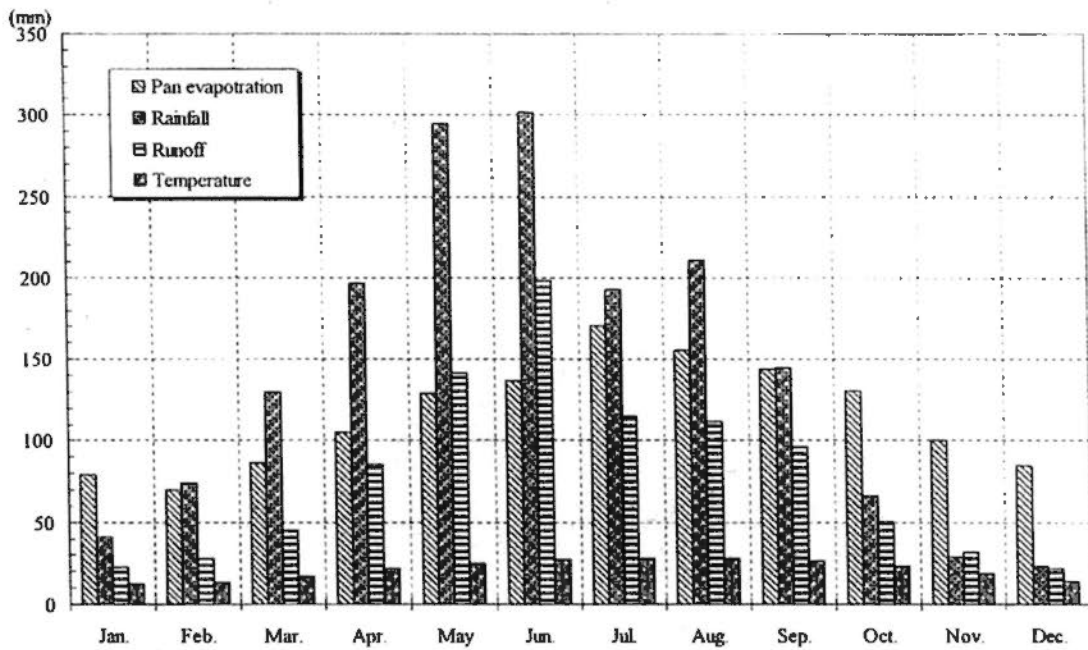


Figure 4.3 Areal mean monthly pan evaporation, rainfall, runoff and temperature of the East River Basin from 1980 to 2000

4.2.3 Satellite Data

The NOAA/AVHRR data are employed to conduct this study. The Advanced Very High Resolution Radiometer (AVHRR) is a cross-track scanning system with five spectral bands having a resolution of 1.1 km and a frequency of earth scans twice per day (0230 and 1430 local solar time). AVHRR data provide opportunities for studying and monitoring vegetation conditions in ecosystems including forests, tundra and grasslands. AVHRR data are also used to retrieve various geophysical parameters such as sea surface temperatures and energy budget data (NOAA).

The following NOAA/AVHRR data is employed to conduct this study:

- (1) NOAA AVHRR (LAC/HRRT) level 1B: 1.1 km × 1.1 km, 1982~2000, channel 1~channel 5.
- (2) NOAA AVHRR NDVI/LAI: 1982~2003 (Monthly), 8 km × 8 km.
- (3) Land use/cover data: China land use/cover in 1980 and 2000, 1 km × 1 km.

The NOAA AVHRR (LAC/HRRT) level 1B requires preprocessing work, namely, data calibration (Radiometric correction and Geo-referencing) and resizing, which was conducted with the aid of ENVI 4.6.

4.2.4 Field measurement data

From December 2008 to December 2009, monthly field work was conducted in the East River Basin by our research group (together with research group from Hohai University, Nanjing). A total of 305 sample points are selected for LAI measurement and ground truthing. The field trip itinerary and sample points are illustrated as Figure 4.6.

(1) LAI measurement

At each sample point, the Tracing Radiation and Architecture of Canopies (TRAC), which is developed by Canada Centre for Remote Sensing, was used to measure LAI. The results are shown in Figure 4.7 and Table 4.1.

(2) Ground truthing

At each sample point, digital camera was used to record vegetation types. The selected photos for ground truthing are shown in Figure 4.8.

4.2.5 Other data

DEM: USGS GTOPO30 (1 km × 1 km).

Soil data: Soil Map China.

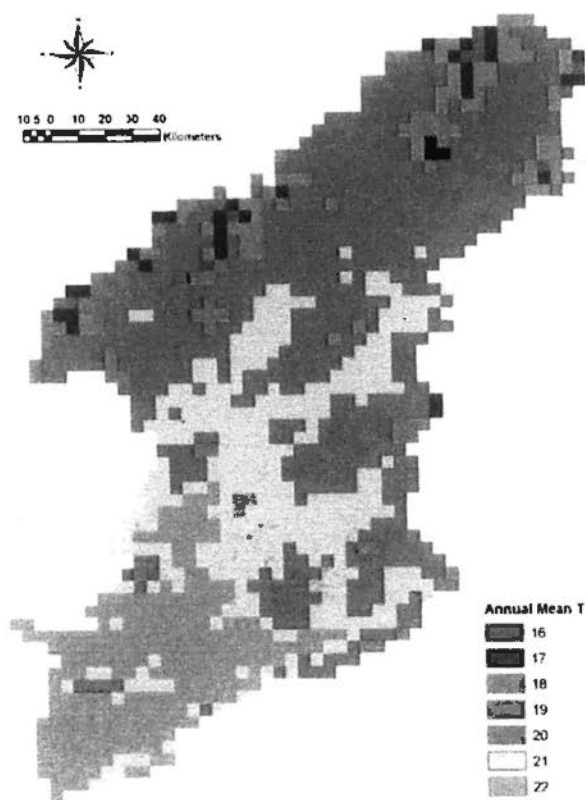


Figure 4.4 Spatial distribution of annual mean temperature

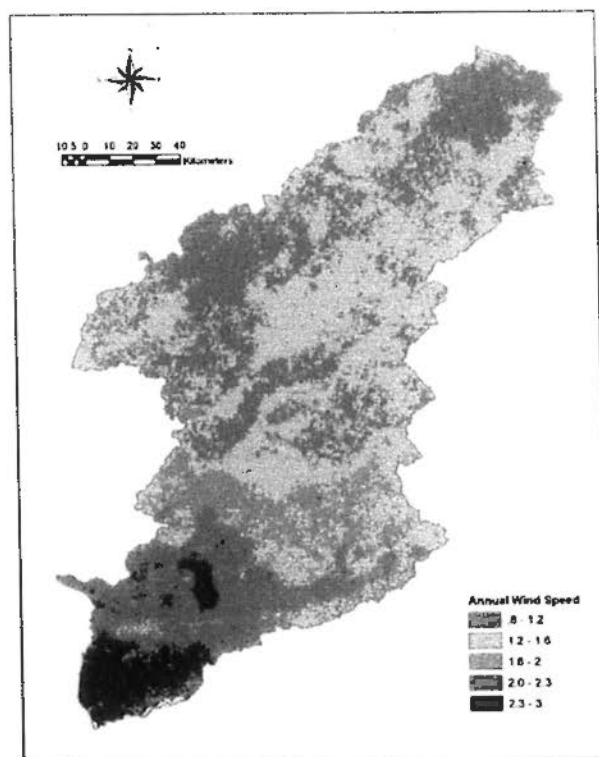


Figure 4.5 Spatial distribution of annual mean wind speed

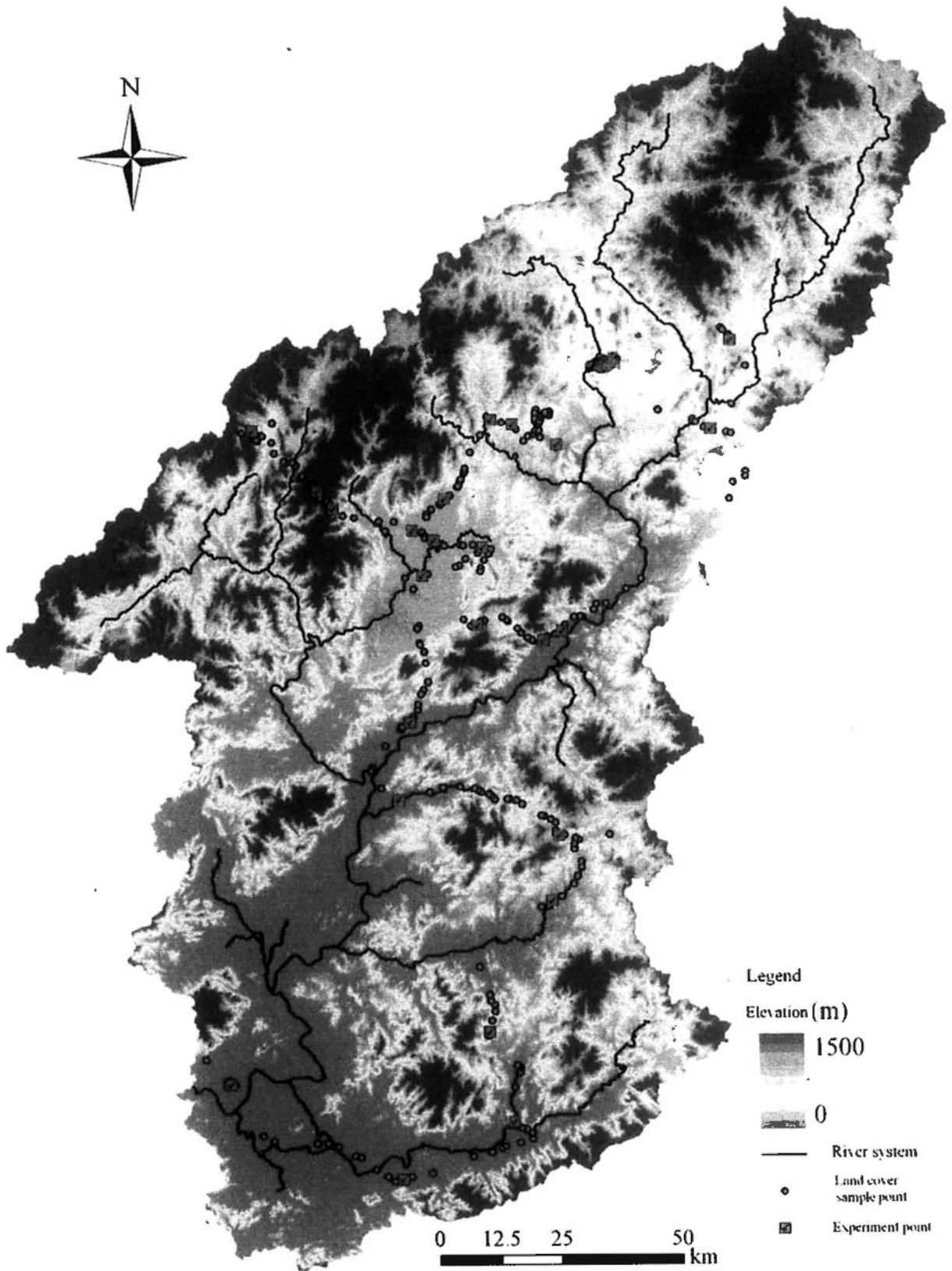


Figure 4.6 Field work for ground truthing and LAI measurement conducted from December 2008 to December 2009

Field-measured monthly LAI for different land cover

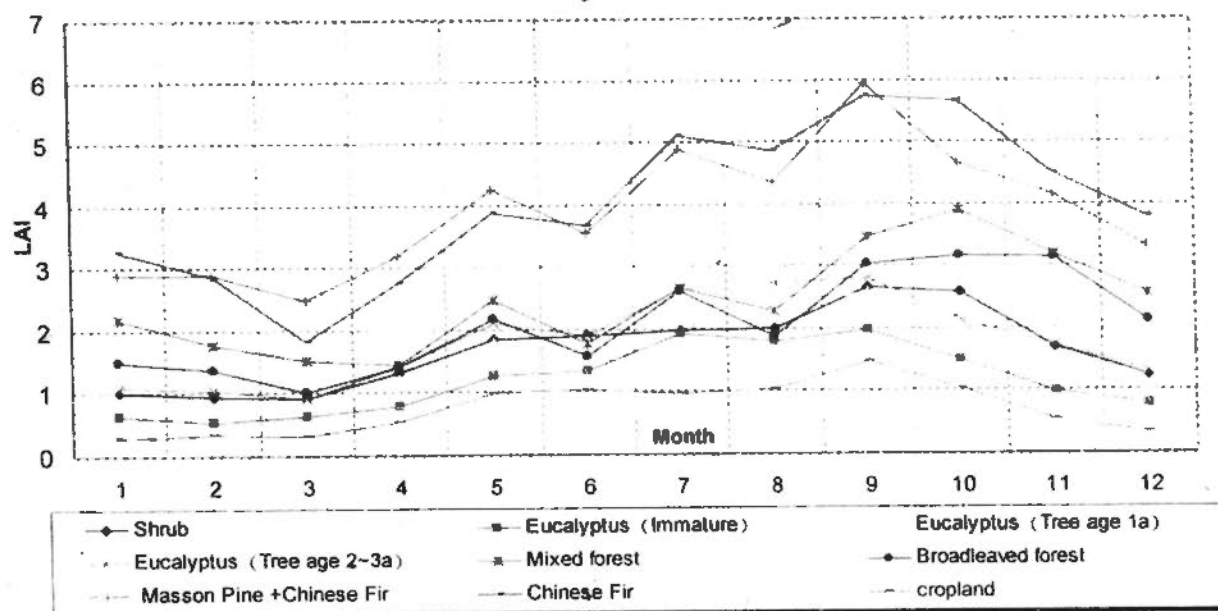


Figure 4.7 Measured LAI by field work from December, 2008 to December, 2009

Table 4.1 Summary of measured LAI for different land cover

Tree species	Mixed forest	Broad-leaved forest	Needle-leaved forest	cropland	Shrub	Eucalyptus			Chinese Fir	Masson Pine
						Immature	1 year	2~3 years		
Month										
January	2.18	1.49	2.88	0.29	1.02	0.63	0.85	1.08	3.27	2.49
February	1.76	1.37	2.88	0.33	0.94	0.54	0.72	1.03	2.86	2.90
March	1.52	1.01	2.46	0.31	0.91	0.62	0.85	0.91	1.83	3.10
April	1.45	1.42	3.18	0.52	1.31	0.78	1.22	1.40	2.75	3.60
May	2.48	2.18	4.25	1.00	1.85	1.27	1.80	2.10	3.87	4.63
June	1.76	1.56	3.55	1.04	1.90	1.35	1.82	1.89	3.68	3.43
July	2.66	2.60	4.87	0.95	1.98	1.92	2.43	2.64	5.11	4.63
August	2.27	1.87	4.35	1.04	2.01	1.80	2.33	2.73	4.85	3.85
September	3.47	3.02	5.93	1.45	2.65	1.98	2.57	2.81	5.74	6.13
October	3.89	3.15	4.64	1.04	2.59	1.50	1.93	2.13	5.66	3.62
November	3.19	3.13	4.16	0.54	1.70	0.99	1.37	1.72	4.50	3.82
December	2.55	2.12	3.30	0.33	1.25	0.78	1.07	1.31	3.78	2.83

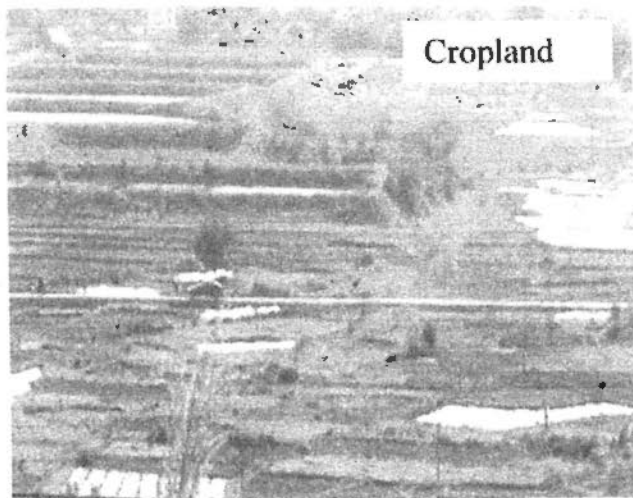
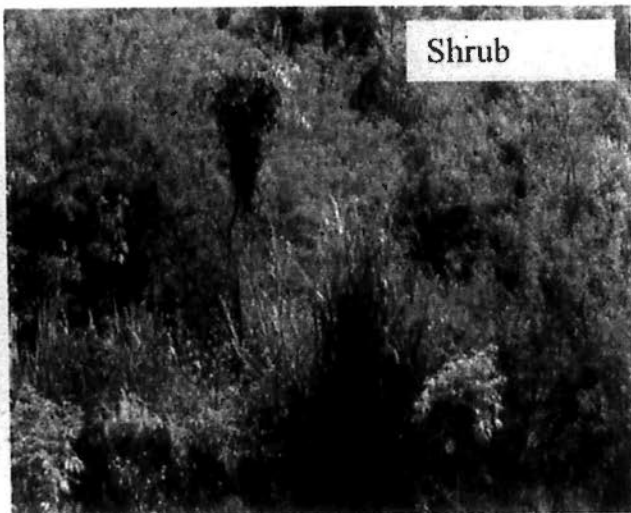
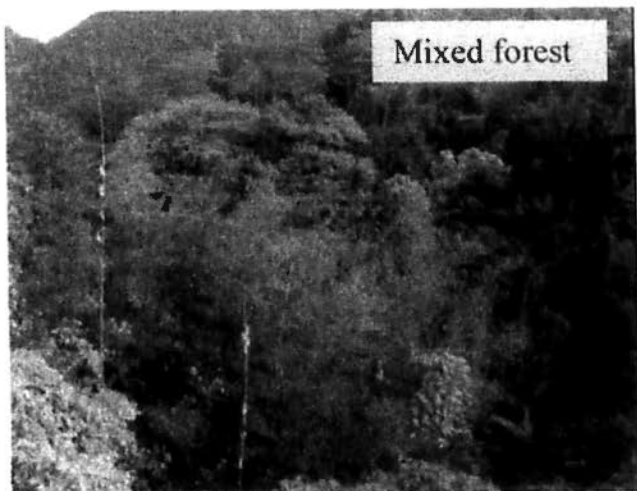
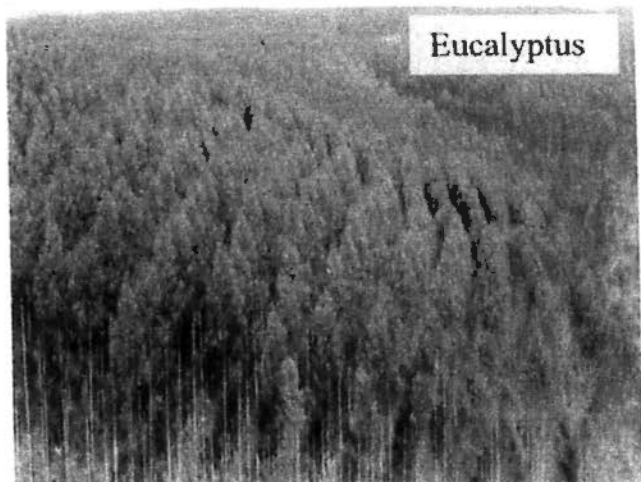


Figure 4.8 Selected photos for land use/cover in the East River Basin

4.3 Surface energy balance system (SEBS)

The SEBS is developed for the estimation of atmospheric turbulent fluxes using satellite earth observation data more coherently. SEBS as developed by Su (2002) consists of: (1) a set of tools for the determination of the land surface physical parameters, such as albedo, emissivity, temperature, vegetation coverage etc. from spectral reflectance and radiance; (2) an extended model for the determination of the roughness length for heat transfer reported by Su et al. (2001); and (3) a new formulation for the determination of the evaporative fraction on the basis of energy balance at limiting cases. In the application SEBS requires as inputs three sets of information. The first set consists of land surface albedo, emissivity, temperature, fractional vegetation coverage and leaf area index, and the height of the vegetation (or roughness height). When vegetation information is not explicitly available, the Normalized Difference Vegetation Index (NDVI) is used as a surrogate. These inputs can be derived from remote sensing data in conjunction with other information about the concerned surface. The second set includes air pressure, temperature, humidity, and wind speed at a reference height. The reference height is the measurement height for point application and the height of the planetary boundary layer (PBL) for regional application (in this latter case, PBL averaged meteorological variables are to be used. See later for detailed discussions). This data set can also be variables estimated by a large scale meteorological model. The third data set includes downward solar radiation, and downward longwave radiation which can either be directly measurements, model output or parameterization.

In SEBS the friction velocity, the sensible heat flux and the Obukhov stability length are obtained by solving the system of non-linear equations. For field measurements performed at a height of a few meters above ground, since the surface fluxes are related to surface variables and variables in the atmospheric surface layer, all calculations use the Monin-Obukhov Similarity (MOS) functions given by Brutsaert (1999). By replacing the MOS stability functions with the Bulk Atmospheric Boundary Layer (ABL) Similarity (BAS) functions proposed by Brutsaert (1999), the system equations can be used to relate surface fluxes to surface variables and the mixed layer atmospheric variables provided either by radiosonde data or obtained from atmospheric model fields. The relevant atmospheric boundary layer that needs to be considered in different scaling is shown in Figure 4.9. The determination of the evaporative fraction (the ratio of latent heat flux to the available energy) on the basis of energy balance at limiting

cases is carried out and finally the turbulent heat fluxes are determined by utilizing the surface energy balance. Furthermore, by utilizing the conservative characteristics of the evaporative fraction, the daily evaporation can be determined given the total daily available energy. The different steps involved in SEBS are discussed as follows.

Structure of the atmospheric boundary layer

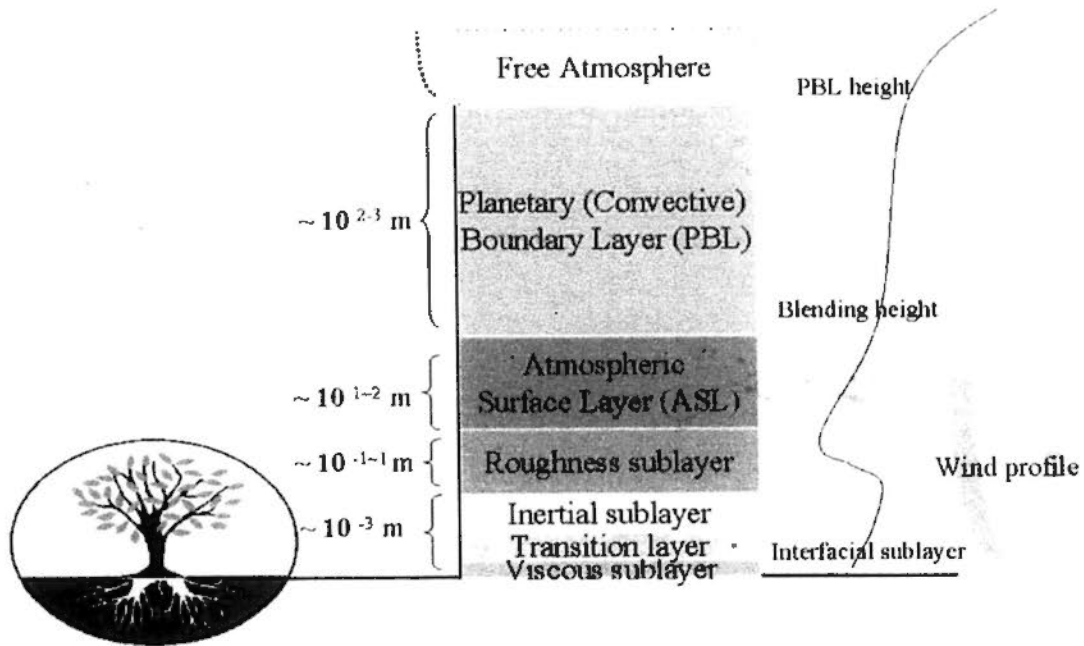


Figure 4.9 Typical structure of the atmospheric boundary layer (Adopted from Su, 2002)

4.3.1 Model description

The surface energy balance (Figure 4.10) is written in SEBS as

$$R_n = G_0 + H + \lambda E \tag{4-1}$$

where R_n is the net radiation, G_0 is the soil heat flux, H is the turbulent sensible heat flux, and λE is the turbulent latent heat flux (λ is the latent heat of vaporization and E is the actual evapotranspiration).

$$LE = R_n - H - G$$

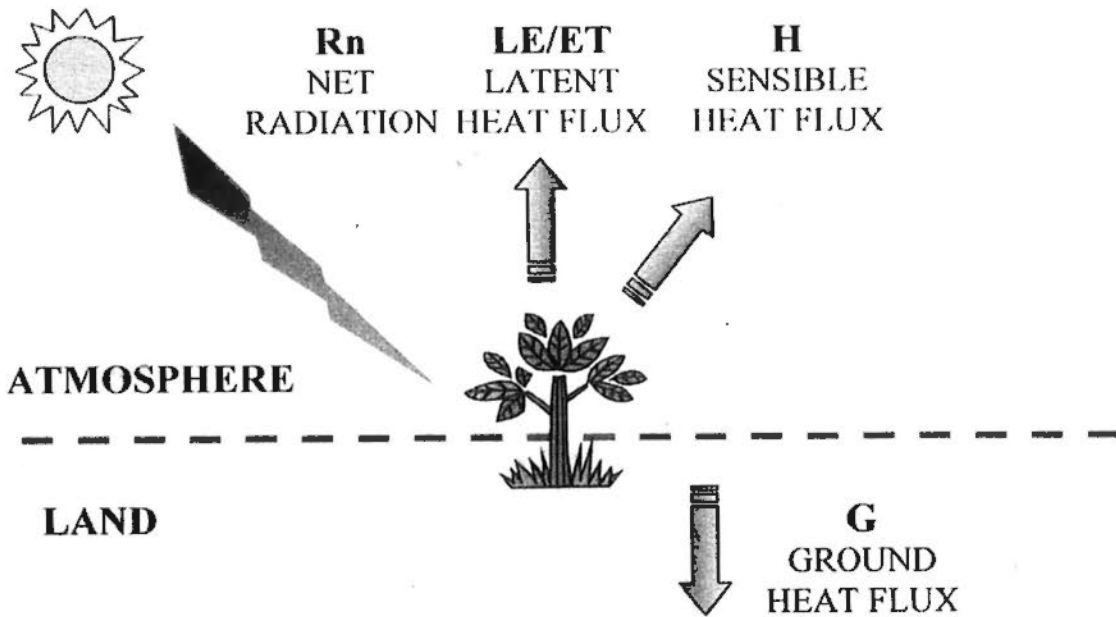
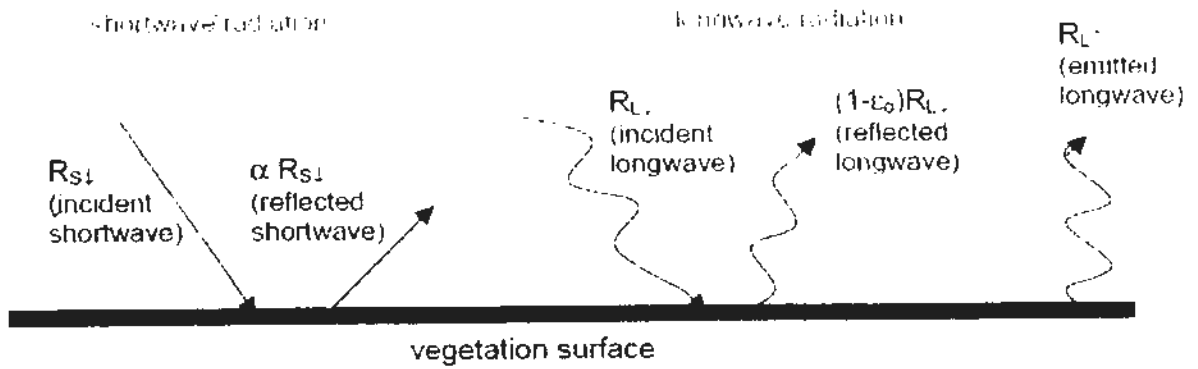


Figure 4.10 Surface Energy Balance for ET

The equation to calculate the net radiation (Figure 4.11) is given by

$$R_n = (1 - \alpha) \cdot R_{swd} + \varepsilon \cdot R_{lwd} - \varepsilon \cdot \sigma \cdot T_0^4 \quad (4-2)$$

where α is the albedo, R_{swd} is the downward solar radiation, R_{lwd} is the downward longwave radiation, ε is the emissivity of the surface, σ is the Stefan-Boltzmann constant, and T_0 is the surface radiative temperature measured by a remote sensor. α , ε and T_0 can be derived from remote sensing data from the visible to the thermal infrared spectral range. The simplest of form to calculate the downward solar radiation is $R_{swd} = I_{sc} \cdot e_0 \cdot \cos\theta_z \cdot \exp(-m \cdot \tau)$, where $I_{sc} = 1367 \text{ W} \cdot \text{m}^{-2}$ is the solar constant, e_0 the eccentricity factor, θ_z the solar zenith angle (Figure 4.12), m the air mass, and τ the optical thickness. Details on the determination of all the parameters can be found in Iqbal (1983). The downward longwave radiation R_{lwd} can be calculated as $R_{lwd} = \varepsilon_a \sigma T_a^4$ when there is no measurement, where ε_a is the emissivity of the atmosphere which can be estimated using the Swinbank formula as given by Campbell and Norman (1998) in the form $\varepsilon_a = 9.2 \cdot 10^{-6} \cdot (T_a + 273.15)^2$, with T_a the air temperature at the reference height. Su et al. (2001) and Su (2002) have shown that equation (4-2) provides accurate estimation of the net radiation.



Net surface radiation = gains – losses

$$R_n = (1 - \alpha) R_{S↓} + R_{L↓} - R_{L↑} - (1 - \epsilon_o)R_{L↓}$$

Figure 4.11 Surface radiation balance (Adopted from SEBAL manual, 2002)

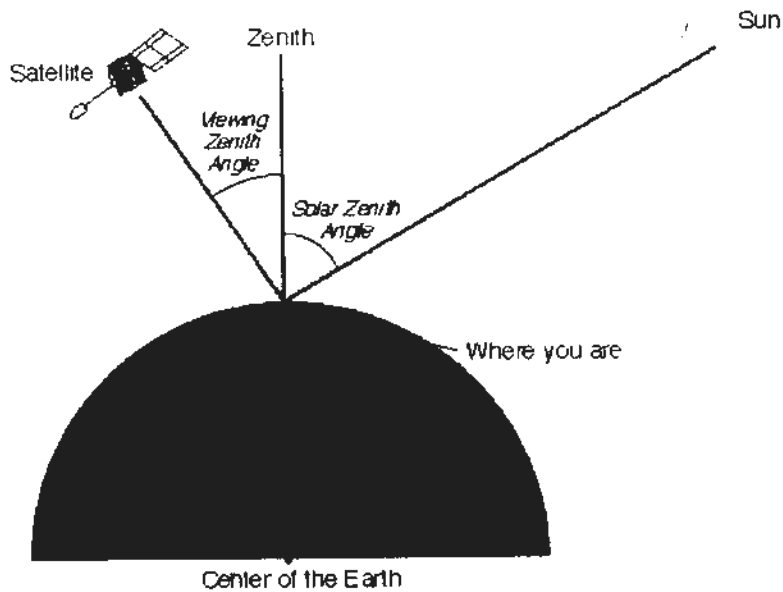


Figure 4.12 Map of solar zenith (Adopted from Su, 2002)

The equation to calculate the soil heat flux is parameterized as

$$G_0 = R_n \cdot [\Gamma_c + (1 - f_c) \cdot (\Gamma_s - \Gamma_c)] \tag{4-3}$$

in which it is assumed that the ratio of soil heat flux to net radiation $\Gamma_c = 0.05$ for full vegetation canopy (Monteith, 1973) and $\Gamma_c = 0.315$ for bare soil (Kustas & Daughtry, 1989). An interpolation is then performed between these limiting cases using the fractional canopy coverage, f_c , which can be determined from remote sensing data.

In order to determine the evaporative fraction, use is made of energy balance considerations at limiting cases. Under the dry-limit, the latent heat (or the evaporation)

becomes zero due to the limitation of soil moisture, and the sensible heat flux is at its maximum value. From Equation (4-1), it follows,

$$\begin{aligned}\lambda E_{dry} &= R_n - G_0 - H_{dry} \equiv 0, \quad \text{or} \\ H_{dry} &= R_n - G_0\end{aligned}\tag{4-4}$$

Under the wet-limit, where the evaporation takes place at potential rate, λE_{wet} , (i.e. the evaporation is only limited by the available energy under the given surface and atmospheric conditions), the sensible heat flux takes its minimum value, H_{wet} , i.e.

$$\begin{aligned}\lambda E_{wet} &= R_n - G_0 - H_{wet}, \quad \text{or} \\ H_{wet} &= R_n - G_0 - \lambda E_{wet}\end{aligned}\tag{4-5}$$

The relative evaporation then can be evaluated as

$$\Lambda_r = \frac{\lambda E}{\lambda E_{wet}} = 1 - \frac{\lambda E_{wet} - \lambda E}{\lambda E_{wet}}\tag{4-6}$$

Substitution of Equations (4-1), (4-5) and (4-4) in Equation (4-6) and after some algebra, one obtains

$$\Lambda_r = 1 - \frac{H - H_{wet}}{H_{dry} - H_{wet}}\tag{4-7}$$

The evaporative fraction is finally given by:

$$\Lambda = \frac{\lambda E}{H + \lambda E} = \frac{\lambda E}{R_n - G} = \frac{\Lambda_r \cdot \lambda E_{wet}}{R_n - G}\tag{4-8}$$

Equations (4-1-4-8) are the basic formulations of SEBS. Furthermore, the actual sensible heat flux H in SEBS is obtained by solving a set of non-linear equations and is constrained in the range set by the sensible heat flux at the wet limit H_{wet} , and the sensible heat flux at the dry limit H_{dry} .

4.3.1.1 Determination of sensible heat fluxes H , H_{dry} , H_{wet}

The similarity theory is used to derive the actual sensible heat flux H . In SEBS, distinction is made between the Atmospheric Boundary Layer (ABL) or Planetary Boundary Layer (PBL) and the Atmospheric Surface Layer (ASL) similarity. ABL refers to the part of atmosphere that is directly influenced by the presence of the Earth's surface and responds to the surface forcings with a timescale of an hour or less, while ASL refers to usually the bottom 10% of ABL but above the roughness sub-layer, i.e. the ASL is where turbulent fluxes and stress vary by less than 10% of their magnitude

(Stull, 1988). The roughness sub-layer (or the interfacial layer) is the near surface thin layer of a few centimeters where the molecular transport dominates over turbulent transport (see Figure 4.11). The thickness of the roughness sub-layer is thought to be around thirty-five times of the surface roughness height, or three times of the vegetation height (Katul & Parlange, 1992). In ASL, the similarity relationships for the profiles of the mean wind speed, u , and the mean temperature, $\theta_0 - \theta_a$, can be written in integral form as

$$u = \frac{u_*}{k} \left[\ln \left(\frac{z - d_0}{z_{0m}} \right) - \Psi_m \left(\frac{z - d_0}{L} \right) + \Psi_m \left(\frac{z_{0m}}{L} \right) \right] \quad (4-9)$$

$$\theta_0 - \theta_a = \frac{H}{ku_* \rho C_p} \left[\ln \left(\frac{z - d_0}{z_{0h}} \right) - \Psi_h \left(\frac{z - d_0}{L} \right) + \Psi_h \left(\frac{z_{0h}}{L} \right) \right] \quad (4-10)$$

where z is the height above the surface, $u_* = (\tau_0 / \rho)^{1/2}$ is the friction velocity, τ_0 is the surface shear stress. ρ is the density of air, $k = 0.4$ is the von Karman constant, d_0 is the zero plane displacement height, z_{0m} is the roughness height for momentum transfer, θ_0 is the potential temperature at the surface, θ_a is the potential air temperature at height z , z_{0h} is the scalar roughness height for heat transfer, Ψ_m and Ψ_h are the stability correction functions for momentum and sensible heat transfer respectively, L is the Obukhov length defined as

$$L = - \frac{\rho C_p u_*^3 \theta_v}{kgH} \quad (4-11)$$

where g is the acceleration due to gravity, θ_v is the potential virtual temperature near the surface.

For field measurements performed at a height of a few meters above ground, all calculations use the Monin-Obukhov Similarity (MOS) stability functions (e.g. Brutsaert, 1999) since the surface fluxes are related to surface variables and variables in the atmospheric surface layer. By replacing the MOS stability functions with the Bulk Atmospheric Boundary Layer (ABL) Similarity (BAS) functions proposed by Brutsaert (1999), the system of Equations (4-9~4-11) can be used to relate surface fluxes to surface variables and the mixed layer atmospheric variables. The criterion proposed by Brutsaert (1999) is used to determine if the MOS or the BAS scaling is appropriate for a given situation. The above functions are only valid for unstable conditions. For stable

conditions the expressions proposed by Beljaars & Holtslag (1991) and evaluated by Van den Hurk et al. (1997) are used for atmospheric surface layer scaling and the functions proposed by Brutsaert (1982) for atmospheric boundary layer scaling.

The friction velocity, the sensible heat flux and the Obukhov stability length are obtained by solving the system of non-linear Equations (4-9~4-11) using the method of Broyden (Press et al., 1997). It is important to note that the derivation of the sensible heat flux using Equations (4-9~4-11) requires only the wind speed and temperature at the reference height as well as the surface temperature and is independent of other surface energy balance terms.

As stated previously, this derived actual sensible heat flux H is further subjected to constraints in the range set by the sensible heat flux at the wet limit H_{wet} , and the sensible heat flux at the dry limit H_{dry} in SEBS.

The sensible heat flux at the dry limit H_{dry} is given by Equation (4-4) and the sensible heat flux at the wet limit H_{wet} can be derived by combining Equation (4-5) and a combination equation similar to the Penman-Monteith combination equation (Monteith, 1965). Menenti (1984) showed, when the resistance terms are grouped into the bulk internal (or surface) and external (or aerodynamic) resistances, the combination equation can be written in the following form,

$$\lambda E = \frac{\Delta \cdot r_e \cdot (R_n - G_0) + \rho C_p \cdot (e_{sat} - e)}{r_e \cdot (\gamma + \Delta) + \gamma \cdot r_i} \quad (4-12)$$

where e and e_{sat} are actual and saturation vapor pressure respectively; γ is the psychrometric constant, and Δ is the rate of change of saturation vapor pressure with temperature (i.e. $\partial e_{sat}(T)/\partial T$); r_i is the bulk surface internal resistance and r_e is the external or aerodynamic resistance. In the above equation it is assumed that the roughness lengths for heat and vapor transfer are the same (Brutsaert, 1982). It is worthwhile to point out that the Penman-Monteith equation is strictly only valid for vegetation canopy, whereas the definition by means of Equation (4-12) is also valid for soil surface with properly defined bulk internal resistance. The difficulty in using Equation (4-12) to estimate latent heat flux lies in the difficulty to determine the bulk

internal resistance r_i , which is strongly regulated by soil water availability. Because the latter is generally not known a priori, an alternative is thus proposed in SEBS to avoid the direct use of r_i in estimating λE .

At the wet-limit, the internal resistance $r_i \equiv 0$ by definition. Using this property in Equation (4-12) and changing the subscripts correspondingly to reflect the wet-limit condition, the sensible heat flux at the wet-limit is obtained as

$$H_{wet} = \left((R_n - G_0) - \frac{\rho C_p}{r_{cw}} \cdot \frac{e_s - e}{\gamma} \right) / \left(1 + \frac{\Delta}{\gamma} \right) \quad (4-13)$$

The external resistance depends also on the Obukhov length, L , which in turn is a function of the friction velocity and sensible heat flux (Equation 4-11). With the friction velocity and the Obukhov length determined by the numerical procedure described previously, the external resistance can be determined from Equation (4-10) as

$$r_e = \frac{1}{ku_*} \left[\ln \left(\frac{z - d_0}{z_{0h}} \right) - \Psi_h \left(\frac{z - d_0}{L} \right) + \Psi_h \left(\frac{z_{0h}}{L} \right) \right] \quad (4-14)$$

Similarly, the external resistance at the wet-limit can be derived as

$$r_{ew} = \frac{1}{ku_*} \left[\ln \left(\frac{z - d_0}{z_{0h}} \right) - \Psi_h \left(\frac{z - d_0}{L_w} \right) + \Psi_h \left(\frac{z_{0h}}{L_w} \right) \right] \quad (4-15)$$

and the wet-limit stability length can be determined as

$$L_w = - \frac{\rho u_*^3}{kg \cdot 0.61 \cdot (R_n - G_0) / \lambda} \quad (4-16)$$

4.3.1.2 Determination of the roughness length for heat transfer

In above derivations, the aerodynamic and thermal dynamic roughness parameters need to be determined firstly. When near surface wind speed and vegetation parameters (height and leaf area index) are available, the within-canopy turbulence model proposed by Massman (1997) can be used to estimate aerodynamic parameters, d_0 , the displacement height, and, z_{0m} , the roughness height for momentum. This model has been shown by Su et al. (2001) to produce reliable estimates of the aerodynamic parameters. The aerodynamic parameters can be related to vegetation indices derived from satellite data. However, more attention has to be paid in this case because the vegetation indices saturate at higher vegetation densities and the relationships are

vegetation-type dependent.

The scalar roughness height for heat transfer, z_{0h} , changes with surface characteristics, atmospheric flow and thermal dynamic state of the surface (Blümel, 1999; Massman, 1999a). Based on the work of Massman (1999a) a simple roughness model for heat transfer was proposed by Su et al. (2001). However, in their model a functional form to describe the vertical structure of the vegetation canopy is needed in order to calculate the within-canopy wind speed profile extinction coefficient, n_{cc} . For local studies, this information is easily obtained, but for large scale applications, it is generally impossible to obtain detailed information on the vertical structure of the canopy. In SEBS, n_{cc} , is formulated as a function of the cumulative leaf drag area at the canopy top,

$$n_{cc} = \frac{C_d \cdot LAI}{2u_*^2 / u(h)^2} \quad (4-17)$$

where C_d is the drag coefficient of the foliage elements assumed to take the value of 0.2, LAI is the one-sided leaf area index defined for the total ground area, $u(h)$ is the horizontal wind speed at the canopy top. The scalar roughness height for heat transfer, z_{0h} , can be derived from

$$z_{0h} = z_{0m} / \exp(kB^{-1}) \quad (4-18)$$

where B^{-1} is the inverse Stanton number, a dimensionless heat transfer coefficient. To estimate the kB^{-1} value, an extended model of Su et al. (2001) is proposed as follows,

$$kB^{-1} = \frac{kC_d}{4C_l \frac{u_*}{u(h)} (1 - e^{-n_{cc}/2})} f_c^2 + 2f_c f_s \frac{k \cdot u_* / u(h) \cdot z_{0m} / h}{C_l^*} + kB_s^{-1} f_s^2 \quad (4-19)$$

where f_c is the fractional canopy coverage and f_s is its complement. C_l is the heat transfer coefficient of the leaf. For most canopies and environmental conditions, C_l is bounded as $0.005N \leq C_l \leq 0.075N$ (N is number of sides of a leaf to participate in heat exchange), The heat transfer coefficient of the soil is given by $C_l^* = Pr^{-2/3} Re_s^{-1/2}$, where Pr is the Prandtl number, the roughness Reynolds number $Re_s = h_s u_* / \nu$, with h_s the roughness height of the soil. The kinematic viscosity of the air is given by $\nu = 1.327 \cdot 10^{-5} (p_0/p)(T_0/T_{a0})^{1.81}$ (Massman, 1999b), with p and T_0 the ambient pressure and temperature and $p_0 = 101.3$ kPa and $T_{a0} = 273.15$ K. Physically and

geometrically, the first term of (19) follows the full canopy only model of Choudhury & Monteith (1988), the third term is that of Brutsaert (1982) for a bare soil surface, while the second term describes the interaction between vegetation and bare soil surface. A quadratic weighting based on the fractional canopy coverage is used to accommodate any situation between the full vegetation and bare soil conditions. For bare soil surface kB_s^{-1} is calculated according to Brutsaert (1982).

$$kB_s^{-1} = 2.46(\text{Re.})^{1/4} - \ln[7.4] \quad (4-20)$$

4.3.1.3 Monin-Obukhov Similarity (MOS) stability correction functions

The MOS stability correction functions for momentum and sensible heat transfer ψ_m and ψ_h respectively are defined in the following integrated form

$$\Psi_i(y) = \int_0^y \frac{[1 - \phi_i(x)] dx}{x} \quad (4-21)$$

where $y = -(z-d)/L$. i equals m , or h for momentum and sensible heat transfer respectively.

The ϕ_i functions are proposed by Brutsaert (1999) as

$$\phi_m(y) = \frac{(a + b \cdot y^{m+1/3})}{a + y^m} \quad (4-22)$$

$$\phi_h(y) = \frac{(c + d \cdot y^n)}{c + y^n} \quad (4-23)$$

On the basis of data reported by Högström (1988), and Kader & Yaglom (1990), Brutsaert (1999) assigned the constants in Equations (4.22-4.23) as $a = 0.33$, $b = 0.41$, $m = 1.0$, $c = 0.33$, $d = 0.057$, and $n = 0.78$.

By integration of equations (4-22) and (4-23) using equation (4-21), the required MOS stability functions for free-convective conditions are obtained

$$\Psi_m(y) = \ln(a+y) - 3 \cdot b \cdot y^{1/3} + \frac{b \cdot a^{1/3}}{2} \ln \left[\frac{(1+x)^2}{(1-x+x^2)} \right] \quad (4.24a)$$

$$+ 3^{1/2} \cdot b \cdot a^{1/3} \tan^{-1} \left[\frac{(2 \cdot x - 1)}{3^{1/2}} \right] + \Psi_0, \quad \text{for } y \leq b^{-3}$$

$$\Psi_m(y) = \Psi_m(b^{-3}), \quad \text{for } y > b^{-3} \quad (4.24b)$$

$$\Psi_n(y) = \left[\frac{(1-d)}{n} \right] \ln \left[\frac{c + y^n}{c} \right] \quad (4-25)$$

where $x = (y/a)^{1/n}$. $\Psi_0 = (-\ln a + 3^{1/2} \cdot b \cdot a^{1/3} \cdot \pi/6)$ is an integration constant.

Equations (4-24-4-25) are extensions to the Businger-Dyer function for unstable conditions. For stable conditions the expressions proposed by Beljaars & Holtslag (1991) and evaluated by Van den Hurk & Holtslag (1995) can be used. These are given in the following:

$$\Psi_m(y_s) = - \left[a_s \cdot y_s + b_s \left(y_s - \frac{c_s}{d_s} \right) \exp(-d_s \cdot y_s) + \frac{b_s \cdot c_s}{d_s} \right] \quad (4-26)$$

$$\Psi_b(y_s) = - \left[\left(1 + \frac{2a_s}{3} y_s \right)^{1.5} + b_s \cdot \left(y_s - \frac{c_s}{d_s} \right) \cdot \exp(-d_s \cdot y_s) + \left(\frac{b_s \cdot c_s}{d_s} - 1 \right) \right] \quad (4-27)$$

where $y_s = (z-d)/L$, $a_s = 1$, $b_s = 0.667$, $c_s = 5$ and $d_s = 1$.

4.3.1.4 Bulk Atmospheric Boundary Layer (ABL) Similarity (BAS) stability correction functions

Since under free convective conditions, the outer region of the ABL is well mixed, such that the mean profiles of wind and potential temperature are nearly constant with height. This is equivalent to state that the unstable ABL consists of two regions, an inner region where MOS is valid, and a slab outer region where the profiles are constant.

According to Brutsaert (1999), experimental evidence suggests that the height of the ASL, h_{st} , should be scaled with the thickness of the ABL over moderately rough surfaces, but with the surface roughness over very rough terrain. More quantitatively, h_{st} , can be determined in the following ways

$$h_{st} = \alpha_b \cdot h_i \quad (4-28)$$

where h_i is the height of the ABL and α_b is around 0.10-0.15, or

$$h_{st} = \beta_b \cdot z_0 \quad (4-29)$$

where β_b is around 100 -150, which ever is larger. Setting typical values of $\beta_b/\alpha_b = 10^3$, and $h_i = 10^3$ m, gives $z_0 = (\alpha_b/\beta_b) \cdot h_i = 1$ m which separates very rough from moderate rough terrain.

For moderately rough terrain satisfying $z_0 < (\alpha_h / \beta_h) \cdot h_i$, joining the inner with the outer region such that $u(z - d_0) = u_m$, $\theta_a(z - d_0) = \theta_m$, at $z - d_0 = h_m$. (where the subscript m indicates average of the variable in question over the lower half of the mixed layer, which is an advise for practical applications because the entrainment of warmer air into the ABL affects both the potential temperature and the wind profiles in the upper half of the ABL), allows to derive the bulk stability functions

$$B_w = -\ln(\alpha_h) + \Psi_m(\alpha_h \cdot h_i / L) - \Psi_m(z_0 / L) \quad (4-30)$$

$$C_w = -\ln(\alpha_h) + \Psi_h(\alpha_h \cdot h_i / L) - \Psi_h(z_{0h} / L) \quad (4-31)$$

Equations (4-30-4-31) show that the bulk stability functions depend on both the surface roughness and the height of the ABL for moderately rough terrain.

Similarly, for very rough terrain, i.e., $z_0 \geq (\alpha_h / \beta_h) \cdot h_i$, it can be obtained

$$B_w = -\ln(h_i / (\beta_h \cdot z_0)) + \Psi_m(\beta_h \cdot z_0 / L) - \Psi_m(z_0 / L) \quad (4-32)$$

$$C_w = -\ln(h_i / (\beta_h \cdot z_0)) + \Psi_h(\beta_h \cdot z_0 / L) - \Psi_h(z_{0h} / L) \quad (4-33)$$

Which state that the bulk stability functions depend on only the surface roughness for very rough terrain.

Finally, for stable conditions, i.e. when $h_i / L > 0$. we use the following Equation (Brutsaert, 1982):

$$B_w = -2.2 \cdot \ln(1 + h_i / L) \quad (4-34)$$

$$C_w = -7.6 \cdot \ln(1 + h_i / L) \quad (4-35)$$

Both stability correction functions may need to be verified using data from more recent large scale field experiment and updated accordingly when necessary.

4.3.1.5 Determination of turbulent heat fluxes and actual evaporation

By inverting Equation (4-8), the actual sensible and latent heat fluxes can be obtained as,

$$\begin{aligned} H &= (1 - \Lambda) \cdot (R_n - G) \\ \lambda E &= \Lambda \cdot (R_n - G) \end{aligned} \quad (4-36)$$

When the evaporative fraction is known, the daily evaporation can be determined as

$$E_{daily} = 8.64 \times 10^7 \times \overline{\Lambda} \times \frac{\overline{R_n - G_0}}{\lambda \rho_w} \quad (4-37)$$

where E_{daily} is the actual evaporation on daily basis ($mm \cdot d^{-1}$). $\overline{\Lambda}$ is the daily average evaporative fraction, which can be approximated by the SEBS estimate since the

evaporative fraction is conservative (Shuttleworth et al., 1989; Sugita & Brutsaert, 1991; Crago, 1996). $\overline{R_n}$ and $\overline{G_0}$ are the daily net radiation flux and soil heat flux, λ is the latent heat of vaporization (JKg^{-1}), ρ_w is the density of water ($Kg \cdot m^{-3}$).

Since the daily soil heat flux is close to zero because of the downward flux in daytime and the upward flux at night balance each other approximately, the daily evaporation only depends on the net radiation flux given by

$$\overline{R_n} = (1 - \alpha)K_{24}^\downarrow + \varepsilon L_{24} \quad (4-38)$$

where K_{24}^\downarrow is the daily incoming global radiation and L_{24} is daily net longwave radiation. The daily average albedo, α , and emissivity, ε , can be approximated easily with the same values as used previously in the energy balance equation.

By summing up the corresponding daily evaporation for a certain period, the actual evaporation for that period (i.e. a week, a month or a year) can be determined. However, errors will occur due to cloud effects. Such effects can be further removed by using the time series processing or by data assimilation procedures. In this study, on one hand, if the cloudy areas are not too large based on visual Interpretation, the cloudy area are masked when conduct ET mapping; on the other hand, if cloudy area is too large, only selected sunny images with good quality are used for ET mapping. A schematic presentation of SEBS is given in Figure 4.13 for clarity of the steps involved.

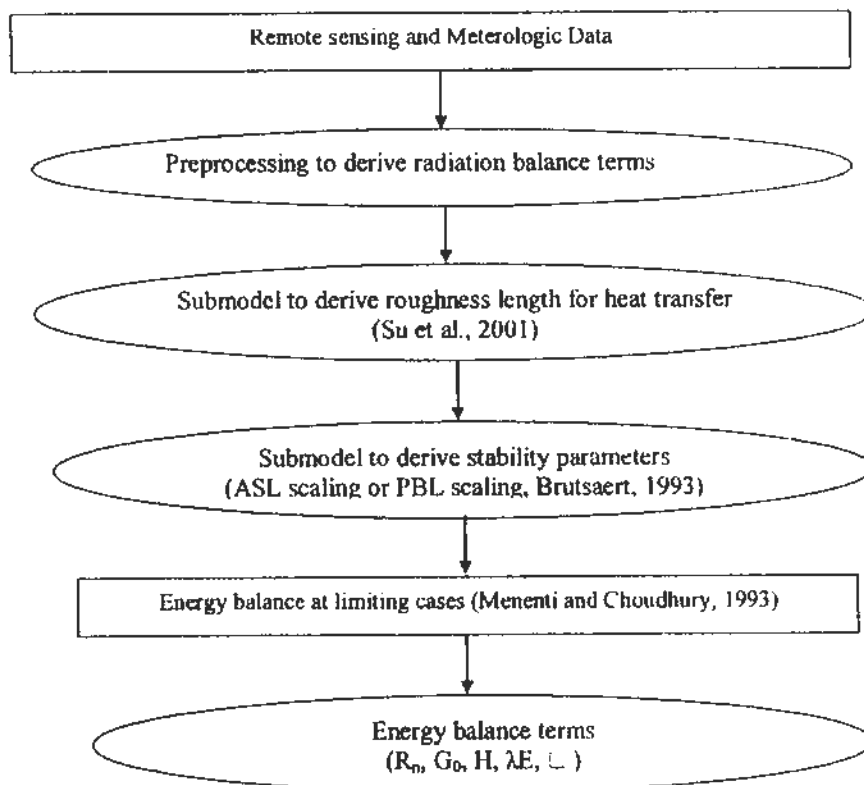


Figure 4.13 Scheme representation of SEBS (Modified from Su, 2002)

4.3.2 Parameterization of surface bio-physical characteristics in the original SEBS

In order to run SEBS, surface bio-physical parameters should be prepared firstly as model inputs. Those inputs can be derived from remote sensing data by applying related empirical equations as follows in the original SEBS.

4.3.2.1 Vegetation fractional cover

Fractional Vegetation Cover is an important parameter that has a key role in the energy exchanges at the land surface. A simple procedure to determine fractional vegetation cover is proposed by Gutman et al. (1998).

$$f = \frac{NDVI - NDVI_{min}}{NDVI_{max} - NDVI_{min}} \quad (4-39)$$

where, $NDVI_{min}$ is the NDVI for bare soil and $NDVI_{max}$ for full vegetation coverage.

4.3.2.2 Leaf Area Index (LAI)

Leaf Area Index (LAI) is the leaf area per unit ground area, which reflects the vertical vegetation amount. The relationship proposed by Su & Jacobs (2001) is used in the original SEBS, this reads

$$LAI = \left(NDVI \cdot \frac{1 + NDVI}{1 - NDVI + \delta NDVI} \right)^{1/2} \quad (4-40)$$

This formula is strictly only good for low vegetation since NDVI saturates at higher LAI values. However, this equation is adopted in most SEBS studies because of limited information for the study area to support more sophisticated formulations. In this study, this formula is improved which will be discussed in the section 4.4.

4.3.2.3 Surface emissivity

By analyzing the relationship between surface emissivity and NDVI, an experimental relationship is obtained by Van de Griend et al. (1993) to determine surface emissivity,

$$\varepsilon = 1.0094 + 0.047 \ln(NDVI) \quad (4-41)$$

4.3.2.4 Aerodynamic roughness height

Aerodynamic roughness height is a very important parameter in surface energy balance model, which influence greatly the turbulent characteristics near the surface where the heat fluxes originate. Aerodynamic roughness height can be estimated by a simple

relationship proposed by Su et al. (2001),

$$z_{0m} = 0.005 + 0.5 \cdot \left(\frac{NDVI}{NDVI_{max}} \right)^{2.5} \quad (4-42)$$

4.3.2.5 Vegetation height and displacement height

A conversion is performed according to Brutsaert (1982) to derive vegetation height and displacement height for a given aerodynamic roughness height in original SEBS,

$$h = \frac{z_{0m}}{0.136} \quad d = \frac{2}{3} h \quad (4-43)$$

4.4 Enhancement of SEBS for application in complex vegetated area

The SEBS model, which has a very clear physical basis and is not data intensive, has been widely applied in the Northwestern China (e.g. Su, 2002; Zhan, 2005; Lin, 2006), Spain (van der Kwast et al., 2009) and Dutch (e.g. Hailegiorgis, 2006; Weligepolage, 2005) in Europe. In practice it performs much better in Europe than in northern China. The reasons have been discussed so much that one major consensus has been reached that the traditional SEBS is well suited for homogeneous low-vegetation region like some parts in Europe. In the original SEBS, LAI is estimated by equation 4-40 based on NDVI, this formula is strictly only good for low vegetation since NDVI saturates at higher LAI values. Therefore, it is not suitable for complex vegetated area, particularly for areas with tall trees (Zhan, 2005). However, in China, particularly in the southern part, due to the complexity of vegetation condition and underlying surface, there is a need to improve SEBS for application in such complex vegetated areas.

As mentioned above, the LAI, aerodynamic roughness height, vegetation height and displacement are often estimated with the empirical equation (see equation 4-40, 4-42 and 4-43) in the original SEBS, however, there are a few limitations for application in China. For LAI, the formula is strictly only good for low vegetation since NDVI saturates at higher LAI values; for aerodynamic roughness height z_{0m} and displacement height d_0 , the empirical simple equations can not represent the real surface conditions (He et al., 2006). The study area located in the southern part of China and has a complex underlying surface condition. Therefore, in order to better apply SEBS for areas with

complicated surface condition, an attempt should be made to improve SEBS for application in complex vegetation conditions.

The procedures for enhancing SEBS for application in complex vegetated area are summarized and shown in Figure 4.14. As shown in Figure 4.14, firstly relationship of LAI and NDVI are identified based on remote sensing data and field measured data using regression model. Secondly, based on the identified LAI-NDVI relationship mentioned above, in combination with the experiments in China as reported in Zhang (1996), aerodynamic roughness height z_{0m} and the displacement height d_0 can be improved using the following equations, which are much more suitable for application in China:

$$\begin{aligned}
 d_0 &= h \left[\ln(1 + x^{1.6}) + 0.031 \ln(1 + x^6) \right] \\
 z_{0m} &= \begin{cases} h_s + 0.28hx^{1/2} & (0 \leq x \leq 0.2) \\ 0.3h(1 - d_0/h) & (0.2 \leq x \leq 2) \end{cases} \\
 x &= 0.2LAI
 \end{aligned} \tag{4-44}$$

where h is vegetation height. The value of h_s ranges from 0.005~0.02. In this study, $h_s = 0.13$. Comparing with the original equations in SEBS (equation 4-42 and 4-43), equation 4-44 estimates z_{0m} and d_0 based on LAI, which is suitable for complex vegetated area. In equation 4-44, there are 2 parameters LAI and h . The parameter h can be determined by field measured data or derived from Land Data Assimilation System (LDAS) (Table 4.2), which has been widely used in numerous land surface models (e.g. Mosaic, BATS, SIB2, and CLM). In this way, the SEBS is enhanced for application in complex vegetated area, which has a much stronger physical basis and a wider applicability.

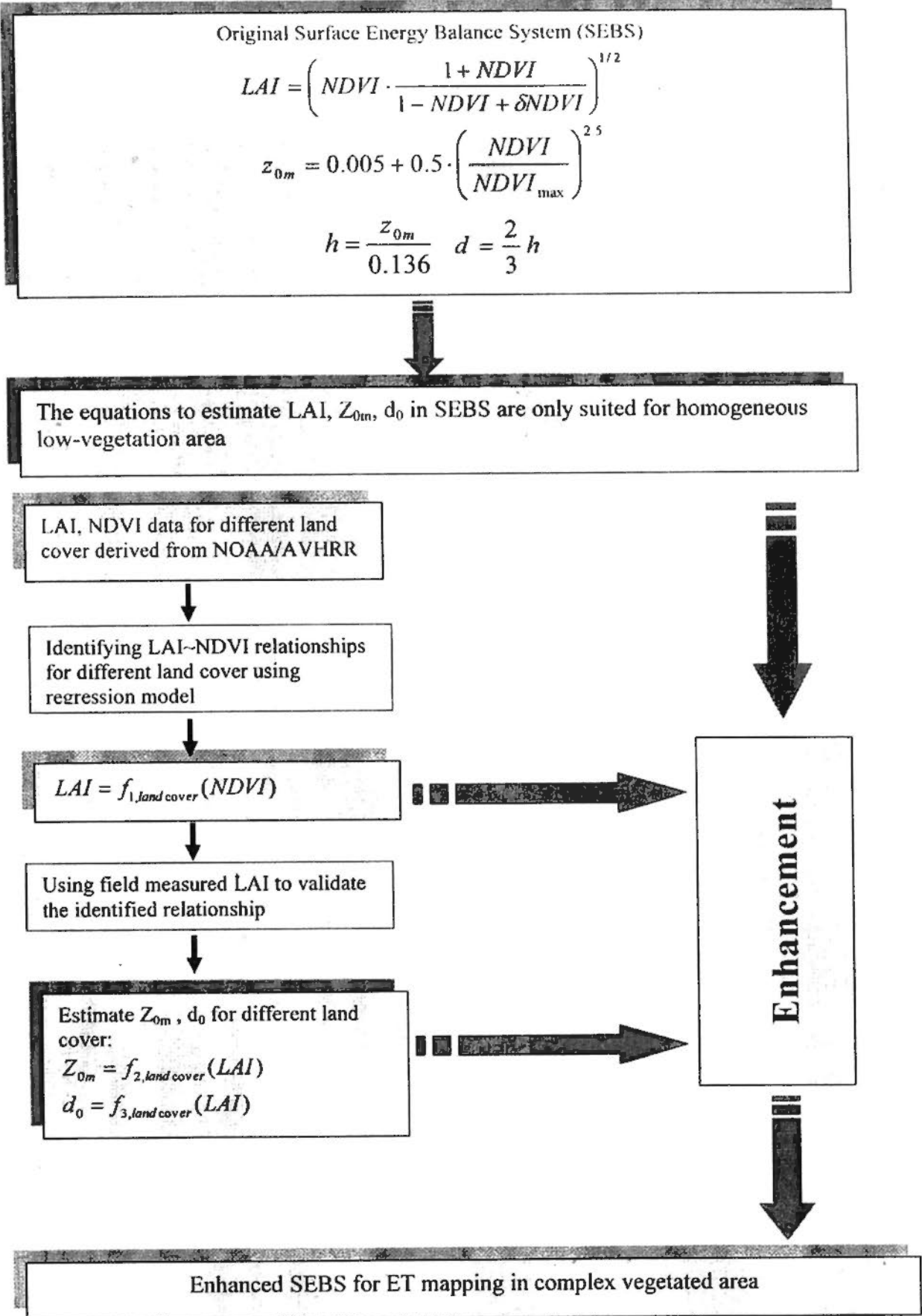


Figure 4.14 The procedures for enhancing SEBS for application in complex vegetated area

Table 2 Vegetation height for different land cover (LDAS, 2010)

Land cover	Vegetation height h (m)
Evergreen needle leaf forest	17.00
Evergreen broadleaf forest	35.00
Deciduous needle leaf forest	17.00
Deciduous broadleaf forest	20.00
Mixed forest	18.50
Woodland	14.02
Wooded grassland	6.89
Closed shrub land	0.60
Open shrub land	0.59
Grassland	0.60
Cropland	0.60

4.4.1 LAI estimation for different land cover based on NDVI

There are numerous studies on relationship of LAI and NDVI (e.g. Asrar et al., 1985; PierceL et al., 1993; Spanner et al., 1990). All these studies show that that LAI has a strong relationship with NDVI, which can be presented in various forms based on regression model (Ramakrishna et al., 1996).

The relationship between areal NDVI and LAI is presented in Figure 4.15 which indicates there is a good agreement between NDVI and LAI when using exponential function. Therefore, in this section, firstly exponential equation is used as a basic principle to identify NDVI~LAI relationship for different land use classes when curve fitting is conducted. The results are presented in Figure 4.16, and the equations of LAI-NDVI relationship for different land cover are described in the following. Secondly, accuracy is always a big challenge for quantitative remote sensing (Liang, 2003). In order to validate the identified relationship, literature-based estimation method and measured LAI are used to validate the results from the regression model.

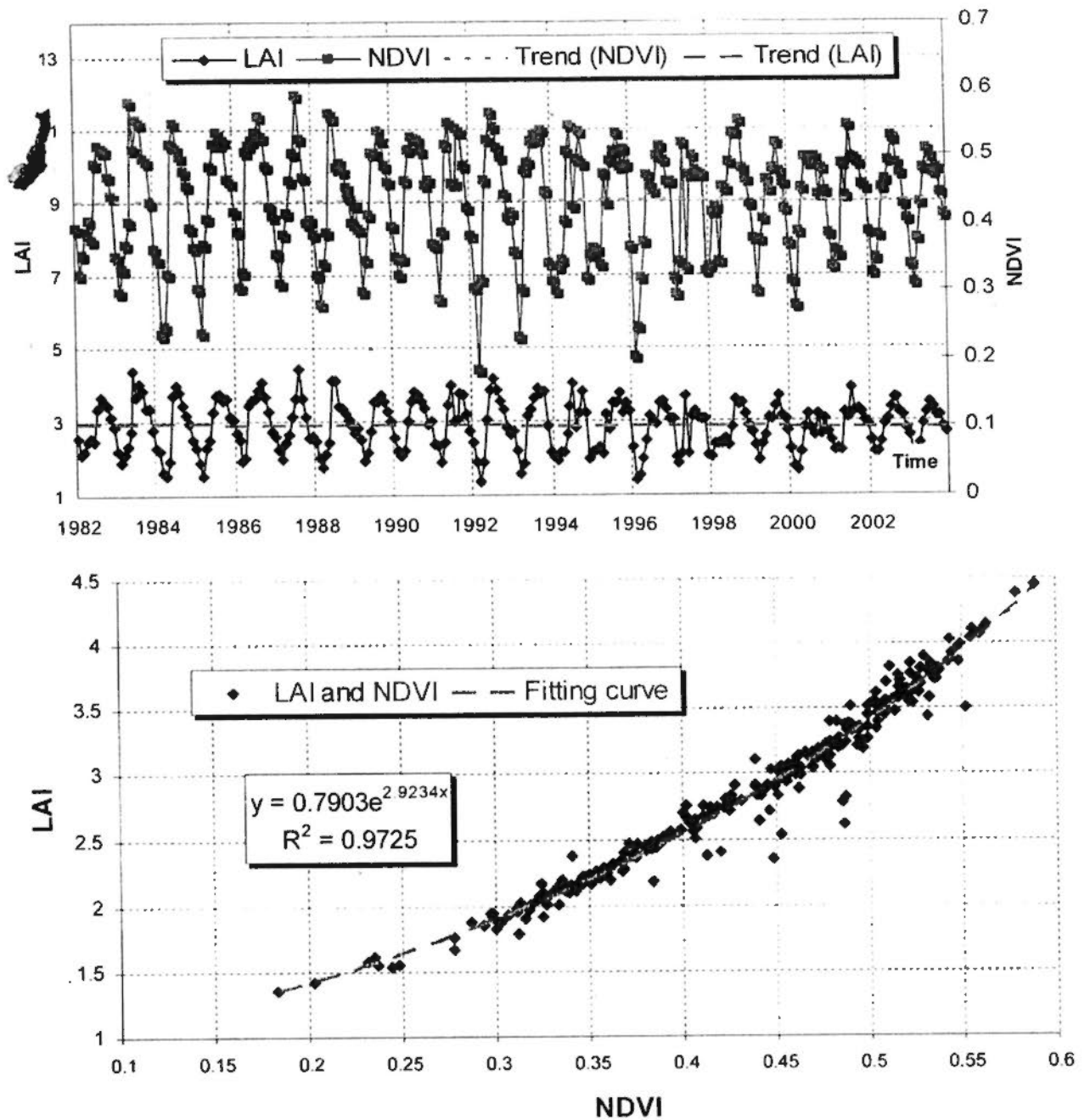


Figure 4.15 Relationship of LAI~NDVI

4.4.1.1 Relationship identification based on regression model

Based on NDVI and LAI data products from NOAA/AVHRR (Myneni et al., 1997), regression equations for different land cover have been obtained as follows.

(1) For overall forest, the relationship can be presented with the following equation

$$\text{LAI} = 0.6346 \exp(2.7929 \times \text{NDVI}) \quad (4-45)$$

(2) For mixed forest, the relationship can be presented with the following equation

$$\text{LAI} = 0.654 \exp(2.356 \times \text{NDVI}) \quad (4-46)$$

(3) For evergreen needle-leaf forest, the relationship can be presented with the following equation

$$LAI = 0.764 \exp(2.91 \cdot NDVI) \quad (4-47)$$

(4) For evergreen broadleaf forest, the relationship can be presented with the following equation

$$LAI = 0.3861 \exp(3.252 \cdot NDVI) \quad (4-48)$$

(5) For cropland, the relationship can be presented with the following equation

$$LAI = 0.198 \exp(2.888 \cdot NDVI) \quad (4-49)$$

(6) For shrub, the relationship can be presented with the following equation

$$LAI = 0.273 \exp(3.245 \cdot NDVI) \quad (4-50)$$

(7) For grasslands, the relationship can be presented with the following equation

$$LAI = 0.494 \exp(3.13 \cdot NDVI) \quad (4-51)$$

4.4.1.2 Relationship identification based on literature

According to Getu (1998), the relationship between NDVI and LAI can be expressed as follows.

(1) For cropland, the equation is:

$$LAI = -2.5 \ln(1.2 - 2 \cdot NDVI) \quad (4-52)$$

(2) For grassland, the equation can be expressed as follows:

$$LAI = (NDVI \times 1.71) + 0.48 \quad (4-53)$$

(3) For mixture forest, the relationship can be represented as follows:

$$LAI = (0.52(NDVI + 1) / (1 - NDVI))^{1.715} \quad (4-54)$$

(4) For coniferous forest, the equation is:

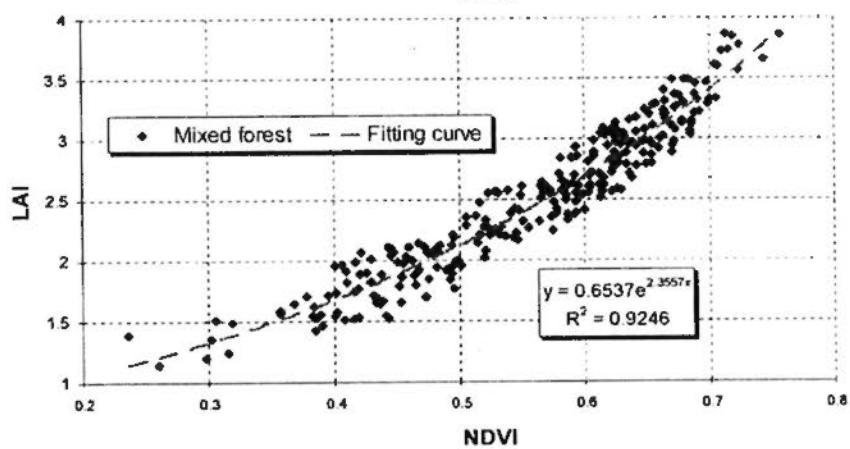
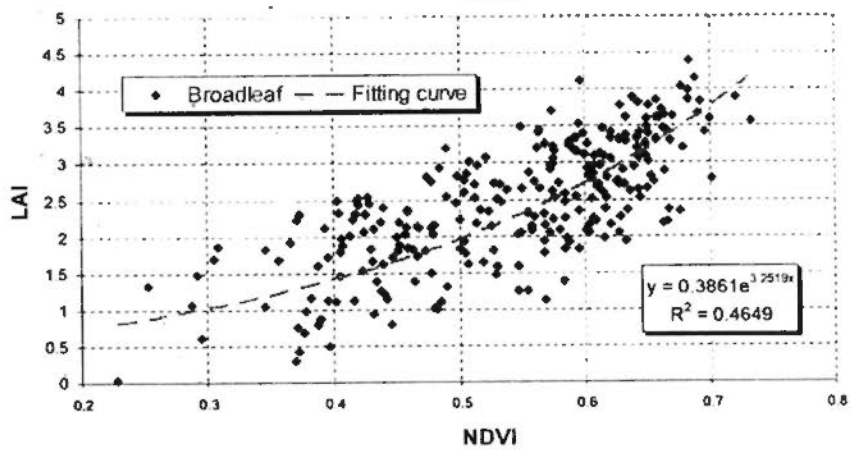
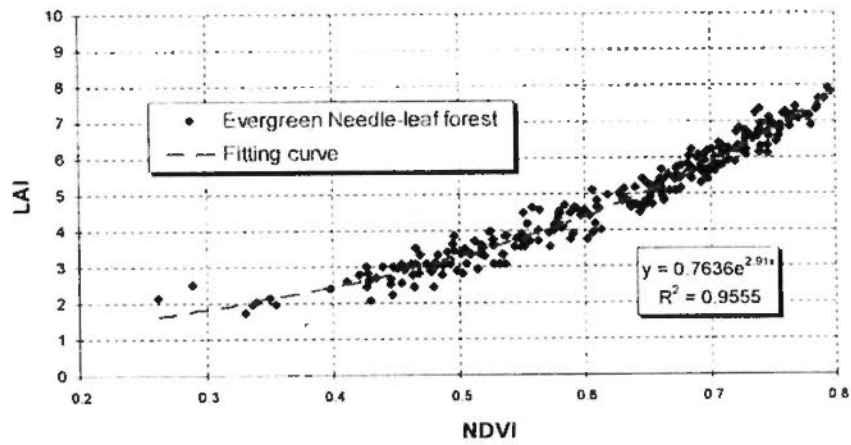
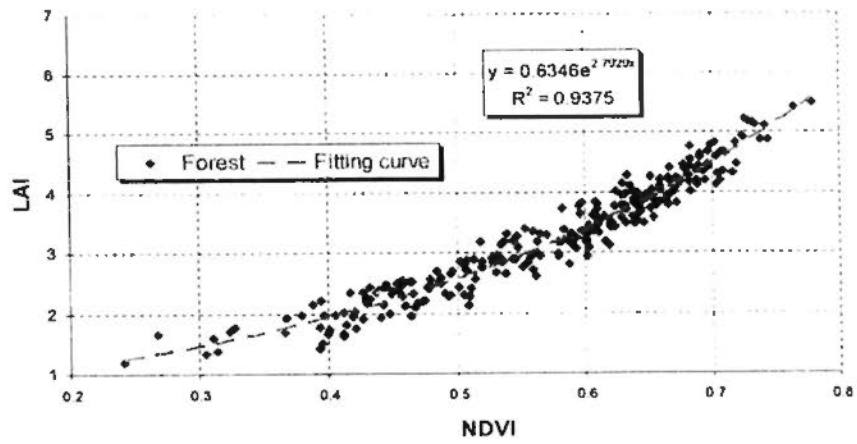
$$LAI = (NDVI / 0.31)^{0.26} \quad (4-55)$$

(5) For broadleaf forest, the equation is:

$$LAI = (NDVI / 0.26)^2 \quad (4-56)$$

(6) For shrub land the equation is:

$$LAI = (NDVI \times 1.71) + 0.48 \quad (4-57)$$



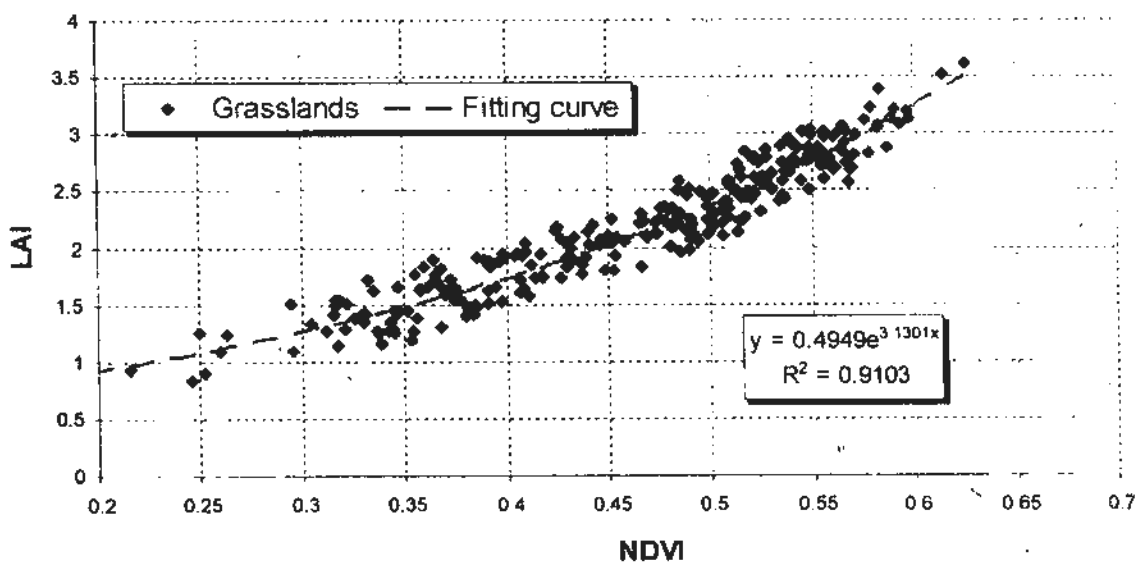
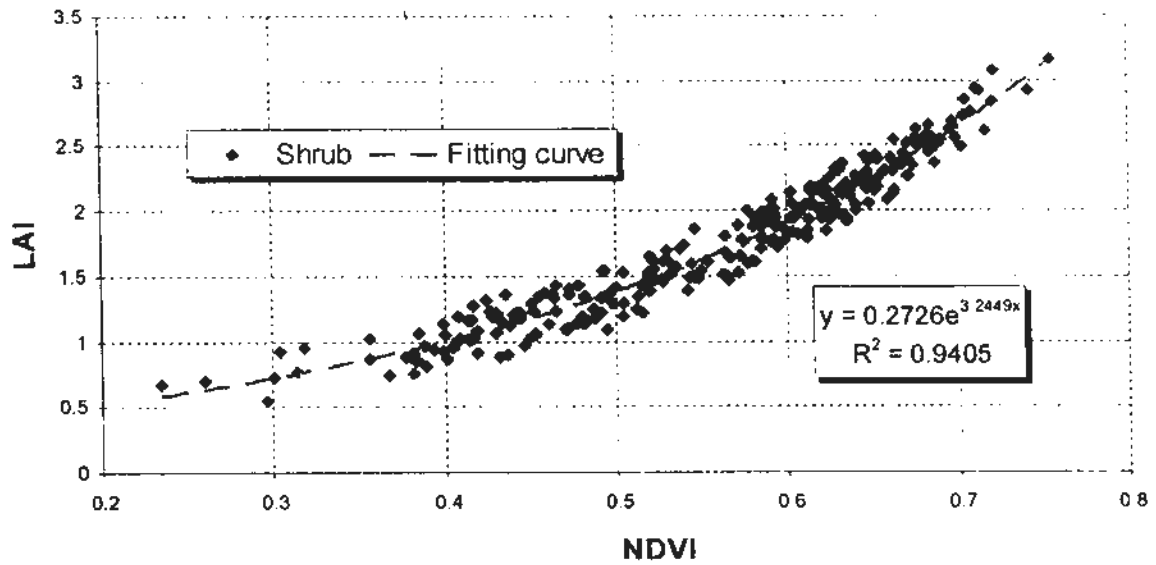
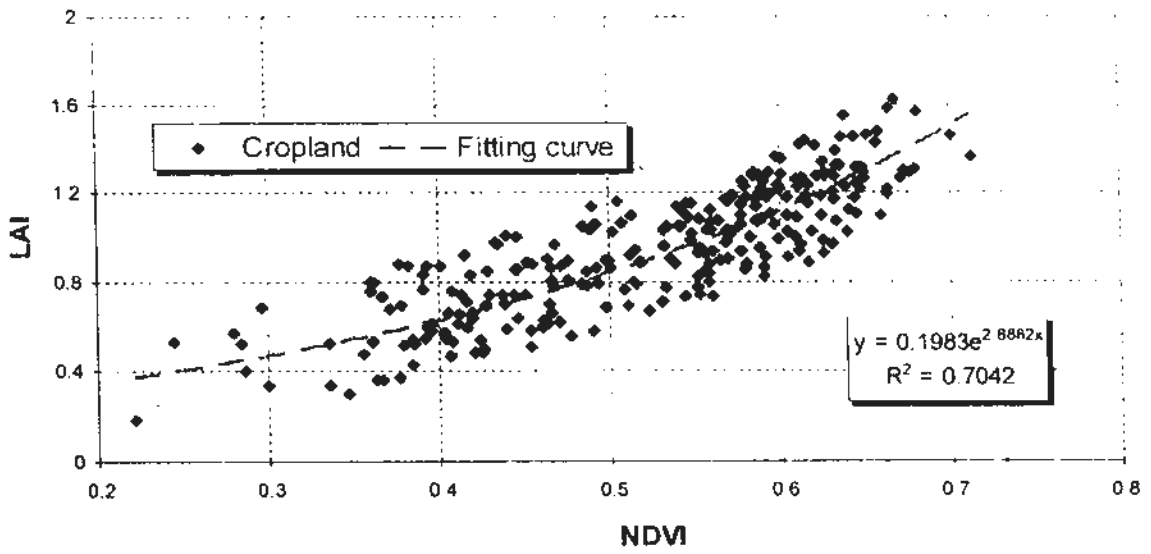


Figure 4.16 Curve fitting results for identification of LAI-NDVI relationship

4.4.1.3 Validation and inter-comparison of LAI-NDVI relationship

The inter-comparison of LAI estimated by curve-fitting-based regression model, literature-based model, SEBS-based model and measured LAI~ NDVI relationships are presented in Figure 4.17. As shown in the Figure, it is clear that the results based on regression model using exponential function show a much better agreement with measured LAI. Therefore, the exponential formula is employed to estimate LAI instead of the simple relationship proposed by Su (2001) in the original SEBS for application in complex vegetated area.

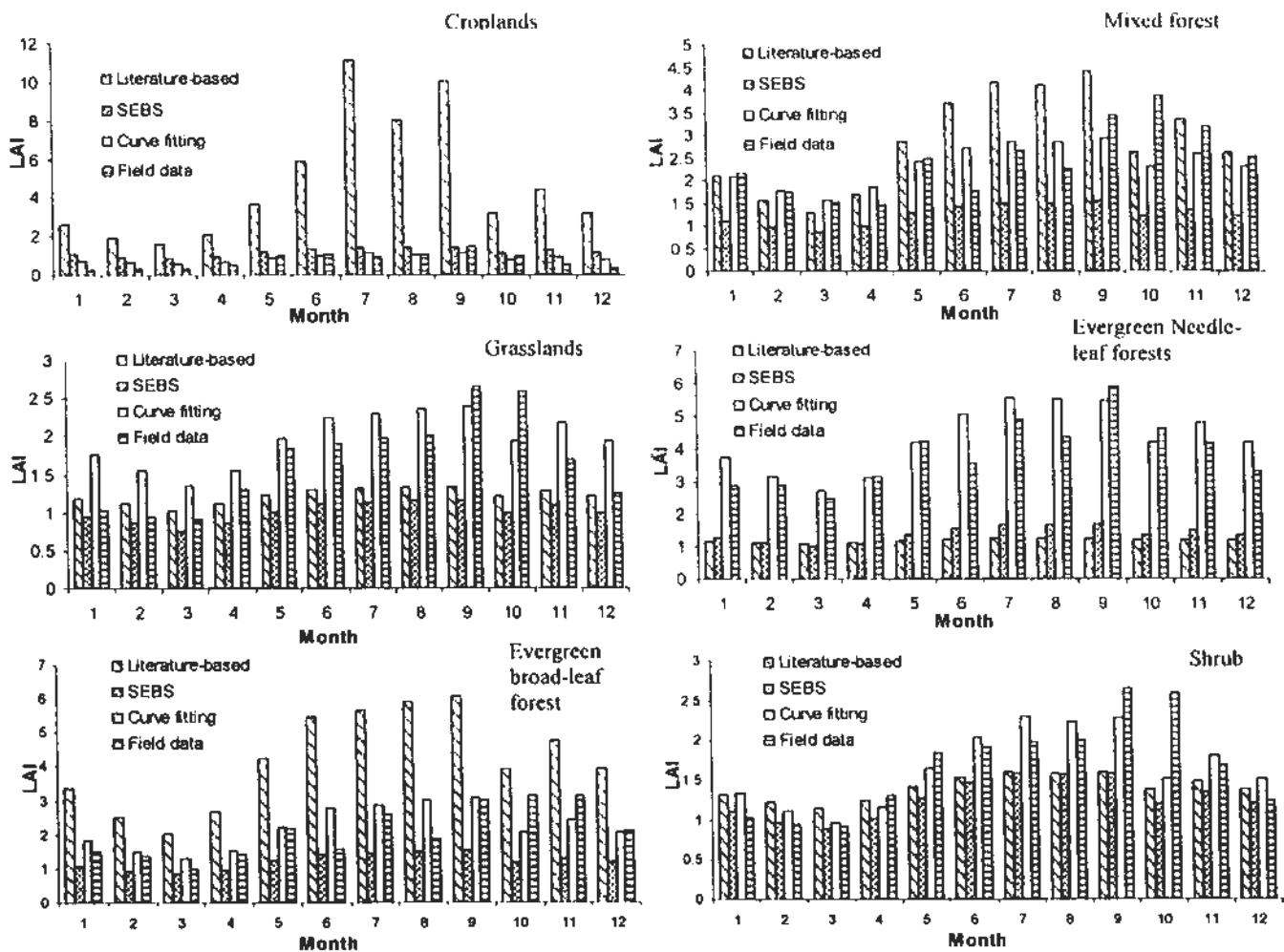


Figure 4.17 Comparison of LAI estimated by different methods

4.5 Validation of ESEBS

ET as a key process in the water budget and the energy budget has traditionally been one of the most difficult hydrological processes to determine, which can not be measured directly (Zhang et al., 2001). Therefore, validation of ET model is of great importance to test the applicability and feasibility.

The complimentary relationship model (AA/GG/CARE) (Xu & Singh, 2005) can estimate actual ET (ET_a) from observations of temperature, humidity, and sunshine duration over a wider range of climate conditions (regions) without calibrations and has been widely used in China, Europe and all over the world. The details of complementary ET model will be described in the following. On the other hand, the hydrological model is capable of yielding an accurate ET amount for a watershed, but cannot provide high resolution ET distribution data like the remote sensing-based models. The remote sensing based model is capable of generating reasonable ET distribution, but the ET amount at pixel scale is in doubt and needs to be evaluated (Gao & Long, 2008). The details of the model will be presented in Chapter 5.

In this section, the complimentary relationship model and the distributed monthly water balance model developed by Chen et al. (2006) are employed to validate the ESEBS model by inter-comparison of annual ET and monthly processes at the watershed level.

4.5.1 Complimentary ET model

Complementary relationship of ET estimation was proposed by Bouchet (1963). For areal estimation, this method is usually preferred because it requires only standard meteorological variables and does not require local parameter calibration. Different models have been derived using the complementary relationship concept, which include the advection-aridity (AA) model proposed by Brutsaert & Stricker (1979), the complementary relationship areal evapotranspiration (CRAE) model derived by Morton (1978), and the complementary relationship model proposed by Granger & Gray (1989) using the concept of relative evaporation (the ratio of actual to potential evaporation). In this study this model is named as GG model. Although the above three models are derived using the complementary relationship concept, the assumptions and derived models forms are different. Besides the above cited references, there are a number of

studies that evaluate the validity of complementary relationship model (e.g. Doyle, 1990; Lemeur & Zhang, 1990; Chiew & McMahon, 1991; Granger & Gray, 1990; Xu & Li, 2003). A comparative study that evaluates the performance of these three models (i.e., CRAE, $\Lambda\Lambda$, and GG) in terms of climate regions and calculation seasons using the same data sets has not been done.

4.5.1.1 Model Description

Using an analysis based on energy balance, Bouchet (1963) corrected the misconception that a larger potential evaporation necessarily signified a larger actual evaporation by demonstrating that as a surface dried from initially moist conditions the potential evaporation increased while the actual evaporation was decreasing. The relationship that he derived has come to be known as the complementary relationship between actual and potential evaporation; it states that as the surface dries the decrease in actual evaporation is accompanied by an equal, but opposite, change in the potential evaporation; the potential evaporation thus ranges from its value at saturation to twice this value (Figure 4.18). This relationship is described as:

$$ET_a + ET_p = 2ET_w \quad (4-58)$$

Where ET_a , ET_p and ET_w are actual, potential and wet environment evapotranspiration, respectively.

The complementary relationship has formed the basis for the development of some evaporation models (Morton, 1983; Brutsaert & Stricker, 1979; Granger & Gray, 1989), which differ in the calculation of ET_p and ET_w . ET_a is usually calculated as a residual of (4-58). For the sake of completeness, the model equations are briefly summarized in what follows using the same notations as used by the original authors. For a more complete discussion, the reader is referred to the cited literature.

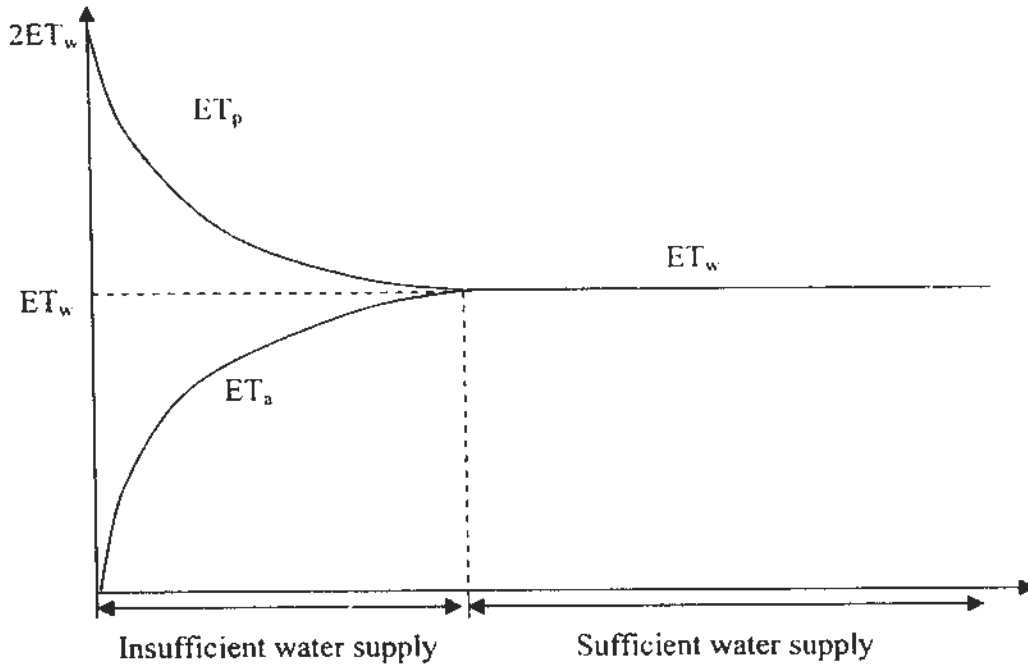


Figure 4.18 Illustration of complimentary relationship ET model
(Modified from Liu et al., 2006)

(1) The AA model

In the AA model, the ET_p is calculated by combining information from the energy budget and water vapor transfer in the Penman (1948) equation:

$$ET_p = \frac{\Delta}{\Delta + \gamma} \frac{R_n}{\lambda} + \frac{\gamma}{\Delta + \gamma} E_a \quad (4-59)$$

where R_n is the net radiation near the surface, Δ is the slope of the saturation vapor pressure curve at the air temperature, γ is the psychrometric constant, λ is the latent heat, and E_a is the drying power of the air which in general can be written as

$$E_a = f(U_z)(e_s - e_a) \quad (4-60)$$

where $f(U_z)$ is some function of the mean wind speed at a reference level z above the ground, and e_a and e_s are the vapor pressure of the air and the saturation vapor pressure at the air temperature, respectively. In this study, the Penman (1948) originally suggested an empirical linear approximation for $f(U_z)$ which was used here:

$$f(U_z) \approx f(U_2) = 0.0026(1 + 0.54U_2) \quad (4-61)$$

which, for wind speeds at 2-m elevation in m/s and vapor pressure in Pa, yields E_a in mm/d. This formulation of $f(U_2)$ was first proposed by Brutsaert and Stricker (1979) for use in the AA model operating at a temporal scale of a few days. Substituting (4-60) and

the wind function (4-61) into the Penman equation (4-60) yields the expression for ET_p used by Brutsaert and Stricker (1979) in the original $\Lambda\Lambda$ model:

$$ET_p^{AA} = \frac{\Delta}{\Delta + \gamma} \frac{R_n}{\lambda} + \frac{\gamma}{\Delta + \gamma} f(U_2)(e_s - e_a) \quad (4-62)$$

The AA model calculates ET_w (Brutsaert and Stricker, 1979) using the Priestley and Taylor (1972) partial equilibrium evaporation equation:

$$ET_w^{AA} = \alpha \frac{\Delta}{\Delta + \gamma} \frac{R_n}{\lambda} \quad (4-63)$$

where $\alpha = 1.26$. Different values for α have been reported in the literature (Xu et al., 2005), the original value was tested in this study. Substitution of (4-62) and (4-63) into (4-58) results in the expression for ET_a (4-64) in the AA model:

$$ET_a^{AA} = (2\alpha - 1) \frac{\Delta}{\Delta + \gamma} \frac{R_n}{\lambda} + \frac{\gamma}{\Delta + \gamma} f(U_2)(e_s - e_a) \quad (4-64)$$

(2) The GG model

Assuming that advection is negligible Granger and Gray (1989) derived the GG model from the energy balance equation (with the terms expressed as an equivalent depth of evaporation) as:

$$E + H = Q \quad (4-65)$$

where E is the actual evaporation (ET_a), H is the sensible heat, and Q is the total energy available from the net radiation and soil heat. Applying the Bowen ratio:

$$\beta = \frac{H}{ET_a} = \frac{\gamma(T_s - T_a)}{(e_s - e_a)} \quad (4-66)$$

and the slope of the saturation vapor pressure curve, $\Delta = de^*/dT$, equal to:

$$\Delta = \frac{(e_s^* - e_a^*)}{(T_s - T_a)} \quad (4-67)$$

to (4-65) one obtains:

$$Q = ET_a \left[1 + \frac{\gamma(e_s^* - e_a^*)}{\Delta(e_s - e_a)} \right] \quad (4-68)$$

where γ = the psychrometric constant: e_s^* and e_s = the saturation and actual vapor pressures at the evaporating surface at a temperature, T_s ; and e_a^* and e_a = the saturation and actual vapor pressures of the air at a temperature, T_a .

Evaporation can also be expressed by the Dalton-type bulk transfer equation:

$$ET_a = f(u) (e_s - e_a) \quad (4-69)$$

or

$$(e_s - e_a) = \frac{ET_a}{f(u)} \quad (4-70)$$

where $f(u)$ is a wind speed function. Substituting (4-47) into (4-68) and rearranging terms the following is obtained:

$$ET_a = Q + \frac{\gamma}{\Delta} f(u)(e_a^* - e_s^*) \quad (4-71)$$

If the vapor pressure of the air, e_a , is added to and subtracted from the difference in the vapor pressure, (4-71) becomes:

$$ET_a = Q + \frac{\gamma}{\Delta} f(u)(e_a^* - e_a)(e_s^* - e_s) \quad (4-72)$$

The term in (4-72), $f(u)(e_a^* - e_a)$, the product of the wind function and the vapor pressure deficit of the air, is generally referred to as the "drying power" of the air (E_a). The second term, $f(u)(e_s^* - e_s)$, is the evaporation rate which would occur under the same atmospheric conditions for wind and humidity, if the surface were saturated at the temperature of the surface. This term therefore represents the potential evaporation, ET_p (Van Bavel, 1966). (4-72) is a general equation relating evaporation to the net energy available by radiation and conduction, the drying power of the air and the potential evaporation. It can be used to calculate ET_a when an adequate expression for ET_p is available.

The formulation for ET_a , although quite simple, has the major drawback of requiring a measurement of the surface temperature, a parameter which is rarely observed. Consider the general case of evaporation from an unsaturated surface at some rate less than the potential, i.e., $0 < ET_a < ET_p$. The relative evaporation, the ratio of actual to potential evaporation, $G = ET_a / ET_p$, should be a unique parameter for each set of atmospheric and surface conditions. Using (4-73) and the equivalent expression for ET_p , G can be expressed as:

$$G = \frac{ET_a}{ET_p} = \frac{f(u)(e_s - e_a)}{f(u)(e_s^* - e_a)} \quad (4-73)$$

(4-73) shows that the relative evaporation is governed by the vapor pressure deficit at the evaporating surface, $(e_s^* - e_s)$, or by the availability of water at the surface. In other words, surface conditions play a predominant role in the partitioning of the available energy to evaporation, and thus also control the potential evaporation. For a wet surface, where $e_s = e_s^*$, G will be equal to unity; for a very dry surface, e_s approaches e_a and G will approach zero, thus, $0 < G \leq 1$. Substituting $ET_a = G ET_p - G f(u) (e_s^* - e_a)$ into (4-72) and simplifying, one gets the general expression for evaporation from an unsaturated surface:

$$ET_a^{GG} = \frac{\Delta G Q}{\Delta G + \gamma} + \frac{\gamma G E_a}{\Delta G + \gamma} \quad (4-74)$$

(4-74) is similar in form to the Penman equation, but differs through the inclusion of the relative evaporation, G , which accounts for departures from saturated conditions.

Granger and Gray (1989) further derived that the relative evaporation G can be calculated as:

$$G = \frac{1}{1 + 0.028e^{8.045D}} \quad (4-75)$$

where $D = E_a / (E_a + Q)$ is the relative drying power.

(3) The CRAE model

There are different forms of the CRAE model that have been reported in the literature; in this study the original form presented by Morton (1983) is used. To calculate ET_p in the CRAE model, Morton (1983) decomposed the Penman equation into two separate parts describing the energy balance and vapor transfer process. A refinement was developed by using an “equilibrium temperature” T_p , which is defined as the temperature at which Morton’s (1983) energy budget method and mass transfer method for a moist surface yield the same result for ET_p . The energy-balance and vapor transfer equations can be expressed, respectively, as:

$$ET_p^{CRAE} = R_T - \lambda_p f_T (T_p - T) \quad (4-76)$$

$$ET_p^{CRAE} = f_T (e_p - e_d) \quad (4-77)$$

in which ET_p is the potential evapotranspiration in the units of latent heat; T_p and T are the equilibrium and air temperatures, respectively, in °C; R_T is the net radiation for soil-plant surfaces at the air temperature; f_T is the vapor transfer coefficient; e_p is the

saturation vapor pressure at T_p ; e_d is the saturation vapor pressure at the dew-point temperature, and

$$\lambda_p = \gamma + 4\varepsilon\sigma(T_p + 273)^3 / f_T \quad (4-78)$$

$$f_T = (P_o / P)^{0.5} f_z \xi^{-1} \quad (4-79)$$

where γ is the psychrometric constant, σ is the Stefan--Boltzmann constant, ε is the surface emissivity, P is the atmospheric pressure, and P_o is the atmospheric pressure at sea level. In (4-79), f_z is a coefficient whose value is $28.0 \text{ Wm}^{-2}\text{mbar}^{-1}$ for above-freezing temperatures. For below-freezing temperatures the value of f_z is increased by a factor of 1.15, the ratio of the latent heat of sublimation to the latent heat of vaporization. Exponent 0.5 represents the effect of atmospheric pressure on the evapotranspiration process and the vapor transfer coefficient. Here ξ represents a dimensionless stability factor with values greater than or equal to 1. Morton (1983) proposed that ξ can be calculated as

$$1/\xi = 0.28(1 + e_d/e_a) + \Delta R_{TC} / [(P_o/P)^{0.5} b_o f_z (e_a - e_d)] \quad (4-80)$$

$$1/\xi \leq 1 \quad (4-80a)$$

in which b_o is 1.0 for areal evapotranspiration, R_{TC} is R_T with $R_{TC} \leq 0$, and other symbols are as defined previously.

If T_p is the sum of a trial value (T'_p) and a correction ($[\delta T_p]$), and if $\delta e_p = \Delta'_p [\delta T_p]$, the solution of (4-76) and (4-77) is:

$$[\delta T_p] = \left[\frac{R_T}{f_T} + e_d - e'_p + \lambda_p (T - T'_p) \right] / (\Delta'_p + \lambda_p) \quad (4-81)$$

in which e'_p and Δ'_p are the saturation vapor pressure and the slope of the saturation vapor pressure curve at T'_p , respectively.

During the iterative process R_T , f_T , e_d , and T remain constant and the effects of changes in λ_p are so small that it is assumed constant at its initial value. For the initial trial T'_p is set equal to the air temperature (T), e'_p is set equal to the saturation vapor pressure at the air temperature, and Δ'_p is set equal to the slope of the saturation vapor pressure curve at the air temperature (T). With each application of (4-81) these three quantities change and the process is repeated until the absolute value of $[\delta T_p]$ becomes less than 0.01°C . The use of (4-81) ensures that this will take place within four trials even in arid climates

where the difference between air and equilibrium temperatures may exceed 10°C. The present study shows that two trials are usually sufficient.

The potential evapotranspiration estimate is obtained by using in (4-76) the value of T_p obtained by the iterative process. Morton (1983) noted that the value of T_p obtained from the first iteration would give the same value of potential evapotranspiration as Kohler and Parmele's (1967) modification of the Penman (1948) equation. In calculating the wet-environment evapotranspiration, Morton (1983) modified the Priestley-Taylor equilibrium evaporation equation (4-63) to account for the temperature dependence of both the net radiation term and the slope of the saturated vapor pressure curve Δ . The Priestley-Taylor factor α is replaced by a smaller factor $b_2 = 1.20$, while the addition of $b_1 = 14 \text{ Wm}^{-2}$ accounts for large-scale advection during seasons of low or negative net radiation and represents the minimum energy available for ET_w but becomes insignificant during periods of high net radiation:

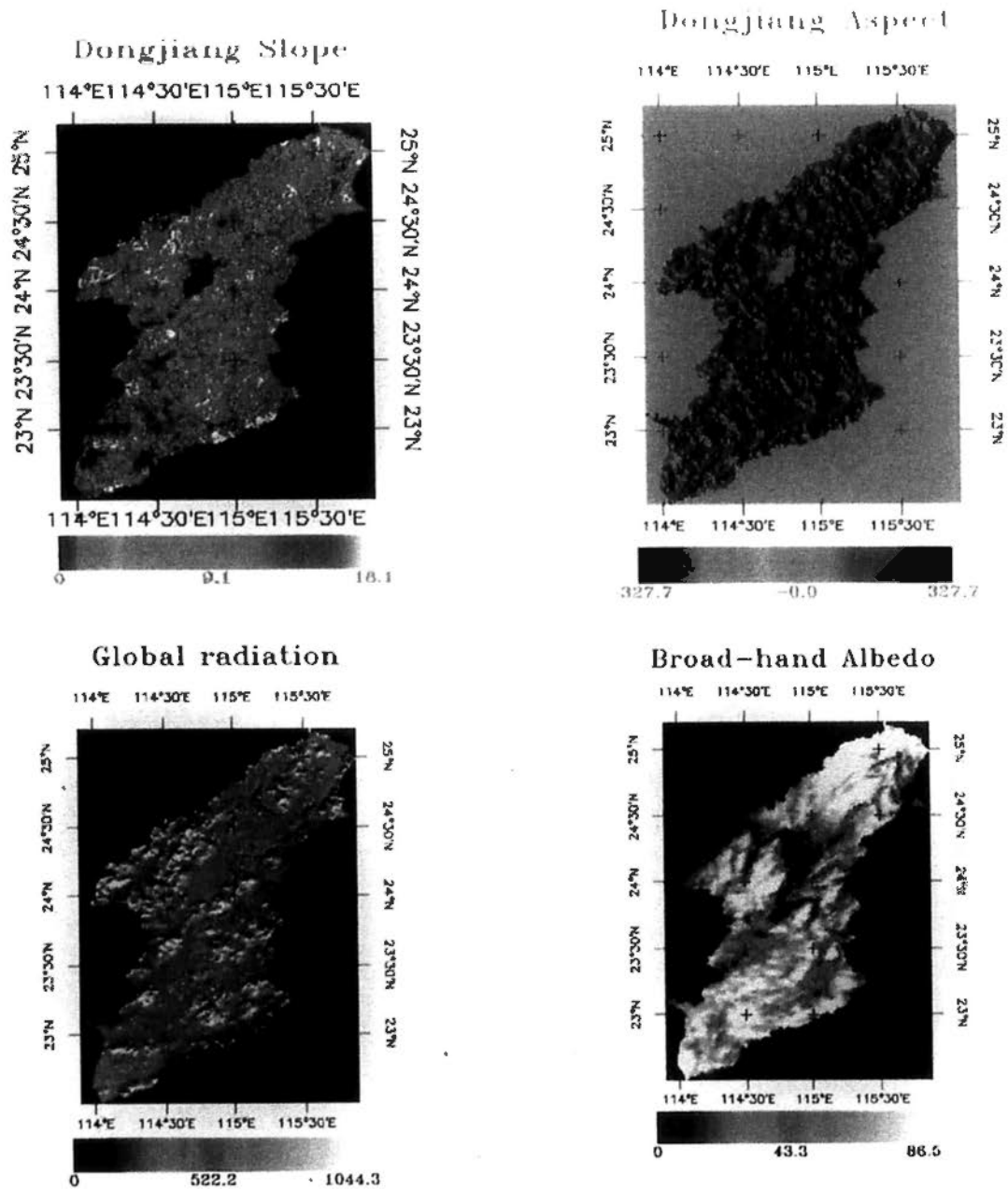
$$ET_w^{CRAE} = b_1 + b_2 \frac{\Delta p}{\Delta p + \gamma} R_{TP} \quad (4-82)$$

where R_{TP} is the net radiation for soil-plant surfaces at T_p and other symbols are as defined previously. Actual evapotranspiration is calculated as a residual of (4-58).

4.6 Results and discussion

4.6.1 ET mapping based on ESEBS from 1982 to 2000

ET mapping was conducted by using ESEBS based on NOAA/AVHRR and meteorological data from 1982 to 2000. For illustrative purpose, one selected daily results of ESEBS on 02/02/1992 are shown in Figure 4.19. The output includes albedo, net radiation, soil heat flux, sensible heat flux, latent heat flux, evaporative fraction and daily evaporation. The annual variation of ET estimated by ESEBS from 1982 to 2000 is presented in Figure 4.20. Moreover, the spatial distribution of annual mean ET is presented in Figure 4.21.



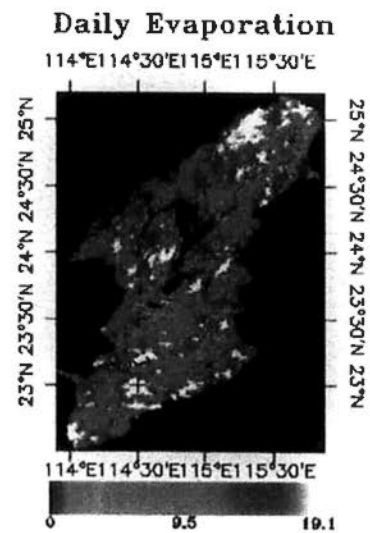
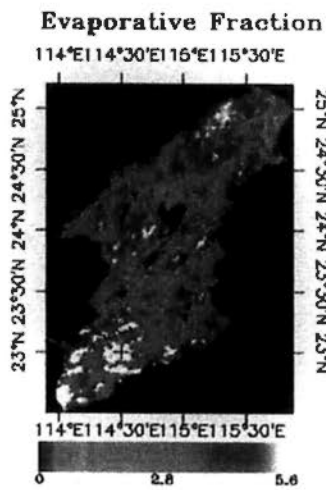
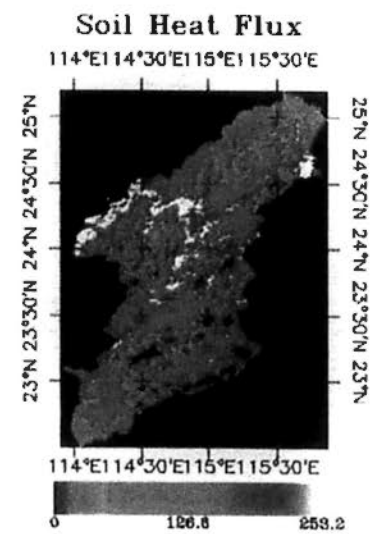
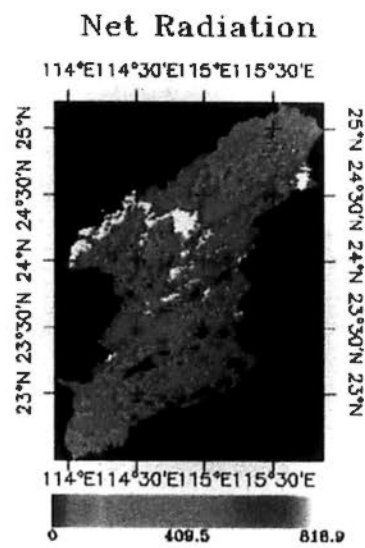
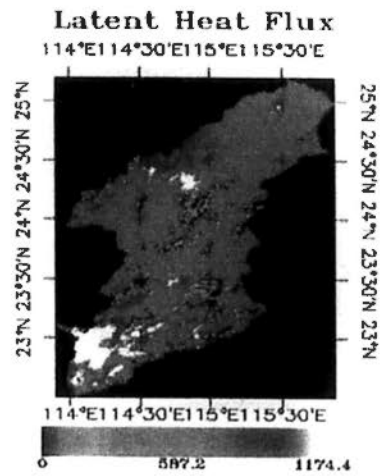
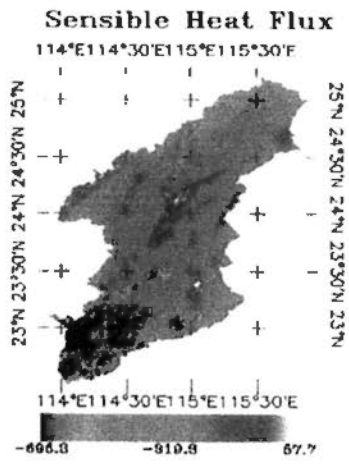


Figure 4.19 ESEBS output on 02/02/1992

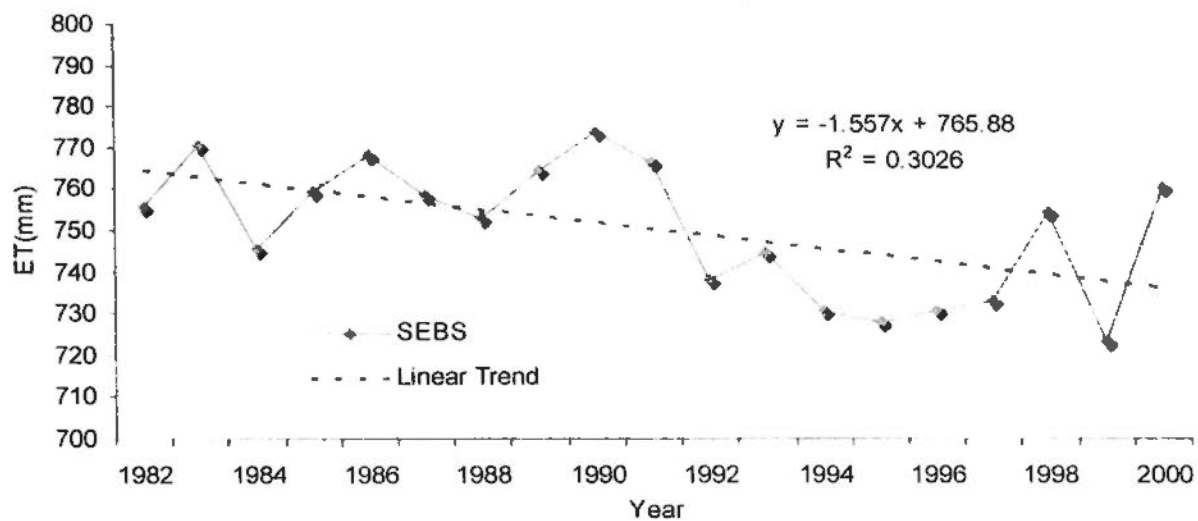


Figure 4.20 Annual variation of ET from 1982 to 2000

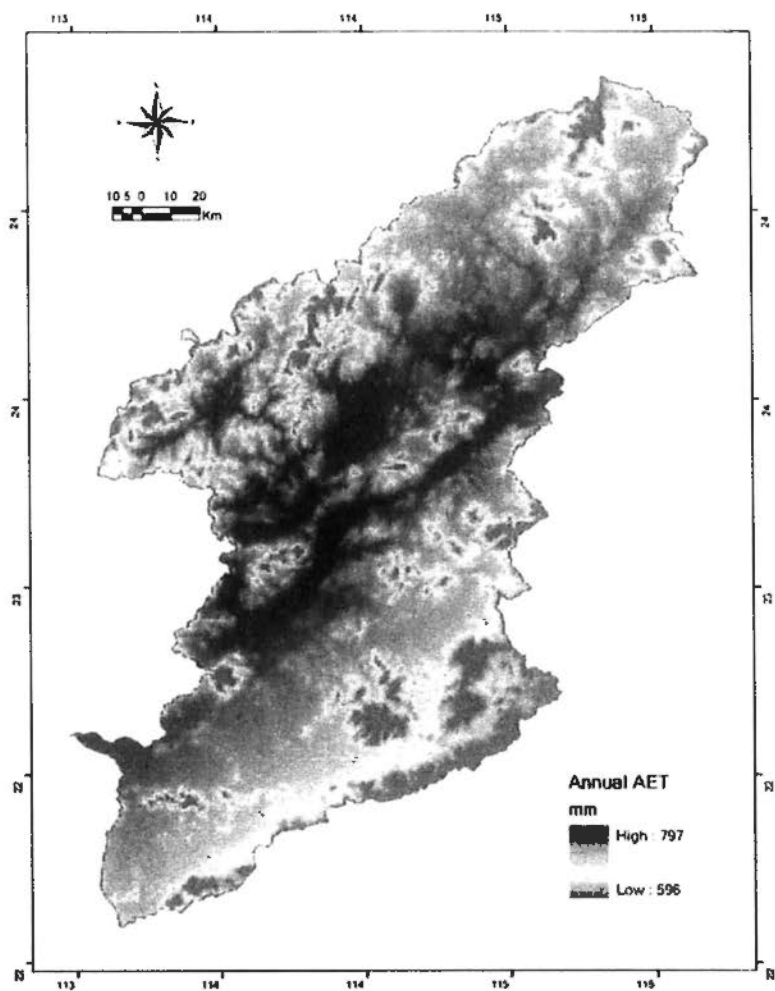


Figure 4.21 Spatial distribution of annual mean ET from 1982 to 2000

4.6.2 Inter-comparison with complimentary ET model and hydrologic model

The inter-comparison results are presented in Figure 4.22 and Figure 4.23. As shown in the figures, there is no significant variation in terms of annual ET. The annual ET generated by SEBS is a little greater than other models. However, the results are still reasonable. On a monthly basis, the results of AA model tend to be homogenization, and the reason is that the AA model does not consider dynamics of topography and soil moisture. GG and CARE model are sensitive to temperature and therefore the models overestimate ET in summer and underestimate ET in winter. However, it makes no difference in annual amount. Hydrologic model shows reasonable results on a monthly and annually basis and the results of SEBS show a good agreement with that of hydrologic model.

By inter-comparison with each other, the results of ESEBS are validated, and the comparison results show that ESEBS agree well with all the other four models with respect to annual ET amount. On a monthly basis, the ESEBS shows a good agreement with hydrologic model. In summary, the feasibility and applicability of ESEBS has been tested by inter-comparison with the other four ET models, which can lay a solid foundation for ET mapping, model integration and studies of hydrologic impact of LUCC.

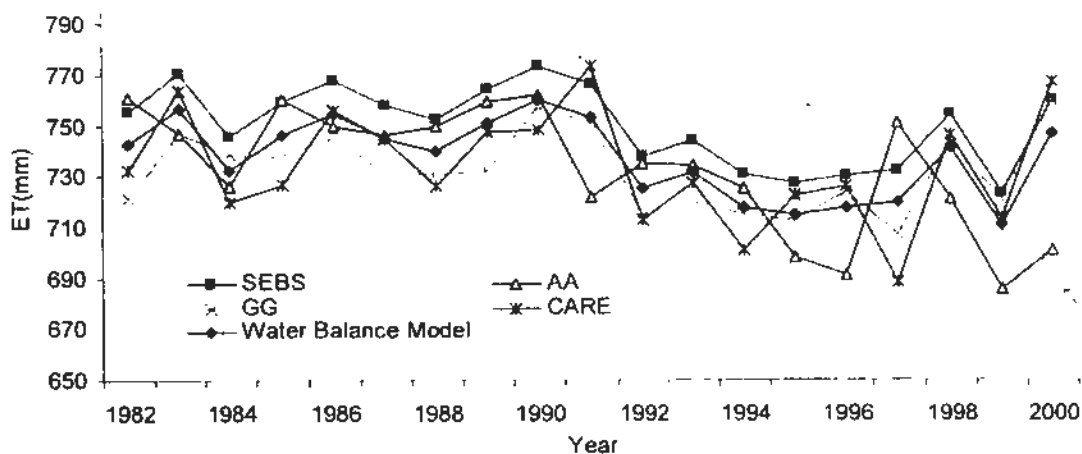


Figure 4.22 Inter-comparison of ET estimated by different models

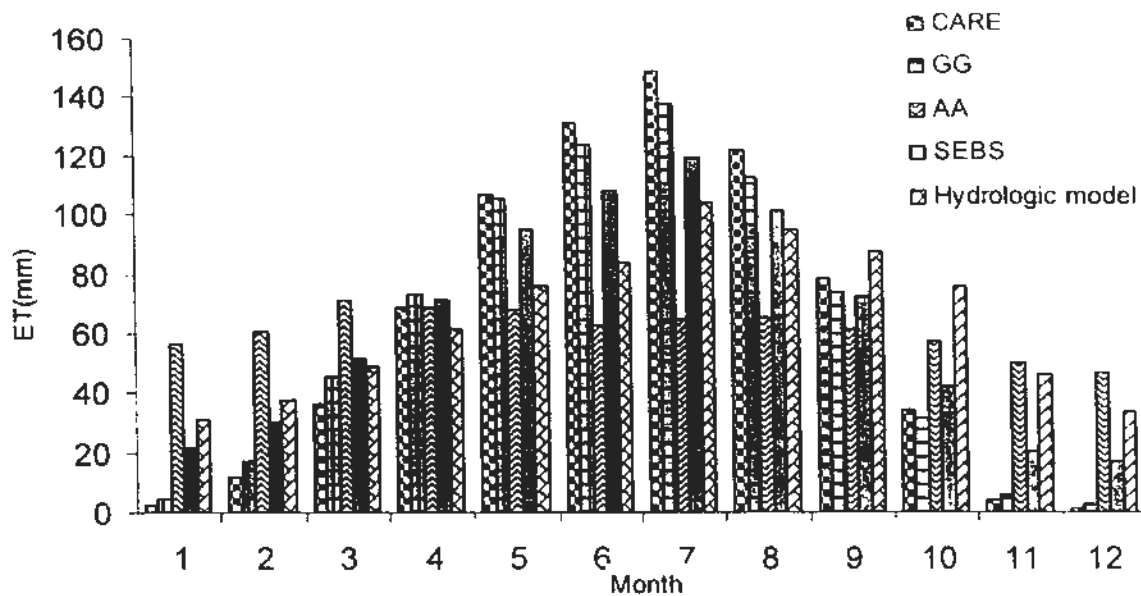


Figure 4.23 Monthly mean ET process of different models

4.6.3 Spatio-temporal analysis of ET in the East River Basin

4.6.3.1 Temporal analysis of ET in the East River Basin

(1) Analysis of annual ET

The annual ET estimated by SEBS is shown in Figure 4.24. As shown in Figure 4.24, it can be observed that a decrease of ET from 1982 to 2000. The Z value of M-K test is -1.782, which indicates a significant decrease of ET during the study period.

The four climatic variables related to ET, namely temperature, relative humidity, wind speed and sunshine duration, are presented in Figure 4.24 ~ 4.27. The Z values for temperature, relative humidity, sun duration, wind speed are 2.446, -2.099, -1.329 and 0.630 respectively. The results indicate that there is a significant increase in temperature, however, the relative humidity and sunshine duration decrease significantly and an insignificant decrease can be found in wind speed. The relative humidity has a negative relationship with ET while the other three climatic variables have positive relationships with ET, therefore, it can be concluded that the decrease of annual ET may probably be caused by decrease of sunshine duration and humidity.

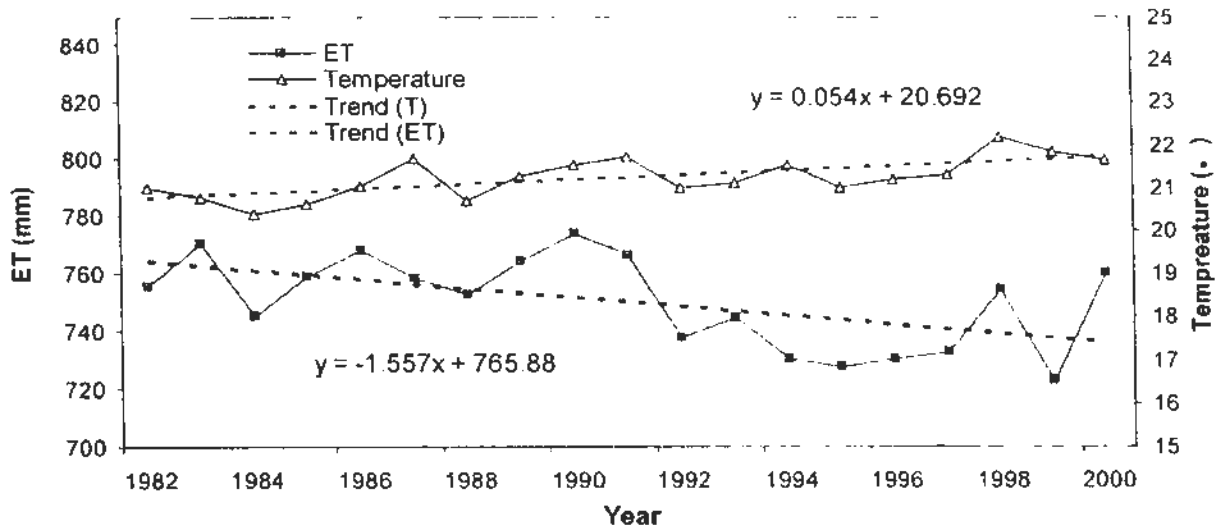


Figure 4.24 Variation of annual mean ET and Temperature from 1982 to 2000

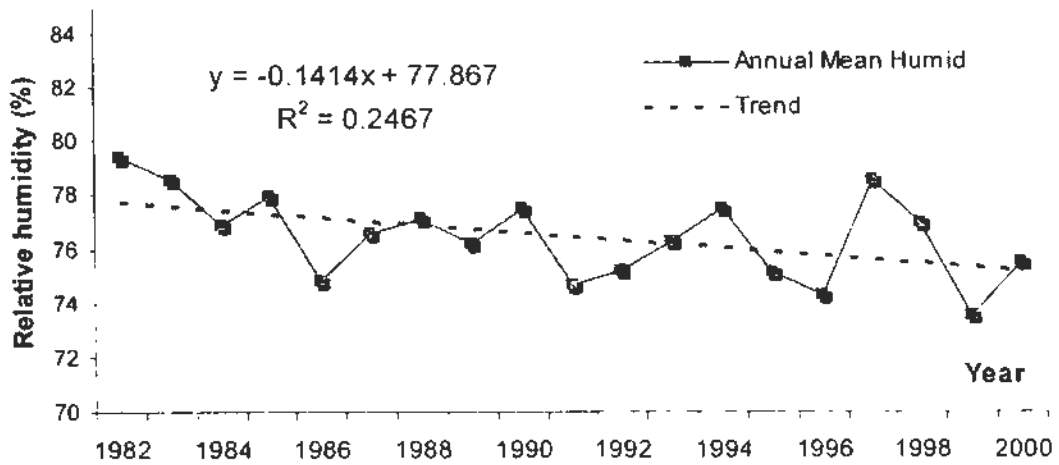


Figure 4.25 Variation of annual mean relative humidity from 1982 to 2000

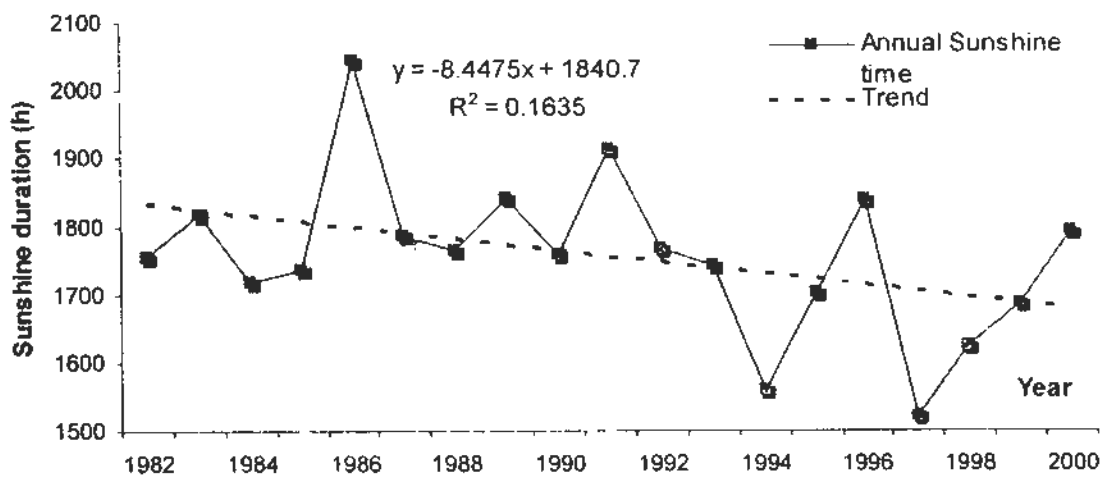


Figure 4.26 Variation of annual mean sunshine duration from 1982 to 2000

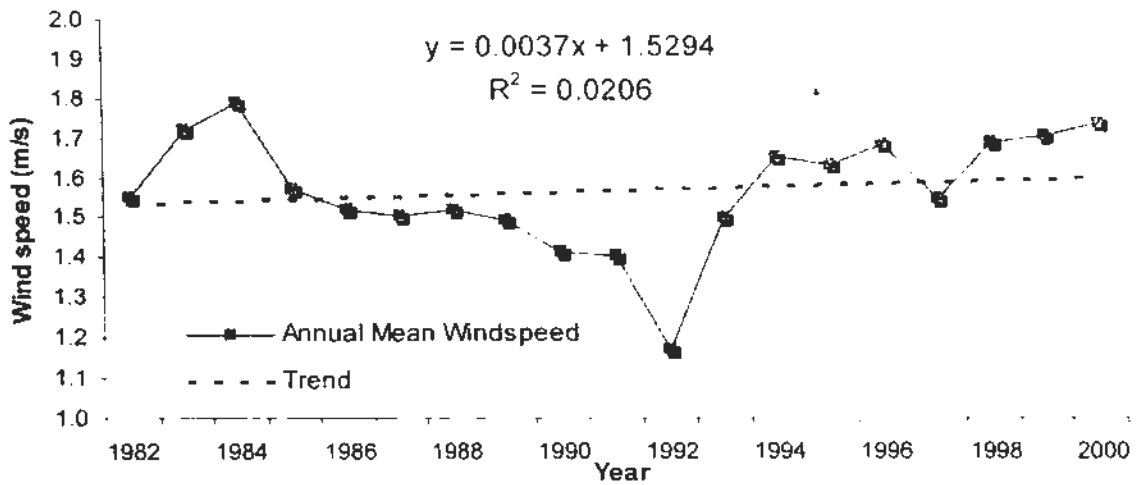


Figure 4.27 Variation of annual mean wind speed from 1982 to 2000

(2) Analysis of monthly ET

Monthly ET estimated by SEBS, monthly LAI, and monthly NDVI are presented in Figure 4.28 and 4.29. As shown in the two figures, it is clear that there is a good agreement of the trend among ET, LAI and NDVI, which indicates ET has a positive relationship with vegetation indexes on a monthly basis. In terms of monthly process, ET reaches the highest value in July and goes down to lowest value in December and January, which agrees well with monthly variation of temperature. Therefore, it can be concluded that ET has close relationship with LAI and temperature on a monthly basis.

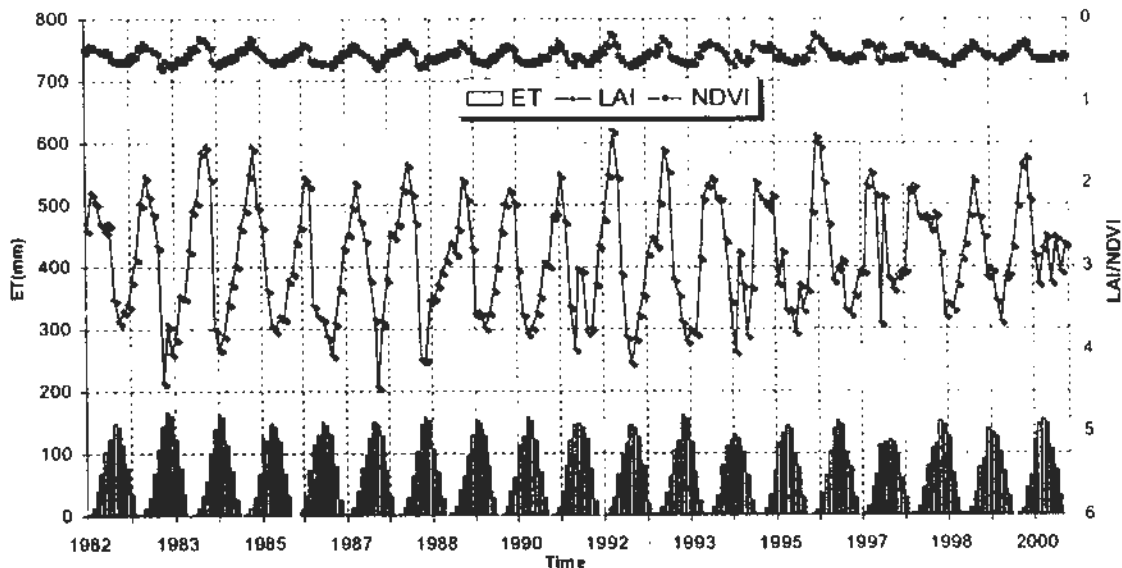


Figure 4.28 Comparison of monthly ET, NDVI and LAI from 1982 to 2000

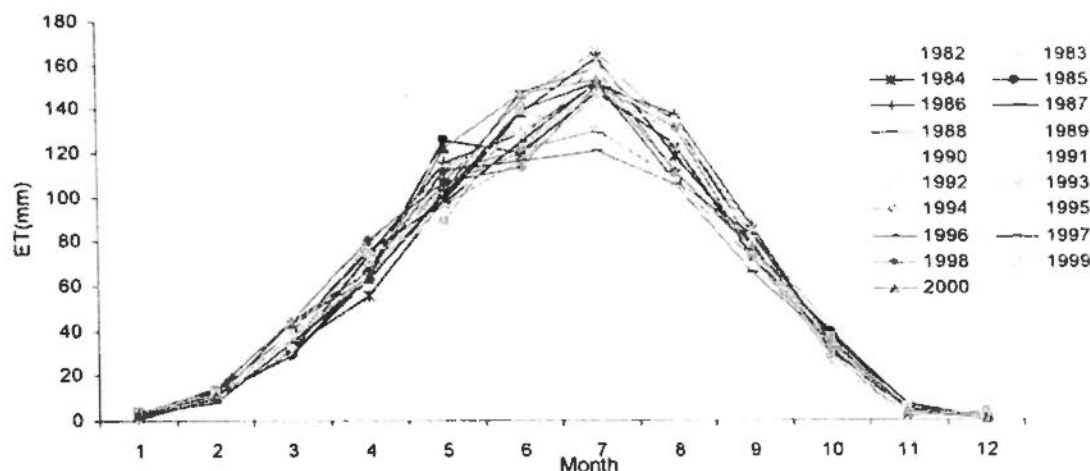


Figure 4.29 Monthly process of ET estimated by ESEBS

4.6.3.2 Spatial analysis of ET in the East River Basin

As shown in Figure 4.21, it can be found that the forest area in the upper-middle-part (northern part) has higher ET, while the urban area in the southern part has lower ET. Moreover, ET has a negative relationship with elevation (Table 4.3). The higher elevation represents lower ET. This can be explained that temperature decreases with the increase of elevation.

Moreover, as mentioned in Chapter 1, ET is closely linked with land cover. Relationship of ET and land cover will be further discussed in Chapter 6.

Table 4.3 Elevation and ET

Elevation (m)	ET (mm)			
	Min	Max	Range	Mean
0-150	689	797	108	765
150-300	664	794	130	762
300-500	626	784	158	744
500-700	613	770	157	719
700-1500	596	739	143	688

4.7 Summary and conclusion

The aim of this chapter is to use remote sensing to estimate areal ET rather than traditional point measurement. The data and SEBS are firstly described. Secondly, the SEBS is enhanced for application in complex vegetated area by estimating LAI, Z_{0m} and d_0 for different land cover. Furthermore, the enhanced SEBS (ESEBS) is employed to estimate surface fluxes and estimate areal ET spatially for a large area. Moreover, the results of SEBS are validated with complimentary relationship ET models (AA/GG/CARE) and Distributed Monthly Water Balance Model. The validation results show that the ESEBS has a good accuracy both monthly and annually and can be applied in the East River Basin. Lastly, spatio-temporal variation of ET in the East River Basin is analyzed. The ET mapping results demonstrate that actual ET in the East River Basin decreased significantly during the last two decades. By inter-comparison with trends of the corresponding climatic variables, namely, temperature, relative humidity, wind speed and sunshine duration, it is concluded that the decrease of ET is probably caused by decrease of sunshine duration.

In summary, the application of ESEBS shows a good accuracy and applicability in the East River Basin. With the ESEBS, physically-based ET mapping can be conducted in complex vegetated area with aid of GIS/RS. Based on the ET mapping, spatially-distributed ET estimates can be obtained, which can lay a solid foundation for future studies of hydrologic impacts of LUCC.

CHAPTER 5

INTEGRATED DISTRIBUTED MONTHLY WATER BALANCE MODEL (IDMWBM)

5.1 Introduction

As mentioned previously, one of the most promising hydrological modeling techniques for assessing regional effects of land use change is water-balance modeling on a monthly basis. Since the objective of land use change impact studies is to project the average hydrological behavior of a watershed under different land use change scenarios, the use of monthly water balance models for studying the hydrological impact of potential land use change has several merits (Figure 5.1). Firstly, hydrological modeling on a large spatial scale which is not data intensive and requires only averages of watershed characteristics as model input that can be performed. Secondly, the structure of monthly water balance models is not so complicated and the physical basis is clear that make them applicable. Thirdly, monthly water balance models are suitable for assessing hydrologic impacts of LUCC because land use changes are often studied on monthly basis. Fourthly, water resources management and planning for a large basin or region is generally on monthly or longer time scales. However, there is no universally accepted water balance model for all the areas due to land surface heterogeneity. Moreover, most of the water balance models applied in China can do a fairly good job for the prediction of spatially averaged catchment response; however they are limited in assessing the effect of land use and other changes in basin hydrology (e.g. Zhao, 1980; Guo et al., 2002; Chen et al., 2006; Wang, 2007). The distributed monthly water balance model (DMWBM) developed by Chen et al. (2006) is well suited for the East River Basin in practice, however it has several limitations in assessing hydrologic impacts of LUCC. On one hand, it does not have any direct links with vegetation which makes them not capable of predicting hydrologic impacts of LUCC. On the other hand, it has only one set of parameters for the whole basin. As mentioned by Beven (2001) and Singh (1995), distributed hydrologic models have a set of effective parameters for each cell or spatial unit. In this sense, it is a semi-distributed model and more efforts have to be made for estimating distributed parameter at each spatial unit.

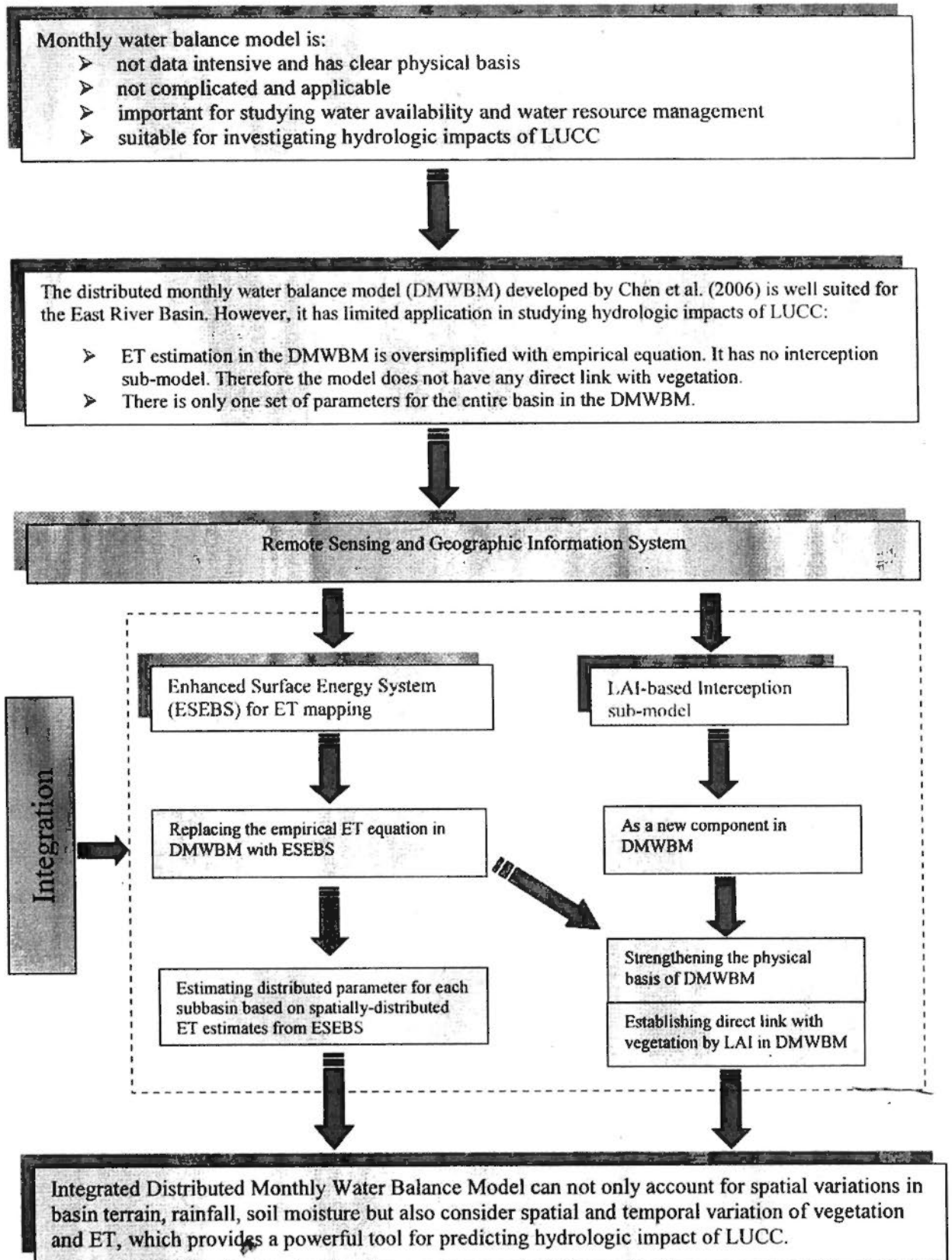


Figure 5.1 Integration of ESEBS and LAI-based interception sub-model into monthly water balance model for assessing hydrologic impact of LUCC

The integration procedures of ESEBS and LAI-intercept sub-model into monthly water balance model for assessing hydrologic impact of LUCC are illustrated in Figure 5.1. As shown in Figure 5.1, in this chapter firstly an integrated distributed monthly water balance model accounting for the spatial variations of basin topography and precipitation and considering vegetation effects is developed with the aid of GIS/RS. This integrated model is capable of simulating the runoff generation processes by accounting for the spatial and temporal dynamics of soil moisture storage over the entire basin. Furthermore, the model is integrated with a physically-remote-sensing-based ET sub-model and a LAI-based interception sub-model, which can strengthen the physical basis of the model and establish direct links between hydrologic processes and vegetation. Therefore it can be used for predicting hydrologic impact of LUCC. Finally, with the spatially-distributed ET estimates from the ESEBS sub-model, the integrated model can estimate distributed parameters at sub-basin scale, which moves one more step in the development of distributed hydrologic model. In a word, the Integrated Distributed Monthly Water Balance Model can not only account for spatial variations in basin terrain, rainfall, soil moisture but also consider spatial and temporal variation of vegetation and ET, which provides a powerful tool for predicting hydrologic impact of LUCC.

5.2 Conceptual framework of Monthly Water Balance Model

Regional terrestrial hydrological processes occurring in a warm and humid region are presented in Figure 5.2. The hydrological response of a catchment is mainly governed by the local combination of topography, vegetation, soil and geology. Heterogeneity of the hill slope forms, properties of soils and vegetation in combination with rainfall variability to produce different runoff processes and responses across hill slope, different soil moisture conditions and inter-storm (dry period) moisture redistribution and evapotranspiration (Wood, 1995).

To simulate the complete hydrological processes accurately would call for a very detailed knowledge of the catchment, of the physical processes governing water movement and of the ways by which these factors interact. Even if these processes are understood completely, at the present level of field observations, it is impossible to simulate the overall catchment responses. Therefore conceptualization has to be made.

What to conceptualize and to what extent are problems that relate to scale issues since different hydrological processes occur at different scales of space and time (Dooge, 1988; Klemes, 1983).

The terrestrial water balance components, including precipitation, interception, infiltration, evapotranspiration and runoff is highly nonlinear and involves spatially variable processes. However, on a longer time scale, such non-linearity would decrease, e.g. the degree of nonlinearity of a catchment response on a monthly time scale is much smaller than that on shorter time scales such as daily and hourly. This has been illustrated in previous studies (e.g., Jiang, 2005; Chen et al., 2006; Wang, 2007).

The response characteristics of a catchment on a monthly scale can be explained by fast response and slow response. Fast response, which usually occurs during and immediately after rainfall events and generates fast runoff (direct runoff and return flow), mainly depends on the rainfall amount and the state of soil moisture content. Slow response, which dominates in low flow periods and generates the slow runoff or base flow, is mainly dependent on groundwater storage. All the fast and slow runoff forms the currently monthly streamflow at the catchment outlet. Therefore, a monthly model does not distinguish between the runoff generating and routing processes.

Water balance models simulate the movement of water through a catchment from the time that it enters as precipitation to the time that it leaves as evapotranspiration or runoff. Both evapotranspiration and runoff generation are strongly dependent on the volume of precipitation and soil moisture characteristics of the catchment on a monthly scale. In a humid catchment, rainfall amount exceeding the soil moisture capacity becomes fast runoff. Evapotranspiration is a function of potential evapotranspiration and soil moisture (Chen et al., 2006). Soil moisture is an important factor influencing the hydrological processes of a catchment. Since soil moisture is dominated by the characteristics of catchment topography, vegetation and soils, the heterogeneity of topography, vegetation and soil on spatial dimensions lead to spatial variation of soil moisture. On the other hand, ET is a dominant hydrologic component on a monthly basis and a complex process between water and energy fluxes subjected to changing atmosphere, soil and vegetation conditions. Therefore, if a model can represent the

spatial variation of soil moisture and ET and their effects on hydrological processes, the ability of the model to simulate the catchment responses will be improved.

Accounting for the spatial variation of soil moisture capacity and the influence of topography on soil moisture storage, considering vegetation effects on hydrologic cycle, the Integrated Distributed Monthly Water Balance Model developed in this study can establish direct links between vegetation and hydrologic process and represent hydrologic processes in a distributed way. It is simple in structure with three parameters for calibration so that the reliable relationship between model parameters and catchment characteristics can be obtained. Using monthly precipitation and potential evapotranspiration data as input and integrating with physically-remote-sensing-based ET model and LAI-based interception model, the physical basis of the integrated model is strengthened. Moreover, through the integration, a direct link between hydrologic processes and vegetation is established. In a word, through the integration, the Integrated Distributed Monthly Water Balance Model can not only account for spatial variations in basin terrain, rainfall, soil moisture but also consider spatial and temporal variation of vegetation and ET, which provides a powerful tool for evaluating the impact of land use change on regional water resources and hydrological regimes.

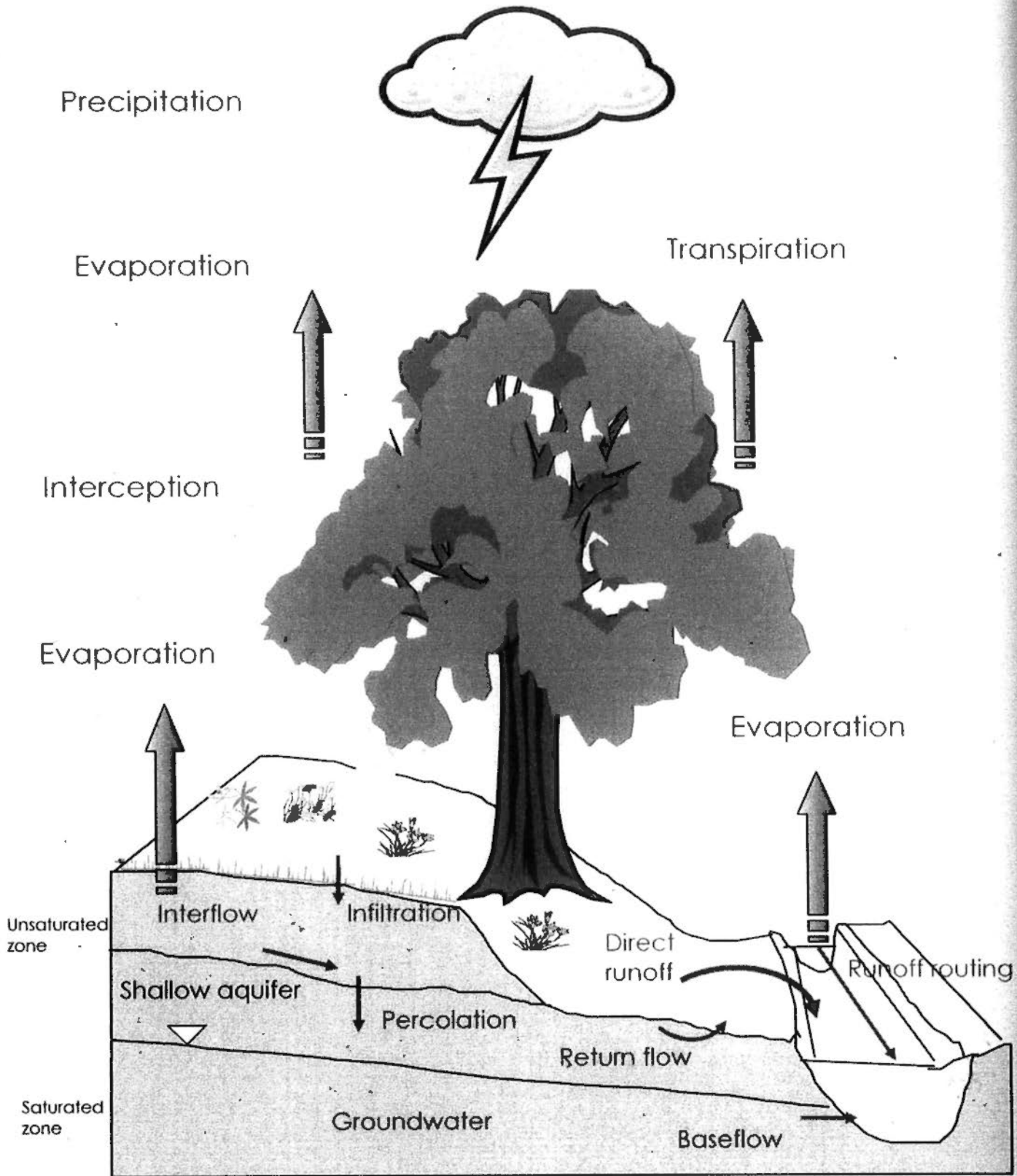


Figure 5.2 Regional terrestrial hydrological processes in warm and humid area

5.3 Distributed Monthly Water Balance Model

The following local mass balance equation in continuum form is essential for the hydrologic model development (Beven, 2002):

$$\frac{dS}{dt} = \nabla q + p - e \quad (5-1)$$

where s is a local mass storage, ∇q is the divergence in local mass flux, p is a local source term (such as precipitation) and e is a local loss term (such as evapotranspiration). More sophisticated mathematical equations for dynamic hydrology can be developed if spatial variations of topographical effects are taken consideration. The equations can be used to develop a practical watershed hydrological model in discrete space and time increments. The distributed hydrological model is based on description of spatial variation of hydrological components. Theoretically, numerical solutions of the hydrodynamic equations can be used to describe the spatial variations. The spatial discretization at the scale of finite elements or finite volumes representing discretized soil profiles or hill slope. This method is time consuming and needs lots of data. An alternation is to find mathematical functions to describe the spatial variations. This method is relatively easy to be used in application. However, selection of a proper mathematic function to represent spatial distribution of hydrologic components is difficult because of heterogeneity and variability of catchment characteristics and hydrological response. Rodriguez-Iturbe (2000) pointed out that the final product from equation (5-1) is the probabilistic description of soil moisture at a point as a function of climate, soil, and vegetation. Soil moisture is a key variable for hydrological modeling. Viable attempts to link the spatial structure of the soil moisture field and inherent temporal fluctuations with organization and scaling has been found and has been successfully modeled in the interlocked system of hillslopes and channels which make up the river basin. The description involves both the probability distribution of soil moisture content as well as its correlation structure in time.

Chen et al. (2006) developed a spatially distributed monthly water balance model (DMWBM) that can make use of readily available meteorological and topographic data to simulate spatial distribution of hydrological variables for the purpose of planning and management of environment and water resources over large geographical regions. It adopts the technique of implicit representation of soil moisture characteristics in the

Xinanjiang model and uses the TOPMODEL concept to integrate terrain variations into runoff simulation. With the help of Digital Elevation Model (DEM) program and topography data, the proportion of soil moisture reaching field capacity in Xinanjiang model is substituted by an index of relative difficulty of runoff generation (IRDG) which is a function of topographic index. Streamflow from the watershed outlet is routed by a simple storage routing approach. There are in total only three parameters need to be determined in the DMWBM. For the purpose of completeness, some important equations are briefly summarized as follows.

5.3.1 The TOPMODEL

The TOPMODEL, proposed by Beven & Kirby (1979), is a physically based watershed model that simulates the variable-source-area concept of streamflow generation. This model requires DEM data and a sequence of rainfall and potential evapotranspiration data for predicting stream discharge.

Since the theoretical basis of the TOPMODEL has been clearly reported in the literature (Beven & Kirby, 1979; Beven & Wood, 1983; Beven, 1997b), a brief description of the model is provided herein. The TOPMODEL makes use of a topographic index of hydrological similarity based on an analysis of the topographic data. The topographic index at any location x in the basin is defined as:

$$TI_x = \ln \frac{a}{\tan \beta}, \quad (5-2)$$

where a is the upstream contributing area per unit contour length that drains through location x , and $\tan \beta$ is the local slope. Large values of $\ln(a/\tan \beta)$ indicate that the locations are topographically convergent and more likely to be saturated. Small values correspond to uphill areas of flow divergence.

In general TOPMODEL predicts the catchment responses following a series of rainfall events. Also, it maintains a continued accounting of the storage deficits allowing the identification of the saturated source areas within the catchment. This model involves several important hydrological equations and variables for its simulation purpose.

Based on this exponential approximation, the local deficit is derived as:

$$S_i = \bar{S} + m[\Lambda - \ln(a/\tan \beta)_i] \quad (5-3)$$

Where \bar{S} is the average storage deficit, Λ is the areal average of $\ln(\alpha/\tan\beta)$. The equation (5-3) is used to predict the saturated contributing areas at each time step. The negative value of S_i indicates that the area is saturated and the saturation overland flow is generated, while the positive value of S_i indicates the area is unsaturated. Unsaturated zone calculations are made for each $\ln(\alpha/\tan\beta)$ increment.

The calculations use two storage elements, SUZ and SRZ , representing a root zone storage, the deficit of which is 0 at 'field capacity' and becomes more positive as the soil dries out; and an unsaturated zone storage which is 0 at field capacity and becomes more positive as storage increases. Storage subject to drainage is represented by SUZ_i for the i -th increment of $\ln(\alpha/\tan\beta)$.

The subsurface flow rate per unit width of contour length, q_s , vertical flow to the zone, and outflow from the saturated zone, Q_b are all dependent on the topographic index.

5.3.2 The Xinanjiang model

The Xinanjiang model was first developed in 1973 and published in English in 1980 (Zhao et al., 1980). It is a well-known lumped watershed model and has been widely used in China. In comparison with other lumped hydrologic models, the Xinanjiang model describes watershed heterogeneity using a parabolic curve of field capacity (FC) distribution (Zhao et al., 1980).

$$\frac{f}{F} = 1 - \left(1 - \frac{WM'}{WMM}\right)^b \quad (5-4)$$

where WM' is FC at point and varies from zero to the maximum of the whole watershed WMM , b is a power index. The $\frac{f}{F}$ versus WM' curve is shown in Figure

5.3. Watershed average field capacity (WM) is the integral of $1 - \frac{f}{F}$ between $WM' = 0$ and $WM' = WMM$, obtaining

$$WM = WMM / (1 + b) \quad (5-5)$$

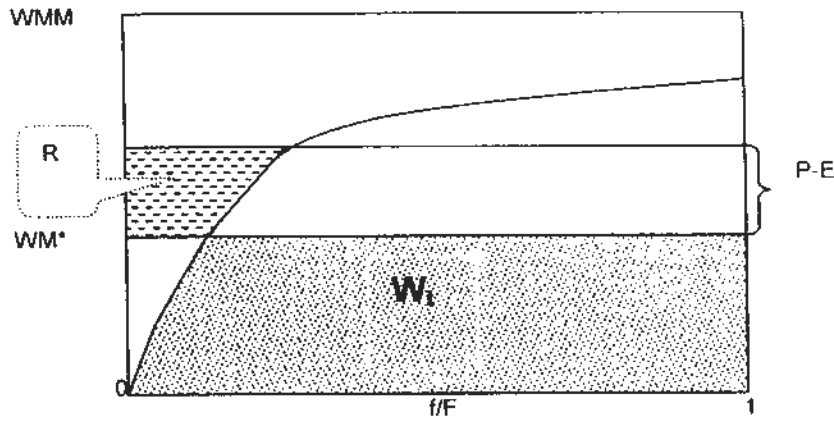


Figure 5.3 Field capacity curve of soil moisture and rainfall-runoff relationship

For the watershed-average soil moisture storage W_t at time t , is the integral of $1 - \frac{f}{F}$ between zero and WM_t^* , a critical FC at time t (Figure 5.3).

$$W_t = \int_0^{WM_t^*} \left(1 - \frac{f}{F}\right) dWM' = WM \left(1 - \left(1 - \frac{WM_t^*}{WMM}\right)^{1+b}\right) \quad (5-6)$$

Thus, the critical FC WM_t^* corresponding to watershed-average soil moisture storage W_t is

$$WM_t^* = WMM \left[1 - \left(1 - \frac{W_t}{WM}\right)^{\frac{1}{1+b}}\right] \quad (5-7)$$

Runoff occurs where soil moisture reaches FC . As shown in Figure 5.3, if the net rainfall amount (precipitation amount minus actual evaporation) in a calculation time interval $[t, t+\Delta t]$ is $P_t - E_t$ and initial average soil moisture (tension water) is W_t , then runoff yields in the time interval R_t can be calculated as

If $P_t - E_t - WM_t^* < WMM$

$$\begin{aligned} R_t &= P_t - E_t - \int_{WM_t^*}^{P_t - E_t + WM_t^*} \left(1 - \frac{f}{F}\right) dWM' \\ &= P_t - E_t - WM + W_t + WM \left[1 - \left(\frac{P_t - E_t - WM_t^*}{WMM}\right)^{1+b}\right] \end{aligned} \quad (5-8)$$

If $P_t - E_t - WM_t^* \geq WMM$

$$R_t = P_t - E_t - WM + W_t \quad (5-9)$$

5.3.3 DEM-based FC distribution and runoff generation

The parameter b represents spatial heterogeneity of FC , uniform distribution for $b=0$ and significant spatial variation for larger b . In the hilly mountain area, Topography

index indicates that topography dominated spatial variations of soil wetness. Larger topography index at a local area means less soil moisture deficit or easier runoff generation in a rainfall period. On contrast, larger $\frac{f}{F}$ means larger soil moisture storage capacity in a local area and difficulty in runoff generation in a rainfall period. Comparing distribution of $\frac{f}{F}$ and $\ln(\alpha / \tan \beta)$, Guo et al. (2000) found that $\frac{f}{F}$ is able to be substituted by an index of relative difficulty of runoff generation (IRDG):

$$IRDG = \frac{\max(\ln(\alpha / \tan \beta)) - \ln(\alpha / \tan \beta)}{\max(\ln(\alpha / \tan \beta)) - \min(\ln(\alpha / \tan \beta))} \quad (5-10)$$

where $\max(\ln(\alpha / \tan \beta))$ and $\min(\ln(\alpha / \tan \beta))$ represent maximum and minimum topographic index, respectively.

The cumulative frequency of IRDG is used to substitute FC distribution in equation (5-4). Thus, $\frac{f}{F}$ in equation (5-4) can be calculated from DEM. Soil moisture and runoff yield in each subbasin are calculated by a numerical method. If soil moisture storage capacity in the basin varies from 0 to WMM , and it is divided into N segments, the storage capacity WM_i corresponding to the i -th segment is equal to $i \times WMM / N$ and IRDG is equal to f_i / F . Then, areal mean storage capacity of the basin WM corresponding to equation (5-5) is:

$$WM = \frac{WMM}{N} \sum_{i=1}^N (1 - \frac{f_i}{F}) \quad (5-11)$$

Then equation (5-6) for determining relationship between WM_i^* and W_i is substituted by following two equations

$$W_i = \sum_{j=1}^{N_{WM_i^*}} (1 - \frac{f_j}{F}) \frac{WMM}{N} \quad (5-12)$$

where $N_{WM_i^*}$ is the $N_{WM_i^*}$ -th segment of WMM , and the WM_i^* corresponding to that segment is given by

$$WM_i^* = N_{WM_i^*} \cdot WMM / N \quad (5-13)$$

$N_{WM_i^*}$ and WM_i^* can be obtained from equations 5-12 and 5-13 using an iteration method.

When $P_r - E_t > 0$, runoff begins to be formed and its amount is calculated with following equations:

$$R_t = \int_{WMM^*}^{P_r - E_t + WMM^*} \frac{f}{F} dWMM' \approx \sum_{N_p} \frac{f_t}{F} \frac{WMM}{N} \quad \text{when } P_r - E_t + WMM_t^* \geq WMM \quad (5-14)$$

where N_p is calculated by equations (5-12) and (5-13) if WMM_t^* in equations (5-12) and (5-13) is substituted for $P_r - E_t + WMM_t^*$.

$$R_t = P_r - E_t - (WM - W_t) \quad \text{when } P_r - E_t + WMM_t^* \geq WMM \quad (5-15)$$

Where W_t is the watershed-average soil moisture at time t in the unsaturated zone and can be calculated by the following equation (Zhao et al., 1980)

$$W_t = W_{t-1} + P_r - E_t - R_t \quad (5-16)$$

where E_t is actual evapotranspiration and can be estimated by

$$E_t = \eta E_p \left[1 - \left(1 - \frac{W_t}{WM} \right)^{1/\eta c} \right] \quad (5-17)$$

where η is a conversional coefficient from pan evaporation to potential evaporation, and Be approximately equals to 0.6 (Ripple et al., 1972).

5.3.4 Storage routing of watershed

Point or local runoff will be regulated by watershed surface, subsurface and stream system before it reaches watershed outlet. Most surface water and a portion of subsurface water in shallow layer will flow out the watershed within one calculation time interval; the left will storage in the subsurface soil and flow out in successive months. If the watershed regulation in a monthly scale is treated as a linear reservoir, the following simple storage routing approach could be used to simulate water flow.

$$Q_t = Q_{t-1} e^{-\alpha} + I(1 - e^{-\alpha}) \quad (5-18)$$

$$I = R_t F / \Delta t \quad (5-19)$$

where Q_t and Q_{t-1} are the discharge at time t and $t-1$; α is a parameter used to describe the watershed regulation of monthly runoff, and F is watershed area and t is time.

5.3.5 Model parameters

There are only three parameters, WM , η and α that need to be determined in the DMWBM. The first two parameters influence runoff generation, and the last one, α ,

influences the slope of streamflow hydrograph. Previous studies (e.g., Zhao, 1984; Zhao & Wang, 1988; Huang, 1993) indicate that watershed-average field capacity, WM , is mainly dependent on climatic dryness or wetness. It is smaller in the humid region and larger in the dry region of China. Zhao (1984) demonstrated that runoff generation is insensitive to WM and a certain value can be set depending on the climatic zone. Approximate values of 120 mm for regions south of the Yangtze River and 160 mm for regions north of Yanshan Mountains and northeastern China are recommended by Zhao (1984) and Zhao & Wang (1988). According to MWR (1992), the parameter η varies between 0.72 and 1.00 for an evaporation pan of 80 cm in diameter and between 0.53 and 0.80 for an evaporation pan of 20 cm in diameter, with larger values for humid climate in the southeastern China and smaller values for dry climate in the northwestern China. Therefore, values of WM and η are fairly consistent for basins located in the same climatic zone (Chen et al., 2006).

5.4 Integration of ESEBS and LAI-based interception model into DMWBM

Although the DMWBM developed by Chen et al. (2006) is capable of simulating the runoff generation processes by accounting for the spatial and temporal dynamics of soil moisture storage over the entire basin, there are still some limitations for assessing hydrologic impacts of LUCC in southern China. First and foremost, the ET component in DMWBM is oversimplified with empirical equation (equation 5-17) which can only be obtained through model calibration. Therefore, it does not have clear physical meaning or any direct links with vegetation. Furthermore, there is no interception sub-model in the DMWBM. Interception is an important process in hydrologic cycle, especially in humid southern China, it may account for 20% of annual precipitation (Yuan, 2006). With the empirical ET estimation sub-model and no interception sub-model, the original DMWBM does not have a clear physical basis or any direct links with vegetation, which makes it not capable of predicting hydrologic impacts of land use/cover changes. Moreover, although it is distributed in terms of accounting for spatial variation of rainfall and soil moisture, however, there is only one set of parameters for the entire basin. Since distributed hydrologic models should have a set of effective parameters for each cell or spatial unit, it is not a fully-distributed model regarding to distributed parameters.

This chapter is to integrate ESEBS and LAI-based interception sub-model into the DMWBM for strengthening the physical basis of the DMWBM, establishing a direct link with vegetation, estimating distributed parameters at sub-basin scale and modeling land use/cover changes on hydrologic regimes with GIS/RS. Specifically,

- (1) To integrate the enhanced physically remote-sensing-based ET model (ESEBS) into the DMWBM with RS/GIS by replacing the empirical ET sub-model in the original DMWBM, for strengthening the physical basis of the DMWBM, establishing direct links between hydrologic process and vegetation in DMWBM;
- (2) To integrate the LAI-based interception sub-model as a new component into the DMWBM with aid of RS/GIS, for strengthening the physical basis of the DMWBM, establishing direct links between hydrologic process and vegetation in DMWBM;
- (3) To estimate distributed parameter η and α of DMWBM based on spatially-distributed ET estimates from ESEBS at basin scale.

The flowchart for integrating models of ESEBS, LAI-interception model and DMWBM to predict hydrologic impacts of LUCC is presented in Figure 5.4. On one hand, the enhanced SEBS (ESEBS) is integrated into the distributed monthly water balance model (DMWBM) by replacing the empirical ET sub-model in the original DMWBM with aid of GIS/RS. In addition, the LAI-based interception model (Yi. et al., 1996) as new component is integrated into the DMWBM. Through the integration, the physical basis of the model is strengthened and direct links between hydrologic process and vegetation is established, which makes the integrated model capable of assessing hydrologic impacts of LUCC. On the other hand, based on spatially-distributed ET estimates from ESEBS, the parameters, pan coefficient η and regulation coefficient α can be estimated for each subbasin, which moves one more step in the development of distributed hydrologic model. The details of integration procedure of interception sub-model and ESEBS sub-model are described in the following.

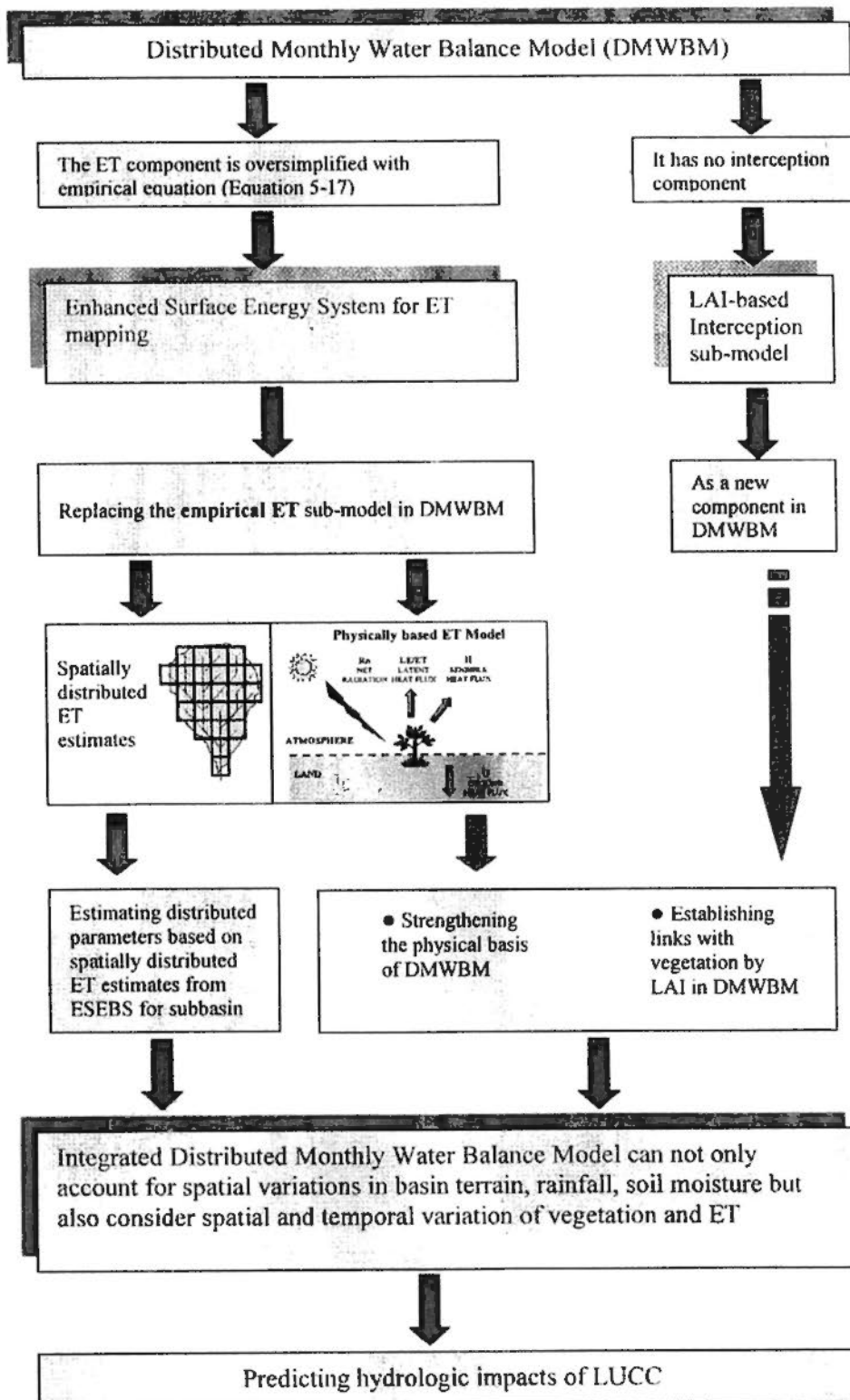


Figure 5.4 Flowchart for integration of ESEBS and LAI-based interception model into DMWBM with aid of GIS/RS

5.4.1 Integration of LAI-based interception sub-model into DMBWM

Rainfall interception is also an important hydrological process that has a close link with vegetation. The amount of water intercepted by the canopy and the net precipitation reaching the ground surface depend on the type and density of vegetation (Yi, et al., 1996; Getu, 1998). Some experiments indicate that the percentage of rainfall intercepted by forest canopies to total annual rainfall varies from 11.4 to 34.3% (Wang & Xue, 1997). However, it has received little attention in most traditional monthly water balance models. Therefore, simulation of interception in monthly water balance model can strengthen the physical basis of model and establish a direct link between hydrologic processes and vegetation, which is important for studying hydrologic impact of LUCC.

Rainfall interception is affected by a number of factors such as canopy characteristics and rainfall regime. Detailed studies of interception processes require accurate and frequent measurements. In practice, such data are not always available. However, for most catchments water balance modeling the interception process can be approximated using a simple equation related to LAI (Yi, et al., 1996; Getu, 1998). According to Yi et al. (1996), interception can be represented by the following equation:

$$E_I = a \times F \times LAI \quad (5-19)$$

where E_I is the interception storage; a is mean canopy storage capacity (mm), which varies from 0.1~0.2, in this study a is 0.15 according to the interception experiments in the same climatic and geomorphologic zone in Taoyuan, Hunan province, which was conducted by research group from Hohai university (Wei, 2010); F is vegetation fractional cover; and LAI is leaf area index, which has already been discussed in Chapter 4.

By integrating this LAI-based interception model as a new component into DMWBM, the net precipitation reaching the ground surface can be estimated in a more accurate way. Moreover, through the integration, the physical basis of DMWBM can be strengthened and direct links between vegetation and hydrologic process can be established in the DMWBM.

5.4.2 Integration of the Enhanced SEBS ET sub-model into DMWBM

As discussed previously, the ET in the DMWBM is oversimplified by empirical equation through model calibration, which does not have clear physical meaning or any direct links with vegetation. Moreover, the DMWBM has only one set of parameters for the whole basin. It is well understood that distributed hydrologic models should have a set of effective parameters for each cell or spatial unit (Singh, 1995; Beven, 2001). Therefore it is still a semi-distributed model and more efforts have to be made for estimating parameters for each subbasin. The Enhanced SEBS (ESEBS) model is a remote-sensing-based model for areal ET estimation, which has a clear physical meaning. Integrating the ESEBS into the DMWBM by replacing the empirical ET estimation model would make significant contributions to strengthening the physical basis and providing the model a direct link with vegetation. Furthermore, through the integration of ESEBS and DMWBM, spatially distributed information of ET is readily available for each subbasin. As a result, for each subbasin, rainfall P and actual Evapotranspiration (spatially-distributed estimates from ESEBS) as the model input are readily available, and therefore the parameter α can be calibrated against observed runoff. On the other hand, the distributed parameter η can also be determined directly based on spatially-distributed ET estimates from ESEBS. In a word, through the integration, the physical basis of the DMWBM can be strengthened, a direct link between vegetation and hydrologic process can be established and distributed parameters for each sub-basin can be estimated, which makes the DMWBM well suited for modeling hydrologic impact of LUCC.

In summary, by the integration of the ESEBS, LAI-based interception sub-model into the DMWBM with aid of GIS/RS, the physical basis of the model is strengthened in terms of ET mapping and interception simulation and the model moves one more step to fully-distributed hydrologic model by estimating distributed parameters for each subbasin. Moreover, it has a direct link with vegetation through ET and interception simulation. In a word, it is a distributed model that can not only account for spatial variations in basin terrain, rainfall, soil moisture but also consider spatial and temporal variation of vegetation and ET, which provides a powerful tool for modeling effects of land use changes on hydrologic regimes.

5.5 Application of the integrated DMWBM in the East River Basin

5.5.1 Basin division and terrain analysis

5.5.1.1 Topographic division of sub-basins

The integrated distributed model has been developed to evaluate the impact of land use change on water resources and hydrological regimes in the East River Basin. The basin exhibits spatial variability of rainfall and the heterogeneity of topography and soil. To improve the accuracy of hydrological simulation and understand the spatial distribution of water balance components, it is necessary to divide the basin into relatively homogenous units (sub-catchments).

Traditionally division of sub-catchments is derived from a topographic map manually. Technological advances in GIS, however, make it possible to delineate sub-catchments from digital elevation models (DEMs) or digital terrain models (DTMs). As shown in Figure 5.5, three data sets must be produced at the initial conditioning stage. The three data sets, in the order that they are produced, are a DEM with sinks filled (or a depressionless DEM), a data set of flow directions and a flow accumulation data set. These three procedures are also required for the delineation of specific watershed, watershed linkages, the generation of drainage networks and overland paths from a DEM.

A sink is a cell or a set of spatially connected cells whose elevation is lower than all of its neighbors' elevation. A DEM almost always contains sinks that hinder flow routing. The objective of the filling sinks is to create an adjusted depressionless DEM in which the cells contain in depressions are raised to the lowest elevation value on the rim of the depression. Sinks can be removed by a smoothing approach (O'Callaghan & Mark, 1984) or filling depression approach (Mark et al., 1984; Douglas, 1986).

The flow direction procedure is applied to a depressionless DEM to build the flow direction data set in where each cell has a definable flow direction value and a flow path to the data set edge. Upon the completion of flow direction data set indicating the direction for each cell, the flow accumulation data set is created by the procedure of the flow accumulation. In this phase, each cell receives a value equal to the total number of cells that drain into it. Cells having a value of zero (to which no other cells flow) generally correspond to the pattern of ridges. The pattern formed by highlighting cells

with values higher than some threshold values delineates a fully connected drainage network. The density of the drainage network decreases with the increase of the value of the threshold. The drainage network is then used to identify watersheds, sub-catchments, overland paths and so on.

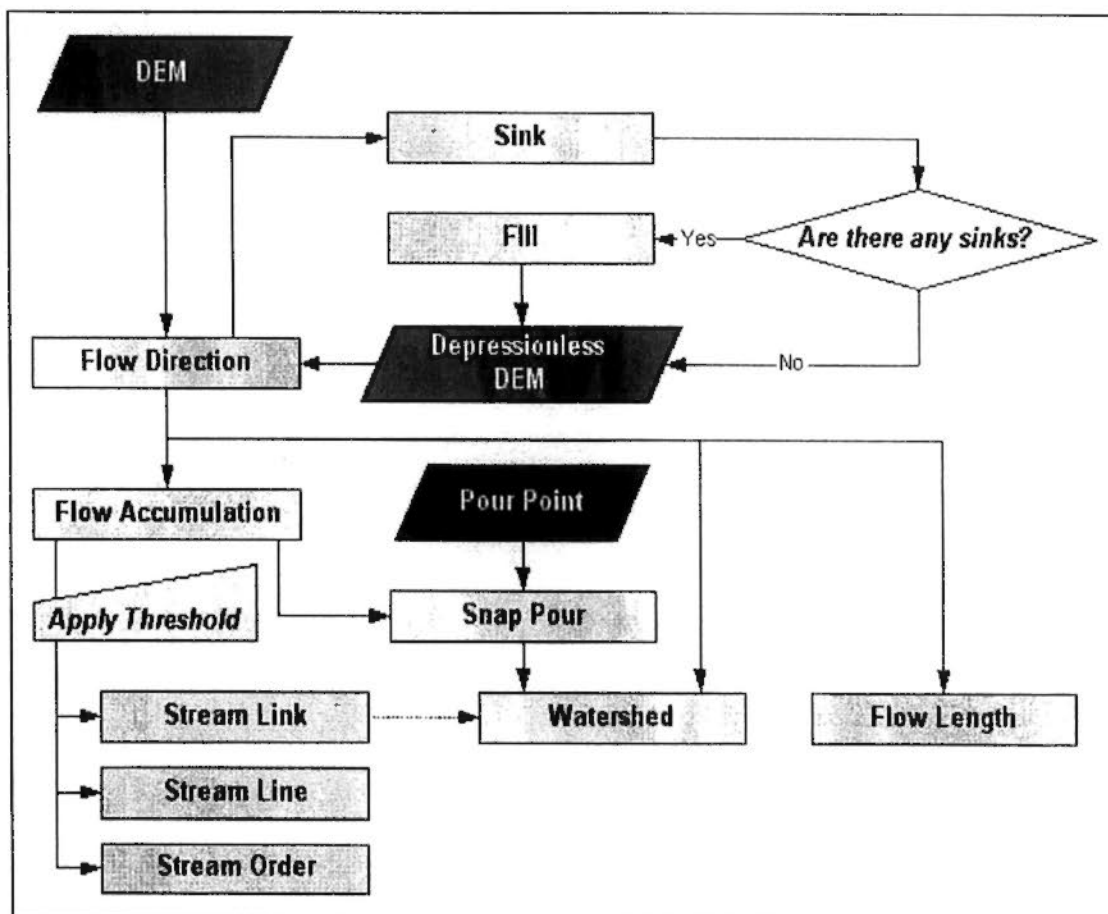


Figure 5.5 Flow chart for the delineation of subbasin from a DEM
(Adapted from ARCGIS 9.2 Manual, 2007)

Over the last two decades, techniques have been developed for extracting a wealth of hydrological information from a DEM. Every technique has its limitations. Research on such a technique is out of the scope of this study. In this study, the techniques developed by Band (1986) and Jenson & Domingue (1987) are directly used to delineate sub-basins. The procedures for the partition of sub-catchments in the East River Basin were presented in Figures 5.6–5.10. All the procedures are achieved by using ARCGIS 9.2 with hydrology extension. The original DEM of the East River Basin at a resolution of $50 \times 50 \text{ m}^2$ is derived from 10 m equidistance contour lines of 1:250000 topographic maps. The entire East River Basin is divided into 17 sub-catchments with areas ranging from 517 km^2 to 2780 km^2 . Each sub-basin represents a consistent unit in terms of hydrological response in that runoff flows out of the sub-catchments through one flow point, and that the surface runoff fluxes across the other boundaries are zero.

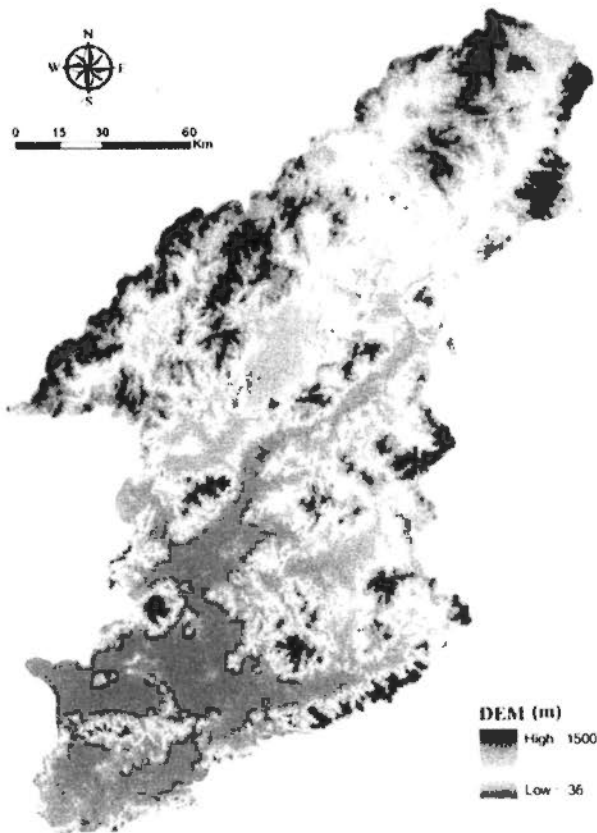


Figure 5.6 DEM for the East River Basin

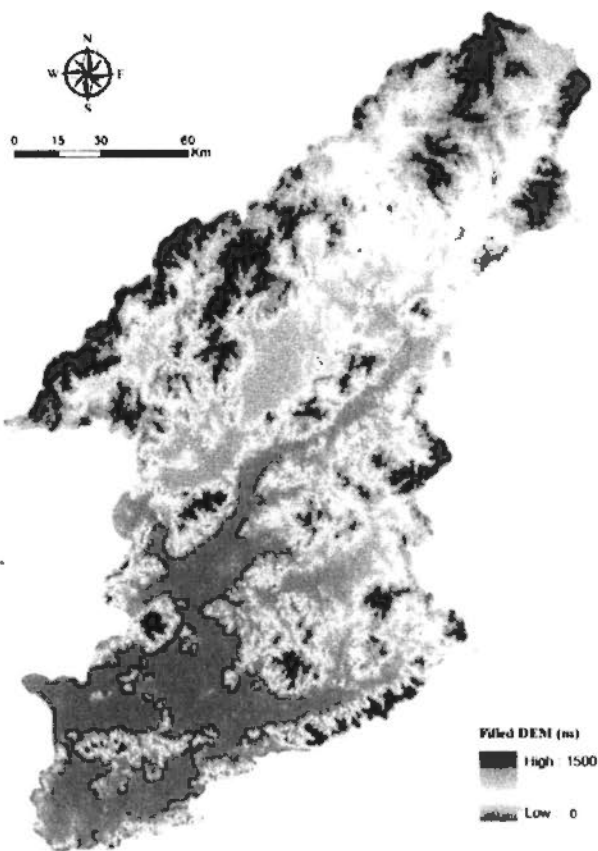


Figure 5.7 Depressionless DEM for the East River Basin

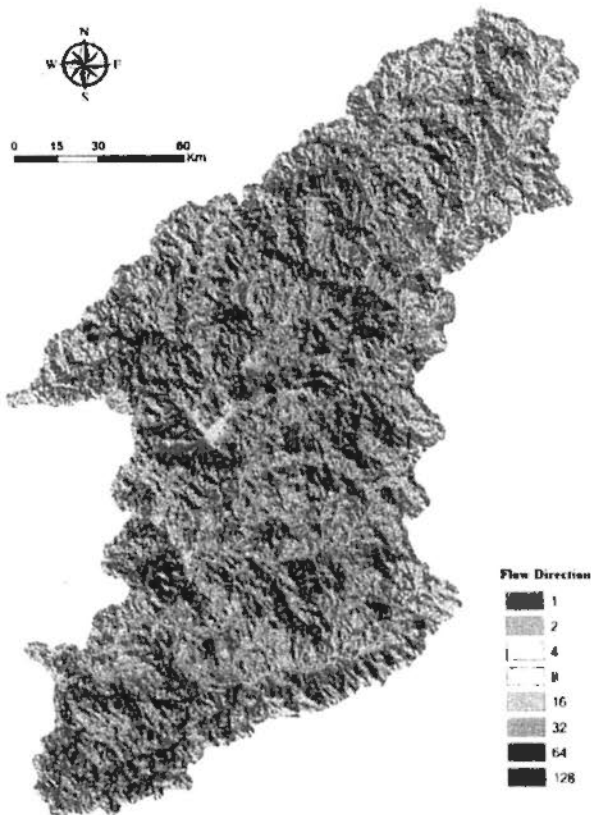


Figure 5.8 Flow directions for the East River Basin
(1=E, 2=SE, 4=S, 8=SW, 16=W, 32=NW, 64=N, 128=NE)

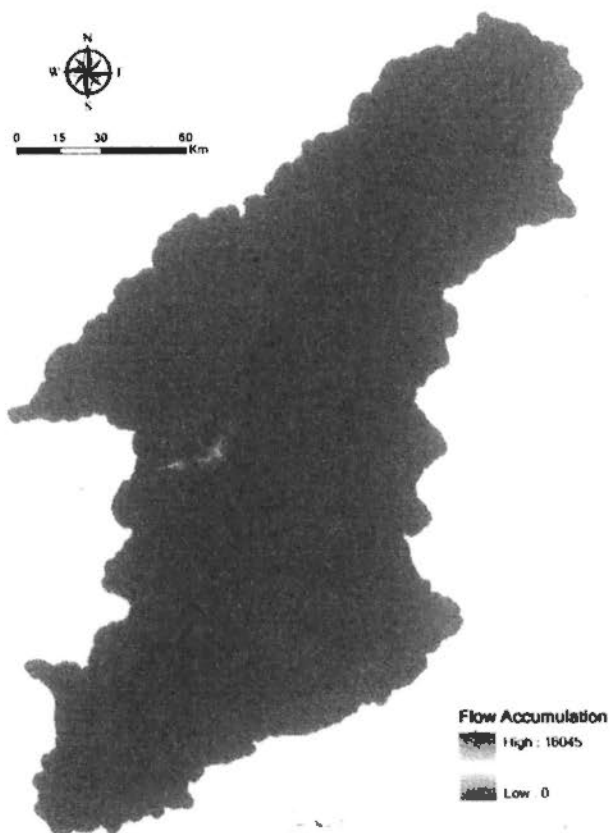


Figure 5.9 Flow accumulation for the East River Basin

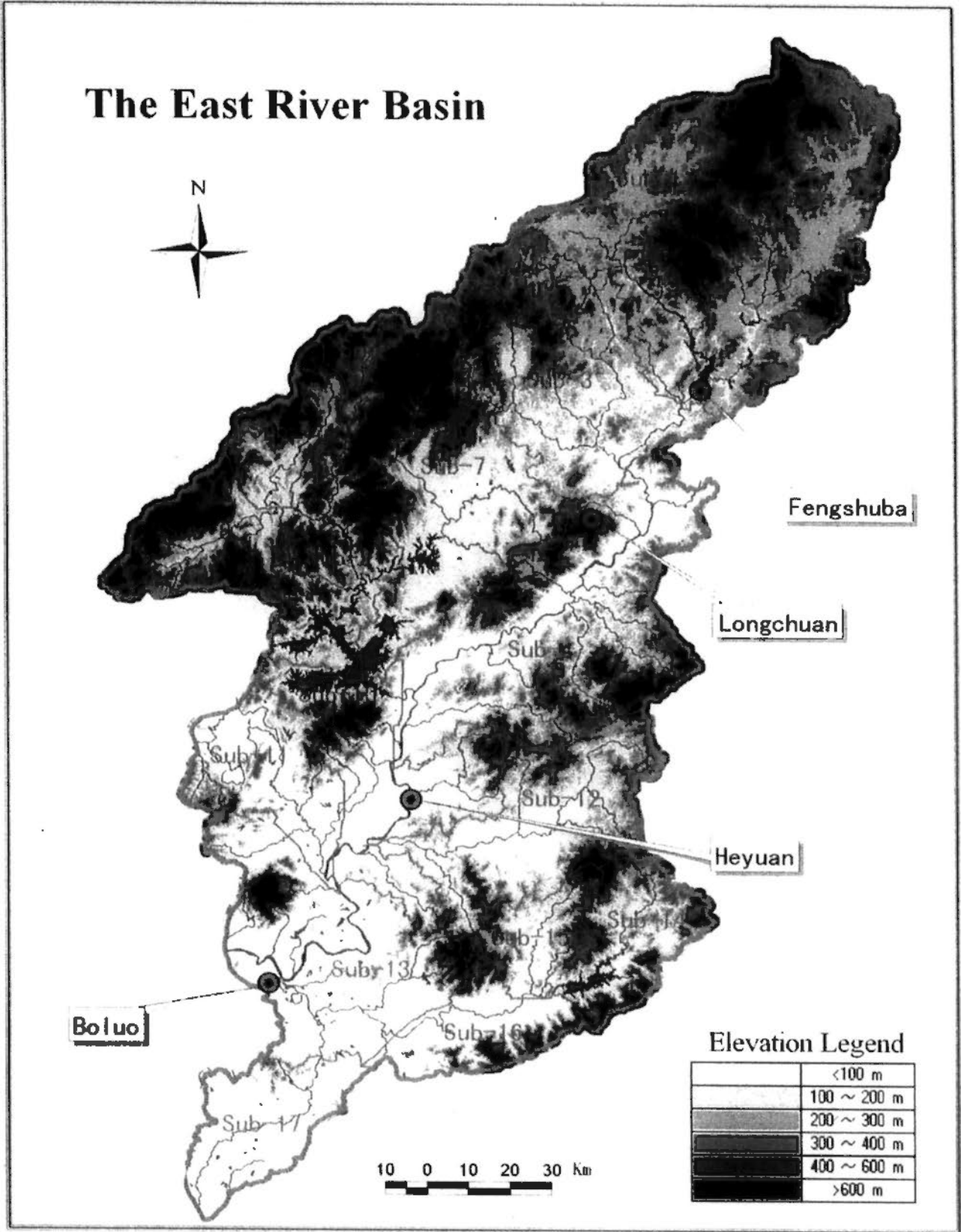


Figure 5.10 Division of the East River Basin into 17 sub-basins

5.5.1.2 Index of Relative Difficulty in Runoff Generation (IRDRG)

Topographic index was originally used in the TOPMODEL as an index of hydrological similarity that any location in a basin with the same value of topographic index has the same hydrological response (Kirkby, 1975). The topographic index at any location x in the basin is defined as Equation 5-2.

In the early days after the TOPMODEL was developed, the derivation of the $\ln(a/\tan\beta)$ distribution function was obtained by manual analysis of local slope angles $\tan\beta$, upslope contributing area A_c and cumulative areas A from topographic maps. Beven and Kirkby (1979) first outlined a computerized approach used to derive the distribution function based by the partition of the basin into sub-basin units. On the basis of dominant flow path inferred from lines of the greatest slope, each unit was then discretised into small 'local slope' elements. The $(a/\tan\beta)$ was calculated for the downslope edge of each element. Although the calculation was an approximation, this method was felt to be justified by its relative efficiency and because the slope element can be defined by field observations and the effects of field drains and roads on upslope contributing areas can be taken into account (Beven et al., 1995).

Figure 5.11 shows the distributions of topographic index $\ln(a/\tan\beta)$ for 17 sub-basins in the East River Basin. The topographic index is derived from the sub-basin DEM with a grid spacing of 100 m using the multiple direction flow algorithm proposed by Quinn et al. (1991). By using Equation (5-2), the cumulative frequency distributions of IRDRG are derived from the distributions of topographic index for the 17 sub-catchments (see in Figure 5.10).

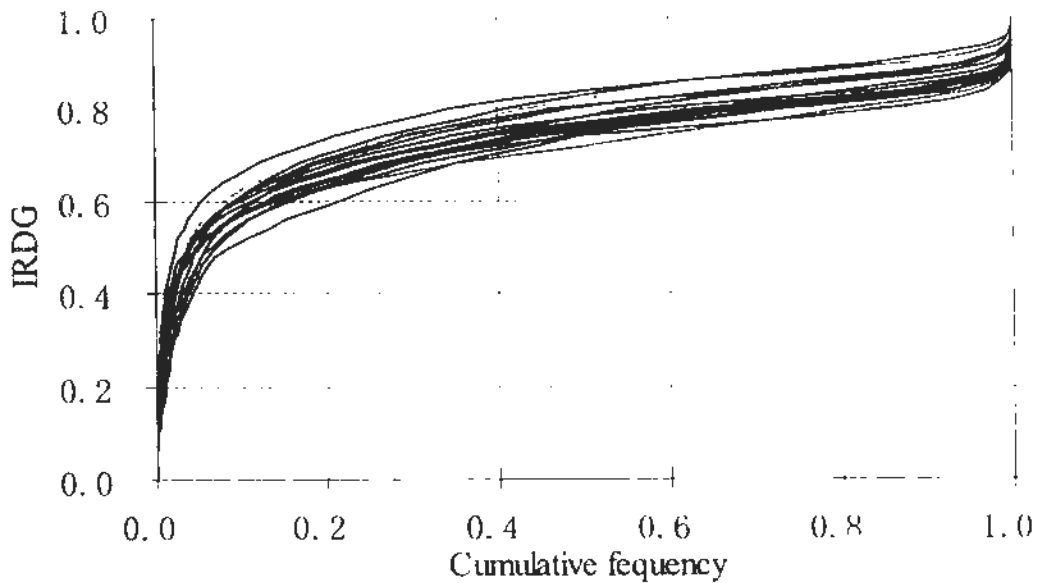


Figure 5.11 Cumulative frequency distributions of IRDRG for 17 sub-basins in the East River Basin

5.5.2 Model Calibration and Validation

Observed streamflows from Boluo stream gauging stations in the East River Basin were first selected to test the model using a split-sample procedure. The data of the whole study period from two additional sites within the basin, Longchuan and Heyuan stations, were also used to validate the model. The Longchuan station is in the upstream region, and the Heyuan station in the middle of the East River Basin (Figure 4.1). Characteristics of the three watersheds are shown in Table 5.1.

The model was applied to simulate the monthly runoff for the period of 1980-1994 for model calibration and for the period of 1995-2000 for validation at the Boluo station, and then validated for the period 1980-2000 at the Heyuan, Longchuan stations, respectively. The areal mean rainfall of each sub-basin is the arithmetic average of gauged quantities within and around the sub-basin.

Table 5.1 Watershed Characteristics

Drainage basin	Longchun	Heyuan	Buluo
Drainage area (km ²)	7,699	15,750	25,325
Mainstem length (km)	165	293	435
Numbers of rainfall gages	10	20	46
Numbers of evaporation stations	1	2	3
Mean annual rainfall (mm)	1,616	1,936	1,747
Mean annual pan evaporation (mm)	1,168	1,407	1,391
Mean annual runoff (mm)	831	944	935

5.5.2.1 Methods for model calibration and validation

The model has a few parameters which can not be directly determined from field measurement or estimated from catchment characteristics and must, therefore, be estimated through model calibration. Model calibration is a process which generates a reasonable set of parameter values. Using the calibrated parameter values, the model can reproduce the response of the catchment under study within some desired accuracy or “goodness-of-fit”. This goodness-of-fit must be based on some criterion or objective function so that a comparison can be made between observed and simulated values of interest.

Selection of such an objective function is an important step in rainfall-runoff model calibration and therefore provides the basis for adjustment of parameter values. Currently there is no standard and universal criterion for model calibration. Blackie and Eeles (1985) reviewed the objective functions commonly used to calibrate hydrological model. Most require minimizing the sum of the squared differences between observed and simulated flow when discharge at the basin outlet is the only variable which is used to establish a criterion of the goodness of fit. In a study on the effect of objective functions on hydrological modeling, Gan et al. (1997) found that different objective functions gave rise to significantly different values of calibrated parameters.

Optimization methods are usually used to calibrate conceptual hydrological models. Generally there are three methods, i.e., manual calibration through trial-and-error;

automatic calibration; and a combination of trial-and-error calibration to achieve a first approximation of the parameters followed by a constrained automatic search to refine the initial approximation. Manual calibration is an iterative process in which users of hydrological models use their knowledge and experience to obtain a satisfactory set of parameters based on visual comparisons between the observed and simulated results. Automatic calibration attempts to achieve the parameter values that are the optimum or “best” to satisfy the criterion of accuracy through automatic computation routines. Over the past few decades, with the development in computer technology a number of techniques have been developed for automatic calibration such as the Simplex method (Nelder & Mead, 1965), the simulated annealing (Kirkpatrick et al., 1983), the Newton-Raphson method (Gupta & Sorooshian, 1985), the Genetic algorithm (Wang, 1991), and the shuffled complex evolution method (Duan et al., 1992). The main problem with automatic calibration is that there may be many local optima, which is relative to the number of parameters to be optimized (Jiang, 2005).

The calibrated model then needs to be tested to confirm whether it can provide adequate information for answering the relevant questions. This second stage of model testing is called validation. For the purpose of evaluating the hydrological impacts of land use change, the standard method of split sample test was used for model calibration and validation in this study. In other words, the available historical record is split into two parts. The model is calibrated using the first sample and validated using the second sample, and then the model is calibrated using the second sample and validated using the first sample. If the model results well match with the observed data and the errors are judged acceptable, the model itself can be considered to be acceptable.

In this study, values of model parameters were optimized to minimize the values of the following objective function:

$$OBJ = \sum_{t=1}^n (qobs_t - qsim_t)^2 \quad (5-14)$$

where $qobs_t$ and $qsim_t$ is the observed and simulated streamflow, respectively, of month t , and n is the total number of months of the simulation. Equation (5-15) is the commonly used sum of squared differences between observed and simulated streamflow discharges. Although it places more importance on the high flow, it is used to reflect the model’s ability to estimate catchment yields.

In this study, as there are only three parameters, WM , η and α that need to be determined. According to Jiang et al. (2005) and Chen et al. (2006), WM is approximately 120 mm in the East River Basin. Moreover, the η can be determined if the information of ET at subbasin is available. As discussed in Section 5.3.2, the ESEBS can map ET spatially thus information of ET at sub-watershed level is readily available. Therefore, η can also be determined directly from spatially-distributed ET estimates generated from ESEBS. As a result, there is only one parameter α need to be estimated. The Simplex method of Nelder & Mead (1995), in combination with manual calibration through trial-and-error (Figure 5.13), is chosen to conduct parameter optimization in this research. The Simplex method is a local, direct search algorithm that has been commonly used for calibration of hydrological models (e.g., Gan & Biftu, 1996; Hendrickson et al., 1988; Johnston & Pilgrim, 1976).

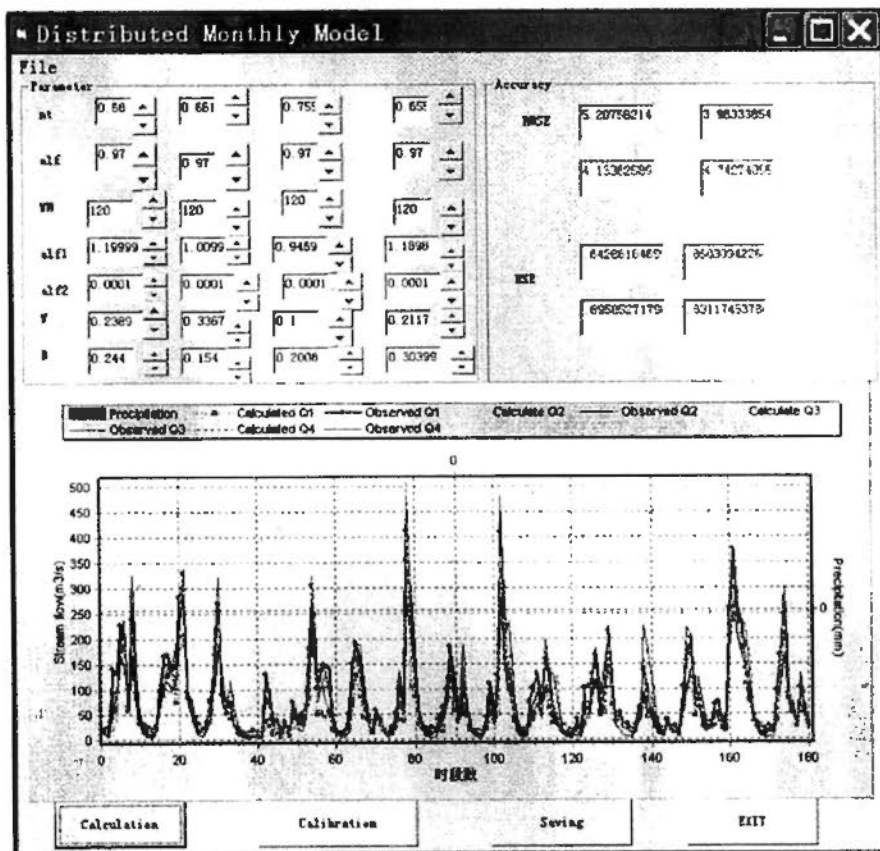
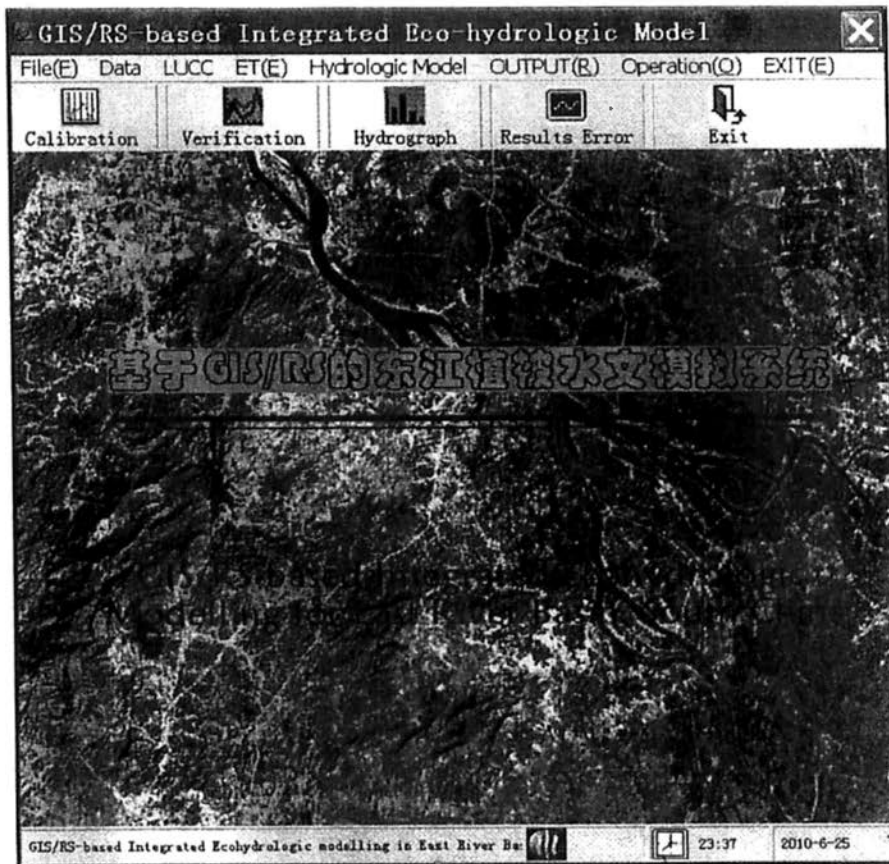


Figure 5.12 Model calibration interface

5.5.2.2 Evaluation of model performance

It is a common practice to employ some criteria of model performance in order to test the accuracy of modeling results. Judgment of the model performance in the calibration and validation periods in this study is based essentially on statistical and numerical comparisons, aided by visual assessment of joint plots of the observed and computed hydrographs. These methods of judgment can provide directional hints for hydrological calibration and a clear indication of how well the computed results fit the observed values.

The first requirement of a model should have the ability to reproduce the mean of the observed streamflow. However, mean value cannot fully indicate how well individual simulated values match the observed values. To overcome this limitation, root mean squared error (*RMSE*), coefficients of efficiency or Nash-Sutcliffe coefficient *NSC'* (Nash & Gleick, 1991) are employed. These numerical tests were first proposed and tested by Aitken (1973) and have been extensively used in the evaluation of hydrological model performance.

RMSE is simply the average of the squared errors for all simulation results and provides an objective measure of the difference between the observed and simulated values. That is:

$$RMSE = \sqrt{\frac{1}{n} \sum_{t=1}^n (q_{obs,t} - q_{sim,t})^2} \quad (5-15)$$

Nash-Sutcliffe efficiency coefficient (NSC'), as shown below, is a deterministic coefficient for measuring the degree of association between the observed and simulated values:

$$NSC' = \frac{\sum_{t=1}^n (q_{obs,t} - \overline{q_{obs}})^2 - \sum_{t=1}^n (q_{obs,t} - q_{sim,t})^2}{\sum_{t=1}^n (q_{obs,t} - \overline{q_{obs}})^2}, \quad (5-16)$$

where $\overline{q_{obs}}$ is the mean of the observed discharges. The value of *NSC'* is always less than unity. A value of *NSC'* equal to unity represents a perfect agreement between the observed and simulated streamflow.

The optimum set of the model parameters were obtained by the methods described above. The optimized values for the areal mean soil moisture storage capacity WM is 120 mm. Distributed parameters estimation results are presented in Table 5.2 and Figures 5.13 and 5.14. As shown in the Table and the two Figures, the runoff regulation coefficient α ranges from 0.917 to 0.963, and has a negative relationship with area. Moreover, it is also related to geologic characteristics, for example, subbasin 13, 16, 17 are dominated by granite and quartz sandstone. Therefore the α value for subbasin 13, 16, 17 are lower. The parameter η varies from 0.67 to 0.70, which also increases from the upstream to downstream. Comparing with DEM map, it can be found that it also has a negative relationship with elevation.

Table 5.2 Distributed parameters at sub-basin scale

Subbasin NO.	Area (km ²)	Annual rainfall (mm)	Elevation (m)	α	η
1	2303	1604	397	0.931	0.67
2	2700	1640	413	0.924	0.66
3	2042	1616	288	0.936	0.68
4	3075	1796	398	0.917	0.66
5	698	1818	487	0.960	0.64
6	671	1788	304	0.960	0.67
7	2074	1787	469	0.935	0.66
8	877	1876	290	0.957	0.67
9	947	1936	177	0.955	0.69
10	1583	1754	256	0.944	0.68
11	1061	1921	141	0.953	0.69
12	1705	1663	237	0.942	0.68
13	2297	1693	266	0.931	0.68
14	867	2044	321	0.957	0.67
15	536	1771	115	0.963	0.70
16	756	1819	202	0.959	0.69
17	1131	1747	99	0.952	0.70

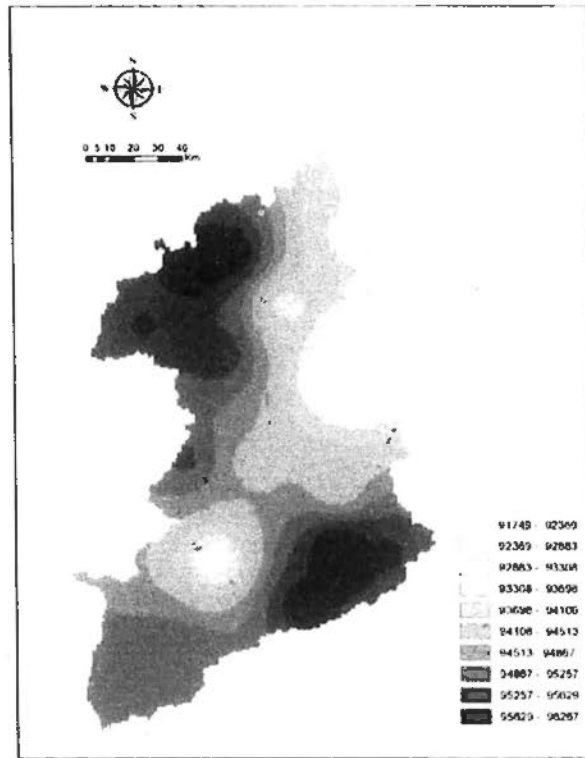


Figure 5.13 Spatial distribution of the runoff regulation coefficient α

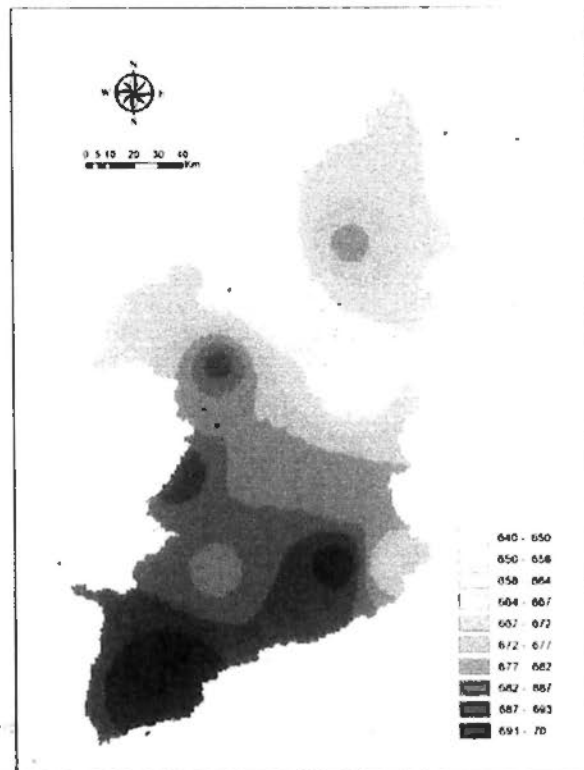


Figure 5.14 Spatial distribution of the pan coefficient η

The results of the model calibration and validation are given in Table 5.3. The model overestimates the mean monthly runoff volumes by 0.5% for the calibration period. For the validation periods, the model overestimates the mean runoff at the Boluo and Heyuan stations by 0.5% and 0.2%, respectively, and underestimates at the Longchuan stations by 0.8%.

Table 5.3 Calibration and validation results for the integrated model

Station	Test period	Mean annual runoff (mm)		RMSE (mm)	NSC
		Observed	Simulated		
Boluo	Calibration	945	940	13.8	0.91
	Validation	977	973	9.74	0.96
Heyuan	Validation	983	985	11.7	0.92
Longchuan	Validation	869	876	11.9	0.93

The values of *RMSE* decreases very slightly from the calibration stage to the validation stage. This indicates that the differences between the simulated and observed values tend to be small in the validation periods. The coefficient of efficiency *R* is 0.91 for the calibration period. The values of *R* are improved by 0.05 for the validation run with the Boluo station and reduced by 0.01 and 0.02, respectively, with the Longchuan and Heyuan stations.

Table 5.4 presents the observed and simulated mean monthly runoff depths for the test periods. The model performs quite well during the rainy months and moderately during dry months. The largest value of percentage errors in mean monthly runoff is 4.8% occurring in the January at the Boluo outlet. The model performs relatively better in simulating the mean monthly runoff for the Heyuan and Longchuan stations.

Simulated and observed runoff hydrographs for all the test periods are presented in Figures 5.15-5.18. In general, the model miscalculates both the peak and low flows, especially for months with the highest and lowest flows, in each of test period. Besides the errors in observed data supplied to models, this miscalculation may be caused by no single groundwater storage in the model and the smoothing effect of using a DEM with a 50m resolution. Nevertheless, Figures 5.15-5.18 reveal that the model can capture the

main features of the observed hydrographs and inter- and intra-annual variability of the flows at each of the three outlets in the East River Basin.

The capability of the developed model to simulate monthly runoff in the East River Basin has been tested. The results of the calibration and validation can be considered to be reasonably acceptable in terms of the quantitative and qualitative criteria. The developed model has been shown to perform satisfactorily well in the East River Basin. As compared with other conceptual lumped models, the features of the developed model are its simple structure with three calibrated parameters and its capacity to represent the spatial distribution of runoff generation.

Table 5.4 Comparison of mean monthly observed and simulated runoff (mm)

Month	Boluo			Heyuan			Longchuan		
	OBS	SIM	ERR (%)	OBS	SIM	ERR (%)	OBS	SIM	ERR (%)
January	44.8	42.6	-4.8	61.6	61.4	-0.3	39.1	40.3	2.9
February	42.9	44.9	4.6	55.8	59.6	6.8	42.1	44.3	5.0
March	67.6	71.7	6.1	85.6	87.8	2.5	79.2	79.1	-0.1
April	93.6	91.3	-2.4	96.6	94.9	-1.8	102.4	103.8	1.4
May	108.9	106.6	-2.2	110.9	112.2	1.2	115.6	115.8	0.2
June	129.6	132.9	2.6	116.4	114.0	-2.1	108.6	108.7	0.1
July	112.7	115.7	2.6	100.1	96.7	-3.4	85.8	79.8	-6.9
August	119.2	116.9	-2.0	102.8	101.9	-0.9	86.6	86.3	-0.3
September	90.3	84.3	-6.7	79.8	81.7	2.4	67.5	73.1	8.3
October	55.8	54.4	-2.6	59.5	59.7	0.3	49.1	53.8	9.5
November	44.7	46.5	4.1	55.0	54.0	-2.0	48.7	48.5	-0.5
December	43.2	42.8	-1.0	59.5	60.7	2.0	44.3	42.1	-4.9

OBS=Observed; SIM=Simulated; ERR=100×(SIM-OBS)/OBS %. The values with the Boluo station were the mean of the period of 1980-2000.

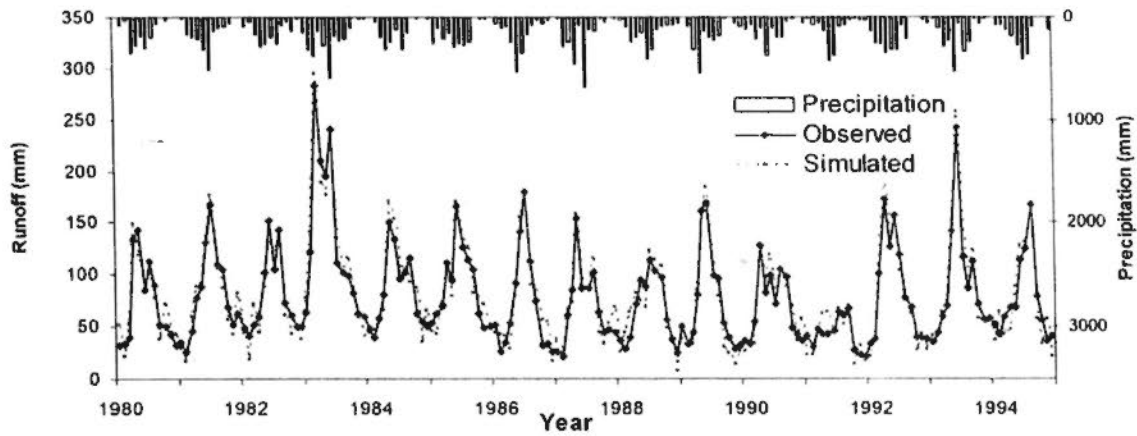


Figure 5.15 Comparison of monthly observed and simulated runoff for the calibration period at the Boluo station

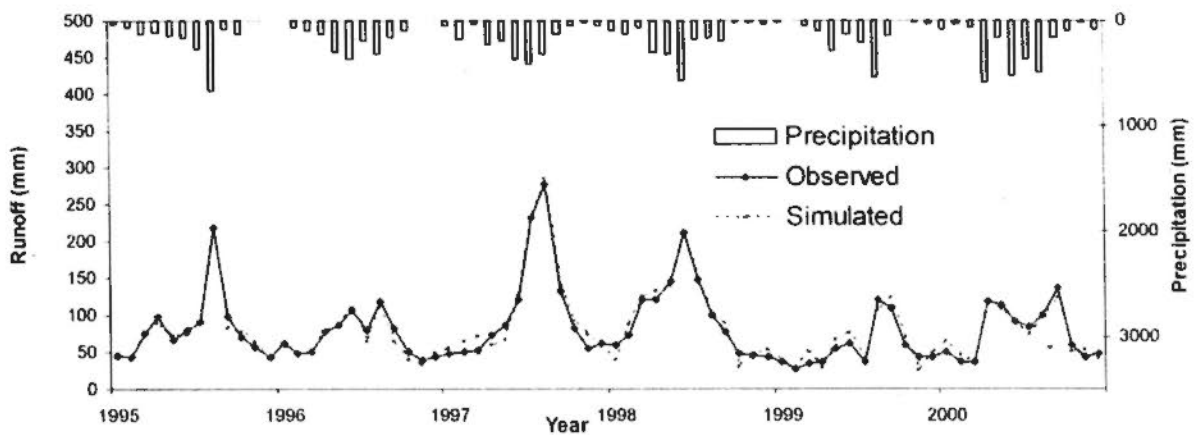


Figure 5.16 Comparison of monthly observed and simulated runoff for the validation period at the Boluo station

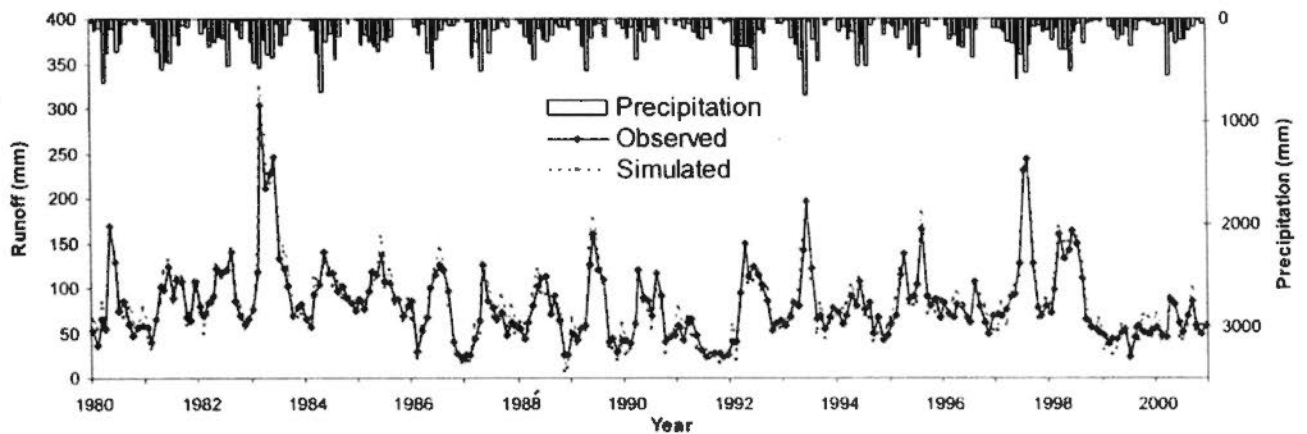


Figure 5.17 Comparison of monthly observed and simulated runoff for the validation period at the Heyuan station

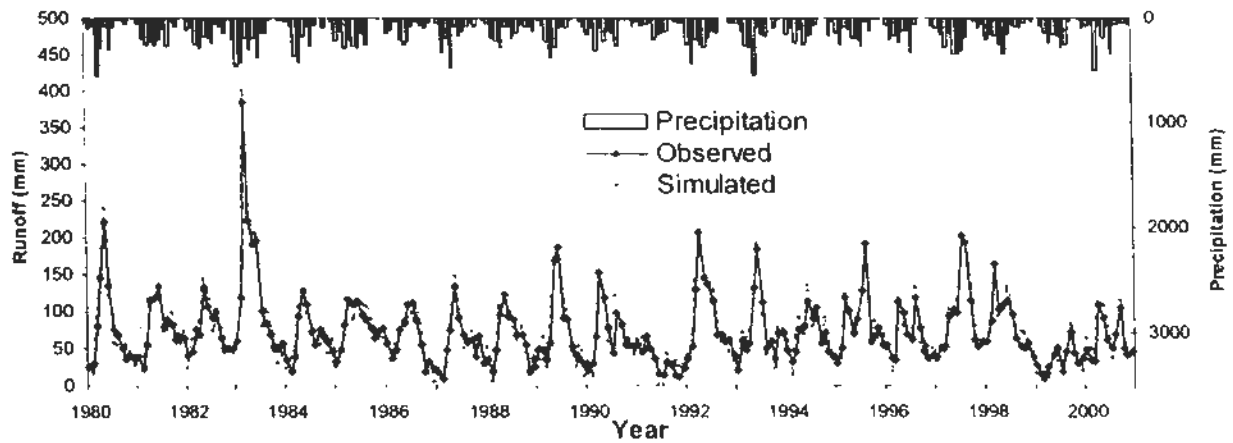


Figure 5.18 Comparison of monthly observed and simulated runoff for the validation period at the Longchuan station

5.5.3 Parameter sensitivity analysis

Sensitivity analysis usually suggests that the model performance is much more sensitive to some parameters than others (Calver, 1988). To test how sensitive is the model output to the variations in the values of three parameters of areal mean soil moisture storage capacity WM , coefficient of runoff regulation α and pan coefficient η , a sensitivity analysis is conducted for the East River Basin by using conventional “one-at-a-time” method that changes one parameter at a time while holding the rest of the factors constant (Jiang, 2005).

The result of sensitivity analysis is presented in Figure 5.19. Relative changes of annual streamflow (the ratio of streamflow changes to annual mean streamflow, dR/R) resulted from the relative changes of each parameter (the ratio of parameter changes to the calibrated model parameter, dP/P) is used as an indicator of the sensitivity of runoff to parameter changes. The considered percentage changes in the parameters were $\pm 5\%$, $\pm 10\%$, $\pm 15\%$, $\pm 20\%$. The relationship between parameter changes and the corresponding streamflow changes in the East River watershed is shown in Figure 5.20. For the three parameters, α has the most significant effect on streamflow. A 10% change in parameter α results in approximately the same percentage of streamflow changes, as compared to 5.8% for η , and only 0.5% for WM . The results show that parameter WM is least sensitive to streamflow and using fixed values of 120 mm for the East River Basin. Effect of change of rainfall amount on model output is also tested; as expected, rainfall had the most significant effect on annual streamflow. A 5% change in rainfall amount changed streamflow approximately by 10% in the two watersheds.

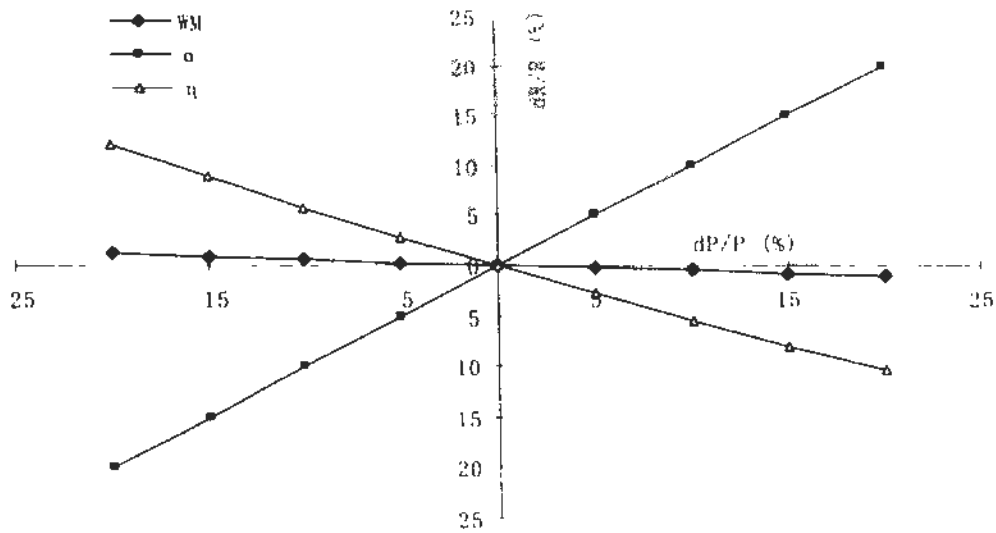


Figure 5.19 Sensitivity of parameters to runoff in the East River Basin

5.6 Summary and conclusion

In this chapter, an integrated distributed monthly water balance model accounting for the spatial variations of basin topography and precipitation and considering vegetation effects is developed with the aid of GIS/RS. This integrated model can not only account for the spatial and temporal dynamics of soil moisture storage but also consider spatial and temporal variation of ET. Furthermore, the integrated model has a clearer physical basis by integrating the physically-remote-sensing-based ESEBS sub-model and the LAI-based interception sub-model. Moreover, the integrated model has direct links between hydrologic processes and vegetation, which makes it capable of predicting hydrologic impact of LUCC. In addition, with the spatially-distributed ET estimates from the ESEBS sub-model, distributed parameters, i.e. regulation parameter α and pan coefficient η can be estimated for each sub-basin, which moves one more step in distributed hydrologic modeling and makes a valuable contribution to spatial representation of catchment responses. In a word, it is a distributed model that can not only account for spatial variations in basin terrain, rainfall, soil moisture but also consider spatial and temporal variation of vegetation and ET in particular, which provides a powerful tool for modeling effects of land use changes on hydrologic regimes.

Based on topography, soil characteristics and spatial distribution of precipitation, the East River Basin is divided into seventeen relatively homogenous units (sub-basins). The model inputs are monthly areal precipitation and potential evaporation values of each sub-basin and the outputs are monthly values of actual evapotranspiration, soil moisture storage and runoff for each sub-basin. The model is calibrated for one gauged station (Boluo) and validated for three stations (Boluo, Heyuan, Longchuan) in the East River Basin. Evaluation of the hydrologic simulation results demonstrate that: a) simulated runoff matches observed values very well on monthly and annual basis and b) the degree of association between the simulated and observed stream flows is quite high for monthly mean values. In summary, the calibration and validation results suggest that the new model is suitable for simulating monthly runoff processes and assessing hydrologic impacts of LUCC in the East River Basin.

Sensitivity analysis of the model was carried out to reveal that runoff regulation parameter α and pan coefficient η have the most significant effects on runoff and soil moisture capacity WM is an insensitive parameter. Depending on the geographical location of the study basin, the value of parameter WM can be determined by experience. With the input data of precipitation and potential evapotranspiration and through calibration of the parameters, the integrated model (IDMWBM) of DMWBM, ESEBS sub-model and LAI-based interception sub-model can be easily and efficiently applied to evaluate the impacts of land use change on regional water resources and hydrological regimes.

CHAPTER 6

ASSESSMENT OF HYDROLOGIC IMPACTS OF LAND USE/COVER CHANGE

6.1 Introduction

As an important theme in eco-hydrology, the hydrologic impacts of land use changes have received a considerable amount of interest in modern hydrology studies. Early field studies to determine the effects of land management and land use change on hydrology date back to the nineteenth century. Much of the earlier understanding of land-use effects on hydrology is derived from paired watershed studies (DeFries & Eshleman, 2004) and statistical analysis (Wang, 2007). The paired watershed studies refer to controlled, experimental manipulations of the land surface, coupled with pre- and post-manipulation observations of hydrological processes, commonly precipitation inputs and stream discharge outputs. A major limitation of paired watershed studies is the obvious lack of experimental replication across a full range of natural conditions. The statistical methods are mainly based on statistical analysis of runoff in different periods. The main problems of statistical methods are lack of physical basis and limited in distinguishing the impacts from climate change and land use change. The development of distributed and semi-distributed hydrological models has bridged the research gaps mentioned above and provided powerful tools for modeling the hydrological response to land use and land cover change, which has received a great deal of attention worldwide (e.g., Mutiah & Wurbs, 2002; Fohrer et al., 2005; Gosain et al., 2006).

Theoretically, vegetation cover, soils, and topography are the three primary watershed properties governing hydrologic variability in the form of rainfall-runoff response. While topographic characteristics can be modified on a small scale (such as the implementation of contour tillage or terracing), variation in watershed-scale hydrologic response through time is primarily due to changes in the type and distribution of land use and land cover. Improved understanding of the relationships among land use/cover, ET, runoff, soil moisture at a watershed scale is helpful for predicting watershed-scale hydrologic response to LUCC, which will benefit regional eco-environmental and water resources management (Gao et al., 2009). On the other hand, LUCC is such a

complicated process that it is difficult to accurately predict. Therefore understanding future effects of LUCC on hydrological regimes is required to understand hydrologic response to LUCC under different scenarios, which is important for supporting water resources management and environmental change monitoring.

This chapter analyzes the impacts of land use and land cover changes on hydrologic regimes using the IDMWBM for the East River Basin. Firstly, streamflow simulation is made and effects of LUCC on hydrologic regimes are analyzed using the integrated model (IDMWBM) under current and historic conditions with land use and land cover maps in 1980 and 2000 from CAS. Secondly, as human activities are intensive in the East River Basin, which has caused significant changes in vegetation types (Wang et al., 2006; Wei, 2010), and there is an urgent call for providing an insight into hydrologic response to changes of different vegetation types (e.g., broad-leaf forest, needle-leaf forest, mixed forest, cropland, grassland). As a result, the land use maps from CAS are too coarse and hence detailed land use/cover maps are needed. However, detailed land use classification map and results of LUCC prediction are not readily available. In this case, scenario analysis is one of the most promising ways to bridge the gap. Based on the LUCC analysis in Chapter 3, six extreme LUCC scenarios are constructed and their impacts on the hydrological regimes are analyzed under what-if scenario from 1980 to 2000.

6.2 Effects of land use/cover on hydrologic regimes

The role of vegetation in the dynamics of soil moisture, runoff, and ET has been acknowledged to be very important (e.g., Neave, 2002; Newman et al., 1998; Wilcox et al., 2003; Fernández-Illescas, 2004), and understanding the influence of vegetation on hydrological changes is part of the foundational basis of eco-hydrology (e.g., Azzali, 2000; Bradford et al., 2003; Li et al., 2006; Newman et al., 2006). Therefore, studies on quantifying the relationship between vegetation and hydrologic regimes represent a critical step in developing advanced eco-hydrological approaches, supporting water resource management and environmental change monitoring.

In this section, effects of land use/cover on hydrologic regimes, i.e. relationship between land use/cover and ET/runoff/soil moisture, are assessed using the integrated model

(IDMWBM). The details of the results are summarized and discussed in details as follows.

6.2.1 Relationship of ET and land use/cover

The spatial distribution maps of ET modeled by the IDMWBM for different level year (1980 and 2000) are presented in Figure 6.1. Table 6.1 summarizes the mean ET for different land use types. As shown in Figures 6.1 and Table 6.1, in 1980, the order of annual amount of ET for different land use types is as follows: Urban and built-up area < Grassland < Cropland < Forest land < Water. Water area has the highest annual ET of 767 mm while the Urban and built-up area has the lowest annual ET of 392 mm. The same conclusions can be drawn from the analysis of year 2000.

Urban and built-up area is impervious, which has limited water for evaporation, and therefore it has the lowest ET. Water body is sufficient in water supply for evaporation in southern China, and therefore it has the highest ET. Moreover, ET has a positive relationship with LAI. The LAI of forestland is greater, and therefore it has a higher ET. This can be explained by surface energy balance as follows. Firstly, the high LAI represents low surface albedo because surface albedo has a negative relationship with LAI (Yuan, 2006; Xie, 2009). However, a low surface albedo indicates that land surface receives more net shortwave radiation, i.e., there is more energy for evaporation, which produces a higher ET. Secondly, vegetation with high LAI has low stomatal resistance and high transpiration rate in the same climatic zone (Xie, 2009). Thirdly, forest trees with high LAI have deeper roots than grassland and cropland, which can absorb more moisture from soil. Therefore, ET has a positive relationship with LAI. The results are in good agreement with several studies in southern China (Zhang, 2008; Xie, 2009; Wei, 2010).

Table 6.1 Summary of mean ET for different land use

Land use/cover	1980		2000	
	Area (km ²)	ET (mm)	Area (km ²)	ET (mm)
Urban and built-up	323.0	392.1	840.9	398.3
Grassland	1581.1	412.4	726.6	420.3
Cropland	3999.5	576.5	3299.2	625.2
Forest land	20780.5	749.0	21814.1	734.4
Water	526.4	767.7	529.9	773.3

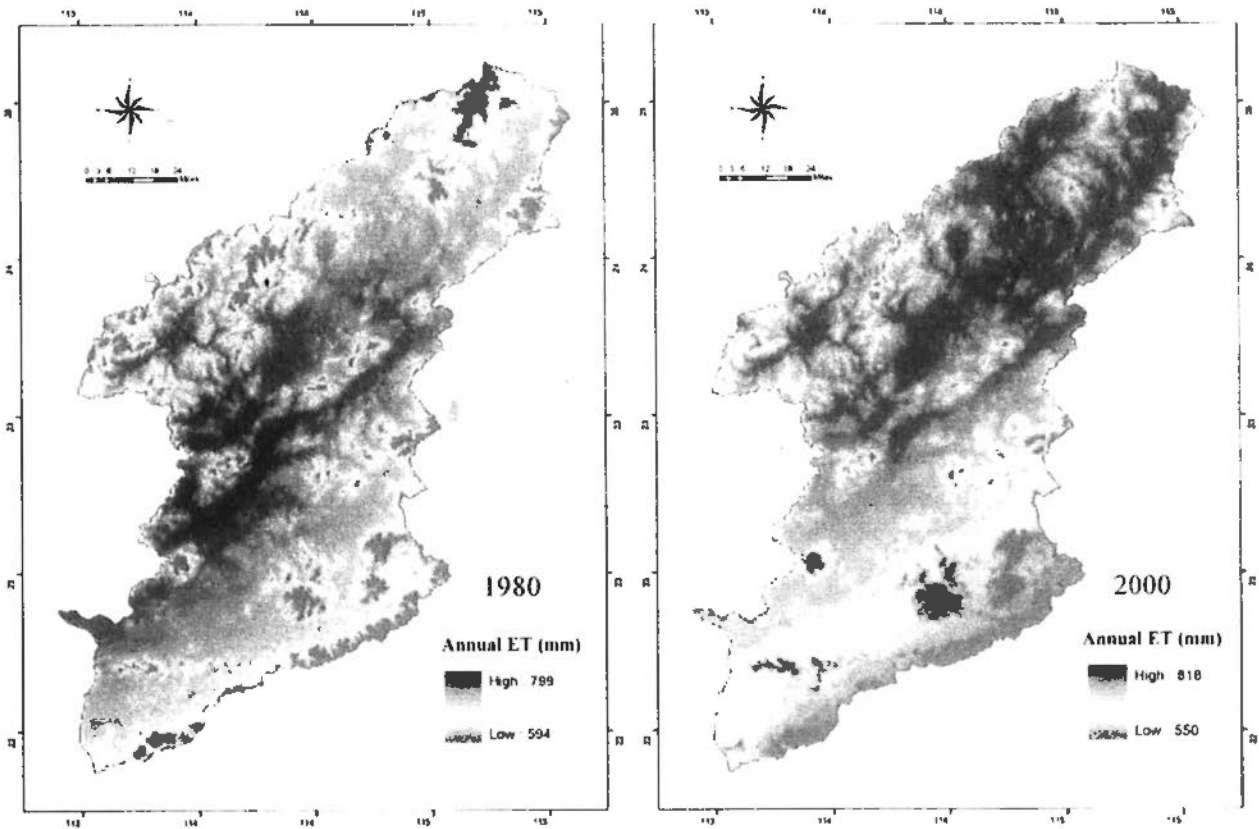


Figure 6.1 Spatial distribution of annual mean ET in 1980 and 2000

6.2.2 Relationship of runoff and land use/cover

Figures 6.2~6.4 present the distribution of annual mean runoff (1980~2000), annual runoff of 1980 and 2000, respectively. Table 6.2 summarizes the mean runoff depth for different land use types. As shown in Figures 6.2~6.4 and Table 6.2, in terms of annual amount, the order of runoff for different land use is ranked as follows: Urban and built-up area > Grassland > Cropland > Forestland. Urban and built-up area has the greatest annual runoff of 1243 mm while forest area yields the least runoff of 855 mm. The same conclusions can be drawn from the analysis of year 2000.

The results can be explained as follows. Urban and built-up area is impervious and has less infiltration and generates more direct runoff, and it has limited water for evaporation. Therefore, it has the highest runoff. According to water balance equation on an annual basis, annual runoff has a negative relationship with annual ET. As mentioned above, forest has much higher ET and cropland has a much lower ET. Therefore, runoff of forest is lower and runoff of cropland and grassland is much higher. The results reveal that urbanization can increase annual runoff while afforestation can decrease annual runoff. These conclusions are in good agreement with related studies in Germany (DeFries & Eshleman, 2004) and China (Yuan, 2007; Xie, 2009; Wei, 2010).

Table 6.2 Summary of annual mean runoff depth for different land use

Land use/cover	1980		2000	
	Area (km ²)	Runoff (mm)	Area (km ²)	Runoff (mm)
Forest land	20780.5	854.7	21814.1	812.4
Cropland	3999.5	1044.9	3299.2	914.2
Grassland	1581.1	1219.0	726.6	1126.4
Urban and built-up	323.0	1243.2	840.9	1205.1

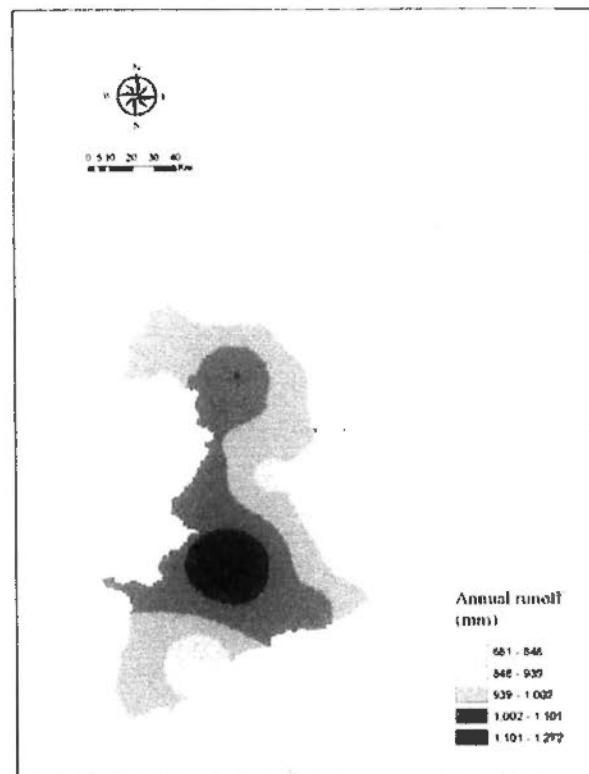


Figure 6.2 Spatial distribution of annual mean runoff from 1980 to 2000

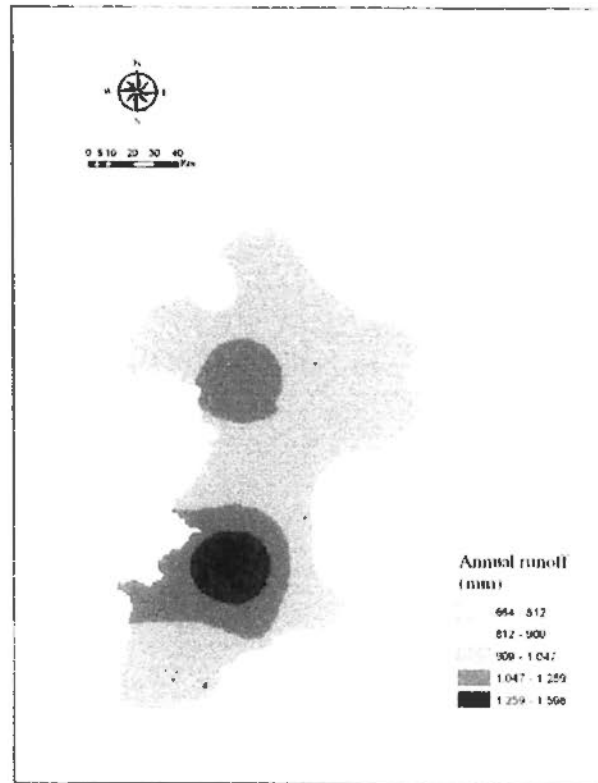


Figure 6.3 Spatial distribution of annual runoff in 1980

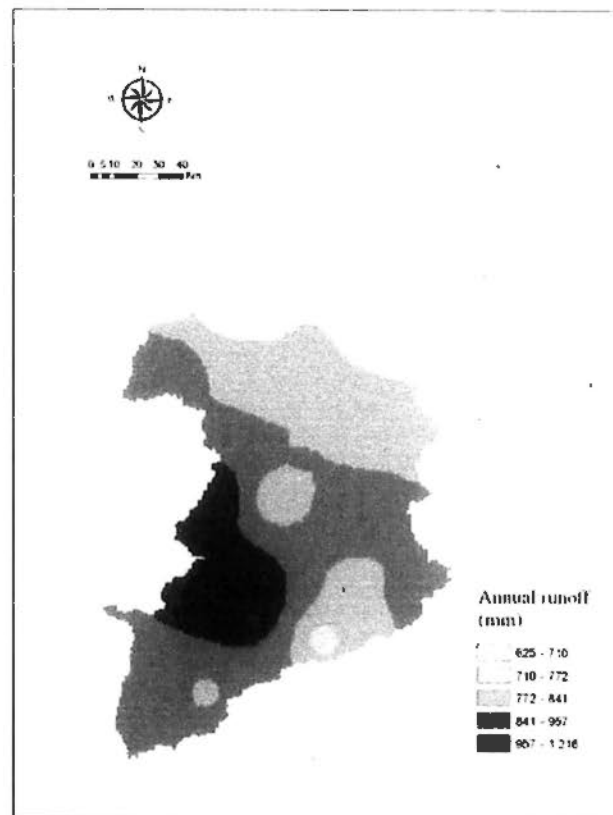


Figure 6.4 Spatial distribution of annual runoff in 2000

6.2.3 Relationship of soil moisture and land use/cover

As far as monthly soil moisture is concerned, there is hardly any change in most of the months and only slight variation in the dry season (November to February for the study period) in the East River Basin. For illustrative purpose, selected monthly soil moisture of January and February in the dry season are analyzed to investigate the relationship between monthly soil moisture and land use.

Table 6.3 summarizes the selected monthly soil moisture for different land use types in the dry season. Figures 6.5 ~ 6.8 present distribution of monthly soil moisture in January and February of 1980 and 2000, respectively. As shown in Figures 6.5 ~ 6.8 and Table 6.3, it is clear that there is slight change in monthly soil moisture. Forest has the highest value of soil moisture while cropland has the lowest value. The results indicate that there is no significant variation in soil moisture for different land use types on a monthly basis in the East River Basin. In other words, vegetation has limited effects on soil moisture on a monthly basis in the East River Basin. The reason is probably that soil moisture is only sensitive on a small time scale (e.g., on an hourly or daily scale). The results agree well with related studies conducted in southern China (Yuan, 2007; Zhang, 2008; Xie, 2009).

Table 6.3 Summary of monthly soil moisture for different land use

Land use/cover	Monthly Soil Moisture (mm)			
	1980		2000	
	January	February	January	February
Cropland	62.7	94.4	55.4	37.1
Grassland	68.2	104.6	59.9	41.4
Forest land	74.3	105.0	60.7	42.3

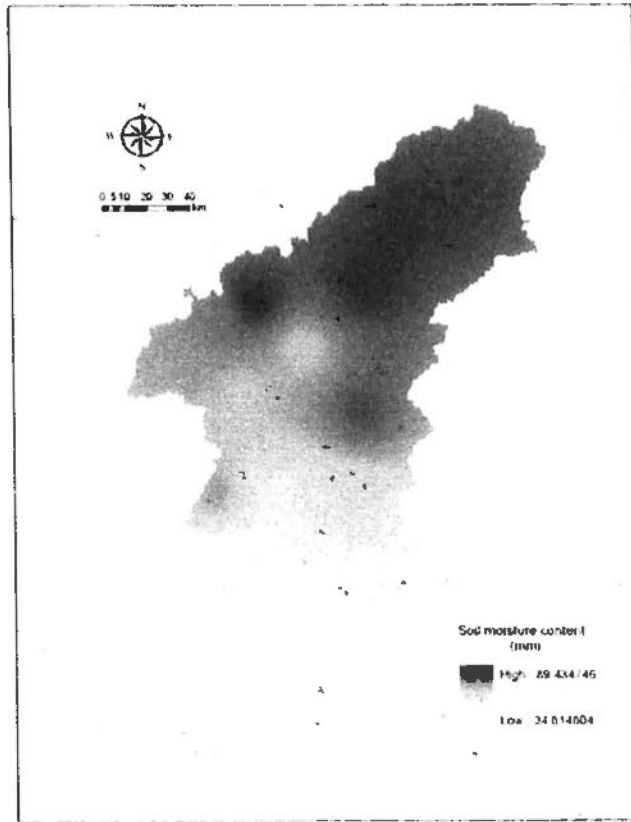


Figure 6.5 Spatial distribution of monthly soil moisture in January 1980

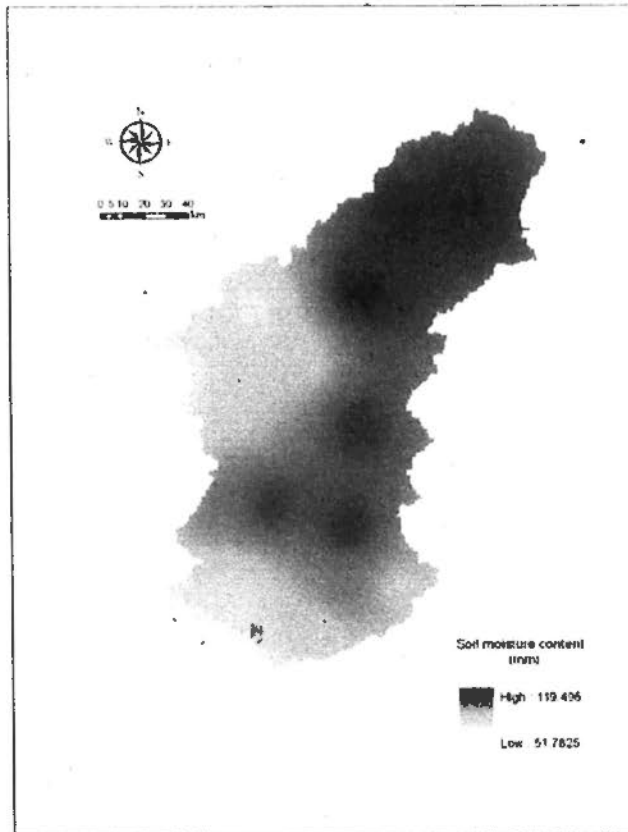


Figure 6.6 Spatial distribution of monthly soil moisture in February 1980



Figure 6.7 Spatial distribution of monthly soil moisture in January 2000



Figure 6.8 Spatial distribution of monthly soil moisture in February 2000

6.3 Hydrologic response to land use/cover change

Human activities are intensive in the East River Basin (Wang et al., 2006; Wei, 2010), which has caused significant changes in vegetation types. There is an urgent call for providing an insight into hydrologic response to changes of different vegetation types. Although effects of land use/cover on hydrologic regimes are evaluated and analyzed in section 6.2, the analysis is mainly based on land use maps in 1980 and 2000 from CAS, which is too coarse to provide an insight into hydrologic response to change of different vegetation types in details. Therefore, a better idea is needed for further studying hydrologic response with more detailed LUCC maps. Scenario analysis is one of the most promising ways to bridge the gap.

Scenarios, as defined by the Intergovernmental Panel on Climate Change, are “plausible and often simplified descriptions of how the future may develop based on a coherent and internally consistent set of assumptions about driving forces and key relationships” (Houghton et al., 2001). Scenario analysis is an approach for evaluating various rational choices and the respective trajectories that lead to alternative future events. In the realm of natural sciences this is typically accomplished by using a combination of land-use change and process models to develop an artificial representation of the physical manifestations of scenario characteristics and to establish a multidisciplinary framework within which scenario characteristics may be analyzed. Scenarios are also usually conducted over long time periods (20–50 yrs) and develop a range of stakeholder-driven perspectives (scenarios), which are analyzed in detail for the consequences or benefits of their selection (Kepner et al., 2008). The process of building a scenario is the creation of a new digital map of land uses, based on the one that depicts the present state of land cover in the watershed. The scenarios are mainly focused on the possibly changes that can occur in the near future. This is employed by changing percentage of one land use and land cover class into another based on the pre-defined criteria.

Basically, four commonly used methods for scenario analysis of predicting hydrologic impact of LUCC (Wan, 2005; Yuan, 2006) include: (1) paired watershed comparison (Liu & Zhong, 1978), (2) prediction based on historic land use conditions (Wang, 2003), (3) prediction based on LUCC prediction model (Nichoff, 2002), and (4) Prediction based on extreme scenario analysis (e.g., Dunn & Mackay, 1995; Yuan, 2006; Zhang,

2008; Wei, 2010). The former three methods need specific land use/cover maps under current condition or in the future. However, the detailed land use maps are not readily available for the East River Basin, and detailed land use classification to distinguish different tree species for a large area is a hard nut to crack and needs intensive studies, which is not the focus of hydrologic studies. On the other hand, LUCC is a very complicated process that is the result of complex interaction among climatic, socio-economic and biotic system, and therefore accurate prediction of land use calls for intensive studies due to so many driving forces, which is beyond the scope of this dissertation. In this case, extreme scenario analysis is a promising method to conduct hydrologic impacts of LUCC (Yuan, 2006; Wei, 2010).

In this section, firstly six hypothetical extreme scenarios are constructed based on LUCC analysis in Chapter 3. Secondly, the IDMWBM developed in Chapter 5 is employed to perform simulations under different scenario conditions in order to analyze impact on the catchment hydrology of possible changes in land use that may occur in the near future.

6.3.1 Hypothetical scenarios

The land use map of 2000 from CAS is used as a base map (Figure 3.9) for scenario setting. Based on the analysis in Chapter 3, there is little change in water, urban and built-up area after year 2000. Therefore, these two land use types remain constant in scenario setting.

As mentioned in Chapter 3, according to LUCC analysis based on MODIS land cover/use products obtained from the Land Processes Distributed Active Archive Center (LP DAAC) of Earth Resources Observation and Science (EROS), broad-leaf forest and needle-leaf forest are two dominant land cover types in the East River Basin. Therefore, these two extreme scenarios are constructed for assessment of hydrologic impact of LUCC. The LUCC studies conducted in the East River Basin (e.g., Wang, et al., 2006; Hu, 2008; Wei, 2010) reveal that mixed forest is also a dominant land cover, and therefore extreme scenario of mixed forest is also constructed for assessment of hydrologic impact of LUCC. Based on the analysis in Chapter 3, significant changes occurred in grassland and cropland from 1980 to 2000; as a result, extreme scenarios of grassland and cropland can also be set as two scenarios for assessment of hydrologic

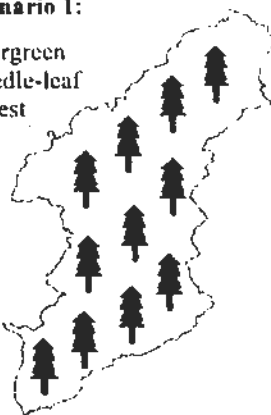
impact of LUCC. The predicted scenario based on Markov chain provides one possible scenario for future LUCC which has a stronger scientific meaning can also be constructed as one scenario for assessment of hydrologic impact of LUCC. Therefore, totally six extreme scenarios are built to investigate hydrologic response to LUCC. The six scenarios are described in Table 6.4 and illustrated in Figure 6.9.

Table 6.4 Summary of six hypothetical scenarios

Scenario No.	Description
1	All land cover (i.e., forest, grassland, and cropland in the land use map of 2000) will be changed to evergreen needle-leaf forest
2	All land cover (i.e., forest, grassland, and cropland in the land use map of 2000) will be changed to evergreen broad-leaf forest
3	All land cover (i.e., forest, grassland, and cropland in the land use map of 2000) will be changed to mixed forest
4	All land cover (i.e., forest, grassland, and cropland in the land use map of 2000) will be changed to cropland
5	All land cover (i.e., forest, grassland, and cropland in the land use map of 2000) will be changed to grassland
6	Land use/cover will be as projected in 2010 by Markov chain model

Scenario 1:

Evergreen
Needle-leaf
Forest



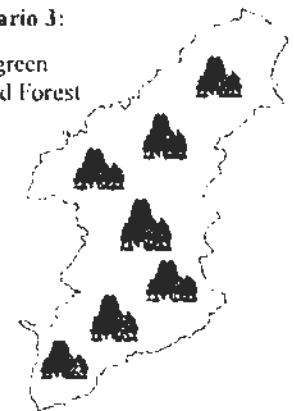
Scenario 2:

Evergreen
Broad-leaf
Forest



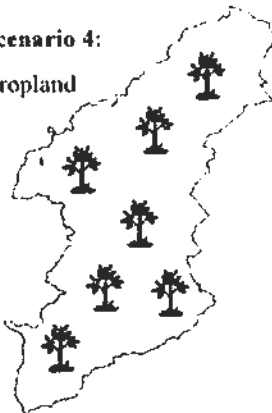
Scenario 3:

Evergreen
Mixed Forest



Scenario 4:

Cropland



Scenario 5:

Grassland



Scenario 6:

Predicted
scenario

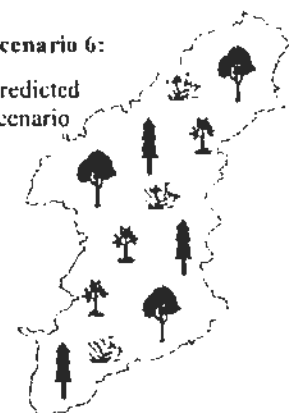


Figure 6.9 Illustration of scenario setting

6.3.2 ET in response to LUCC

The results of ET in response to LUCC are presented in Table 6.5 and Figures 6.10 ~ 6.12. In Table 6.5, change amount and change ratio are defined as follows:

$$\text{Change amount} = H_s - H_c \quad (6-1)$$

$$\text{Change ratio} = (H_s - H_c) / H_c \times 100\% \quad (6-2)$$

where H_s is the value of hydrologic regime under the scenario condition, and H_c is the value of hydrologic regime under the current condition.

As shown in Table 6.5 and Figure 6.10, in terms of annual mean amount, the order of ET for different land cover is ranked as follows: Grassland scenario < Cropland scenario < Projected scenario < Broad-leaf forest scenario < Mixed forest scenario < Need-leaf forest scenario. The results show that ET has a positive relationship with LAI. This can be explained by surface energy balance. Firstly, high LAI represents low surface albedo because surface albedo has a negative relationship with LAI (Yuan, 2006; Xie, 2009). However, a low surface albedo indicates that land surface receives more net shortwave radiation, i.e., there is more net radiation for evaporation, which produces a higher ET. Secondly, vegetation with high LAI has low stomatal resistance and high transpiration rate in the same climatic zone (Xie, 2009). Thirdly, forest trees with higher LAI have deeper roots than grassland and cropland, which can absorb more moisture from soil for evaporation. Therefore, vegetation with high LAI produces high ET.

On a monthly basis, the monthly processes of ET (Figure 6.11) are consistent with monthly processes of LAI (Table 4.1), which indicates a positive relationship between LAI and ET (van der Kwast et al., 2009). As shown in Figure 6.11, ET reaches highest value in summer and the lowest value in autumn and winter. This phenomenon can be elaborated as follows. In winter and autumn, due to the lower temperature and weaker sunshine radiation, the values of LAI for different land cover types are close to each other. Therefore, the values of ET for different land cover types are near to each other. However, in spring and summer, there are significant variations in LAI for different land cover types, therefore, there are the most significant variations of ET for different land cover types in spring and summer.

As far as the change of ET comparing with current situation is concerned (Figure 6.12), on an annual basis, the grassland scenario has the greatest change ratio, which would

cause 45% decrease of ET compared with current situation. It indicates that there would be significant decrease in ET when the watershed changes from forest-dominated to grass-governed. The mixed forest scenario has the lowest change ratio, which would cause 2% decrease of ET. It indicates that mixed forest scenario is similar to current situation. The broadleaf forest scenario is of practical significance because eucalyptus, as a type of broad-leaf tree, has been widely planted in the East River Basin. This scenario would cause 14% decrease of ET. The projected scenario would cause 16% decrease of ET. On a monthly basis, comparing with the current situation, the most significant changes occur in summer. The reasons are that ET has a positive relationship with LAI and monthly processes of ET are consistent with monthly processes of LAI, which has been explained with surface energy balance in details above.

In summary, on an annual basis, ET has a positive relationship with LAI. On a monthly basis, the monthly processes of ET are consistent with monthly processes of LAI. In terms of the change of ET comparing with current situation, all of the hypothetical scenarios except for the need-leaf forest scenario would cause decrease of annual ET. The most significant decrease of ET occurs in summer. The reasons have already been elaborated above based on surface energy balance. The results demonstrate that deforestation (forest changed to grassland/cropland) would cause decrease of annual ET in the East River Basin. Particularly, deforestation would cause significant decrease of ET in summer. The results can be well understood based on land surface balance equation and agree well with related studies in Guizhou (Zhang, 2008), the Hanjiang River Basin (Yuan, 2006), the Yellow River Basin (Liu et al., 1978) and the Pearl River Delta (Xie, 2009; Wei, 2010) in China.

6.3.3 Runoff in response to LUCC

As shown in Table 6.6 and Figures 6.13 ~ 6.15, in terms of annual mean runoff, the order of annual runoff depth for different land cover is ranked as follows: Grassland scenario > Cropland scenario > Projected scenario > Broad-leaf forest scenario > Mixed forest scenario > Need-leaf forest scenario. This can be explained by water balance equation. There is no significant variation of annual rainfall for a specific climatic zone in southern China, therefore, for annual water balance, runoff approximately equals to precipitation minus ET. Therefore, runoff has a negative relationship with ET when rainfall keeps constant. On a monthly basis, monthly runoff processes for different land

cover types are in the inverse order of ET processes for different land cover types. The reason is mainly that runoff has a negative relationship with ET if there is no significant dynamics of precipitation and soil moisture. The results agree well with related studies conducted in southern China (Yuan, 2007; Zhang, 2008; Xie, 2009).

As far as the change of annual mean runoff comparing with current situation is concerned, grassland scenario would cause the greatest increase of 37% in comparison with current situation, which indicates that there would be significant increase in runoff when all the land cover change to grass. There would be the least increase of 2% in runoff for mixed forest scenario, which is the most similar to the current situation. As eucalyptus has been widely planted in the East River Basin, the broad-leaf forest scenario is practically meaningful and reveals that there would be 13% increase of runoff when all the land cover change to evergreen broad-leaf forest. The projected scenario would cause 14% increase in runoff depth. On a monthly basis, the most significant changes occurred in the rainy season (May to September) in the East River Basin. It can be explained that runoff has a negative relationship with ET according to water balance model. Comparing the change amount of monthly ET (Figure 6.12) and the change amount of monthly runoff (Figure 6.15), they generally tally with each other. As shown in Figure 6.16, for most scenarios, particularly for grassland and cropland scenario, the most significant changes occurred in the rainy season. It indicates deforestation (forest changed to grassland or cropland) would cause significant increase of monthly runoff in the rainy season in the East River Basin.

In summary, it is concluded that all of the hypothetical scenarios except for the needle-leaf forest scenario would cause increase of annual runoff comparing with current situation. Particularly the grassland and cropland scenarios would cause significant increase of annual runoff. On a monthly basis, monthly runoff processes for different land cover types are in the inverse order of ET processes for different land cover types. On the other hand, the most significant changes occurred in the rainy season. The reasons have been explained above based on water balance equation. The results reveal that deforestation would cause significant increase of annual runoff and significant increase of monthly runoff in the rainy season in the East River Basin.

Table 6.5 Summary of estimated ET for different scenarios (unit: mm)

Year	Current	Evergreen Needle-leaf forest	Evergreen broad-leaf forest	Mixed forest	Cropland	Grassland	Projected scenario
1980	750.1	873.7	648.6	743.2	570.6	404.3	628.0
1981	718.2	840.6	623.6	701.0	535.9	381.8	599.1
1982	753.3	877.4	653.2	749.7	572.6	408.4	632.0
1983	768.3	869.8	623.1	717.0	642.1	424.7	631.3
1984	731.7	830.7	620.5	700.6	590.6	402.6	613.3
1985	745.7	857.6	613.5	704.9	549.9	377.1	597.0
1986	759.2	882.1	686.0	789.7	605.0	439.7	665.0
1987	755.1	882.6	655.6	735.5	565.5	401.7	630.4
1988	739.2	850.4	610.2	702.1	545.4	373.0	593.4
1989	755.2	876.8	681.7	784.5	606.6	436.9	662.3
1990	755.9	878.6	682.0	786.1	603.6	437.4	661.8
1991	762.4	885.6	685.9	789.8	606.3	442.3	665.4
1992	716.9	813.5	583.4	672.0	597.3	397.4	590.0
1993	733.6	831.7	596.2	686.5	613.2	406.7	603.8
1994	709.0	824.9	614.1	704.9	541.4	387.6	595.1
1995	714.3	822.7	588.4	677.3	522.9	360.7	571.4
1996	714.5	829.0	641.1	737.6	568.1	411.3	622.2
1997	710.5	805.3	575.3	664.4	593.8	399.9	583.4
1998	738.6	863.7	642.1	718.7	554.2	393.8	617.4
1999	702.2	815.3	630.6	726.5	557.5	405.7	611.8
2000	745.6	844.7	604.4	696.8	622.5	415.3	612.4
Average	737.1	850.3	631.4	723.3	579.3	405.2	618.4
Change amount	0.0	113.2	-105.7	-13.8	-157.8	-332.0	-118.7
Change ratio (%)	0.0	15.4	-14.3	-1.9	-21.4	-45.0	-16.1

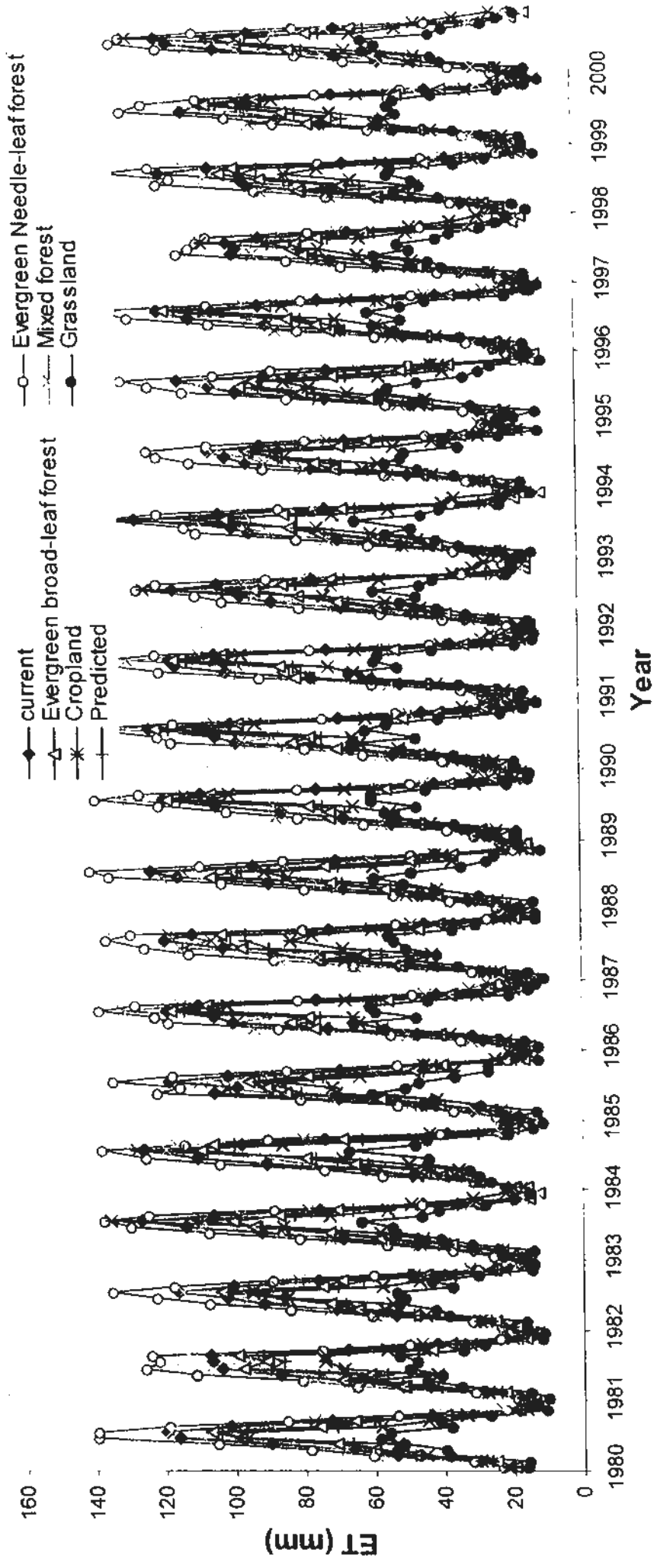


Figure 6.10 Comparison of ET processes for different scenarios

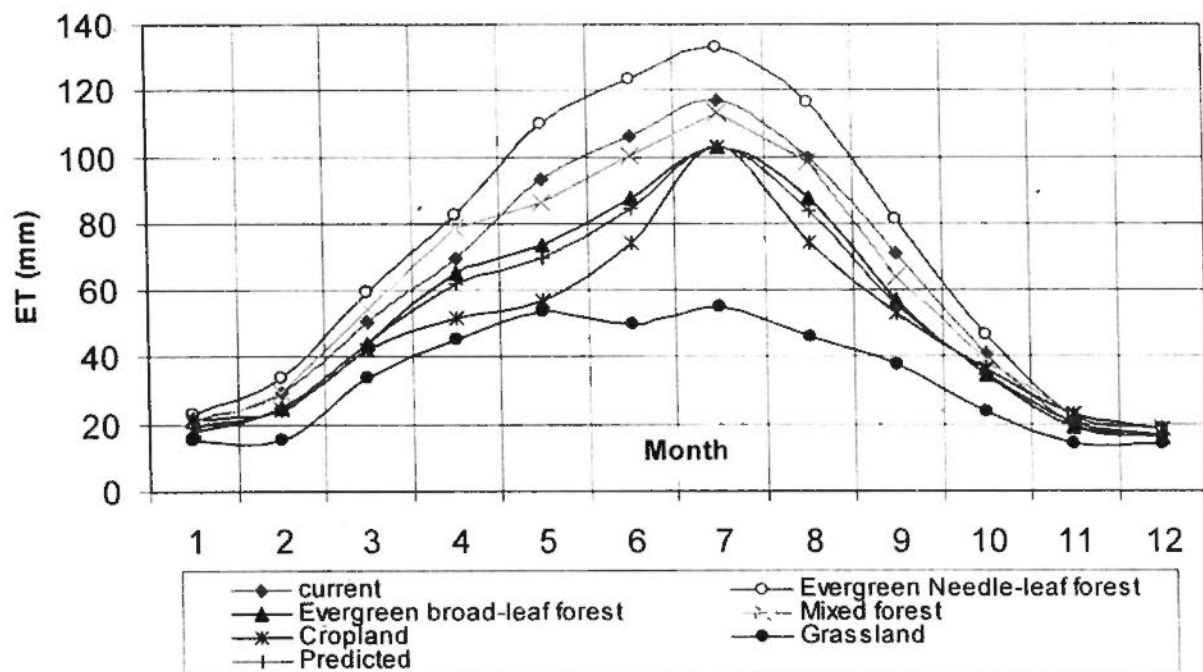


Figure 6.11 Monthly mean ET for different scenarios

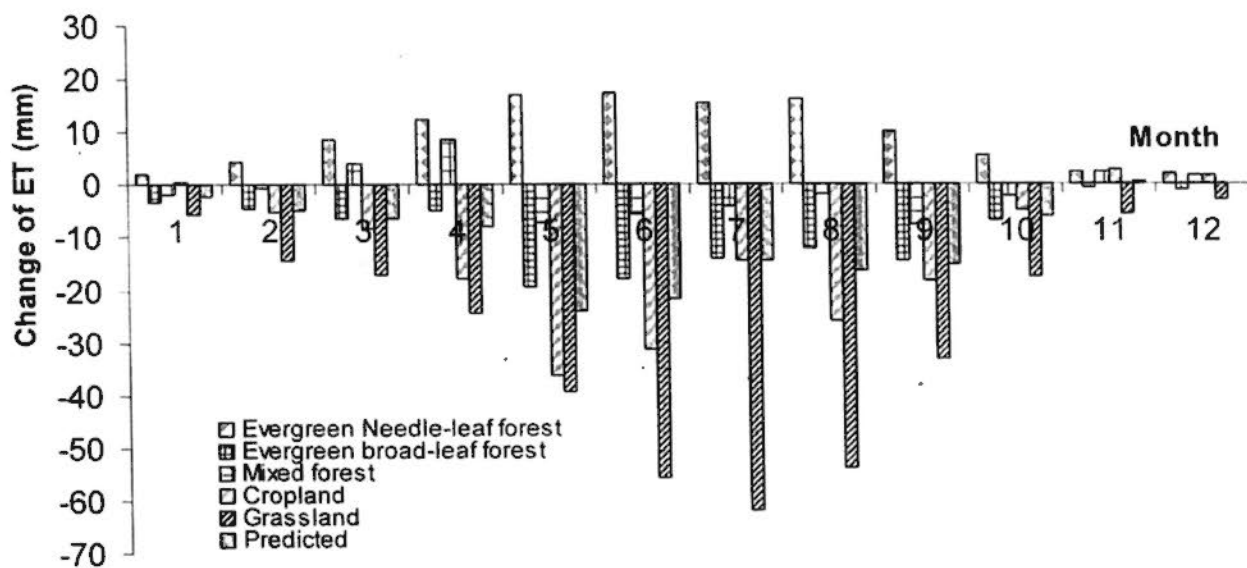


Figure 6.12 Change of ET compared with current situation for different scenarios

Table 6.6 Summary of runoff depth for different scenarios (unit: mm)

Year	Current	Evergreen needle- leaf forest	Evergreen broad-leaf forest	Mixed forest	Cropland	Grassland	Projected scenario
1980	891.0	766.8	983.9	886.0	1059.4	1199.9	1003.1
1981	972.6	828.7	1138.4	996.3	1219.8	1466.4	1158.4
1982	970.9	838.6	1072.6	969.2	1154.8	1307.8	1093.7
1983	1660.2	1547.8	1815.0	1695.3	1837.0	2020.2	1817.0
1984	972.4	861.3	1118.3	1037.6	1126.1	1407.5	1120.5
1985	1069.4	956.0	1236.5	1118.4	1276.7	1460.0	1244.2
1986	823.7	713.0	921.9	825.2	982.8	1190.7	938.0
1987	757.5	646.5	877.5	774.8	938.1	1111.3	892.4
1988	789.5	703.5	905.6	826.4	947.4	1078.1	915.4
1989	877.1	758.3	973.4	874.7	1043.7	1226.1	991.7
1990	840.6	725.4	939.2	840.0	1001.7	1214.5	955.8
1991	455.5	392.7	510.5	455.5	537.2	666.1	517.5
1992	1055.8	974.2	1168.7	1081.8	1179.7	1313.6	1168.6
1993	1025.0	941.8	1145.9	1052.4	1159.3	1294.8	1146.1
1994	851.6	736.3	940.6	849.0	1010.6	1144.8	958.4
1995	1058.0	945.2	1218.9	1106.6	1261.0	1450.0	1227.7
1996	834.9	715.8	935.8	834.6	997.3	1225.6	952.2
1997	1245.9	1125.0	1407.9	1282.7	1404.3	1615.2	1402.2
1998	1145.9	979.4	1341.2	1140.2	1411.9	1694.1	1354.7
1999	543.6	462.8	612.1	546.7	655.3	824.5	624.2
2000	801.6	730.5	899.5	824.7	909.4	1039.1	899.8
Average	935.4	826.2	1055.4	953.2	1100.6	1283.3	1065.8
Change amount	0.0	-109.2	120.0	17.9	165.3	348.0	130.4
Change ratio (%)	0.0	-11.7	12.8	1.9	17.7	37.2	13.9

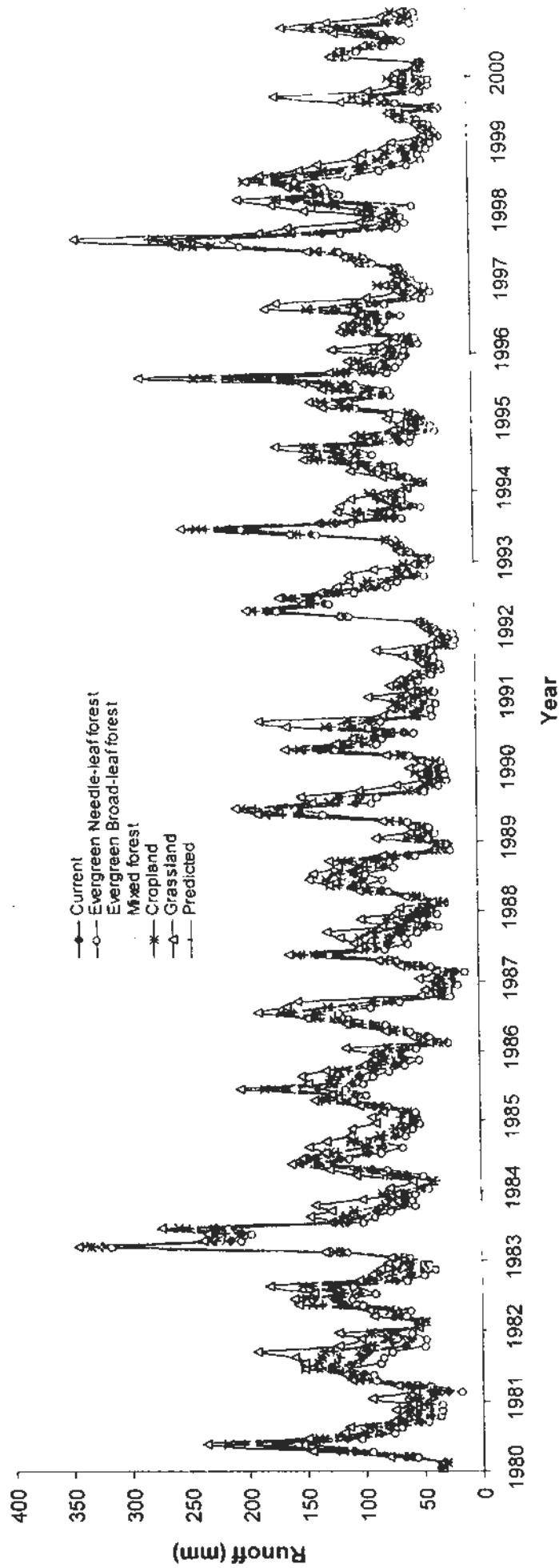


Figure 6.13 Comparison of runoff processes for different scenarios

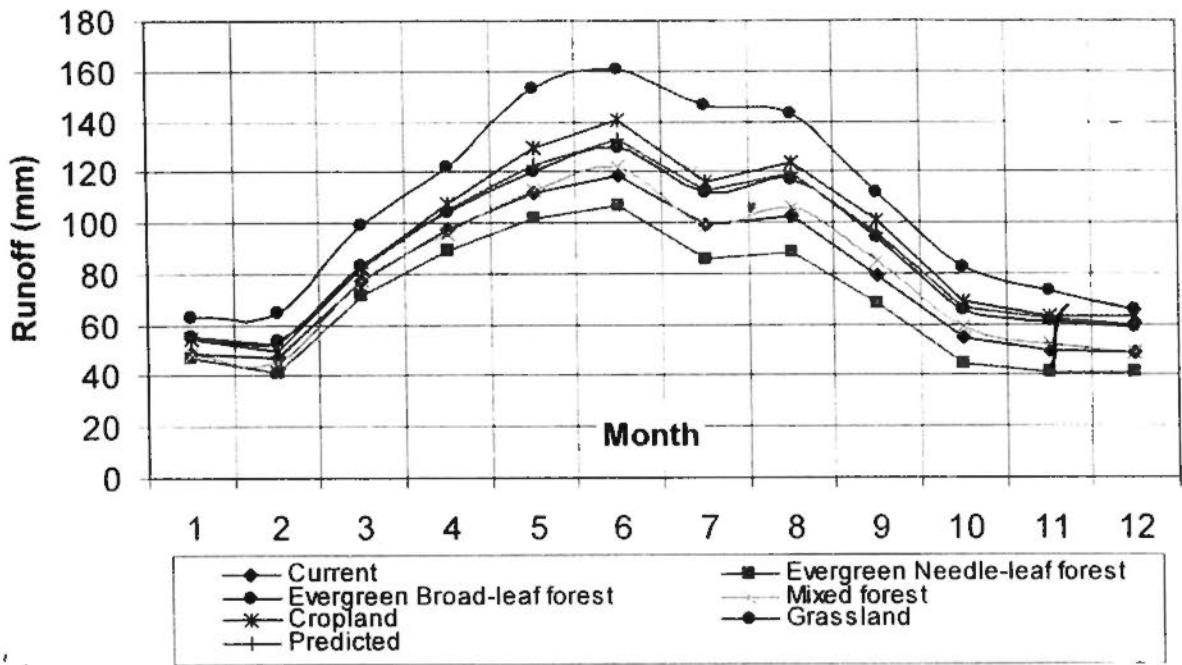


Figure 6.14 Monthly runoff depth for different land cover

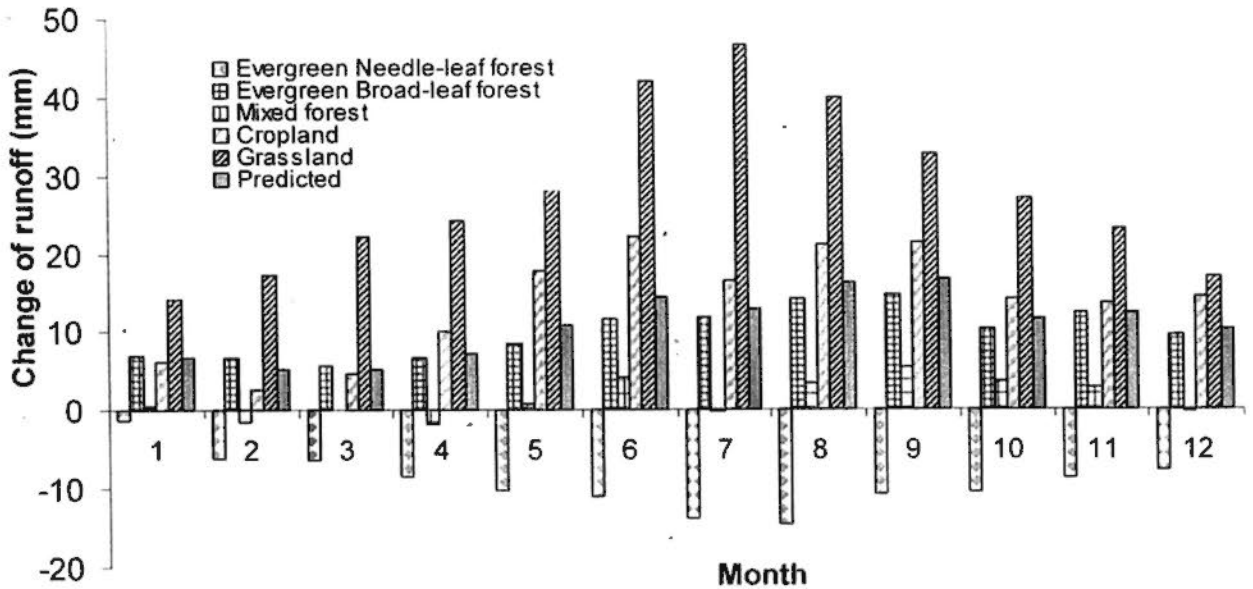


Figure 6.15 Change of monthly runoff depth compared with current situation for different scenarios

6.4 Summary and conclusion

This chapter analyzes the impacts of land use and land cover changes on hydrologic regimes using the IDMWBM for the East River Basin. Firstly, streamflow simulation is calculated and the effects of LUCC on hydrologic regimes are analyzed using the integrated model (IDMWBM) under current-historic conditions using land use and land cover maps in 1980 and 2000 from CAS. The results of effects of LUCC on hydrologic regimes show that Urban and built-up area has the lowest ET and the highest runoff. It is elaborated that urban and built-up area is impervious, which has limited water for evaporation and yields runoff directly. Moreover, ET has a positive relationship with LAI while runoff has a negative relationship with LAI in the same climatic zone, which can be elaborated by surface energy balance and water balance. In addition, there is little change in monthly average soil moisture. All the results mentioned above agree well with related studies in Germany (DeFries & Eshleman, 2004) and southern China (Yuan, 2007; Zhang, 2008; Xie, 2009; Wei, 2010).

Secondly, scenario analysis is employed to further study hydrologic response to different vegetation cover based on detailed land use/cover maps under different scenarios. Based on the LUCC analysis in Chapter 3, six hypothetical LUCC scenarios are constructed and their impacts on the hydrological regimes are analyzed under what-if scenario from 1980 to 2000. The results show that ET has a positive relationship with LAI while runoff has a negative relationship with LAI in the same climatic zone, which can be elaborated by surface energy balance and water balance equation. The results indicate that deforestation would cause increase of annual runoff and decrease of annual ET in southern China. On a monthly basis, monthly runoff processes for different land cover types are in the inverse order of ET processes for different land cover types. On the other hand, for most of the scenarios, particularly for grassland and cropland scenarios, the most significant changes occurred in the rainy season, which indicates that deforestation would cause significant increase of monthly runoff in the rainy season in the East River Basin. The conclusions agree well with related studies in southern China (Yuan, 2007; Zhang, 2008; Xie, 2009; Wei, 2010).

Because of the limitations of hydrological modeling techniques and the uncertainty of prediction of land use change, the results of this modeling study are not definitive

statements as to what will happen to ET, runoff and soil moisture regimes in the East River Basin in the future. But the modeling outcome does show the plausible changes in ET, runoff and soil moisture based on the current state of science. Therefore the results in this research carry not only important scientific merit but also valuable practical significance for future water resources planning and management.

CHAPTER 7

SUMMARY AND CONCLUSIONS

7.1 Summary of the study

An integrated modeling system of enhanced surface energy balance system, LAI-based interception model and distributed monthly water balance model has been developed to quantify LUCC, conduct physically-remote-sensing-based ET mapping and predict hydrologic impacts of LUCC.

To understand the state-of-the-art, this dissertation began with a review of the techniques and approaches for assessing the impacts of land use change on water resources, the historical development of hydrological models, land use/cover change detection with remote sensing and ET estimation with aid of remote sensing. Furthermore, spatio-temporal analysis of vegetation dynamics based on NDVI and LUCC analysis based on post-classification comparison were made to understand LUCC and its implications at basin scale during the study period (1980 to 2000), which lays a solid foundation for future studies on hydrologic impacts of LUCC.

ET is a major hydrologic component in the water budget and an important ecological element (plant physiological processes) in the energy budget, which can not be measured directly and has become the most difficult process to quantify in ecohydrologic modeling. In order to estimate areal ET for the whole watershed rather than traditional point measurements at local scales, a physically remote-sensing-based model SEBS was firstly enhanced for application in complex vegetated area and then employed for ET mapping in the East River Basin. Then the inter-comparison with complimentary ET model and distributed monthly water balance model was made to validate the enhanced SEBS (ESEBS). The application and test of ESEBS show that it has a good accuracy both monthly and annually and can be effectively applied in the East River Basin.

In addition, an integrated distributed monthly water balance model of enhanced surface energy balance system, LAI-based interception model and distributed monthly water balance model was developed for effectively predicting hydrologic impacts of LUCC.

The integrated model is capable of considering basin terrain and the spatial distribution of precipitation and soil moisture. Particularly, the model is unique in accounting for spatial and temporal variation of vegetation cover and ET by integration of physically-remote-sensing-based ET sub-model ESEBS and LAI-based interception sub-model. This unique feature makes it have several merits. On one hand, through the integration, the physical basis of the model is strengthened and a direct link between hydrologic process and vegetation is established in the model. On the other hand, spatially-distributed ET estimates for each subbasin are readily available through the integration, which makes the model capable of estimating distributed-parameters for each subbasin and makes a valuable contribution to spatial representation of catchment responses. In a word, it is a distributed model that can not only account for spatial variations in basin terrain, rainfall, soil moisture but also consider spatial and temporal variation of vegetation and ET in particular, which provides a powerful tool for studying hydrologic impact of LUCC. The calibration and validation of the model suggest that the new model is suitable for simulating monthly runoff processes and assessing hydrologic impacts of LUCC in the East River Basin.

Finally the newly integrated model was applied to evaluate of hydrological impacts of land use change in the East River Basin. Firstly the impact of LUCC on the hydrologic regimes in past and present were analyzed and then hypothetical land use scenarios were developed and examined.

7.2 Major findings and conclusions

This study concentrates on developing an integrated modeling system of enhanced surface energy balance system, LAI-based interception model and distributed monthly water balance model to quantify LUCC, conduct physically-remote-sensing-based ET mapping and predict hydrologic impacts of LUCC. During the studies, a great number of data were collected and then LUCC were quantified and its implications were analyzed. Moreover, with the aid of GIS/RS, areal ET for a large area was estimated rather than traditional point measurement on local scales. Furthermore, an integrated model that can not only account for spatial variations in basin terrain, rainfall, soil moisture but also consider spatial and temporal variation of vegetation and ET were developed and finally the hydrologic impacts of LUCC were quantified using the

integrated model. The contributions to regional eco-hydrological modeling, large-scale ET estimation and major findings of this dissertation, as well as the directions for future work, are summarized below.

7.2.1 Development of database for the hydrologic and LUCC studies in the East River Basin with the aid of GIS/RS

Hydrologic models are generally built according to data availability (Schultz, 2000). Particularly, modeling hydrologic impact of LUCC requires intensive data. In this dissertation, a great number of data, including hydrologic data, meteorological data, land use/cover data, soil data, DEM data, remote sensing data and field measurement data were collected and manipulated. Particularly, the measured monthly LAI and ground truthing data collected (together with research group from Hohai University, China) at 305 sample points from December, 2008 to December, 2009 are primary data, which provides vital role in LUCC studies in the East River Basin. Then GIS database including land use/cover layer, meteorological layer, hydrologic data layer and DEM layer were constructed, which lays a solid foundation for hydrologic and LUCC studies in this area.

7.2.2 Findings in LUCC analysis

Spatio-temporal variations of vegetation dynamics were analyzed based on NDVI and changes of land use/cover were analyzed based on post-classification comparison with aid of GIS/RS. The major findings and contributions are summarized as following.

(1) From spatio-temporal analysis of vegetation dynamics based on NDVI, it can be concluded as follows. Spatially speaking, the NDVI value decreased from the upper-middle-part (agricultural region) to the lower-part (urban area) in the study area, which demonstrates that human activities can influence vegetation activities (plant growth). Temporally speaking, NDVI decreased significantly in summer (June to September) over the years. According to relevant studies conducted in this area (e.g. Wei, 2010; Hu, 2008; Wang et al., 2006), there is little influence of climate change on vegetation in southern China due to plentiful rainfall and suitable temperature, particularly in summer. Therefore, it can be concluded that the major driving force for the decrease of vegetation activities is probably human activity.

(2) From post-classification comparison of LUCC, it is concluded that the East River Basin had experienced a significant change in land use and land cover over the past two decades. Particularly there was a sharp increase of urban and built-up area and a significant decrease of grassland and cropland. Spatially speaking, the change ratios for Dongguan, Huizhou urban and Baoan, Longgang in the lower-part were greater than others. It is in good agreement with the urban growth and economic development.

(3) Furthermore, based on land use prediction with aid of Markov chain model, it can be concluded that the dominant land cover in the study area in 2010 remain forest and cropland and there is slight change in water area and urban and built-up area.

7.2.3 Contributions to areal ET estimation

ET as a key component in the water budget and energy budget has traditionally been one of the most difficult hydrological processes to determine, which can not be measured directly (Zhang et al., 2001). Therefore, mapping ET becomes a very important step in integrated eco-hydrologic modeling for assessment of hydrologic impact of LUCC.

Conventional techniques that employ point measurements to estimate ET are only representative at local scales and can not be extended to large areas. Remote sensing is probably the only technique which can provide representative measurements of several relevant physical parameters at scales from a point to the large scale. In this dissertation, the physically remote-sensing-based ET estimation model, SEBS was employed to areal ET for a large area rather than traditional point measurements at local scales.

The SEBS has a very strong physical basis, which does not require too many parameters or other intensive data; therefore, it has been widely applied in Spain (van der Kwast et al., 2009) and Dutch (e.g. Hailegiorgis, 2006; Weligepolage, 2005) in Europe and northwestern China (Li, 2001; Su et al., 2003). The practical application has proved that it has a clear physical meaning and good accuracy for lowland-shrub region with relatively heterogeneous underlying surface (Su, 2002; Su et al., 2003; Zhan, 2005; Lin et al., 2008). However, there are few studies on its application in southern China. Moreover, the applicability in the area with heterogeneous underlying surface and complex vegetation conditions has been challenged by many scholars (e.g., Zhan, 2005; He et al., 2006; Lin et al., 2008). In the original SEBS, for LAI, the formula is strictly

only good for low vegetation since NDVI saturates at higher LAI values: for aerodynamic roughness height (Z_{0m}) and displacement height (d_0), there is only one empirical equation for all types of land cover can not represent the complex vegetation conditions. Therefore, an enhancement has to be made for its application in complex vegetated area.

In order to enhance the SEBS for application in complex vegetated area, firstly relationship of LAI and NDVI were identified based on remote sensing data and field measured data using regression model. Secondly, based on the identified LAI-NDVI relationship mentioned above, in combination with the experiments in China as reported in Zhang (1996), estimation of aerodynamic roughness height z_{0m} and the displacement height d_0 can be improved for application in complex vegetated area. Through model enhancement, the SEBS has a much stronger physical basis and a wider applicability, particularly for the complex vegetated area in southern China.

The ESEBS was applied to estimate areal ET from 1980~2000 based on NOAA/AVHRR Data and meteorologic data. Moreover, the results of SEBS were validated with complimentary relationship ET models (AA/GG/CARE) and Distributed Monthly Water Balance Model. The application and test of ESEBS show that it has a good accuracy both monthly and annually and can be effectively applied in the East River Basin.

The results of ET mapping based on ESEBS demonstrate that actual ET in the East River Basin decreased significantly in the last two decades. By inter-comparison with trend of corresponding climatic variable, such as temperature, relative humidity, wind speed and sunshine duration, it can be concluded that the decrease of ET is probably caused by decrease of sunshine duration.

7.2.4 Contributions to basin-scale hydrologic modeling

Most water balance models account for runoff generation processes evenly over a whole watershed and are limited in assessing the effect of land use and other changes in basin hydrology. The integrated distributed monthly water balance model developed in this study is capable of considering basin terrain and the spatial distribution of precipitation

and soil moisture. Particularly, the model is unique in accounting for spatial and temporal variation of vegetation cover and ET by integration of physically-remote-sensing-based ET sub-model ESEBS and LAI-based interception sub-model. This unique feature makes it have several merits. On one hand, in the original DMWBM, ET is oversimplified by empirical equation which does not have clear physical meaning and thus there is no direct links between hydrologic processes and vegetation. Through the integration, the physical basis of the model is strengthened and a direct link between hydrologic process and vegetation is established in the model. On the other hand, the new model can account for spatial and temporal variation of vegetation cover and ET through the integration, therefore spatially-distributed ET estimates for each subbasin are readily available which makes the model capable of estimating distributed parameters for each subbasin and makes a valuable contribution to spatial representation of catchment responses. In a word, the integrated model developed in this study is a distributed model that can not only account for spatial variations in basin terrain, rainfall, soil moisture but also consider spatial and temporal variation of vegetation cover and ET in particular, which provides a powerful tool for studying hydrologic impact of LUCC.

Based on topography, soil characteristics and spatial distribution of precipitation, the East River Basin was divided into seventeen relatively homogenous units (sub-basins). The model inputs are monthly areal precipitation and potential evaporation values of each sub-basin and the outputs are monthly values of actual evapotranspiration, soil moisture storage and runoff for each sub-basin. The model was calibrated for one gauged station (Boluo) and validated for three stations (Boluo, Heyuan, Longchuan) in the East River Basin. Evaluation of the hydrologic simulation results demonstrate that: a) simulated runoff matches observed values very well on monthly and annual basis and b) the degree of association between the simulated and observed stream flows is quite high for monthly mean values. In summary, the calibration and validation results suggest that the new model is suitable for simulating monthly runoff processes and assessing hydrologic impacts of LUCC in the East River Basin.

Sensitivity analysis of the model was carried out to reveal that runoff regulation parameter α and pan coefficient η have the most significant effects on runoff and soil moisture capacity WM is an insensitive parameter. Depending on the geographical

location of the study basin, the value of parameter WM can be determined by experience. With the input data of precipitation and potential evapotranspiration and through model calibration and validation, the integrated model (IDMWBM) of DMWBM, ESEBS sub-model and LAI-based interception sub-model can be efficiently applied to evaluate the impacts of land use change on regional water resources and hydrological regimes.

7.2.5 Findings on hydrological impacts of land use change

Hydrologic impacts of LUCC were quantified using the integrated distributed monthly water balance model rather than traditional statistical analysis or paired watershed studies. The relationship of land use/cover and hydrologic regimes were firstly quantified based on the simulation of IDMWBM with land use maps in 1980 and 2000. Then potential impacts of land use change on water availability in the East River Basin were simulated by using hypothetical land use/cover scenarios and the newly integrated model in this dissertation. The modeling study has led to the following findings.

7.2.5.1 Analysis of ET for different land use

From the simulation of IDMWBM with land use maps in 1980 and 2000, the order of annual amount of ET for different land use types is ranked as follows: Urban and built-up < Grassland < Cropland < Forest land < Water. Water area has the highest annual ET of 767 mm while the urban and built-up area has the lowest annual ET of 392 mm. It is elaborated that urban and built-up area is impervious and has limited water for evaporation, and therefore it has the lowest ET. Water body is sufficient in water supply for evaporation in southern China, and therefore it has the highest ET. Moreover, it demonstrates that ET has a positive relationship with LAI. The results can be understood and explained by energy balance equation and are in good agreement with several studies in southern China (Zhang, 2008; Xie, 2009; Wei, 2010).

7.2.5.2 Analysis of runoff for different land use

In terms of annual amount, the order of runoff for different land use is ranked as follows: Urban and built-up > Grassland > Cropland > Forestland. Urban and built-up has the greatest annual runoff of 1243 mm while forest area yields the least runoff of 855 mm. It is elaborated that urban and built-up area is impervious, which has less infiltration and generates more direct runoff. Moreover, it has limited water for evaporation. Therefore, it has the highest runoff. Moreover, it demonstrates that runoff has a negative

relationship with LAI. Therefore, annual runoff of forest is less than that of grassland/cropland. The results reveal that urbanization can increase annual runoff while afforestation can decrease annual runoff. These conclusions can be understood and explained by water and energy balance equations and are in good agreement with related studies in Germany (DeFries & Eshleman, 2004) and China (Yuan, 2007; Xie, 2009; Wei, 2010).

7.2.5.3 Analysis of soil moisture for different land use

As far as monthly soil moisture is concerned, there is hardly any change in most of the months and only slight variation in the dry season (November to February for the study area) in the East River Basin. Moreover, there is no significant variation in soil moisture for different land use types on a monthly basis in the East River Basin. In other words, vegetation has limited effects on soil moisture on a monthly basis in the East River Basin. The results are in good agreement with related studies conducted in southern China (Yuan, 2007; Zhang, 2008; Xie, 2009).

7.2.5.4 ET in response to LUCC

In terms of annual mean amount, the order of ET for different land cover is ranked as follows: Grassland scenario < Cropland scenario < Projected scenario < Broad-leaf forest scenario < Mixed forest scenario < Need-leaf forest scenario. The results show that ET has a positive relationship with LAI in the same climatic zone. On a monthly basis, the monthly processes of ET are consistent with monthly processes of LAI, and monthly ET reaches the highest value in summer and the lowest value in autumn and winter, which again indicates a positive relationship between LAI and ET for the same climatic zone.

As far as the change of ET comparing with current situation is concerned, on an annual basis, the grassland scenario has the greatest change ratio, which would cause 45% decrease of ET compared with current situation. It indicates that there would be significant decrease in ET when the watershed changes from forest-dominated to grass-governed. The mixed forest scenario has the lowest change ratio, which would cause 2% decrease of ET. It indicates that mixed forest scenario is similar to current situation. The broadleaf forest scenario is of practical significance because eucalyptus, as a type of broad-leaf tree, has been widely planted in the East River Basin. This scenario would

cause 14% decrease of ET. The projected scenario would cause 16% decrease of ET. On a monthly basis, comparing with the current situation, the most significant changes occur in summer. The results show again that ET has a positive relationship with LAI and monthly processes of ET are consistent with monthly processes of LAI in the same climatic zone.

In summary, on an annual basis, ET has a positive relationship with LAI. On a monthly basis, the monthly processes of ET are consistent with monthly processes of LAI. In terms of the change of ET comparing with current situation, all of the scenarios except for the need-leaf forest scenario would cause decrease of annual ET. The most significant decrease of ET occurs in summer. The results demonstrate that deforestation (forest changed to grassland/cropland) would cause decrease of annual ET in the East River Basin. Particularly, deforestation would cause significant decrease of ET in summer. All the results can be well understood based on surface energy balance equation and agree well with related studies in Guizhou (Zhang, 2008), the Hanjiang River Basin (Yuan, 2006), the Yellow River Basin (Liu et al., 1978) and the Pearl River Delta (Xie, 2009; Wei, 2010) in China.

7.2.5.5 Runoff in response to LUCC

In terms of annual mean runoff, the order of annual runoff depth for different scenarios is ranked as follows: Grassland scenario > Cropland scenario > Projected scenario > Broad-leaf forest scenario > Mixed forest scenario > Need-leaf forest scenario. The results show that runoff has a negative relationship with LAI in the same climatic zone. On a monthly basis, monthly runoff processes for different land cover types are in the inverse order of ET processes for different land cover types, which again reveal that runoff has a negative relationship with LAI in the same climatic zone.

As far as the change of annual mean runoff comparing with current situation is concerned, grassland scenario would cause the greatest increase of 37% in comparison with current situation, which indicates that there would be significant increase in runoff when all the land cover change to grassland. There would be the least increase of 2% in runoff for mixed forest scenario, which is the most similar to the current situation. As eucalyptus has been widely planted in the East River Basin, the broad-leaf forest scenario is practically meaningful and reveals that there would be 13% increase of

runoff when all the land cover change to evergreen broad-leaf forest. The projected scenario would cause 14% increase in runoff depth. On a monthly basis, the most significant changes occurred in the rainy season (May to September) in the East River Basin. Comparing the change amount of monthly ET and the change amount of monthly runoff, they generally tally with each other. For most scenarios, particularly for grassland and cropland scenario, the most significant changes occurred in the rainy season. It indicates deforestation (forest changed to grassland or cropland) would cause significant increase of monthly runoff in the rainy season in the East River Basin.

In summary, it is concluded that all of the hypothetical scenarios except for the needle-leaf forest scenario would cause increase of annual runoff comparing with current situation. Particularly the grassland and cropland scenarios would cause significant increase of annual runoff. On a monthly basis, monthly runoff processes for different land cover types are in the inverse order of ET processes for different land cover types. On the other hand, the most significant changes occurred in the rainy season. The results reveal that deforestation would cause significant increase of annual runoff and significant increase of monthly runoff in the rainy season in the East River Basin. The conclusions can be explained based on surface energy balance and water balance and agree well with related studies in southern China (Yuan, 2007; Zhang, 2008; Xie, 2009; Wei, 2010).

Because of the limitations of hydrological modeling technique and the uncertainty of land use prediction of land use change, the results of this modeling study are not definitive statements as to what will happen to ET, runoff and soil moisture regimes in the East River Basin in the future. But the modeling outcome does show the plausible changes in ET, runoff and soil moisture based on the current state of science. The results in this research carry not only important scientific merit but also valuable practical significance for future water resources planning and management practices.

7.3 Recommendation for future study

Both of land use/cover change and the responses of hydrologic systems are complicated problems involving interactions and feedbacks between atmospheric, hydrologic and biologic system. Although hydrologic modeling with aid of GIS/RS is powerful in

studying hydrologic impacts of LUCC, there are still several assumptions and limitations in this study, which are summarized and discussed as follows.

(1) One major assumption is that climate remains constant under current and altered scenarios. Although global warming has been widely debated, there is still a consensus that climate change occurs. Computer simulation with change in climate taken into account will surely increase the reliability of modeling results. For future research, first and foremost, statistic analysis of long-term climate change (e.g. temperature, precipitation) and runoff variation will be conducted during the last three decades, and then the newly integrated model (IDMWBM) developed herein will be employed to test the sensitivity of hydrologic regimes to climate change under a wide range of scenarios (both hypothetical and GCM-based scenarios).

(2) The land use/cover maps in this study are mainly obtained from existing products of other research groups, which can not provide enough information for studies of hydrologic impact of LUCC. In the future, more efforts have to be made in the studies of land use/cover classification and prediction.

(3) The traditional eco-hydrologic models oversimplify the vegetation growth model. The integrated model in this research uses LAI and NDVI to represent vegetation dynamics, which also has the same limitation. In order to further understand vegetation effects on hydrologic cycle, crop growth sub-model under unstationary condition should be developed and incorporated in the model.

(4) Hydrologic models are generally not built the way which would be scientifically most sound, but rather according to data availability (Schultz, 2000). In the future, more in-situ experiments and ground monitoring works of soil moisture, LAI and other land surface parameters would be very helpful for validating the results from hydrologic simulation or retrieved from remote sensing data.

(5) In order to provide an insight into detailed ecohydrologic process for a small scale on a short-term basis, the integrated model developed in this study can be further modified as a daily model and several representative small sub-basins (e.g. Danshui,

Xinfeng, Lianping, Yuecheng) can be selected to conduct small-scale and short-term studies of eco-hydrologic process by using the modified model and in-situ experiments.

(6) As stated by Peter (1986), "He who controls the future of global-scale models controls the future of hydrology". The IDMWBM presented by this research can output hydrologic regimes(runoff, ET, soil moisture) and land surface parameters (e.g. albedo, emissivity, sensible heat flux, latent heat flux, net radiation, soil heat flux), which can be further developed to be land surface model, which can also be integrated with climate models like GCMs to study macro-scale hydrologic processes.

(7) The model developed in this research has been used in the East River Basin. Further studies are required to test the model over a wide variety of basins under a wide range of climate conditions to test its applicability.

REFERENCES

- Abbott, M.B., Bathurst, J.C., Cunge, J.A., O'Connell, P.E., & Rasmussen, J. (1986). An introduction to the european hydrological system - systeme hydrologique europeen. "SHH", 1: history and philosophy of a physically-based, distributed modeling system. *Journal of Hydrology*, 87, 45-59.
- Abbott, M., & Refsgaard, J. (Eds.). (1996). *Distributed Hydrological Modeling*. The Netherlands: Kluwer Academic Publishers.
- Andrea, W., Nicala, F., & Detlev, M. (2001). Long-term land use changes in a mesoscale watershed due to socio-economic factors — effects on landscape structures and functions. *Ecological Modeling*, 140(1-2), 125-140.
- Aikten, A. (1973). Assessing systematic errors in rainfall-runoff models. *Journal of Hydrology*, 20, 121-136.
- Al-Soufi, R.A. (1987). A physically based model for the agrohydrological processes. *Journal of Hydrology*, 93, 199-219.
- Allen, R., Tasumi, M., Morse, A., & Rezza, R. (2005). A landsat-based energy balance and evapotranspiration model in Western US water rights regulation and planning. *Irrigation and Drainage Systems*, 19(3/4), 251-268.
- Andersen, J., Dybkjaer, G., Jensen, K.H., Refsgaard, J.C., & Rasmussen, K. (2002). Use of remotely sensed precipitation and leaf area index in a distributed hydrological model. *Journal of Hydrology*, 264(1-4), 34-50.
- Asrar, G., Kanemasu, E.T., & Yoshida, M. (1985). Estimates of leaf area index from spectral reflectance of wheat under different cultural practices and solar angle. *Remote sensing of Environment*, 1(7), 1-11.
- Axayacatl, M.E. (2007). Assessment of impacts of land cover change on the san juan river watershed. Retrieved from ProQuest Digital Dissertations (AAT 1445781).
- Azzali, S., & Menenti, M. (2000). Mapping vegetation-soil-climate complexes in southern Africa using temporal Fourier analysis of NOAA-AVHRR NDVI data. *International Journal of Remote Sensing*, 21(5), 973-996.
- BAHC. (1993). *The Biospheric Aspects of the Hydrological Cycle - The Operational Plan*. BAHC core project office. Retrieve from <http://www.igbp.net/>.

- Baird, A.J., & Rober, L.W. (1999). *Eco-hydrology: Plants and Water in Terrestrial and Aquatic Environments* (p. 402). London: Routledge.
- Bastiaanssen, W.G.M (1998). Remote sensing in water resources management: The state of the art. Colombo, Sri Lanka: International Water Management Institute (IWMI).
- Bastiaanssen, W.G.M. (2000). SEBAL-based sensible and latent heat fluxes in the irrigated Gediz Basin, Turkey. *Journal of Hydrology*, 229(1-2), 87–100.
- Beljaars, A.C.M., & Holtslag, A.A.M. (1991). Flux Parameterization over Land Surfaces for Atmospheric Models. *Journal of Applied Meteorology*, 30, 327-341.
- Bell, E.J. (1974). Markov analysis of land use change—an application of stochastic processes to remotely sensed data. *Socio-Economic Planning Sciences*, 8(6), 311-316.
- Bergstrom, S. (1995). The HBV model. In Singh, V. (Ed.), *Computer Models of Watershed Hydrology* (pp. 443-476). Colorado: Water Resources Publications.
- Beven, K.J., Calver, A. & Morris, E.M. (1987). The institute of hydrology distributed model, Internal Report, Institute of Hydrology, Wallingford.
- Beven, K.J. (1997). TOPMODEL: a critique. *Hydrological Processes*, 11(9), 1069-1085.
- Beven, K.J. (2001). *Rainfall-Runoff Modeling, The Primer*. Chichester: Wiley.
- Beven, K.J. (2002). Towards an alternative blueprint for a physically based digitally simulated hydrologic response modeling system. *Hydrological Processes*, 16(2), 189-206.
- Beven, K.J., & Kirby, M.J. (1979). A physically based variable contributing area model of basin hydrology. *Hydrological Sciences Bulletin*, 24(1), 43-69.
- Bhaduri, B., Harbor, J.O., Engel, B., & Grove, M. (2008). Assessing Watershed-Scale, Long-Term Hydrologic Impacts of Land-Use Change Using a GIS-NPS Model. *Sciences-New York*, 26(6), 643- 658.
- Blackie, J., & Eeles, C.W. (1985). Lumped catchment models. In M. Anderson & T. Burt, *Hydrological Forecasting* (Eds.). Chichester: John Wiley & Sons.
- Blanchard. (1973). Measuring watershed runoff capability with ERTS data. In Mercanti, E.P., Freden, S.C. & Becker, M. (Eds.), *Third Earth Resources Satellite Symposium*. Washington, D.C.: NASA.

- Blümel, K. (1999). A simple formula for estimation of the roughness length for heat transfer over partly vegetated surfaces. *Journal of Applied Meteorology*, 38, 814-829.
- Boegh, E., Soegaard, H., Hanan, N., Kabat, P., & Lesch, L. (1999). A remote sensing study of the NDVI-Ts relationship and the transpiration from sparse vegetation in the Sahel based on high resolution satellite data. *Remote Sensing of Environment*, 69, 224-240.
- Bosch, J., & Hewlett, J. (1982). A review of catchment experiments to determine the effect of vegetation changes on water yield and evapotranspiration. *Journal of hydrology*, 55, 3-23.
- Boughton, W.C. (1984). A simple model for estimating the water yield of ungauged catchments. *Civil Engineering Transactions*, 26 (2), 83-88.
- Bowen, I.S. (1926). The ratio of heat losses by conduction and by evaporation from any water surface. *Physical Review*, 27(6), 779-787.
- Bradford, D.W., Breshears, D.D., & Allen, C.D. (2003). Ecohydrology of resource-conserving semiarid woodland: effects of scale and disturbance. *Ecological Monographs*, 73(2), 223-239.
- Briassoulis, H. (2000). *Analysis of Land Use Change: Theoretical and Modeling Approaches*. (Unpublished dissertation). Regional Research Institute, West Virginia University, Morgantown, West Virginia, USA
- Brutsaert, W. (1975). On a derivable formula for long - wave radiation from clear skies. *Water Resources Research*, 11(5), 742 - 744.
- Brutsaert, W. (1982). *Evaporation into the Atmosphere: Theory, History and Applications*. New York: Kluwer Academic Publishers.
- Brutsaert, W. (1999). Aspects of bulk atmospheric boundary layer similarity under free-convective conditions. *Reviews of Geophysics*, 37(4), 439-452.
- Brutsaert, W. & Stricker, H. (1979). An advection–aridity approach to estimate actual regional evapotranspiration. *Water Resources Research*, 15(2), 443–450.
- Brutsaert, W., & Sugita, M. (1992). Application of Self - Preservation in the Diurnal Evolution of the Surface Energy Budget to Determine Daily Evaporation. *J. Geophys. Res.*, 97(D17), 18377-18382.

- Calcagno, G., Mendicino, G., Monacelli, G., Senatore, A., & Versace, P. (2007). Distributed estimation of actual evapotranspiration through remote sensing techniques. In Rossi, G. et al. (Eds.), *Methods and tools for drought analysis and management*. Europe: Springer.
- Calver, A. (1988). Calibration, sensitivity and validation of a physically based rainfall-runoff. *Journal of Hydrology*, 103, 103-115.
- Campana, N., & Tucci, C. (2001). Prediction floods from urban development scenarios: case study of the Diluvio Basin, Porto Alegre, Brazil. *Urban Water*, 3, 113-124.
- Campbell, G., & Norman, J. (1998). *An introduction to environmental biophysics*. New York: Springer.
- Carlson, T., Gillies, R., & Schmugge, T. (1995). An interpretation of methodologies for indirect measurement of soil water content. *Agricultural and Forest Meteorology*, 77, 191-205.
- CAS. (2004). Data sharing infrastructure of earth system science. Retrieved from <http://www.geodata.cn>.
- Chen, D., & Brutsaert, W. (1998). Satellite-Sensed distribution and spatial patterns of vegetation parameters over a tall grass Prairie. *Journal of the Atmospheric Sciences*, 55, 1225- 1238.
- Chen, J., He, Y., & Chen, M. (2004). Water budget analysis of red soils in central Jiangxi Province, China. *Pedosphere*, 14(2), 241-246.
- Chen, X., & Hu, Q. (2004). Groundwater influences on soil moisture and surface evaporation. *Journal of Hydrology*, 297(1-4), 285-300.
- Chen, X., Chen, Y., & Xu, C.Y. (2006). A distributed monthly hydrological model for integrating spatial variations of basin topography and rainfall. *Hydrological Processes*, 21, 242-252.
- Choudhury, B., Ahmed, N., Idso, S., Reginato, R., & Daughtry, C. (1994). Relations between evaporation coefficients and vegetation indices studies by model simulations. *Remote Sensing of Environment*, 50, 1-17.

- Cognard-Plancq, A., Marc, V., Didon-Lescot, J., & Normand, M. (2001). The role of forest cover on stream flow down sub-Mediterranean mountain watersheds: a modeling approach. *Journal of hydrology*, 254(1-4), 229-243.
- Congalton, R.G. & Macleod, R.D. (1998). A Quantitative Comparison of Change Detection Algorithms for Monitoring Eelgrass from Remotely Sensed Data. *Photogrammetric Engineering & Remote Sensing*, 64(3), 207 - 216.
- Consoli, S., D'Urso, G., & Toscano, A. (2006). Remote sensing to estimate ET-fluxes and the performance of an irrigation district in southern Italy. *Agricultural Water Management*, 81, 295–314.
- Coppin, P., & Bauer, M. (1996). Digital Change Detection in Forest Ecosystems with Remote Sensing Imagery. *Remote Sensing Reviews*, 13, 207-234.
- Cosandey, C., Andreassian, V., Martin, C., Didonlescot, J., Lavabre, J., & Folton, N. et al. (2005). The hydrological impact of the Mediterranean forest: a review of French research. *Journal of Hydrology*, 301(1-4), 235-249.
- Costa, M., Botta, A., & Cardille, J. (2003). Effects of large-scale changes in land cover on the discharge of the Tocantins River, Southeastern Amazonia. *Journal of Hydrology*, 283(1-4), 206-217.
- Courault, D., Seguin, B., & Olioso, A. (2005). Review on estimation of evapotranspiration from remote sensing data: From empirical to numerical modeling approaches. *Irrigation and Drainage Systems*, 19(3-4), 223-249.
- Crago, R. (1996). Comparison of the evaporative fraction and the Priestley-Taylor α for parameterizing daytime evaporation. *Water Resource Research*, 32(5), 1403-1409.
- Crawford, N.H., & Linsley, R.K. (1966). Digital simulation in hydrology: Stanford Watershed Model IV. Technical Report 39, Dept. of Civil Engineering, Stanford University, California.
- Dickinson, R.E. (1984). Modeling evapotranspiration for three-dimensional global climate models. In Hansen, J.E., & Takahashi, T. (Eds.). *Climate Processes and Climate Sensitivity* (pp. 58-72). Washington DC: American Geophysical Union.
- Dan, H., Zhou, J., Cai, J.M., & Qiao, Z.P. (2009). The analysis of land use dynamic change and driving force in the Olympic village periphery area. *Proceedings of Urban Remote Sensing of Event, 2009 Joint* (pp. 1-7). Shanghai: IEEE.

- Daniel, E.A., James, D.H., Emily, H.W., Song, M.J., & Zhang, Z.K. (2002). A comparison of Landuse and Landcover Change Detection Methods. , 12. Retrieved from http://clear.uconn.edu/publications/research/tech_papers/Civco_et_al_ASPRS2002.pdf.
- Dawes, W.R., & Short, D.L. (1994). The significance of topology for modeling the surface hydrology of fluvial landscapes. *Water Resources Research*, 30, 1045- 1055.
- DeFries, R., Asner, G., & Houghton, R. (2004). *Ecosystems and Land Use Change*. Geophysical Monograph Series, American Geophysical Union, 153, 344.
- Defries, R., & Eshleman, K.N. (2004). Land-use change and hydrologic processes: a major focus for the future. *Hydrologic Process*, 18, 2183-2186.
- Denisenko, E.A., & Lozinskaya, E.A. (1994). The space and time variability of LAI, transpiration and évapotranspiration (KUREX88 Case Study). Unpublished paper, Russian Academy of Science.
- Dimiyati, M., Mizuno, K., Kobayashi, S., & Kitamura, T. (1995). An Analysis of Land Use/Land Cover Change Using the Combination of MSS Landsat and Land Use Map- A case study of Yogyakarta Indonesia. *International Journal of Remote Sensing*, 17(5), 931 – 944.
- Dolman, A.J., Schulze, E.D., & Valentini, R. (2003). Analyzing carbon flux measurements. *Science*, 301(5635), 916-9177.
- Dooge, J. (1988). Hydrology in perspective. *Hydrological Sciences Journal*, 33, 61-85.
- Dooge, J. (1992). Hydrologic models and climate change. *Journal of Geophysical Research*, 97(D3), 2677-2686.
- Doyle, P. (1990). Modeling catchment evaporation: An objective comparison of the Penman and Morton approaches. *Journal of Hydrology*, 121, 257-276.
- Droogers, P., & Bastiaanssen, W. (2002). Irrigation performance using hydrological and remote sensing modeling. *Journal of Irrigation and Drainage Engineering ASCE*, 128(1), 11–18.
- Duan, Q., Sorooshian, S., & Gupta, V. (1992). Effective and efficient global optimization for conceptual rainfall-runoff models. *Water Resources Research*, 28(4), 1015-1031.

- Duchon, C.E., Salisbury, J.M., Lee, T.H., & Nicks, A.D. (1992). An example of using Landsat and GOES data in a water budget model. *Water Resource. Research*, 28(2), 527–538.
- Dunn, S.M., & Mackay, R. (1995). Spatial variation in evapotranspiration and the influence of land use on catchment hydrology. *Journal of Hydrology*, 171, 49-73.
- Engman, E. (1996). Remote sensing applications to hydrology: future impact. *Hydrological Sciences*, 41, 637–647.
- Engman, E., & Gurney, R.J. (1991). *Remote sensing in hydrology*. London: Chapman and Hall.
- ESRI. (2007). ARCGIS 9.2 Desktop help. Retrieved from <http://webhelp.esri.com/arcgisdesktop/9.2/index.cfm?TopicName=Tutorials>.
- Evans, J.P. (2000). Modeling climate-surface interaction in data sparse area. (Unpublished doctoral dissertation). The Australian National University, Canberra.
- Fang, J., Piao, S., & Huo, J. (2003). Vegetation activity is increasing in the last two decades. *China Science (C series)*, 33(6), 554-565.
- FAO. (1998). *Land Cover Classification System (LCCS): Classification Concepts and User Manual* Environment and Natural Resources Service, GCP/RAF/287/ITA. Gregorio, A. Di & Jansen, L. (Eds.) (pp. 157). Rome, Italy: Africover - East Africa Project and Soil Resources, Management and Conservation Service.
- Fernández-Illescas, C.P., & Rodríguez-Iturbe, I. (2004). The impact of interannual rainfall variability on the spatial and temporal patterns of vegetation in a water-limited ecosystem. *Advance in water resource*, 27, 83-95.
- Fitzpatrick-lins et al. (1987). Producing Alaska Interim Land Cover Maps from Landsat Digital and Ancillary Data. In *Proceedings of the 11th Annual William T. Pecora Memorial Symposium: Satellite Land Remote Sensing: current programs and a look into the future* (p. 339 – 347). Sioux Falls, SD: American Society of Photogrammetry and Remote Sensing.
- Fohrer, N. (2001). Hydrologic Response to land use changes on the catchment scale. *Physics and Chemistry of the Earth, Part B: Hydrology, Oceans and Atmosphere*, 26(7-8), 577-582.

- Gan, T.Y., & Bifu, G. (1996). Automatic calibration of conceptual rainfall-runoff models: optimization algorithms, catchment conditions, and model structure. *Water Resources Research*, 32(12), 3513-3524.
- Gan, T.Y., Dalamini, E.M., & Biftu, G.F. (1997). Effects of model complexity and structure, data quality, and objective functions on hydrologic modeling. *Journal of Hydrology*, 192, 81-103.
- Gao, J., & Wen, Y. (2002). Impact of land use change on runoff of Taihu Basin. *Acta Geogr Sin*, 57, 194-200.
- Gao, Y., & Long, D. (2008). Intercomparison of remote sensing-based models for estimation of evapotranspiration and accuracy assessment based on SWAT. *Hydrological Processes*, 22(25), 4850- 4869.
- Gao, Z., Zhang, Z., & Zhang, X. (2009). Responses of water yield to changes in vegetation at a temporal scale. *Frontiers of Forestry in China*, 4(1), 53-59.
- Garatuza-Payan, J., & Watts, C. (2005). The use of remote sensing for estimating ET of irrigated wheat and cotton in Northwest Mexico. *Irrigation and Drainage Systems*, 19(3/4), 301-320.
- Garbrecht, W. & Martz, J.A. (1998). An automated digital landscape analysis tool for topographic evaluation, drainage identification, watershed segmentation and subcatchment parameterization. Retrieved from <http://duke.usask.ca/~martzl/tonaz/index.html>.
- Getu, F.B. (1998). Semi-distributed hydrologic modeling using remotely sensed data and GIS. Retrieved from ProQuest Digital Dissertations. (AAT NQ34736).
- Geoghegan, J., Pritchard, L., Ogneva-Himmelberger, Y., Chowdhury, R.R., Sanderson, S., & Turner, B.L. (1998). "Socializing' the Pixel and 'Pixelizing' the Social in Land-Use and Land-Cover Change." In Liverman D., Moran, E.F., Rindfuss, R.R., & Stern, P.C. (Eds.), *People and Pixels: Linking Remote Sensing and Social Science*, (pp 151-169). Washington, D.C.: National Academy Press.
- Gholz, H.L., Fitz, F.K., & Waring, R.H. (1976). Leaf area differences associated with old growth forest communities in the Western Oregon Cascades. *Canadian Journal of Forest Research*, 6(1), 49-57.

- Gowda, P.H., Colaizzi, P.D., Evett, S.R., Howell, T.A., & Tolck, J.A. (2007). Remote sensing based energy balance algorithms for mapping ET: current status and future challenges. *Transactions of the ASABE*, 50(5), 1639-1644.
- Gower, S.T., & Norman, J.N. (1991). Rapid estimation of Leaf Area Index in conifer and broadleaf plantations. *Ecology*, 72(5), 1896-1900.
- Granger, R., & Gray, D. (1990). Examination of Morton's CRAE model for estimating daily evaporation from field-sized areas. *Journal of Hydrology*, 120, 309-325.
- Gupta, V., & Sorooshian, S. (1985). The relationship between data and the precision of parameter estimates of hydrologic models. *Journal of Hydrology*, 81, 57-77.
- Gutman, G., & Ignatov, A. (1998). The derivation of the green vegetation fraction from NOAA/AVHRR data for use in numerical weather prediction models. *International Journal of Remote Sensing*, 19(8), 1533-1543.
- Guo, S.L., Wang, J.X., Xiong, L.H., Ying, A.W., & Li, D.F. (2002). A macro-scale and semi-distributed monthly water balance model to predict climate change impacts in China. *Journal of Hydrology*, 268(1-4), 1-15.
- Guo, F., Liu, X.R., & Ren, L.L. (2000). A Topography Based Hydrological Model: TOPMODEL and Its Widened Application. *Advances in water science*, 11(3), 296-301.
- GWP-WATAC. (2000). Water for the 21st Century-Vision to Action for the West Africa. Presented at the Hague 2nd World Water Forum 17-22 March 2000. Stockholm, Sweden.
- Haan, C.T. (1977). *Statistical Methods in Hydrology*. In Ames, Iowa: The Iowa State University Press.
- Hailegiorgis, W. (2006). Remote sensing analysis of summer time evapotranspiration using SEBS algorithm: a case study in Regge and Dinkel. (Unpublished Master thesis). ITC, The Netherlands.
- He, Y.B., Su, Z.B., Li, J., & Wang, S.L. (2006). Estimation of Surface Energy Flux Using Surface Energy Balance System (SEBS) in the Yellow-Huaihe-Haihe River Regions, China. *Plateau Meteorology*, 25(6), 1092-1100.

- Heilman, J., Heilman, W., & Moore, D. (1982). Evaluating the crop coefficient using spectral reflectance. *Agronomy Journal*, 74, 967–971.
- Hibbert, A. (1967). Forest treatment effects on water yield. In Sopper, W. E., & Lull, H.W. (Eds.), *Forest Hydrology* (p. 527-534). Pergamon, Oxford.
- Hu, H.X. (2008). Land Cover Change Detection Based on MODIS EVI Data for Dongjiang River Basin (Unpublished Master thesis). Hohai University, Nanjing.
- Huang, Y. (1993). Calculation methods on runoff generation and flow concentration in ungauged regions (Unpublished PhD dissertation). Hohai University, Nanjing.
- Huang Y.L., Fu, J.B., & Chen, L.D. (2003). Advances in ecohydrological process research. *Acta Ecologica Sinica*, 23(3), 580-587.
- Högström, U. (1998). Non-dimensional wind and temperature profiles in the atmospheric surface layer: A re-evaluation. *Boundary-Layer Meteorology*, 42(1-2), 55-78.
- IGBP. (1994). Land-Use and Land-Cover Change. Local processes and Global Impacts. Retrieve from <http://www.igbp.net/page.php?pid=250>
- IGBP-IHDP. (1999). Land-use and land-cover change, implementation strategy. IGBP Report 46/IHDP Report 10. Prepared by Scientific Steering Committee and International Project Office of LUCC. Stockholm and Bonn.
- Iqbal, M. (1983). An introduction to solar radiation. Toronto: Academic Press.
- Jackson, R.D., Idso, S.B., Reginato, R.J., & Printer, P.J. (1981). Canopy temperature as a crop water stress indicator. *Water Resources Research*, 17(4), 1133 - 1138.
- Jackson, R., Reginato, R., & Idso, S. (1977). Wheat canopy temperature: a practical tool for evaluating water requirements. *Water Resources Research*, 13, 651–656.
- Jacob, F., Oliosio, A., Gu, X., Su, Z.B., & Seguin, B. (2002). Mapping surface fluxes using airborne visible, near infrared, thermal infrared remote sensing data and a spatialized surface energy balance model. *Agronomie*, 22(6), 669–680.
- Jaiswal, R.K., Saxena, R., & Mukherjee, S. (1999). Application of remote sensing technology for land use/land cover change analysis. *Journal of the Indian Society of Remote Sensing*, 27(2), 123-128.

- James, S., Par'fel, M., & Wilson, S.D. (2003). Temporal heterogeneity of soil moisture in grassland and forest. *Journal of Ecology*, 91, 234-239.
- Jia, L., Su, Z., Hurk, V.D., Menenti, M., & Moene, A.F. et al. (2003). Estimation of sensible heat flux using the Surface Energy Balance System (SEBS) and ATSR measurements, *J. Phys. Chem. Earth*, 8, 75-88.
- Jiang, T. (2005). Monthly water balance modeling for hydrological impact assessment of climate change in the Dongjiang (East River) Basin, south China. Retrieved from ProQuest Digital Dissertations. (AAT 3203231).
- Jin, X. (2009). Ecohydrology in water-limited environments using quantitative remote sensing – the Heihe River basin (China) case. (Unpublished doctoral dissertation). Wageningen University, Netherlands.
- Jonathan, A.F., Levis, S., Costa, M.H., Wolfgan, C. & David, P. (2000). Incorporating Dynamic Vegetation Cover Within Global Climate Models. *Ecological Applications*, 10(6), 1620-1632.
- Kader, B.A., & Yaglom, A.M. (1990). Mean fields and fluctuation moments in unstably stratified turbulent boundary layers. *Journal of Fluid Mechanics*, 212, 637-662.
- Katul, G., & Parlange, M. (1992). A Penman-Brutsaert model for wet surface evaporation. *Water Resource Research*, 28(1), 121-126.
- Kendall, M. (1975). Rank correlation methods. Griffin. London, UK.
- Kepner, W.G., Semmens, D.J., Hernandez, M., & Goodrich, D.C. (2008). Evaluating Hydrological Response to Forecasted Land-Use Change : Scenario Testing with the Automated Geospatial Watershed Assessment (AGWA) Tool. In Proceedings, 3rd Interagency Conference on Research in the Watersheds, Estes Park September 08 – 11, 2008 (pp. 79-84). USGS, Corvallis.
- Kirkby, M. (1975). Hydrograph modeling strategies. In Peel, M. R., & Chisholm, H.P. (Eds.), *Process in physical and human geography* (pp. 69-90). Heinemann.
- Kirkpatrick, S., Gelatt, D., & Vecchi, M.P. (1983). Optimization by simulated annealing. *Science*, 220, 671-680.

- Kite, G.W. (1989). Using NOAA data for hydrological modeling. In: Quantitative Remote Sensing: An Economic Tool for the Nineties, Proceeding of IGARSS, 1989 (pp. 553-558). New York: IEEE.
- Kite, G.W. (1995). Manual for the SLURP Hydrological Model. Saskatoon, Canada: NHRI.
- Kite, G.W., & Kouwen, N. (1992). Watershed modeling using land classifications. *Water Resource Research*, 28(12), 3193-3200.
- Kite, G.W., & Pietroniro, A. (1996). Remote sensing applications in hydrological modeling. *Hydrological Sciences Journal*, 41(4), 563 - 591.
- Klemes, V. (1986). Operational testing of hydrological simulation models. *Hydrological Sciences Journal*, 31(1), 13-24.
- Kustas, W., & Daughtry, C. (1989). Estimation of the soil heat flux/net radiation ratio from spectral data. *Agricultural and Forest Meteorology*, 49(3), 205-223.
- Kustas, W., & Norman, J. (1996). Use of remote sensing for evapotranspiration monitoring over land surfaces. *Hydr. Sci. J.*, 41(4), 495-516.
- Lagouarde, J. (1991). Use of NOAA-AVHRR data combined with an agrometeorological model for evaporation mapping. *International Journal of Remote Sensing*, 12, 1853-1864.
- Larsson, H. (2002). Analysis of variations in land covers between 1972 and 1990, Kassala Province, Eastern Sudan, using Landsat MSS data. *International Journal of Remote Sensing*, 23(2), 325-333.
- LDAS. (2010). LDAS Vegetation Parameters. Retrieved from <http://ldas.gsfc.nasa.gov/gldas/GLDASmapveg.php>.
- Lemeur, R., & Zhang, L. (1990). Evaluation of three evapotranspiration models in terms of their applicability for an arid region. *Journal of Hydrology*, 114, 395-411.
- Li, K.Y., Coe, M.T., Ramankutty, N. & Jong, R.D. (2007). Modeling the hydrological impact of land-use change in West Africa. *Journal of Hydrology*, 337(3-4), 258- 268.
- Li, X. (2001). Estimation of Urumqi River Basin Evaporation with Remote Sensing, (Unpublished M.Sc. Thesis). Wageningen University. Netherlands.

- Li, X., & Wang, X. (2003). Changes in agricultural land use in China: 1981-2000. *Asian Geographer*, 22(1-2), 27-42.
- Li, C., Ge, J., Liu, S., & Sun, P.S. (2006). Landscape pattern and eco-hydrological characteristics at the upstream of Minjiang River , China. *Frontiers Biology of China*, 1(4), 455-462.
- Liang, S.L. (2003). *Quantitative Remote Sensing of Land Surfaces*. Hoboken, NJ, USA: Wiley & Sons.
- Lin, W.J., Su, Z.B., Dong, H., Chen, L., & Wang, G.L. (2008). Regional Evapotranspiration Estimation Based on MODIS Products and Surface Energy Balance System (SEBS) in Hebei Plain, Northeastern China. *Journal of remote sensing*, 12(4), 663-672.
- Liu, C.M., Yang, T.S., & Sun, R. (2006). Study on hydrologic cycle factors based on GIS/RS in the Yellow River Basin. Zhengzhou, China: Water press of the Yellow River.
- Liu, C.M., & Zhong, J.X. (1978). The influence of forest cover upon annual runoff in the Loes Plateau of China. *Acta Geographical Sinica*, 33(2), 112-127.
- Liu, H. & Zhou, Q. (2004). Accuracy analysis of remote sensing change detection by rule-based rationality evaluation with post-classification comparison. *International Journal of Remote Sensing*, 25(5), 1037-1050.
- Liu, Q., Ou, M.H., & Peng, X.Y. (2005). The forecast of land use structure based on Markov process - A case study of Kunshan City. *Journal of Nanjing Agricultural University*, 28 (3), 107~112
- Los, S.O., & Collatz, B.L. (2001). Global international Variations in sea surface temperature and land surface vegetation, air temperature and precipitation. *Journal of Climate*, 14, 1535-1549.
- Lørup, J.K., Refsgaard, J.C., & Mazvimavi, D. (1998). Assessing the effect of land use change on catchment runoff by combined use of statistical tests and hydrological modeling: case studies from Zimbabwe. *Journal of hydrology*, 205, 147–163.
- LPDAAC. (2010). Land Cover Type Yearly L3 Global 500 m SIN Grid. Retrieved from https://lpdaac.usgs.gov/lpdaac/products/modis_products_table/land_cover/yearly_l3_global_500_m/mcd12q1.

- LUCC. (1999). Land Use and Land Cover: Implementation Strategy. IGBP Report 48, IHDP Report 10, Stockholm: IGBP Secretariat.
- MWR. (1992). Department of Hydrology, Ministry of Water Resources, PRC, Water Resources Assessment for China. Beijing, China: China Water and Power Press. (in Chinese)
- Macleod, R.D. & Congalton, G. (1998). A Quantitative Comparison of Change Detection Algorithms for Monitoring Helgrass from Remotely Sensed Data. *Photogrammetric Engineering & Remote Sensing*, 64(3), 207 - 216.
- Malin, F.J.R. (2004). Balancing Water for Humans and Nature - the new approach in ecohydrology (pp. 3-22). London: Earthscan.
- Mann, H. (1945). Nonparametric tests against trend. *Econometrica*, 13, 245-259.
- Mark, D., Dozier, J., & Frew, J. (1984). Automated basin delineation from digital elevation data. *Geo-Processing*, 2, 299-311.
- Massman, W. (1997). An analytical one-dimensional model of momentum transfer by vegetation of arbitrary structure. *Boundary-Layer Meteorology*, 83, 407-421.
- Massman, W. (1999a). A model study of kBH-1 for vegetated surfaces using 'localized nearfield' Lagrangian theory. *Journal of Hydrology*, 223, 27-43.
- Massman, W. (1999b). Molecular diffusivities of Hg vapor in air, O₂ and N₂ near STP and the kinematic viscosity and the thermal diffusivity of air near STP. *Atmos. Environ.*, 33, 453-457.
- McGregor, D.F.M., & Thompson, D.A. (1995). Geomorphology and land management in a changing environment. In Thompson, D.M. (pp. 107-119). New York: John Wiley & Sons.
- Menenti, M. (1984). Physical aspects of and determination of evaporation in deserts applying remote sensing techniques. Report 10 (special issue). The Netherlands.
- Menenti, M., & Choudhury, B.J. (1993). Parameterization of land surface evapotranspiration using a location dependent potential evapotranspiration and surface temperature range. In Bolle, H.J. et al. (Eds.), *In Proceeding of Exchange Processes at the Land Surface for a Range of Space and Time Scales* (p. 561 - 568). IAHS Publication.

- Mitchell, J., Dzerdzeevskii, B., Flohn, H., & Hofmeier, W.L. et al. (1966). Climate change WMO Technical Note No. 79.
- Mo, X., Liu, S., & Lin, Z. (2004). 2004. Simulating temporal and spatial variation of evapotranspiration over the Lushi basin. *Journal of Hydrology*, 285(1-4), 125-142.
- Monteith, J. (1965). Evaporation and environment. *Symposia of the Society for Experimental Biology*, 19, 205-234.
- Moran, M., Clarke, T., Inoue, Y., & Vidal, A. (1994). Estimating crop water management using the relation between surface-air temperature and spectral vegetation index. *Remote Sensing of Environment*, 49, 246-263.
- Munther, J.H. (2001). Water scarcity impacts and potential conflicts in the MENA region. *Water International*, 26(4), 460-470.
- Myneni, R.B., Nemani, R.R. & Running, S.W. (1997). Estimation of global leaf area index and absorbed par using radiative transfer models. *IEEE Transactions on Geoscience and Remote Sensing*, 35, 1380-1393
- Nachabe, M., Shah, N., Ross, M., & Vomarka, J. (2005). Evapotranspiration of two vegetation covers in a shallow water table environment. *Soil Science Society of American Journal*, 69(2), 492-499.
- Nash, L., & Gleick, P. (1991). Sensitivity of streamflow in the Colorado Basin to climatic changes. *Journal of hydrology*, 125, 221-241.
- Natale, L., & Todini, E. (1977). A constrained parameter estimation technique for linear models in hydrology. In Ciriani, J. T. A. & Malone, U.(Eds.), *Mathematical models for surface water hydrology*, 1974(pp 69-88). London: Wiley.
- Neale, C., Jayanthi, H., & Wright, J. (2005). Irrigation water management using high resolution airborne remote sensing. *Irrigation and Drainage Systems*, 19(3/4), 321-336.
- Neale, C., Jayanthi, H., & Wright, J. (2005). Irrigation water management using high resolution airborne remote sensing. *Irrigation and Drainage Systems*, 19(3/4), 321-336.

- Neave, M., & Abrahams, A. (2002). Vegetation influences on water yields from grasslands and shrubland ecosystems in the Chihuahuan Desert. *Earth Surface Processes and Landforms*, 27, 1011-1020.
- Nelder, J.A., & Mead, R. (1965). A simplex method for functional minimization. *Compute Journal*, 9, 308-313.
- Newman, B.D., Cambell, A.R., & Wilcox, B. (1998). Lateral subsurface flow pathways in a semiarid ponderosa pine hillslope. *Water Resources Research*, 34, 3485-3496.
- Newman, B.D., Wilcox, B.P., Archer, S.R., Breshears, D.D., Dahm, C.N., & Duffy, C. (2006). Ecohydrology of water-limited environments: A scientific vision. *Water Resources Research*, 42, 1-15.
- Niehoff, D., Fristch, U., & Bronster, A. (2002). Land-use impacts on storm-runoff generation: scenarios of land-use change and simulation of hydrological response in a meso-scale catchment in SW-Germany. *Journal of Hydrology*, 267(1-2), 80-95.
- Norman, J.M., & Kustas, W.P. (1995). A two-source approach for estimating soil and vegetation energy fluxes from observations of directional radiometric surface temperature. *Agricultural and Forest Meteorology*, 77, 263-293.
- Nuttle, W. (2002). Is Ecohydrology one idea or many? *Hydrological Sciences. Hydrological Sciences Journal*, 47(5), 805-807.
- Nuttle, W.K. (2002). Eco-hydrology's past and future in focus. *American Geophysical Union*, 83(19), 1-4.
- Olorunfemi, J.F. (1983). Monitoring Urban Land – Use in Developed Countries – An aerial photographic approach. *Environmental International*, 9, 27 – 32.
- Overgaard, J., Rosbjereg, D., & Butts, M. (2006). Land-surface modeling in hydrological perspective-a review. *Biogosciences*, 3, 229-241.
- Owe, M. (1985). Long-term streamflow observations in relation to basin development. *Journal of Hydrology*, 78(3-4), 243-260.
- Pan, D., & Blois, S.D. (1999). Temporal (1958 – 1993) and spatial patterns of land use changes in Haut-Saint-Laurent (Quebec, Canada) and their relation to landscape physical attributes. *Landscape Ecology*, 14(1), 35-52.

- Pandy, A.C., & Nathawat, S.M. (2006). Land Use Land Cover Mapping Through Digital Image Processing of Satellite Data – A case study from Panchkula, Ambala and Yamunanagar Districts. Haryana State, India. Retrieved from <http://www.gisdevelopment.net/application/environment/overview/envo0009.htm>
- Paul, J.W., David, M.H., & Sadler, J.P. (2008). *Hydroecology and Ecohydrology: Past, Present and Future*. Chichester: John Wiley & Sons.
- Penman, H.L. (1948). Natural Evaporation from Open Water, Bare Soil and Grass. *Proceedings of the Royal Society of London. Series A, Mathematical and Physical Sciences*, 193(1032), 120-145.
- Petit, C., Scudder, T., & Lambin, E.F. (2001). Quantifying processes of land cover change by remote sensing: resettlement and rapid land cover changes in South Eastern Zambia. *International Journal of Remote Sensing*, 21(17), 3435-3456.
- Piercel, L., Walker, J., & Dowing, E.L. (1993). Ecohydrological changes in Murray Darling basin. III. A Simulation of regional hydrological changes. *Journal of Applied Ecology*, 30(28), 3-294.
- Pinty, B., & Verstracte, M.M. (1992). GEMI: a non-linear index to monitoring global vegetation from satellite. *Vegetation*, 101, 15-20.
- Press, W., Teukolsky, S., Vetterling, W., & Flannery, B. (1997). *Numerical Recipes in C: The Art of Scientific Computing*. Cambridge University Press, UK.
- Priestley, C. H. B., & Taylor, R. J. (1972). On the Assessment of Surface Heat Flux and Evaporation Using Large-Scale Parameters. *Monthly Weather Review*, 100(2), 81- 92.
- Ramakrishna, R.N., & Steven, W.R. (1996). Global vegetation cover changes from coarse resolution satellite data. *Journal of geophysical research*, 101(D3), 7157-7162.
- Ran, Y.H., Li, X., & Lu, L. (2009). Accuracy evaluation of the four remote sensing based land cover products over China. *Journal of glaciology and geocryology*, 31(3), 490 -500.
- Ragan, R.M. & Jackson, T.J. (1980). Runoff Synthesis Using Landsat and SCS Model. *Journal of the Hydraulics Division*, 106(5), 667-678.
- Rango, A., Feldman, A., George, T., & Rogan, R.M. (1983). Effective use of Landsat data in hydrologic models. *Water Resource Bulletin*, 19(2), 165-174.

- Read, J.M., & Lam, N.S. (2002). Spatial methods for characterizing land cover and detecting land-cover changes for the tropics. *International Journal of Remote Sensing*, 23(12), 2457-2474.
- Ripple, C., Rubin, J., & Van Hylckama, T.E.A. (1972). Estimating steady-state evaporation rates from bare soils under conditions of high water tables. *Geological Survey Water Supply Paper 2019-A*. USA Geological Survey, Washington, DC.
- Robert, M.R., & Jackson, T.J. (1980). Runoff Synthesis Using Landsat and SCS Model. *Journal of the Hydraulics Division*, 106(5), 667-678.
- Rodriguez-Iturbe, I. (2000). Ecohydrology: A Hydrologic Perspective of Climate-Soil-Vegetation Dynamics. *Water Resources Research*, 36(1), 3-9.
- Rodriguez-Iturbe, I.A., Porporato, F., & Laio, A.L. (2001). Plants in water-controlled ecosystems: Active role in hydrologic processes and response to water stress I. Scope and general outline. *Advance in water resources*, 24, 695-705.
- Roerink, G.J., Su, B., & Menenti, M. (2000). S - SEBI: A simple remote sensing algorithm to estimate the surface energy balance. *Physics and Chemistry of the Earth, Part B*, 25(2), 147 - 157.
- Rui, X.F. (2000). *Shui wen xue yuan li*. Beijing, China: China Water Power Press.
- Running, S.W., Patterson, D.L., Spanner, M.A., & Teuber, K.B. (1986). Remote sensing of coniferous forest leaf area. *Ecology*, 67, 273-276.
- Sala, O.E., et al. (2000). Global biodiversity scenarios for the year 210. *Science*, 287, 1770-1774.
- Salomonson, V.V., & Colwell, J. (Eds.). (1983). *Water resources assessment, Manual of remote sensing*. Bethesda MD: American Society of Photogrammetry and Remote Sensing.
- Schneide, N., Eugster, W., & Schichler, B. (2004). The impact of historical land-use changes on the near-surface atmospheric conditions on the Swiss Plateau. *Earth Interactions*, 8(12), 1-27.
- Schultz, G.A., & Engman E.T. (Eds.). (2000). *Remote Sensing in Hydrology and Water Management*. Berlin, Germany: Springer-Verlag.

- Sellers, P. (1985). Canopy reflectance, photosynthesis, and transpiration. *International Journal of Remote Sensing*, 6, 1335-1371.
- Shao, J. (2005). Land use change and its corresponding ecological responses: a review. *Journal of Geographical Sciences*, 15(3), 305-328.
- Sherman, L.K. (1932). Streamflow from rainfall by the unit-graph method. *Engineering News Record*, 108, 501-505.
- Shoshany, M. (1996). Monitoring temporal vegetation cover changes in Mediterranean and arid ecosystems using a remote sensing technique: case study of the Judean Mountain and the Judean Desert. *Journal of Arid Environments*, 33(1), 9-21.
- Shuttleworth, W.J. (1991). The modellion concept. *Reviews of Geophysics*, 29, 589-606.
- Shuttleworth, W., Gurney, R.J., Hsu, A.Y., & Ormsby, J.P. (1989). FIFE: the variation in energy partition at surface flux sites. *IAHS Publication*, 186, 67-74.
- Singh, A. (1989). Digital Change Detection Techniques Using Remotely Sensed Data. *International Journal of Remote Sensing*, 10(6), 989-1003.
- Singh, V.P. (1995). Watershed modeling. In Singh, V.P. (Ed.), *Computer Models of Watershed Hydrology*. (pp. 1-22). Colorado: Water Resources Publications.
- Sivapalan, M. (2003). Prediction in ungauged basins: a grand challenge for theoretical hydrology. *Hydrological Processes*, 17(15), 3163-3170.
- Sorooshian, S., & Gupta, V. (1995). Model calibration. In Singh, V.P. (Ed.), *Computer Models of Watershed Hydrology* (pp. 23-68). Colorado: Water Resources Publications.
- Spanner M.A., Pierce, L.L., & Running, S.W.E. (1990). The seasonality of AVHRR data of temperate coniferous forests: relationship with leaf area index. *Remote Sensing Environment*, 33, 97 - 112.
- Stadimir, K., Vucicevic, S., Markovic, S., & Nikolic, M. (1998). Runoff regime in small watersheds with different degrees of forest cover. In Balkema, A. A. (Ed.), *Fourth International Conference on Headwater Control*, Merano. Italy.
- Stull, R. (1988). *An introduction to boundary layer meteorology*. Dordrecht, The Netherlands: Kluwer Academic Publishers.

- Su, Z. (2002). The Surface Energy Balance System (SEBS) for estimation of turbulent heat fluxes. *Hydrology and Earth System Sciences*, 6(1), 85-100.
- Su, Z., Li, X., Zhou, Y., Wan, L., Wen, J., & Sintonen, K., et al. (2003). Estimating Areal Evaporation from Remote Sensing. In *International Geoscience And Remote Sensing Symposium* (pp. 21-25). Toulouse.
- Su, Z., Schmugge, T., Kustas, W.P., & Massman, W.J. (2001). An Evaluation of Two Models for Estimation of the Roughness Height for Heat Transfer between the Land Surface and the Atmosphere. *Journal of Applied Meteorology*, 40(11), 1933-1951.
- Su, Z., Yacob, A., Wen, J., Roerink, G., He, Y., & Gao, B., et al. (2003). Assessing Relative Soil Moisture with Remote Sensing Data: Theory and Experimental validation, *Phys. Chem. Earth*, 28(1-3), 89-101.
- Sugawara, M., Watanabe, I., Ozaki, E., & Katsuyama, Y. (1983). Reference manual for the TANK model. National. Research Centre for Disaster Prevention, Tokyo.
- Suleiman, A., & Ritchie, J.T. (2003). Modeling soil water redistribution during second-stage evaporation. *Soil Science Society of America Journal*, 67(2), 377-386.
- Sullivan, A., Ternan, J.L., & Williams, A.G. (2004). Land use change and hydrological response in the Camel catchment, Cornwall. *Applied Geography*, 24(2), 119-137.
- Tao, T., & Kouwen, N. (1983). Remote Sensing and Fully Distributed Modeling for Flood Forecasting. *J. Water Resource Planning. and Management*, 115(6), 809-823.
- Tekle, R., & Redlund, L. (2000). Land cover changes between 1958 and 1986 in Kalu district, Southern Wello, Ethiopia. *Mountain Research and Development*, 20(1), 42-51.
- Terpstra, J., & Mazijk, V.A. (2001). Computer aided evaluation of planning scenarios to assess the impact of land-use changes on water balance. *Physics and Chemistry of the Earth Part B*, 26(7-8), 523-527.
- Thompson, S.A. (1999). *Hydrology for Water Management* (p. 362). Rotterdam, Netherlands: A.A. Balkema International Publishers.
- Thomthwaite, C., & Mather, J. (1955). The water balance. In Thomthwaite, C., & Mather, J. (Eds.), *Publications in climatology*. New York: Drexel Institute of Technology.

- Tomo'omi, K., Saitoh, M., & Yet, S. (2005). Annual water balance and seasonality of evapotranspiration in a Bornean tropical rainforest. *Agricultural and Forest Meteorology*, 128(1-2), 81-92.
- Tucker, C.J., & Sellers, P.J. (1986). Satellite remote sensing of primary vegetation. *International Journal of Remote Sensing*, 22, 3827-3844.
- Turner, K.M. (1991). Annual Evapotranspiration of Native Vegetation in a Mediterranean-Type Climate. *Journal of the American Water Resources Association*, 27(1), 1-6.
- UNESCO, (1998), World Science Report 1998, Paris, UNESCO.
- USDA. (1972). National Engineering Handbook. DC, USA: Hydrology Washington, US Government Printing Office.
- Van De Griend, A.A., & Owe, M. (1993). On the relationship between thermal emissivity and the Normalized Difference Vegetation Index for natural surfaces. *International Journal of remote sensing*, 14(6), 1119-1131.
- Van den Hurk, B.J.J.M. & Holtslag, A.A.M. (1997). On the bulk parameterization of surface fluxes for various conditions and parameter ranges. *Boundary-Layer Meteorology*, 82(1), 1573-1472.
- Van der Kawast, J., Timmermans, W., Gieske, A., & Su, Z. (2009). Evaluation of the Surface Energy Balance System (SEBS) applied to ASTER imagery with flux-measurements at the SPARC 2004 site (Barrax, Spain). *Hydrology and Earth System Sciences*, 13, 1337-1347.
- Vorosmarty, C.J., Green, P., Salisbury, J., & Lammers. R. (2000). Global water resources: vulnerability from climate change and population growth. *Science*, 289, 284-288.
- Wan, R.R., & Yang, G.S. (2005). Discussion on Some Issues of Hydrological Effects of Watershed Land Use and Land Cover Change. *Progress in geography*, 24(3), 25-33.
- Wang, J., & Lu, Z. (2003). Study on the impact of land use changes on the hydrological system. *Advance in Earth Sciences*, 18(2), 292-298.
- Wang, L.X., & Xue, M.S. (Eds.). (1997). The hydroecological benefit and information system of upland defend forest on soil and water conservation. Beijing: Forest press.

- Wang, M.R. (2003). Study on application of multi-sources information in hydrologic model based on digital watershed platform. (Unpublished doctoral dissertation). Hohai University, Nanjing, China.
- Wang, Q.J. (1991). The genetic algorithm and its application to calibrating conceptual rainfall-runoff models. *Water Resources Research*, 27(9), 2467-2471.
- Wang, S.P. (2007). Ecohydrologic reponse of small watershed to land use change and climate variation. (Unpublished doctoral dissertation). Beijing Forestry University, Beijing.
- Wang, S.Y., Wang, G.Q., & Chen, Z.X. (2005). Study on graphic information characteristics of land use spatial pattern and its changes in Yellow River Basin, China. In *Geoscience and Remote Sensing Symposium, 2005. IGARSS '05. Proceedings. 2005 IEEE International* (pp. 2492 – 2495).
- Wang, Z.L. (2006). Effect of climatic change and LUCC on hydrologic system in the East River Basin, South China. (Unpublished Ph.D. dissertation). Sun Yat-sen University, Guangzhou, China.
- Wang, Z.L., Chen, X.H., & Li, Y. (2006). Spatio-temporal changes of NDVI in the Pearl River Basin. *Ecologic Science*, 25(4), 303-307.
- Wei, L.N. (2010). Ecohydrologic processes analysis and modeling in the red-soil hilly area, south China. (Unpublished Ph.D. dissertation). Hohai University, Nanjing, China.
- Weligepolage, K. (2005) Estimation of spatial and temporal distribution of evaporatranspiration by satellite remote sensing – A case study in Hupselse Beek, the Netherland. (Unpublished Ph.D. dissertation). International Institute for Geo-information Science and Earth Observation, Netherland.
- Weng, Q.H. (2002). Land use change analysis in the Zhujiang Delta of China using satellite remote sensing, GIS and stochastic modeling. *Journal of Environmental Management*, 64(3), 273-284.
- Weismiller, R., & Momin, S.J. (1977). Change detection in coastal zone environments. *Photogramm Engg. & Remote Sensing*, 43(12), 1533-1539.

- Wheater, H.S., Jakeman, A.J., & Beven, K.J. (1993). Modeling change in environmental systems. In Jakeman, A.J., Beck, M.B., & McAleer, F.M.J. (Eds.), *Progress and directions in rainfall-runoff modeling* (p. 584). John Wiley & Sons Ltd.
- Wickware, G.M., & Howarth, J.P. (1981). Change detection in the Peace-Athabasca Delta using digital Landsat data. *Remote Sensing Environment*, 11(1), 9-25.
- Wilcox, B.P., Breshears, D.D., & Allen, C. (2003). Ecohydrology of a resource-conserving semiarid woodland: Effects of scale and disturbance. *Ecological Monographs*, 73, 223-239.
- Williamson, D., Stokes, R., & Ruprecht, J.K. (1987). Response of input and output of water and chloride to clearing for agriculture. *Journal of Hydrology*, 94(1-2), 1-28.
- WMO (1975). Intercomparison of conceptual models used in operational hydrological forecasting. WMO operational hydrology Rep. No. 7, WNO no. 429.
- WMO (1992). Simulated real-time Intercomparison of hydrological models. WMO Operational hydrology Rep. No. 38, WNO no. 779.
- Wood, E. (1995). Heterogeneity and scaling land-atmospheric water and energy fluxes in climate systems. In Feddes, R. (Ed.), *Space and time scale variability and interdependencies in hydrological processes* (pp. 3-19). The University Press, Cambridge.
- Wu, L., Sun, B., Zhou, S., Huang, S., & Zhao, Q. (2004). A New Fusion Technique of Remote Sensing Images for Land Use/Cover. *Pedosphere*, 14(2), 187-194.
- Xia J., Li, F.H., Ge, T., Sheng, W.G., & Hua, Z.Y. (2003). Eco-hydrology—Concept, Framework and System. *Journal of Irrigation and Drainage*, 22(1), 4-10.
- Xu, C.Y., & Singh, V. (2005). Evaluation of three complementary relationship evapotranspiration models by water balance approach to estimate actual regional evapotranspiration in different climatic regions. *Journal of Hydrology*, 308(1-4), 105-121.
- Xu, Z., & Li, J. (2003). A distributed approach for estimating catchment evapotranspiration: comparison of the combination equation and the complementary relationship approaches. *Hydrologic Process*, 17, 1509-1523.

- Yi, C., Liu, K., & Zhou, T. (1996). Research on a Formula of Rainfall Interception by Vegetation. *Journal of soil erosion and soil and water conservation*, 2(2), 47-49. (In Chinese).
- Yuan, F. (2006). Hydrologic processes modeling considering the effect of vegetation. (Unpublished Ph.D. Dissertation). Hohai University, Nanjing.
- Zhao, G., Yuill, C.G., & Fletcher, J.J. (2004). Cultivated Land Changes and Their Driving Forces—A Satellite Remote Sensing Analysis in the Yellow River Delta, China. *Pedosphere*, 14(1), 93-102.
- Zalewski, M. (2002). Ecohydrology—the use of ecological and hydrological processes for sustainable management of water resources. *Hydrological Sciences Journal*, 47(5), 823-832.
- Zhan, C.S. (2005). Estimation of Land Surface Evapotranspiration from Satellite Data over China and its Temporal-Spatial Patterns. (Unpublished Ph.D. Dissertation), CAS, Beijing.
- Zhang, L., Dawes, W.R., & Walker, G.R. (1999). Catchment hydrology predicting the effect of vegetation changes on catchment. Technical report 10/97, CSIRO Land & Water, Canberra.
- Zhang, L., Dawes, W.R., & Walker, G.R. (2001). Response of mean annual ET to vegetation change at catchment scale. *Water Resources Research*, 37(3), 701-708.
- Zhang, R.H. (1996). Experimental remote sensing model and the land surface basis. Science press, Beijing, China.
- Zhang, Z.C. (2008). Distributed hydrological model and eco-hydrological effect of vegetation in Karst watershed. (Unpublished Ph.D. dissertation). Hohai University, Nanjing, China.
- Zhao, G.X., Lin, G., Fletcher, J.J. & Yuill, C. (2004). Cultivated land changes and their driving forces—A satellite remote sensing analysis in the Yellow River Delta, China. *Pedosphere*, 14(1), 93-102.
- Zhao, H., Wu, Q., & Liu, G. (2001). Advances on research of runoff and sediment yield and hydrological effect in forest watershed. *Journal of Northwest Forest University*, 16, 82–87. (In Chinese).

- Zhao, R. (1984). *Water Hydrological Modeling – Xinanjiang Model and Shanbei Model*. China Water Resources and Waterpower Publication, Beijing .
- Zhao, R., & Wang, P. (1988). Parameter determination of Xinanjiang model. *Hydrology*, 9, 21-24.
- Zhao, R., Zhuang, Y., Fang, L., Liu, X., & Zhang, Q. (1980). The Xinanjiang model hydrological forecasting. In *proceedings Oxford Symposium* (pp. 351-356). IAHS 129.
- Zhou, L.M., Tucker, C.J., Kaufmann, R.K., Slayback, D., Shabanov, N.V., & Myneni, R.B. (2001). Variation in northern vegetation activity inferred from satellite data of vegetation index during 1981 to 1999. *Journal of geophysical research*, 106(D17), 20069-20083.
- Zhou, X.F., Zhao, H.X., & Sun, H.Z. (2001). Proper assessment for forest hydrological effect. *Journal of Natural Resources*, 16, 420–426.